
Tesis doctoral

MINIMALLY INVASIVE DENTAL STRATEGIES FOR BONE REGENERATION AND ENDODONTIC TREATMENTS

Ana Bárbara Giordano

Aquesta tesi doctoral està subjecta a la licència [Reconeixement-NoComercial-SenseObraDerivada 4.0 Internacional \(CC BY-NC-ND 4.0\)](#)



Esta tesis doctoral está sujeta a la licencia [Reconocimiento-NoComercial-SinObraDerivada 4.0 Internacional \(CC BY-NC-ND 4.0\)](#)

This doctoral thesis is licensed under the [Attribution-NonCommercial-NoDerivatives 4.0 International \(CC BY-NC-ND 4.0\)](#)



Universitat Internacional de Catalunya

Bioengineering Institute of Technology

Minimally invasive dental strategies for bone regeneration and endodontic treatments

PhD Thesis in Health Sciences

Ana Barbara Giordano

Director: Dr. Román Pérez Antoñanzas

Barcelona, 2020

*"Cuando creíamos que teníamos todas las respuestas, de pronto, cambiaron
todas las preguntas"*

Mario Benedetti

Agradecimientos

Llegó el gran momento tan esperado, la finalización de mi tesis y con ella el cierre de una etapa muy especial en mi vida. No puedo decir que esta tesis me pertenezca solo a mí, ya que es el fruto de la colaboración de muchas personas e ideas con las que he tenido la suerte de encontrarme a lo largo de estos años. Todas y cada una de estas personas me han aportado algo significativamente valioso. Es por esto que la tesis se la dedico a todas ellas.

A **Román**, mi director, el cual se ha convertido en un amigo. Te agradezco que me adoptaras como doctoranda, tu apoyo incondicional, consejo y tiempo que siempre me has dado, no solo en lo profesional sino también en lo personal. Me encanta que compartamos ese humor que nos caracteriza... aunque no siempre nos entiendan los chistes! Tus "thinking outside the box", tu pasión y tu manera de entender la ciencia y a los que te rodean. Me has enseñado muchísimo. Gracias por todo.

A todos y cada uno de los miembros del **BIT**. Gracias por hacerme formar parte de este gran equipo, aunque yo haya estado a tiempo parcial y a pesar de ser Odontóloga ☺. Gracias por vuestro buen humor y por vuestra inmensa paciencia conmigo. **Bego**, gracias por estar siempre ahí en todo momento, por todo tu apoyo, ayuda y amistad durante todos estos años. **Èlia**, gràcies per la teva ajuda incondicional desde el primer dia, per la teva paciència i serenitat. Juntes hem fet créixer una amistat i una planta invencibles! **Mireia**, gràcies de tot cor per tot el teu suport i ajuda, per entregar-me la teva gran amistat, per compartir tants moments juntes dins i fora de la universitat. **Leire**, gracias por ayudarme y entregar tu tiempo, siempre volcada a solucionar cualquier problema que pudiera surgir. **Luis**, alias MacGyver, muchas gracias por todo tu apoyo, siempre dispuesto a ayudarme en cualquier ocasión. **Raquel** y **María**, gracias por vuestro buen humor y ayuda en todo momento. Al resto de miembros del BIT: **Marina**,

Jennifer, María, Yolanda, Miguel y Emilio, mil gracias por estar ahí siempre y por todos los buenos momentos compartidos, tanto dentro como fuera de la universidad. Lo mismo a **Noelia**, que a pesar de no compartir despacho siempre has formado parte del grupo. Agradecerte toda la ayuda y apoyo durante estos años y todos los buenos momentos compartidos. A **Bea Santiago**, que aunque hayamos coincidido poco tiempo en el BIT siempre me has brindado tu apoyo y amistad. También gracias a **Noelia Galán** por todos los momentos compartidos, siempre con una sonrisa.

A los miembros del antiguo grupo del **Regenerative Medicine**. Con ellos me inicié en la gran aventura de la investigación durante mi etapa en el máster. Desde el primer día me animaron y me dedicaron su tiempo. Especialment a la **Raquel**, qui sempre m'ha brindat la seva amistat i la seva gran ajuda. Gràcies per compartir amb mi la teva passió per la ciència. També gràcies a la **Montse Mercadé** per creure en mi desde el primer moment i fer possible que m'endinsés en aquesta gran aventura.

Al grupo de **Ciencias básicas** por su ayuda y colaboración en estos años compartiendo laboratorio. Gracias también a **Sònia Soriano**, por toda la ayuda durante estos años con las gestiones administrativas.

Muchas gracias al equipo de **Odontología** de la UIC. En especial a **José Antonio González** y **María Arregui**. Os agradezco mucho todo el soporte y ayuda que me habéis proporcionado siempre. A mis compañeros y amigos de trabajo, en especial a los de la **clínica de Maragall**, quienes durante todos estos años han estado escuchándome y apoyándome, y me han ayudado en todo lo que les he pedido y más en este proyecto, siempre con buen humor.

Al meu amic **Marc**, ens coneixem desde que teníem 4 anys, qui ho hagués dit que 30 anys més tard ens trobaríem on som ara. Moltíssimes gràcies per tota la teva ajuda i paCIÈNCIA, sobretot durant aquests últims mesos.

Als meus **amics** i **amigues**, en especial a l'**Eli** i la **Cris**. Sempre heu estat al meu costat, escoltant-me i animant-me en aquest projecte i en tot. Us agraeixo totes les hores de converses i riures infinits. A **Sara**, por apoyarme y estar ahí siempre, gracias por tu gran amistad.

A **Adolfo**, has sido mi guía durante estos últimos años, no solo me has ayudado en este proyecto sinó en la vida en general. Me has aportado muchísimo y me has hecho crecer como persona. Sabes que siempre te estaré agradecida.

A mi gran **familia**, en especial a mi **madre**, a mi **padre** y a mis **hermanas**, quienes siempre han estado a mi lado apoyándome y creyendo en mí. Siempre he intentado seguir vuestro ejemplo, en lo personal y en lo profesional, y saber que os sentís orgullosos de mí es el mejor regalo. A mi **zia Lila**, siempre interesada por los avances en mi tesis, con mucho cariño y humor.

A mis queridos **suegros**, que a pesar de los miles de kilómetros de distancia siempre os he sentido muy cerca, apoyándome y dándome buenas vibras en todo momento.

Mención especial a mi compañero de vida, **Gian Carlo**, siempre me has motivado a seguir mis sueños y a continuar mejorando, me has enseñado que la perseverancia da sus frutos. Gracias por todo tu cariño, amor y comprensión.

ESTOY AGRADECIDA DE CORAZÓN A TODA LA GENTE QUE DIRECTA O INDIRECTAMENTE HA DEJADO SU HUELLA MARCADA EN ESTA ETAPA QUE RECORDARÉ SIEMPRE CON UNA GRAN SONRISA.

Abstract

Nowadays, the most common solution to maintain the teeth of patients that have suffered from a traumatism or a profound caries and have ended with root canal infection is to perform a root canal treatment. For this purpose, Gutta-percha (GP) is one of the main materials used to fill root canals, presenting excellent biocompatibility and good sealing ability. However, GP poor bonding ability to dental tissues has led to high failure rates in endodontic treatments. To address these challenges, many studies have performed research to revise GP. Among the different options that are being explored as novel endodontic materials, bioactive elements are a promising strategy to improve root canal treatments. For instance, silica based microspheres (SiMS) are an example of bioactive elements that present an active surface and chemical composition that may provide a stronger adhesion to dentin tissue, biocompatibility and the possibility to serve as a possible drug delivery system.

In the cases in which the patient presents a more advanced dental pathology, which has led to the tooth loss and/or bone loss surrounding the tooth, the treatment of choice is bone regeneration through a natural bone graft. This is the best option since it presents the same composition as the bone, containing cells with osteogenic potential and growth factors that stimulate cells differentiation into osteoblasts, among others. Nevertheless, this type of grafts present some drawbacks, such as pain, risk of infection, possible disease transmission and limited availability. For this reason, synthetic bone grafts research is one of the main proposals in regenerative medicine. This branch of medicine is based on the development of new biomaterials with the objective of increase the bone healing capacity and, more specific in the dentistry field, to prevent or eliminate bacterial infections at the same time.

The present thesis is divided in two parts: i) a treatment focused on the dental system and ii) a treatment focused on the bone system. The first part presents the fabrication of an endodontic biomaterial to enhance the GP sealing ability and its bonding capacity with the dental tissue; in the second part, two strategies to improve maxillary bone regeneration are presented: the first one through the *in vitro* study of a low level laser to study its osteogenic effect and cellular proliferation; the second one through the fabrication plus optimization of a biomaterial with a drug sustained release for its potential use as a synthetic bone graft.

Resumen

Actualmente, la principal solución para mantener los dientes de los pacientes que han sufrido un traumatismo o una caries profunda, los cuales han desencadenado una infección del conducto radicular, es realizar el tratamiento de endodoncia. Para este fin, la Gutta-percha (GP) es el material más utilizado para rellenar los conductos radiculares, presentando una excelente biocompatibilidad y una buena propiedad de sellado. No obstante, la pobre capacidad de adhesión de la GP a los tejidos dentales ha llevado a alcanzar unas tasas elevadas de fracaso en los tratamientos endodónticos. Para solventar esta problemática, se han realizado muchos estudios para revisar la GP. Entre las diferentes opciones que se están investigando en el diseño de nuevos materiales de sellado de los conductos radiculares, los elementos bioactivos son una estrategia prometedora para mejorar los tratamientos endodónticos. Entre ellos, las microesferas basadas en sílica son un tipo de elementos bioactivos que presentan una superficie activa y una composición química que podrían proporcionar a la GP una adhesión más fuerte con el tejido dentinario, biocompatibilidad y la posibilidad de usarse como un sistema de liberación de fármacos.

En los casos en que el paciente presenta una patología dental más avanzada, la cual haya conllevado a la pérdida del diente y/o una pérdida de tejido óseo alrededor del diente, el tratamiento de elección es el de regeneración ósea mediante un injerto de hueso natural. Es la mejor opción al presentar la misma composición que el hueso, contener células con potencial osteogénico y factores de crecimiento que estimulen la diferenciación de las células a osteoblastos, entre otros. Sin embargo, este tipo de injertos presenta algunas desventajas, tales como dolor, riesgo de infección, posible transmisión de enfermedades y

una disponibilidad limitada. Por este motivo, la investigación con injertos de hueso sintético es una de las principales propuestas en medicina regenerativa, la cual se basa en el desarrollo de nuevos biomateriales con el objetivo de aumentar la regeneración ósea y, más específicamente en el campo de la odontología, a la vez prevenir o eliminar la infección bacteriana.

La presente tesis está dividida en dos partes: i) tratamiento enfocado en el sistema dental y ii) tratamiento enfocado en el sistema óseo. En la primera parte se describe un biomaterial endodóntico diseñado para mejorar el sellado de la GP y la unión con el tejido dental; en la segunda parte se presentan dos estrategias para mejorar la regeneración ósea a nivel maxilar: la primera mediante el estudio *in vitro* de un láser de baja potencia para analizar su efecto osteogénico y de proliferación celular, y la segunda mediante la fabricación y optimización de un biomaterial con liberación de un fármaco para su potencial uso como injerto de hueso sintético.

Conference Participation

Giordano-Kelhoffer, B., Delgado, L.M., Bosch-Rué, E., Hoyos-Nogués, M. & Perez, R. A. Therapeutic microcarriers for bone tissue engineering in Dentistry. *Biomed PhDay Congress*. Barcelona, January 2019. (Oral Communication).

Patent

Perez, R. A., Giordano-Kelhoffer, B., Durán-Sindreu, F. & González Sánchez, J.A., inventors; Universitat Internacional de Catalunya, assignee. An isoprene-based matrix composition. (*Under submission*).

Thesis objectives

The aim of this thesis is the research of different strategies to enhance dental treatments in the field of endodontics and bone regeneration. It has been divided in three main objectives:

- **O1:** To design a bioactive endodontic material to enhance the sealing ability in teeth root canals.
- **O2:** To study the effect of low-level laser therapy in cell proliferation and osteogenesis on dental pulp mesenchymal stem cells.
- **O3:** To fabricate a bone graft biomaterial with sustained drug release to be used in bone regeneration treatments.

1. Fabrication of silica microspheres/Gutta-percha (SiMS-GP) composite

- a. To decrease the melting point of GP in order to increase its flow properties
- b. To fabricate and incorporate bioactive ceramic components into the GP composite
- c. To determine the effect of silica microspheres in the physico-chemical properties of the SiMS-GP composite
- d. To evaluate the *in vitro* response of mesenchymal stem cells on the SiMS-GP composites
- e. To analyze the sealing ability of SiMS-GP composite on simulated root canals and on extracted teeth

2. **Study the effect of cell proliferation and osteogenesis by low-level laser therapy**
 - a. To study different irradiation parameters to obtain the optimal mesenchymal stem cells proliferation rate
 - b. To determine the *in vitro* osteogenic response of mesenchymal stem cells after the irradiation by low-level laser therapy

3. **Fabrication of chitosan/hydroxyapatite/doxycycline bone graft composite**
 - a. To optimize the hydrogel/ceramic ratio to obtain an injectable bone graft composite with good handling and setting properties
 - b. To control the chemical parameters of the bone graft composite
 - c. To study the sustained drug release of doxycycline within the bone graft composite at different time points

Table of contents

Abbreviations

Introduction

1. Biomaterials in Dentistry: Past and present	3
2. Oral tissues	5
2.1 Tooth related	5
2.2 Bone related	8
3. Clinical problems	12
3.1 Tooth related	12
3.2 Bone related	14
4. Conservative clinical treatments	20
4.1 Tooth related	20
4.1.1 Endodontic treatment	20
4.2 Bone related	30
4.2.1 Adjuvant treatment	30
4.2.1.1 Low-level laser therapy	33
4.2.2 Bone substitutes	40
5. References	54
6. List of figures	64
7. List of tables	67
8. Graphical abstract	68

Chapter 1: A Bioactive Endodontic material for conservative treatments	69
1. Introduction	71
2. Objectives	73
3. Materials and methods	74
<i>Improvement of material's flowing ability</i>	74
3.1 Combining isomers to modify flowing properties	74
3.1.1 Synthesis and preparation	75
3.1.2 Samples characterization	75
3.1.2.1 Chemical analysis	75
3.1.2.2 Mechanical properties	76
<i>Improvement of material's bioactivity</i>	77
3.2 Designing a bioactive composite	77
3.2.1 Synthesis and preparation	77
3.2.2 Samples characterization	80
3.2.2.1 <i>In vitro</i> apatite forming ability	80
3.2.2.2 Cell proliferation assay	82
3.2.2.3 Sealing ability assay	85
3.3 Statistical analysis	87
4. Results and discussion	88
4.1 Isomers characterization	88
4.1.1 Chemical analysis	90
4.1.2 Mechanical properties	94
4.2 Composite characterization	97
4.2.1 Chemical analysis	98

4.2.2	Mechanical properties	101
4.2.3	<i>In vitro</i> apatite forming ability	105
4.2.4	Cell proliferation	109
4.2.5	Sealing ability	114
5.	Conclusions and Future perspectives	120
6.	References	122
7.	List of figures	129
8.	List of tables	131
	Chapter 2: Low-Level Laser Therapy for Bone Regeneration	133
1.	Introduction	135
2.	Objectives	137
3.	Materials and methods	137
3.1	Cell culture	137
3.2	Laser irradiation	138
3.3	Cell morphology	141
3.4	Cell proliferation assay	141
3.5	Cell osteogenic assay	142
3.6	Statistical analysis	143
4.	Results and discussion	143
4.1	Cell morphology	143
4.2	Cell proliferation	146
4.3	Cell osteogenic ability	150

5. Conclusions and Future perspectives	156
6. References	157
7. List of figures and tables	162
Chapter 3: Novel Chitosan-based Biomaterial for Bone Regeneration	164
1. Introduction	165
2. Objectives	168
3. Materials and methods	168
3.1 Chitosan fibers synthesis and characterization	168
3.2 Chitosan composite synthesis and characterization	170
3.3 <i>In vitro</i> doxycycline release study	173
3.4 Statistical analysis	174
4. Results and discussion	174
4.1 Chitosan fibers synthesis and characterization	174
4.2 Chitosan composite synthesis and characterization	184
4.3 <i>In vitro</i> doxycycline release study	195
5. Conclusions and Future perspectives	201
6. References	202
7. List of figures	208
8. List of tables	210
Chapter 4: Conclusions and Future perspectives	211
Supplementary data	217

Abbreviations

ADSCs: Adipose Stem Cells

ALP: Alkaline Phosphatase activity

AP-1: Activator Protein-1

ATP: Adenosine Triphosphate

BMPs: Bone Morphogenetic Proteins

BMSCs: Bone Marrow-derived

Mesenchymal Stem Cells

BSA: Bovine Serum Albumin

cAMP: cyclic Adenosine Mono
Phosphate

CCK-8: Cell Counting Kit-8

Co-Cr: Cobalt-Chromium

CPI: *Cis*-Polyisoprene

DMEM: Dulbecco's Modified Eagle
Medium

CS: Chitosan

CSCs: Cardiac Stem Cells

DEJ: Dentin Enamel Junction

DI: Deionized

DMEM: Dulbecco's Modified Eagle
Medium

DPMSCs: Dental Pulp Mesenchymal
Stem Cells

DX: Doxycycline

ECM: Extracellular Matrix

EDS: Energy Dispersive x-ray
Spectroscopy

EDTA: Ethylenediaminetetraacetic Acid

EGF: Epidermal Growth Factor

FBS: Fetal Bovine Serum

FTIR: Fourier Transformed Infrared
spectroscopy

GP: Gutta-Percha

HA: Hydroxyapatite

hDPMSCs: human Dental Pulp
Mesenchymal Stem Cells

HDPSCs: Human Dental Pulp Stem Cells

HGFs: Human Gingival Fibroblasts cells

ITS: Insulin Transferrin Selenium

hPDGF-BB: human Platelet Derived
Growth Factor BB

HSFs: Human Skin Fibroblasts

IKB: Nuclear factor of Kappa light
polypeptide gene enhancer in B-cells
inhibitor

LA-BSA: Linoleic Acid Bovine Serum
Albumin

LLLT: Low-Level Laser Therapy

MAPK/ERK: Mitogen-Activated Protein Kinase/Extracellular signal-regulated kinase

MSCs: Mesenchymal Stem Cells

MTA: Mineral Trioxide Aggregate

NDs-GP: Nanodiamonds-Gutta Percha

NF-KB: Nuclear Factor Kappa-light-chain-enhancer of activated B cells

NO: Nitric Oxide

PBS: Phosphate Buffer Saline

PCL: Polycaprolactone

PDLFs: Periodontal Ligament Fibroblasts

PGA: Polyglycolic Acid

PLA: Polylactic Acid

PLGA: Poly(lactic-co-glicolic Acid)

PMMA: Poly(methylmethacrylate)

PPF: Poly(propylene Fumarate)

PVA: Poly(vinyl Alcohol)

RCF: Root Canal Filling

rMSCs: rat Mesenchymal Stem Cells

ROS: Reactive Oxygen Species

SBF: Simulated Body fluid

SEM: Scanning Electron Microscopy

SF: Silk Fibroin

SiMS: Silica Microspheres

TCP: Tricalcium Phosphate

TEOS: Tetraethyl Orthosilicate

PBS: Phosphate Buffered Saline

PI: Polyisoprene

TPI: *Trans*-Polyisoprene

Introduction

1. Biomaterials in Dentistry: Past and present

Egyptians, Etruscan and Mayan civilizations from 2.500 BC to 600 AD were the first to use dental biomaterials as we know them today. They used nacre teeth from sea shells, ivory and bones and implanted them into maxillary bone obtaining what we nowadays refer to as osseointegration (*Figure 1*). There was no material science, biological understanding or modern medicine at that time. Nevertheless, their success and longevity are remarkable and highlight two aspects: the resilient nature of the human body, and the constant need, even in prehistoric times, to replace the loss of physiological/anatomical function with a biomaterial ^{1,2}. In the 1920s, Reiner Erdle and Charles Prange joined their knowledge of dentist doctor and metallurgy respectively, to develop the alloy Vitallium. This material was the first metallic biomaterial with acceptable mechanical properties, biocompatibility and corrosion resistance for the application on surgical prostheses ³. That fact shows the constant demand of synergies between different specialties to achieve the same goal. Since then, with the aid of technology and material science development, modern dentistry has evolved rapidly. In 1928, the first dental material consensus was organized in the USA, which had a worldwide repercussion. After that, the physical and chemical characteristics of the materials used were investigated and also the different testing methods. In 1955, a chemist and dentist named Michael Buonocore discovered a method to change the roughness of the dental structure at a microscopic level by an acid agent to enhance the retention of a resin material. His research has focused in a sealing agent that could be mechanically adhered in the occlusal faces of the molars preventing children caries development. This discovery is considered the start of the adhesive dentistry era ⁴. Another revolutionary change in the modern history of dental materials was accomplished in 1982. The orthopedic surgeon Per-Ingvar Brånemark highlighted the importance of the biological aspects of body's natural

cicatrizacion after the introduction of a strange body into the bone. After years of research, he was able to demonstrate the titanium dental implants osseointegration ⁵. Even though the excellent progress in the implantology field, the recent development in endodontic materials has changed the mentality from using bioinert materials to the bioactive ones. This dental field is highly important because its main goal is to preserve the teeth that in the past centuries had to be extracted. In 1995, Mahmoud Torabinejad *et al.* patented the biomaterial Mineral Trioxide Aggregate (MTA). Its composition is based on calcium silicate and it has been demonstrated that promotes the apatite deposition on its surface, making it a bioactive material ⁶. A definition of biomaterial endorsed by a consensus of experts in the field is “*A material used in a medical device, intended to interact with biological systems*” ¹. As far as we know, natural and synthetic biomaterials have drawn attention in the past and nowadays in the medical field. Recently, the research in biomaterials is focused on its chemical modification, drug delivery systems and bioactivity, especially for being used in the dentistry field, which we will focus in this thesis.



Figure 1. This Mayan lower jaw found in Honduras is dated from 600 A.D. It shows three implanted incisors made of carved seashells. Calculus formation on these three implants indicates that they were not made solely for a burial display but served as fixed, functional and esthetic tooth replacements (*Image from the Peabody Museum of Archaeology and Ethnology, Harvard University, Cambridge, Mass.*).

2. Oral tissues

Teeth are closely related to the maxillary bone. However, in this chapter, they will be separately described in order to better focus individually in both structures and clinical problems.

2.1 Tooth related

2.1.1 Structure and composition

Teeth are very important organs in our body. They help us with the feeding and with the phonation processes and give us esthetics. Because of their relevance, dentistry is becoming nowadays a more conservative field. Dentists are trying every day to repair teeth of their patients in order to maintain them, instead of extracting them, with a common goal which is enhancing the patient's health.

Tooth can be divided into two parts: **crown** and **root**. The crown is the visible part which is covered by the enamel, whereas the root is covered by the cementum and is the non-visible part, because it is inserted into the maxillary bone (*Figure 2*).



Figure 2. Tooth anatomy. The crown contains the enamel, the dentin and the pulp cavity. The root contains the nerve, blood vessels and dentin inside the root canals, the periodontal ligament and the cement. The root is surrounded by the maxillary bone ⁷.

The more external part of the crown is the **enamel, which** is composed of ~96% calcium apatite, either as hydroxyapatite (HA) ($\text{Ca}_{10}(\text{PO}_4)_6(\text{OH})_2$) or fluorapatite ($\text{Ca}_{10}(\text{PO}_4)_6\text{F}_2$). This high mineral content and its hierarchical organization may explain that teeth are the strongest biological materials in the body. Enamel part is highly mineralized with organized HA crystallites. The microstructure of enamel has aligned prisms aligned perpendicular from the dentin-enamel-junction (DEJ) towards the tooth surface. Each prism consists of packed carbonated hydroxyapatite crystals covered by a nanometer-thin layer of enamelin and disposed along the prism axis. In the other hand, **dentin** is a hard bone-like tissue that is present in the crown (covered by enamel) as well as in the root of teeth (covered by cementum). It is the supporting structure of the tooth and is composed of ~68% HA mineralized collagenous matrix surrounding tubular extensions of the dentinoblast cells ⁷. Dentin formation, dentinogenesis, is accomplished by cells called odontoblasts. Because of these odontoblastic cell processes, dentin is considered a living tissue, with the capability of reacting to

physiologic and pathologic stimuli. Odontoblasts are considered part of pulp and dentin tissues because their cell bodies are in the pulp cavity, but their long cytoplasmic cell processes (Tome fibers) extend well (100-200 μm) into the tubules in the mineralized dentin ^{7,8}.

The **pulp tissue** is inside the pulp cavity of the teeth, which is not exposed to the microflora and subsequently remains usually sterile. Pulp is an unmineralized tissue composed of soft connective tissue, vascular, lymphatic and nervous element that occupies the central pulp cavity of each tooth. Pulp has a soft, gelatinous consistency. The majority of pulp composition is water (75-80%). It extends down through the root of the tooth as the root canal which opens into the periodontium (bone tissue and periodontal ligament) via the apical foramen (*Figure 2*). The blood vessels and nerves of dental pulp enter and leave the tooth through this foramen. This sets up a communication between the pulp and surrounding tissue – clinically important in the spread of inflammation from the pulp out into the surrounding periodontium. Pulp and dentin act as a unit (pulp-dentin complex). Pulp is responsible for dentin formation, whereas enamel and dentin tissues protect the pulp tissue from physical and microbial attacks. Root canal system, which contains the pulp tissue inside, is composed of one or more main canals (depending on the tooth). This root canal is a channel inside the root that extends from the pulp chamber to the apical foramen. The root canal system is also composed by other smaller canals that branch out from the main canal and usually communicates with the external surface of the root (lateral, accessory, furcation canal). Finally, the apical delta is the region near the apical foramen where the main root canal is divided into more than two accessory canals ⁹ (*Figure 3*).

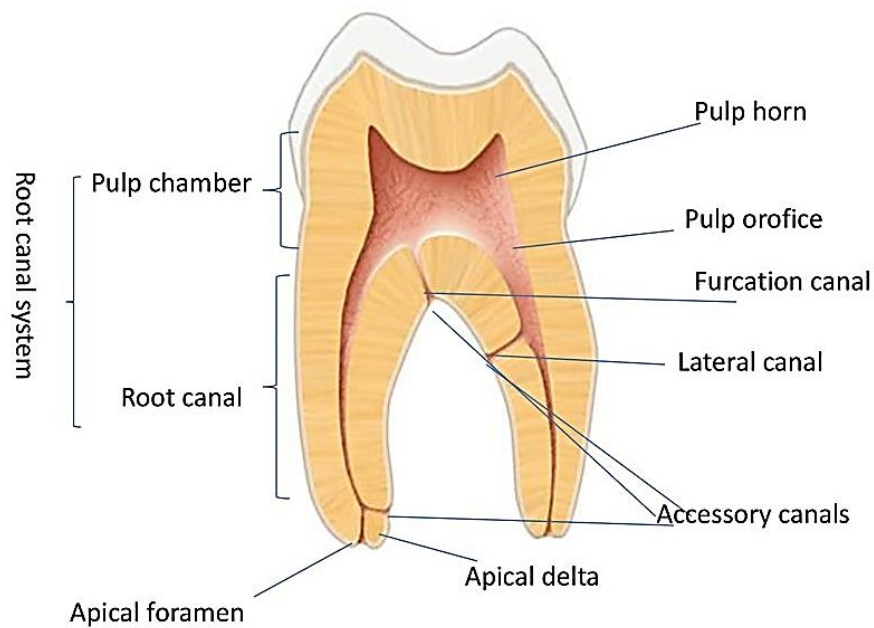


Figure 3. Root canal system that englobes the pulp chamber and the root canal parts. The root canal may have accessory canals (furcation canal, lateral canal) that communicate with the external surface of the root. The apical delta is the region near to the apex (which is the final part of the root), and the main root canal is divided in two or more accessory canals ⁹.

2.2 Bone related

2.2.1 Structure and composition

Bone is a specialized form of connective tissue, with a calcified extracellular matrix, and is the main element of the skeletal tissues. We will focus on the description of the maxillary bone, which englobes both upper and lower jaw. The maxillary bone performs an essential structural and protective function. Important nerves and muscles pass through this bone and emerge from it. Moreover, it is the support of the teeth, being involved in mastication, protection, and in blood cell formation. Alveolar bone properties are similar to bones of other sites of the body. It is formed both by organic and inorganic components which mostly determine its properties, and by three types of cells:

osteoblasts, osteoclasts and osteocytes. The alveolar process is composed of an outer and inner cortical plate of compact bone that encloses the spongiosa, a compartment composed of spongy bone (also called trabecular or cancellous bone). The alveolar bone proper lines the alveolus (or tooth housing) which is contained within the alveolar process. It is composed of a thin plate of cortical bone with numerous perforations (or cribriform plate) that allows the passage of blood vessels between the bone marrow spaces and the periodontal ligament (*Figure 4A*). When teeth are extracted, most of the alveolar process is affected, leaving basal bone as the major constituent of the jawbone. The remaining maxillary bone, therefore, is much reduced in height ¹⁰. Bone contains a relatively small number of cells entrenched in a matrix of collagen fibers that provide a surface of inorganic salt crystals to adhere. These salt crystals form when calcium phosphate and calcium carbonate combine to create hydroxyapatite, which incorporates other inorganic salts like magnesium hydroxide, fluoride, and sulfate as it crystallizes, or calcifies, on the collagen fibers. The hydroxyapatite crystals give bones their hardness and strength, while the collagen fibers give them flexibility so that they are not brittle (*Figure 4B*).

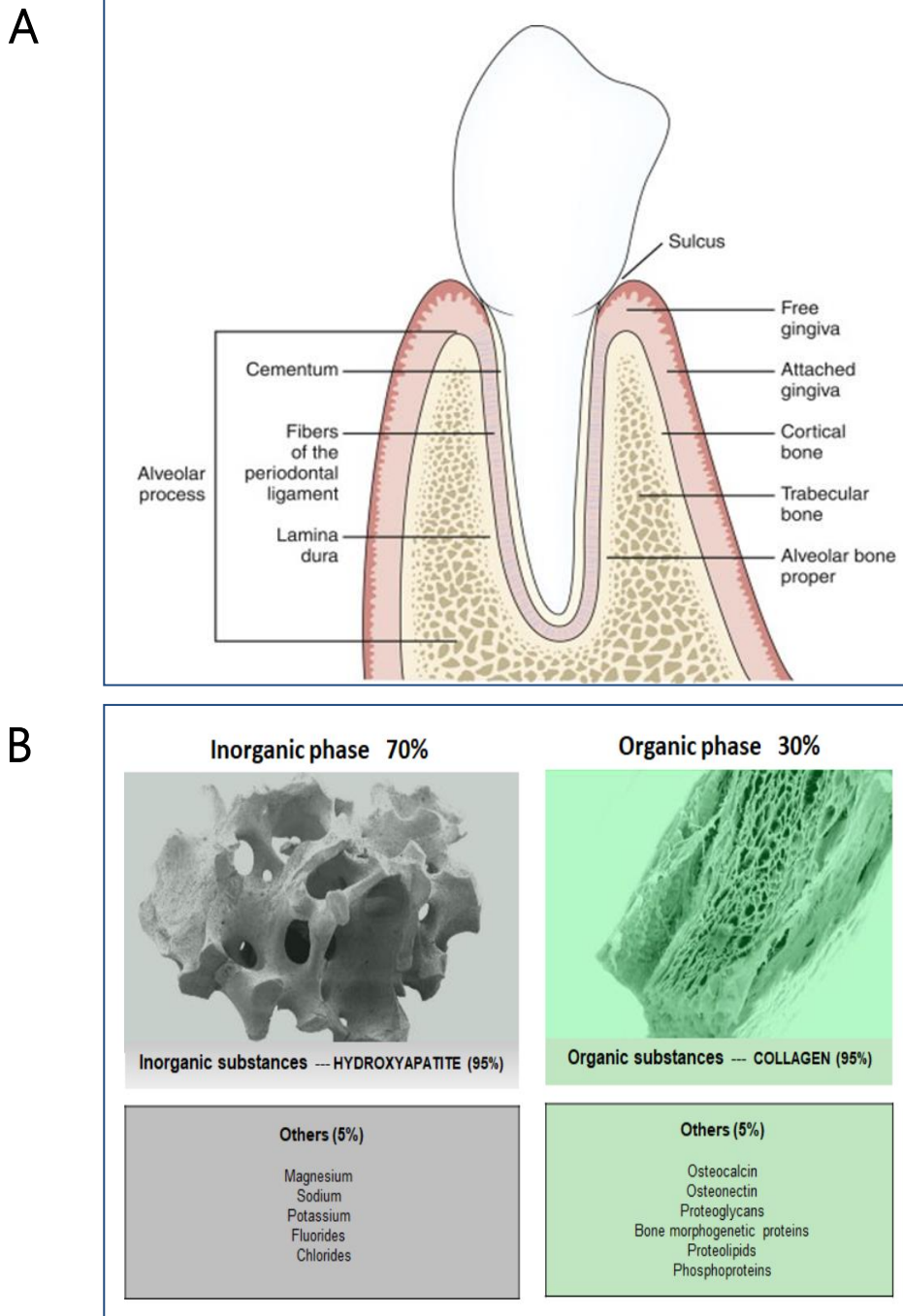


Figure 4. (A) Tooth alveolar process showing the different parts of maxillary bone: cortical, trabecular and alveolar bone. **(B)** Chemical composition of the bone. Bone tissue has an inorganic phase (70%) mostly composed of hydroxyapatite (95%) and an organic phase (30%) mostly composed of collagen (95%)¹⁰. Modified from¹¹.

Despite its solid appearance, maxillary bone is in a constant state of **remodeling**. This means that at all time some parts of the bone are being resorbed, while other parts are growing by apposition of new bone. This process requires coordination between resorption and opposition so that the normal function of the bone can be maintained. Osteoclasts are the cells involved in the bone matrix resorption and remodeling, which are derived from the mononuclear blood cells. In this process, osteoclasts form bone lacunae named Howship's lacunae. Once the resorption process is finished, these lacunae are filled by osteoblast cells of mesenchymal origin, which are in charge of bone neoformation. Different proteins like cytokines and growth factors play important roles in bone remodeling ^{12,13}. Remodeling of the alveolar process allows the normal migration of teeth in a mesial direction, or mesial drift, as their interproximal surfaces wear down. It also allows processes such as orthodontic tooth movement and wound healing (*Figure 5*).

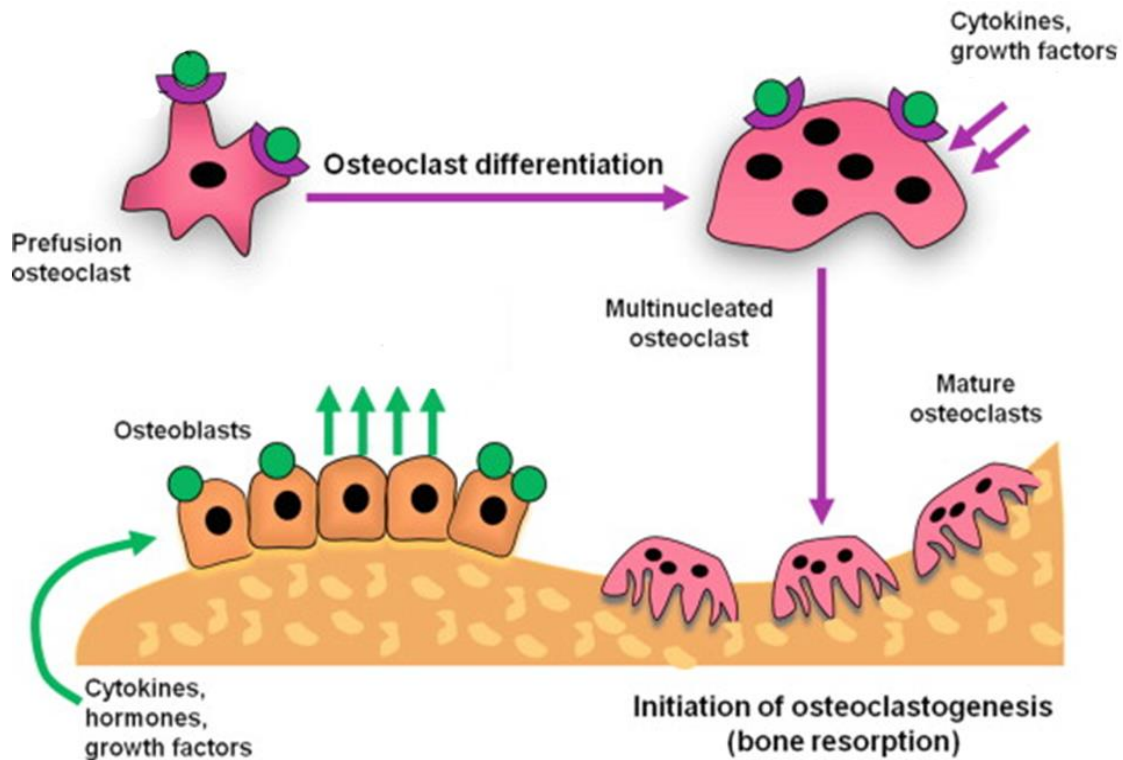


Figure 5. Illustration showing the coordination of different cells and molecules involved in osteoclastogenesis. After osteoclast precursors proliferation they merge in multicellular structures, and differentiate into matured osteoclasts. Both osteoclasts and osteoblasts proliferation is regulated by different cytokines, hormones and growth factors. Modified from ¹³.

3. Clinical problems

3.1 Tooth related

Among the different parts of the tooth, the one that has higher probability to suffer irreversible damage is the dental pulp. Dental pulp affectation can develop from different origins like caries infection, trauma, congenital etiology, among others. We will focus on the caries infection and trauma origin, being both the most common causes of dental pulp affectation causing severe pain to the patient. If these problems are not solved in time, the infection will involve the maxillary bone that surrounds the tooth, affecting the tooth survival which will cause several functional and esthetic problems to the patient.

3.1.1 Caries

Caries, or tooth decay, is the most prevalent chronic disease in humans across the globe ¹⁴. It is caused by acidogenic bacteria fermenting carbohydrates to produce acids, which leads to mineral loss with a degradation of the hard tissues of the teeth (enamel, dentin and cementum) ¹⁵. Symptoms may include pain and difficulty to eat. Complications may add inflammation of tooth surrounded tissue, tooth loss, and infection or abscess formation. If not treated in time, it can develop to a tooth nerve inflammation or infection (necrosis). (*Figure 6*).

3.1.2 Traumatism

Traumatism is one of the main causes of dental pulp affectation. It is characterized by the death of cells and tissues inside the pulp chamber of a tooth, with or without bacterial invasion. When cement around the root is lost and the dentin is exposed, dentin tubules may be a way for bacteria to enter the pulp. The most common clinical signs present in a tooth with necrotic pulp would be a grey discoloration of the crown and/or periapical radiolucency in radiographic exploration. The altered translucency in the tooth is due to disruption and cutting off of the apical neurovascular blood supply (*Figure 6*).

THE STAGES OF CARIES DEVELOPMENT



Figure 6. Caries or tooth decay process. From enamel degradation to pulp involvement ¹⁵.

3.2 Bone related

Maxillary bone defects can develop from different causes like infection, tumor, trauma, surgery, congenital etiology, among others ¹⁶. We will focus on the infection origin being one of the most common causes. As in tooth related clinical problems, if bone problems are not solved in time, they will cause functional and esthetic problems to the patient. As explained in *section 3.1*, the bone that supports the tooth will be reabsorbed because of the infection, compromising the tooth survival. Moreover, if the tooth is lost and we want to replace it with a dental implant, there may not be enough bone to support and osseointegrate it, compromising the dental implant survival.

3.2.1 Periodontal disease

Periodontal disease is a prevalent chronic pathology characterized by an inflammatory destruction of the tooth supporting tissues (periodontium), like gingiva, periodontal ligament and alveolar bone. This pathology is one of the main causes of tooth loss in adults. Although its main etiological agents are bacteria that colonize subgingival tooth surfaces, it is the host inflammatory response to this microbial attack that first damages the periodontium, which may occur through an up-regulation of pro-inflammatory mediators or as a result of particular defects in the host response to the infection, leading extracellular matrix catabolism and bone resorption in periodontitis ^{17,18,19,20} (Figure 7).

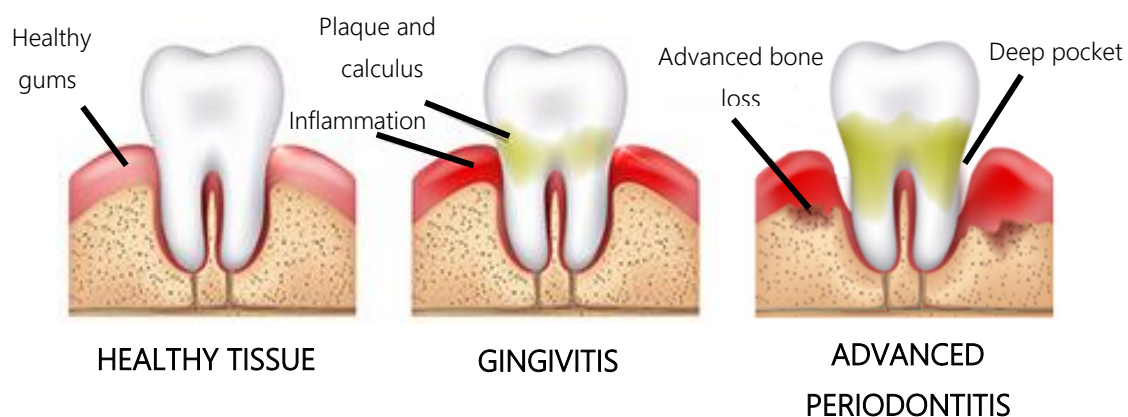


Figure 7. Tooth with healthy periodontal tissue, gingivitis and with advanced periodontitis. Accumulation of plaque and calculus triggers the inflammation of supporting tissues. When there is advanced periodontitis, maxillary bone loss occurs and the tooth stability is in danger ²⁰.

3.2.2 Periapical lesions

Periapical pathology or apical periodontitis is a general term used to englobe the periapical inflammatory process that affects the maxillary bone tissue. This pathology appears in response to the presence of polymicrobial infection and other irritants within the root canal system of a tooth. There are different conditions that can mimic periapical lesions, such as a progression of pulpitis, periodontal disease, occlusal trauma, an accident that has damaged the periodontal ligament and various tumors or cysts ²¹. It can also be a lesion related with a root-filled tooth, because of the presence of resistant bacteria previously or after the moment of the root canal treatment that have reproduced. As explained in *section 2.1*, there is an intimate relationship between the periodontium and pulpal tissues through 3 main avenues which are: apical foramen, lateral and accessory canals and dentinal tubules. These are the pathways through which bacteria arrives to the maxillary bone leading to the bone resorption (*Figure 8*).

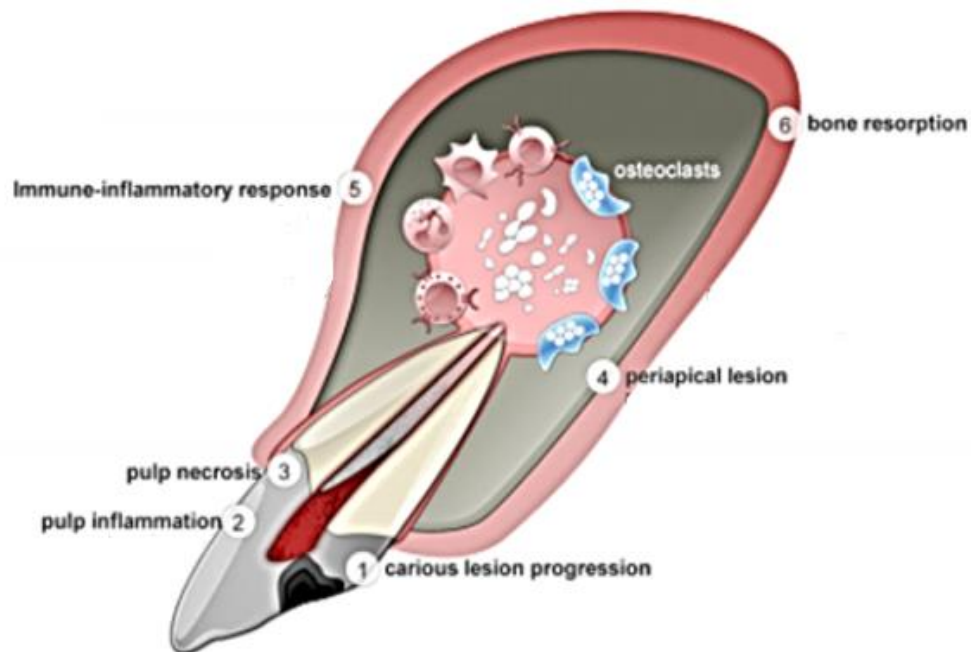


Figure 8. Schematic figure of pulp and periapical pathology evolution. 1. Progress of carious lesion with rupture of enamel and dentin barriers. 2. Pulp inflammation, the first line of pulp defense with the migration of innate immune response cells. 3. Pulp necrosis, to which pulp inflammation evolves. 4. Periapical lesion, in which pulp necrosis makes the immune response migrate to the periapical area. The bone resorption starts. 5. Immune-inflammatory response in periapical area with innate and adaptive cells and products. 6. Bone resorption, started and maintained by osteoclasts and molecules involved, like cytokines among others. Modified from ²².

3.2.3 Bone resorption after tooth loss

When conservative treatments such as endodontic and periodontal treatments fail, or when the infection process is such in an advanced stage that there is an uncertain prognostic, tooth extraction is the last treatment option in order to prevent future major complications (*Figure 9*). When a tooth is extracted from its alveoli, the healing process leads to vertical and horizontal alveolar crest resorption that can make difficult a dental implant installation in a prosthetically suitable position, affecting the functional and esthetic outcomes negatively ²³. This fact explains that alveolar bone is tooth-dependent. The most volumetric

alterations of alveolar bone occur in the first three months after tooth extraction and result in a 50% reduction in the buccolingual dimension of the alveolar crest during 1 year after tooth extraction ^{13,24}. In the cases with an active bone infection, there will be a higher bone loss, first because of the infection process, and secondly, due to tooth extraction. In most cases, the next procedure will be to replace this lost tooth by a dental implant. However, in a stage with bone infection, the dental implant will not be able to osseointegrate to the alveolar bone and it will fail. *Figure 10* illustrates the abstract of this section: clinical problems.



Figure 9. Tooth extraction steps. The maxillary bone will start the resorption process after this procedure.

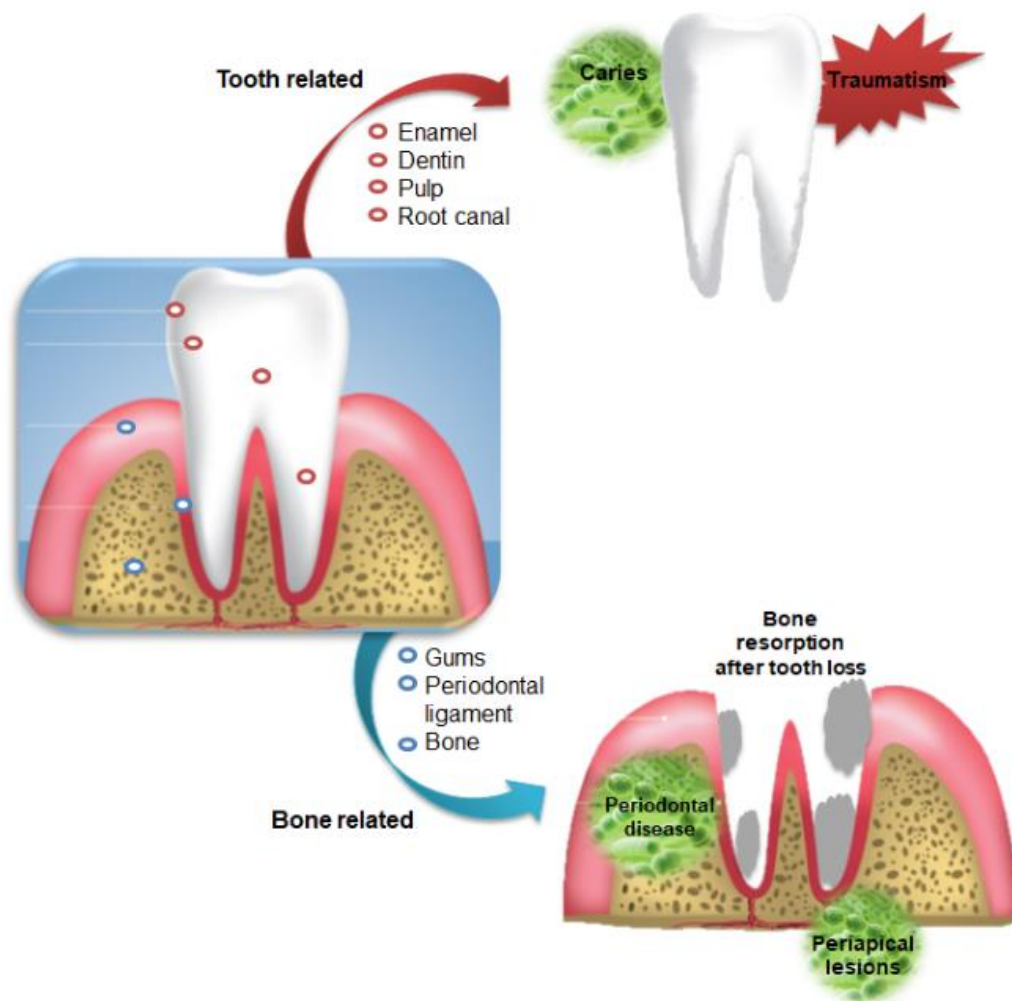


Figure 10. Schematic representation of the tooth related and the bone related parts and their clinical problems. In the tooth related parts we have considered the enamel, dentin, pulp and root canals. Their most common clinical problems are caries and traumatism, which will cause an inflammation/infection of the pulp tissue; regarding the bone related parts we have focused on the gums, periodontal ligament and bone. Their most common clinical problems are periodontal disease and periapical lesions which are both caused by bacterial infections, and the bone resorption after a tooth loss, which may course with or without an infection process.

4. Conservative clinical treatments

4.1 Tooth related

4.1.1 Endodontic treatment

Nowadays, the most common solution to maintain the teeth of patients that have suffered from profound caries or traumatism and have ended with root canal infection is to perform an endodontic treatment. Endodontics has been a specialist since 1867²⁵. Since then, this field has suffered an optimal development in terms of techniques and materials used. These advancements have enhanced the tooth prognosis in the past years. Moreover, they have also changed dentist's and patient's preferences to retain and preserve natural teeth instead of tooth extraction²⁶. *Figure 11A* shows the schematic representation of tooth-related problems and its clinical treatment. The main goal of endodontics is to remove the infected pulp tissue from inside the root canals, to chemically disinfect and mechanically prepare the root canal system in order to seal it hermetically and three dimensionally with a solid core root filling material and a fluid sealer as a shell material to help improve sealing outcomes. The final objective is to prevent bacterial contamination and promote healing of the periradicular bone lesion to maintain the natural tooth function (*Figure 11B*)^{27,28,29,30}. The ideal properties of a root canal filling (RCF) material are presented in *Table 1*.

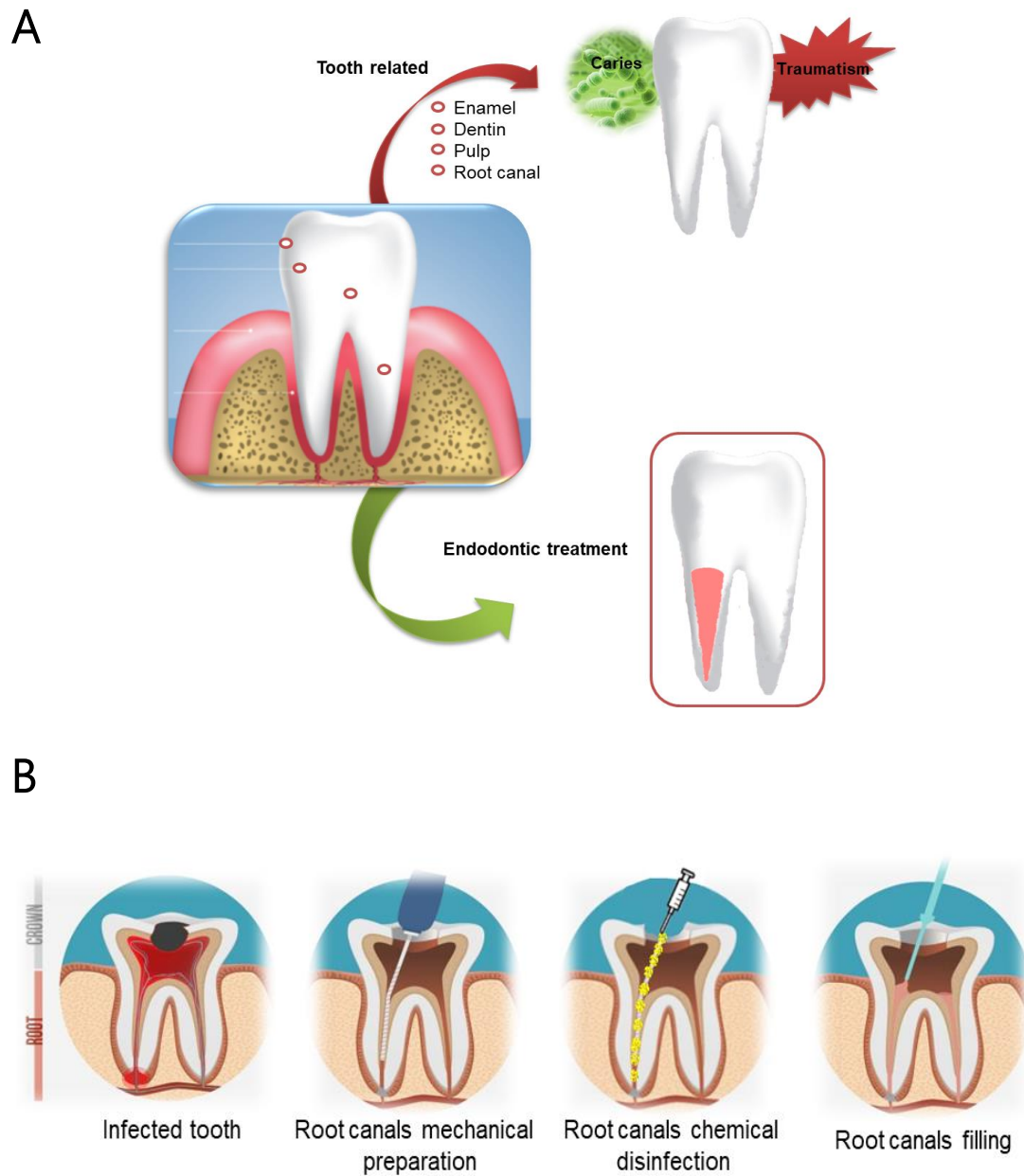


Figure 11. (A) Schematic representation of the tooth related clinical problems and the clinical treatment in which we will focus: the endodontic treatment. It has been represented with the core material used in this treatment. **(B)** Endodontic treatment of a tooth with an infected pulp tissue. This treatment is based 3 main steps: 1. Mechanical preparation and instrumentation by endodontic files in order to extract the pulp tissue and to widen the root canals. 2. The chemical disinfection with sodium hypochlorite solution in order to clean and eliminate the rests of dentin debris and pulp tissue inside the canals and 3. Root canals filling by a core material and a shell material in order to prevent a bacteria reinfection ³¹.

Ideal properties of root canal filling materials
✓ Easily to introduce into the root canal
✓ Seal the canal laterally as well as apically
✓ Not shrink after being inserted
✓ Impervious to moisture
✓ Radiopaque
✓ Prevent tooth staining
✓ Not irritate periapical tissue
✓ Be sterile, or quickly and easily sterilized before insertion
✓ Good flow properties
✓ Excellent mineralization to facilitate sealing the apical part of the root canal and to promote the integration of the material with periapical tissues
✓ Broad-spectrum antibacterial property to inhibit the growth of bacteria

Table 1. Ideal properties of a RCF material which are not fully accomplished by the materials that are used nowadays^{32,33}.

4.1.1.1 Conventional materials

Gutta-percha (GP) has been the material of choice as a solid core root canal filling for more than 150 years. Gutta-percha is a name derived from two words: "getah" meaning sap, and "pertja" meaning tree in Malay language. It is derived from the sap of trees from the Malasyan archipelago, particularly the *Palaquium* gender. The gum extracted is rubberlike, translucent, solid and flexible. This

material is then chemically processed to obtain a polymer, which will be one of the main components of the GP material as known by the clinicians. Contemporary GP-based root filling materials are composed by 20% GP polymer (matrix), 66% zinc oxide (filler), 11% heavy metal sulfates (radiopacifier), and 3% waxes and/or resins (plasticizer)^{31,34,35,36}. The percentages of components may differ depending on the manufacturer³⁷. Once the GP composite is obtained, it is molded in a cone shape to be used as a RCF material (*Figure 12*). GP has been a good material for this purpose because it is biocompatible, inert, easy to introduce into the root canal space and cost efficiency^{29,38,39}. Although with the advanced new filling techniques and materials used in the past decades, there are still high failure rates in endodontic treatments around 18-26%^{40,41}. One of the most important reasons is due to an inadequate root canal filling procedure. This fact may allow microleakage because of the lack of adhesiveness of GP to root canal dentin, being one of the most relevant drawbacks of this material. Moreover, GP does not have ideal mechanical properties to support tooth mechanical forces³⁸.

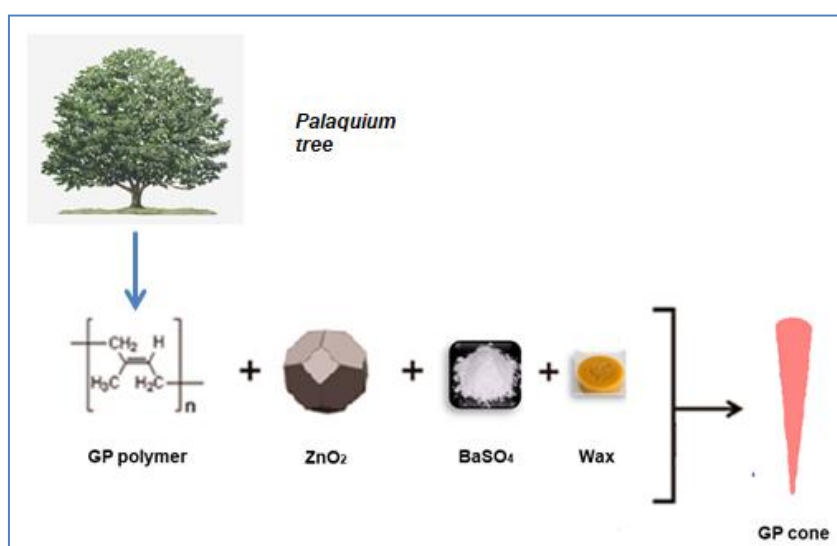


Figure 12. GP polymer is obtained from the sap of the trees of the *Palaquium* gender. Then it is mixed with zinc oxide, barium sulfate and wax and molded into a cone shape to better introduce it in the root canal space⁴⁰.

Moreover, its degradation may occur with some conditions as chemical and biological factors by a slow oxidative process ^{36,42}. *Table 2* summarizes the advantages and the drawbacks of GP-based materials. Because of GP adhesiveness limitation, a sealer material has to be used in combination to get a tight seal, filling the space between the GP and the root canal dentin. Sealers may also penetrate lateral and accessory canals. Different types of sealers have been introduced in the past years, including several components based: zinc oxide eugenol and non-eugenol, glass ionomer, calcium hydroxide, epoxy-resin and methacrylate-resin, silicone, medicated sealers, and the more recently introduced bioceramic and nanoparticles-based sealer materials ^{25,43,44,45,46,47,48}. The sealers penetration into dentinal tubules has often been used for demonstrating the enhancement of sealability to root canals. Nevertheless, studies have shown the lack of correlation between sealer insertion into dentinal tubules and sealability in non-bonded ⁴⁹ or resin-bonded ⁵⁰ root fillings. The same conclusion has been obtained with sealer penetration in apical ramifications ⁵¹ or lateral canals, which resulted in tissue damage and inflammation ^{52,53,54}. Moreover, sealers dissolve in tissue fluid with time and shrink during setting, leaving voids between dentin and GP material which can be colonized by bacteria, compromising the outcome of the endodontic treatment ^{33,42}. To address these challenges, many studies have performed research to revise GP-based materials and some modifications have been made on them in order to better accomplish the filling ability objective.

GUTTA-PERCHA	
ADVANTAGES	DRAWBACKS
✓ Biocompatible	- No chemical bonding ability to dentin tissue
✓ Inert	- Not optimal mechanical properties
✓ Easy to introduce into the root canals	
✓ Cost efficiency	

Table 2. Advantages and drawbacks of GP material ^{38,40}.

4.1.1.2 New generation of endodontic biomaterials

As explained in the previous section, different RCF materials have been introduced in the past years in order to enhance endodontic treatments by improving its bonding ability to dentin tissue. There have been many innovations both in the core and in the shell materials (sealers). This section is focused on the core material development, being the main material that fills the root canal space. We have divided them into GP-based and non GP-based RCF materials (*Table 3*).

GP-BASED	Coated GP	Composite GP	Surface treatment-GP
<p>NON GP-BASED</p>	<ul style="list-style-type: none"> - Iodoform+Tetracycline⁵⁵ - Zinc oxide^{56,57} - Antibiotic^{58,59} 	<ul style="list-style-type: none"> - Glass ionomer (Activ GP®)^{60,61} - Resin (EndoREZ®)^{76,77} - Calcium phosphate⁶⁵ - Bioceramic (TotalFill BC®)^{66,67} - Nanoparticles^{33,39} 	<ul style="list-style-type: none"> - Non-thermal plasma⁶⁸ - Argon plasma²⁸
	<ul style="list-style-type: none"> - Polycaprolactone (Resilon®)^{80,81} 	<ul style="list-style-type: none"> - Niobium phosphate glass composite^{78,79} 	

Table 3. GP-based and non GP-based root canal fillings developed in the last 20 years.

In the first group, GP have been modified in three different manners: by coating its surface with iodoform, zinc oxide or antibiotic components in order to enhance its antibacterial effect ^{55,56,57,58,59}; by manufacturing a composite to improve its sealing ability by adding glass ionomer ^{60,61,62}, resins ^{63,64}, calcium phosphate ⁶⁵ or bioceramics ^{25,66,67} (*Figure 13A*) or to enhance GP antibacterial capacity by adding nanoparticles (*Figure 13B*) ^{33,39}; finally, by modifying GP surface by non-thermal or argon plasma treatments in order to obtain an antibacterial or a higher sealing ability effect (*Figure 13C*) ^{28,68}. Regarding to the bioceramics group, niobium phosphate glass experimental composite and Bio-Gutta[®], which is composed by bioactive glass particles, are the two only RCF materials presented with the advantage of been able to be used without any sealer, simplifying the root canal filling technique step (*Figure 13A*) ⁶⁹. Following this classification, the second group is the non GP-based material. As much as we know, Resilon (RealSeal[®]) is the only material in this group that has been presented as an alternative to GP. Resilon has appeared in 2004 as a new thermoplastic synthetic polycaprolactone-based material that is combined with a self-etching sealer named Epiphany. It also contains methacrylate resin and bioactive glass particles ^{70,71,72}. This material is claimed because of the advantage of bonding to the canal wall and to the core material by the sealer, creating a monoblock in the canal (*Figure 13D*) ⁷³. Resilon good handling properties are similar to those of GP ^{74,75}. Nevertheless, it has a higher cost and its bonding ability have been questioned because of the low adhesion of its methacrylate resin sealer to the core material ³⁶.

Theoretically, an optimal bonding between a RCF material and the root canal dentin is supposed to not present voids or gaps within both structures. A chemical bonding between them may be explained as a reaction of the dentinal fluids with calcium phosphate ions present in the dentin and periradicular bone hydroxyapatite and the material composition (based on calcium or silicate phosphate components), in order to induce an interfacial layer of apatite

formation reaction ^{36,64}. This intracanal bioactive process may contribute to a strongest and more predictable sealing ability (*Figure 14*). Recently, *Lee et al.* fabricated a modified GP with the incorporation of nanodiamonds platforms that were able to absorb amoxicillin on its surface and considered it as a novel GP with antibacterial capacity (*Figure 13B*). The study has performed a contact-mediated inhibition method upon bacterial deposition onto the material surface. The authors claimed this material as an improvement of the mechanical properties of GP, which may lead to an enhancement of the handling properties during clinical procedures. They have studied its sealing ability on extracted tooth by radiographic images showing good results ³⁹. Nevertheless, we believe that the presence of strong solvents such as chloroform could damage the surface adsorbed amoxicillin and hence reduce its efficiency. Furthermore, we believe that the amount of nanodiamonds placed in the matrix could be low to have a significant effect on GP mechanical properties. Moreover, this research only focuses on the antibacterial improvement of the GP and does not take into account the enhancement of the GP sealing ability in order to prevent future microleakage and bacterial reinfection.

Modifications of GP may focus on having better flow properties and being bioactive to enhance dentin adhesion ability, meanwhile simplifying the RCF technique needing only a core material and not a sealer. To address these challenges, we propose a novel bioactive GP RCF material.

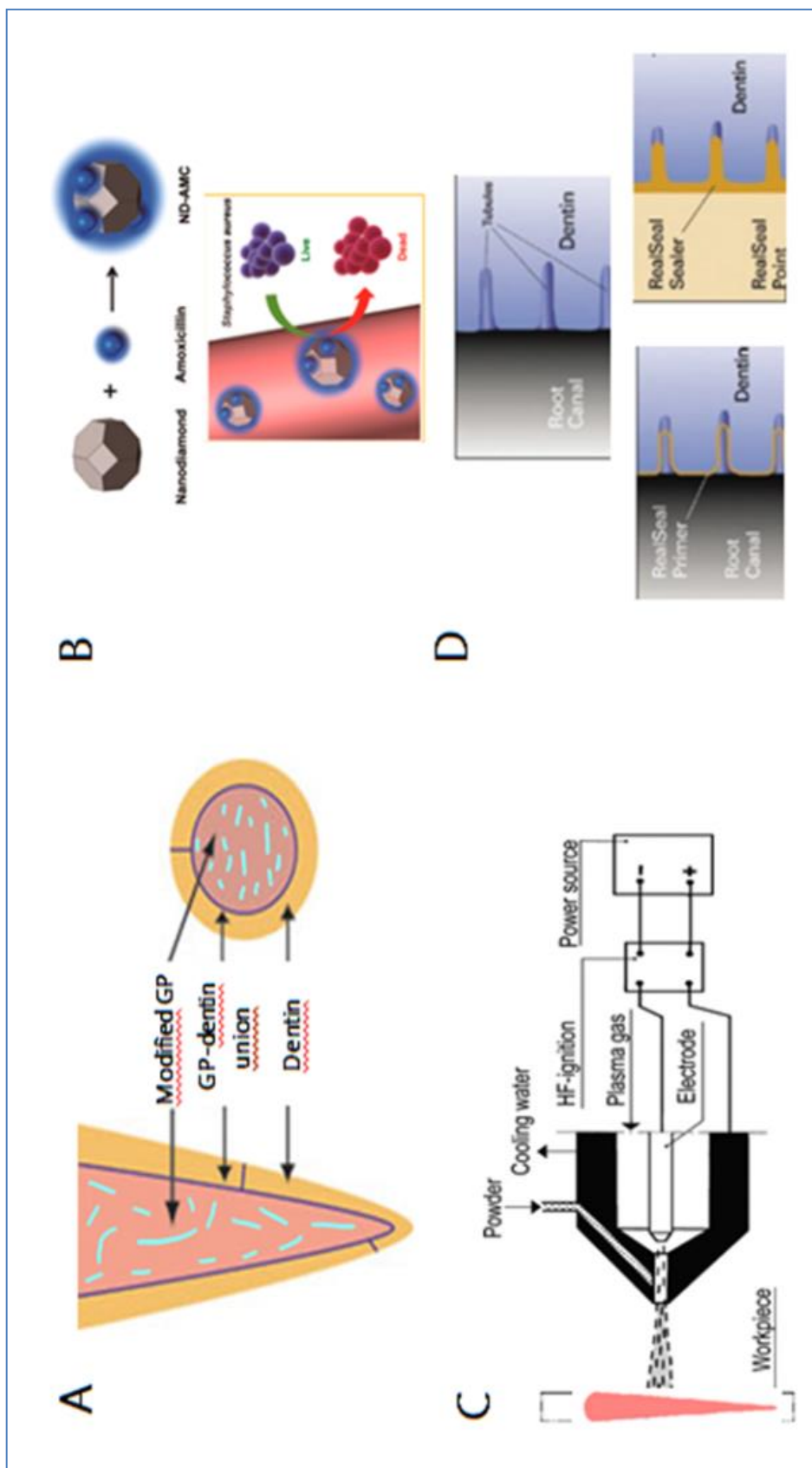


Figure 13. Different strategies of RCF materials to use in endodontic treatments. **(A).** GP-coated with bioactive-glass ²⁵ **(B).** Nanoparticles incorporation into GP ³⁹ **(C).** GP surface treatment modification ⁶⁸ **(D)** Adhesion to dentin technique ⁴⁶ .

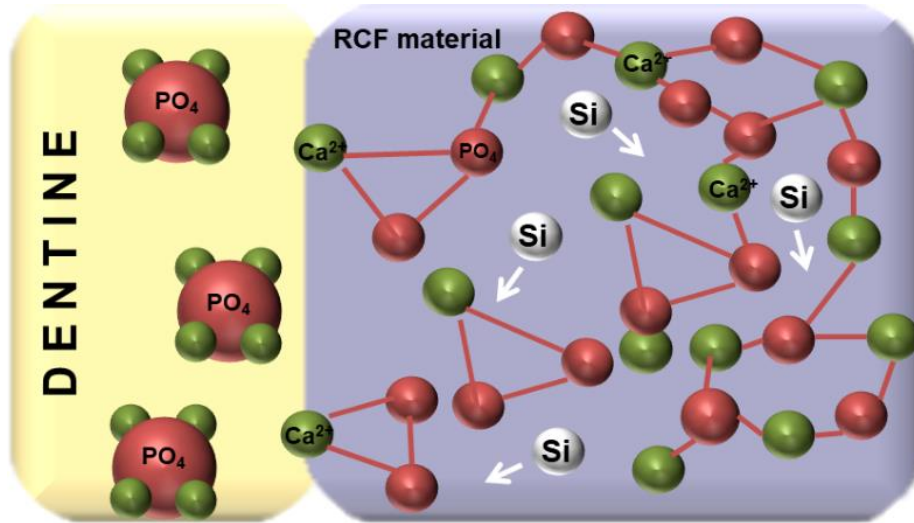


Figure 14. Illustration of the chemical bonding process between dentin tissue and Root Canal Filling (RCF) material. Calcium phosphate ions of dentin may interact with calcium or silicate phosphate components of the RCF material ³⁶.

4.2 Bone related

4.2.1 Adjuvant treatments

As explained in *section 3.2*, we have focused in 3 different situations regarding bone related clinical problems. The first one is the periodontal disease. There are several cases in which conventional treatments such as systemic antibiotic therapy and mechanical treatment (e.g. curettes, ultrasonic systems) are not enough to control advanced periodontitis ⁸². This fact has evoked an interest in the development of innovative therapies to use as adjuvant treatments in order to enhance bone regeneration (*Figure 15A*). In this sense, adjuvant treatments would also be very useful in endodontic microsurgeries, to improve the healing and the regeneration of bone defects produced by periapical lesions (*Figure 15B*). Unfortunately, when tooth or bone related infections have not been treated

in time, or when endodontic or periodontal treatments fail, tooth extraction must be done. After this invasive procedure, the tooth socket will heal through a secondary healing process. First, a blood clot will develop in the alveolar socket. The clot will turn into a fibrin mesh which will facilitate the formation of granulation tissue. Epithelium lined granulation tissue will grow from the bottom of the socket up towards the sides of the socket. A tooth extraction may be complicated by the formation of a haematoma in the surrounding soft tissues, pain of varying degree which starts 2-3 hours after extraction, as the effect of local anesthesia wears off. Surrounding tissues (gum and bone tissues) will have to heal as soon as possible in order to return to healthy state and to let the replacement of the missing tooth by a dental implant ⁸³ (*Figure 15C*).

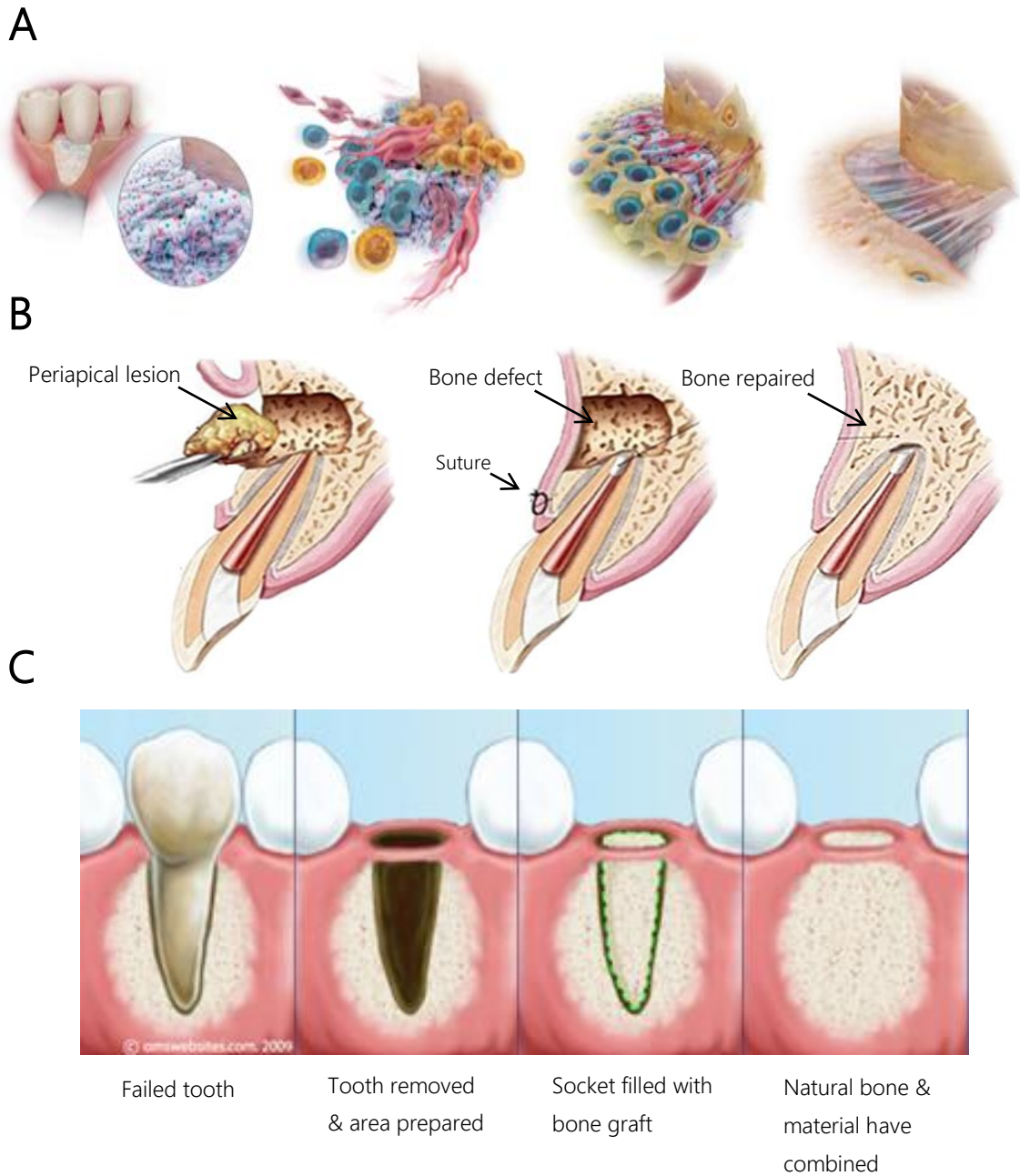


Figure 15. (A) Periodontal surgery for bone augmentation with bone graft placement in a periodontal defect. (B) Endodontic surgery to eliminate a periapical lesion and to repair the bone defect. (C) Tooth extraction and bone graft placement for bone regeneration. In all these cases, adjuvant treatments like low-level laser therapy could enhance wound healing and bone regeneration strategies.

4.2.1.1 Low-level laser therapy

Low-level laser therapy (LLLT) or photobiomodulation has been mainly used in the last 40 years for the treatment of wound healing. In fact, light therapy is known to be one of the oldest therapeutic methods applied by humans. LLLT began with the work of *Mester et al.* reporting non-thermal effects of these lasers on mouse hair growth ⁸⁴. Interestingly, its applicability in pathological conditions such as tissue regeneration, pain relief and anti-inflammatory effects has increased in different branches of regenerative medicine and dentistry. LLLT precise mechanisms on bone repair process is deficient in the literature ⁸³. This device generates an electromagnetic radiation that produces an effect on biologic systems (*Figure 16*). An *in vivo* study has examined its effect on the healing of extraction sockets in healthy and diabetic rats. After 14 days of irradiation, histological observations and gene expression analysis revealed that the irradiated groups showed more new alveolar bone formation than the control groups, both in healthy and diabetic rats ⁸⁵. Several animal studies have shown improved bone healing in extraction sites and in bone fracture defects after LLLT irradiation at a wavelength between 632-930nm (*Table 4*) ⁸⁶. Moreover, some clinical studies have reported the enhancement of bone healing after irradiation with LLLT compared with the control group. A clinical study of 71 patients who have been treated with an endodontic periapical surgery has assessed the LLLT outcomes. The irradiation was applied daily during 7 days, and in the control group patients were not subjected laser therapy. The irradiated group showed better results in terms of edema, wound healing and the number of analgesic drugs used on the first postoperative days. This group also showed significant favorable results in bone density and defect volume area after 3 months of the intervention ⁸⁷. LLLT has also been studied in different cell types including fibroblasts, endothelial cells, skeletal cells, keratinocytes, myoblasts and

stem cells, among other cell types. *Table 5* shows the results of several experiments and as can be observed, depending on the wavelength and potency of the laser, the cellular effect is different. At lower wavelengths there was a higher cell proliferation rate than at higher wavelengths applied. An important point that has been reported by multiple studies is that there is an optimal dose of light for any application, and doses lower or larger than optimum value will exhibit a diminished therapeutic outcome⁸⁸. Although photochemical effects are normally linear in dose, biological responses frequently exhibit a more complex, non-linear dose-response⁸⁹. Evaluating these results, LLLT may induce, at a cellular level, biomodulatory effects during own tissue repair on the molecular and biochemical processes. These effects are: increase epithelial and fibroblast proliferation, enhance collagen synthesis, accelerate the metabolic process of bone repair, increase potential for bone remodeling and repair, induce neovascularization, restoration of nerve function after injury, normalization of hormonal function, immune regulation, inflammation and edema reduction, modulation and relief of pain and improve postoperative analgesia⁹⁰. Although the molecular mechanism associated with the stimulatory effects of LLLT has not been totally understood, there are some theories studied in order to explain how this technique works. The more extended one is that low laser energy is absorbed by intracellular chromophores at the mitochondria. The absorption of photons by molecules contributes to electronically excited states and as a consequence can accelerate the electron transfer reactions. This fact necessarily leads to an increment of ATP synthesis, which means more energy, and induce low levels of reactive oxygen species (ROS). It is known that nitric oxide inhibits respiration by reversible binding to the oxygen attachment site of cytochrom c oxidase. It has previously reported that light can promote the dissociation of nitric oxide from the oxidase at low temperatures^{88,91}. As redox state modulates several regulation pathways, changes in redox state may activate numerous intracellular signaling processes such as nucleic acid and protein synthesis,

enzyme activation and cell cycle progression. These responses may induce changes in transcription factors responsible for gene expression ^{84,92} (Figure 16).

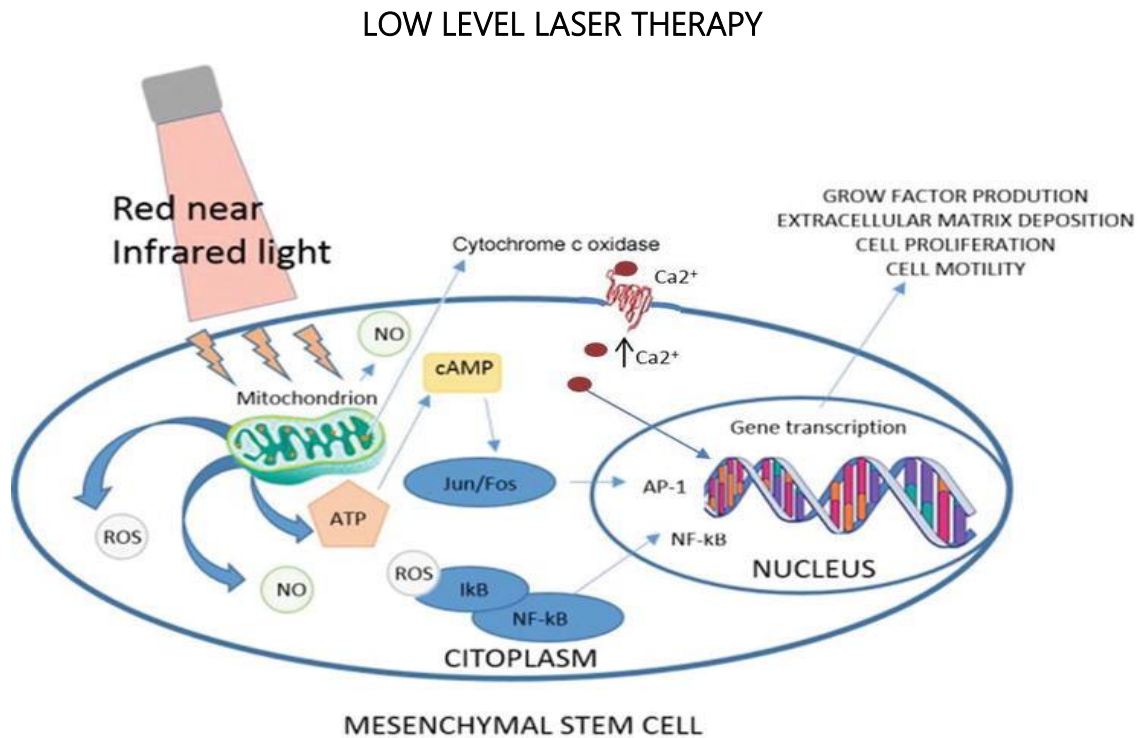


Figure 16. Cell signaling pathways induced by LLLT. LLLT is proposed to act via mitochondria (cytochrome c oxidase) displacing nitric oxide (NO) from the respiratory chain and increasing levels of adenosine triphosphate (ATP) and low levels of reactive oxygen species (ROS). These changes act via intermediaries cyclic adenosine monophosphate (cAMP)-activated transcription factors AP-1. The interaction of the ROS and IκB further transcription factor NF-κB. The LLLT can be photoactive of calcium channels, resulting in higher intracellular calcium concentrations. All stimuli resulting in changes in gene expression and subsequent downstream production of chemical messengers implicated in the cellular changes increase cell proliferation, cell differentiation, cell motility and growth factors production. Modified from ⁹³.

As far as we know, the optimal light parameters to promote cell proliferation and osteogenic differentiation have not yet been established. For this reason, we have studied different parameters of LLLT on mesenchymal stem cells in order to assess the evidenced clinical results.

TYPE OF ANIMAL	WAVELENGTH (nm)	POWER (mW)	RESULTS	STUDY
Rat	904	25	More formation of trabecular osteoid tissue in lased group	⁹³
Rat	632,8	35	Higher maximal load at failure in the irradiated group	⁹⁴
Rabbit	830	75	More bone-to-implant contact in irradiated group	⁹⁵
Rat	830	75	More soft tissue and bone formation in irradiated group	⁹⁵
Rat	830	50	Use of LLLT resulted in a positive effect on the healing of bone defects associated with autologous bone grafts	⁹⁵

Table 4. Effects of low-level laser therapy on different animal models. Adapted from ⁸⁶.

TYPE OF CELLS	WAVELENGTH (nm)	POWER (mW)	RESULTS	STUDY
Mesenchymal and cardiac stem cells (MSCs and CSCs)	804	400	LLLT promoted differentiation of MSCs and CSCs <i>in vitro</i>	⁹⁷
Human skin fibroblasts (HSFs)	632,8	33	Cumulative effect of lower doses (2,5 or 5 J/cm ²) determined the stimulatory effect, while multiple exposures at higher (16 J/cm ²) resulted in an inhibitory effect	⁹⁸
Endothelial and fibroblasts cells	665, 675 and 810	1,58	Fibroblasts proliferated faster than endothelial cells in response to laser irradiation. Maximum cell proliferation occurred with 665- and 675-nm light, whereas 810-nm light was inhibitory to fibroblasts	⁹⁹
Human gingival fibroblasts	670-786	10-50	The infrared laser (780 nm) induced significantly higher cell growth in cells grown in nutritional deficit than the visible laser (670 nm). Lasers of equal power output (red 692 nm and infrared 786 nm) have similar effects on the fibroblasts	¹⁰⁰

TYPE OF CELLS	WAVELENGTH (nm)	POWER (mW)	RESULTS	STUDY
Bone marrow-derived mesenchymal stem cells (BMSCs)	635	60	LLLT significantly stimulated BMSCs proliferation and 0,5 J/cm ² was found to be an optimal energy density	¹⁰¹
BMSCs	632,8	10	Higher ossification levels were observed in the irradiated samples when compared to the control group	¹⁰²
MSCs	647	898-989	Irradiation significantly increased osteoblast mineralization in irradiated cells	¹⁰³
Human dental pulp stem cells (hDPSCs)	660	40	hDPSCs respond positively to LLLT	¹⁰⁴
Adult human adipose-derived stem cells (ADSCs)	635	50	LLLT increased cellular viability, proliferation and expression of $\beta 1$ -integrin	¹⁰⁵

TYPE OF CELLS	WAVELENGTH (nm)	POWER (mW)	RESULTS	STUDY
Human gingival fibroblasts (HGFs)	809	10	The irradiated HGF cells revealed a considerably higher proliferation activity	¹⁰⁶
Rat calvaria osteoblast-like cells	780	10	LLLT increased the proliferation of cells	¹⁰⁷
Human periodontal ligament fibroblasts (PDLFs)	809	10	The irradiated cells revealed a considerably higher proliferation activity than the controls	¹⁰⁸

Table 5. Effects of low-level laser therapy on different cell lines. Adapted from ⁹².

4.2.2 Bone substitutes

As previously explained, LLLT is a technique that can be used as an adjuvant treatment for bone regeneration. This means that there is a need of a combined treatment to obtain optimal bone regeneration results. That is why bone grafts are proposed as the main option to get this goal. The three main clinical situations in which we will focus in this section are the same explained before: the first one is the use of bone grafts for periodontal treatments in order to gain bone volume to have enough support to preserve teeth. This situation may occur when there is a bacterial infection that resorbs the alveolar bone and endangers the tooth survival (*Figure 17A*); the second one, also a very important one in order to preserve teeth, is the use of bone grafts in endodontic surgeries, in situations where there was a periapical lesion that we have eliminated and there remains an extensive bone defect that is not going to regenerate itself (*Figure 17B*). Finally, the third situation, when a functional tooth has to be extracted and there is a requirement to preserve or improve the original alveolar ridge dimensions and to provide an ideal dental implant location, in order to rehabilitate the patient ⁹⁸ (*Figure 17C*).

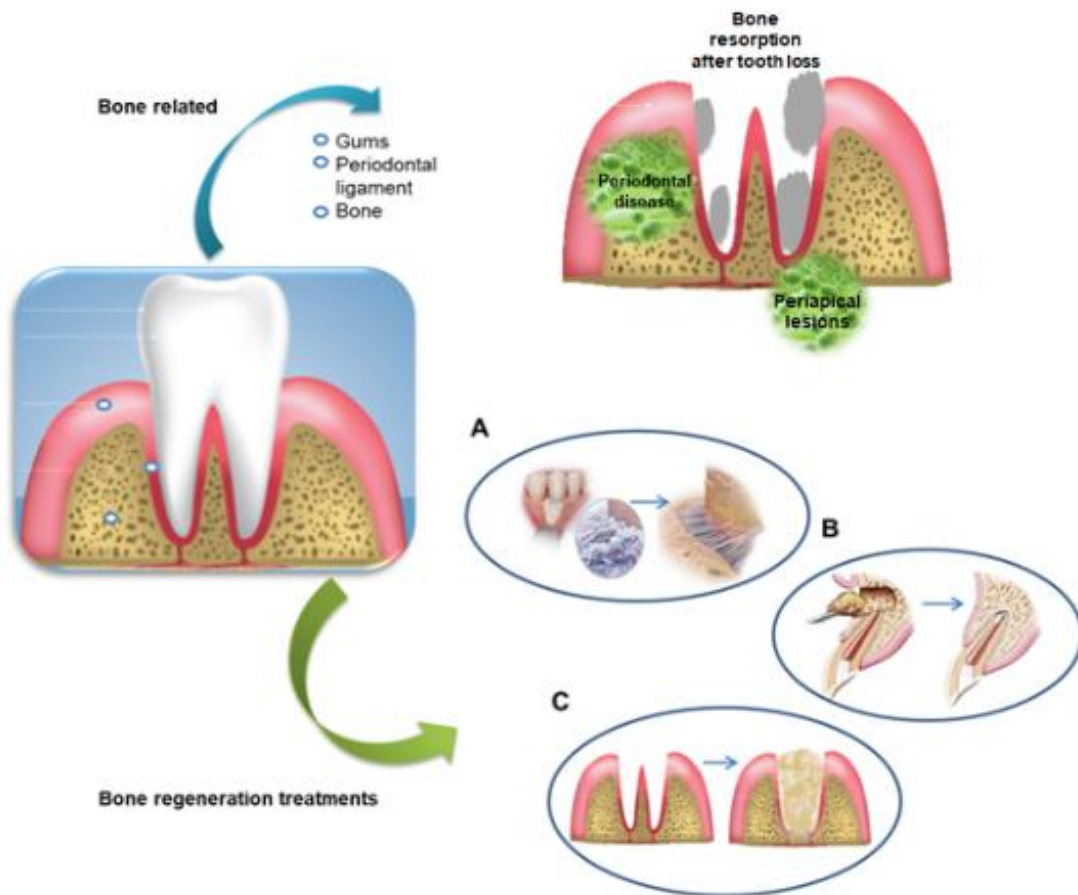


Figure 17. Schematic representation of the bone related clinical problems and the clinical treatment in which we will focus, which is the bone regeneration treatment in three different situations (A) periodontal site, (B) endodontic site and (C) post-extraction site.

Bone grafting is one of the most commonly used surgical methods to replace missing bone. This procedure is accomplished by using material from patient's own body, synthetic or natural material substitute. Bone grafting has dramatically increased in the past two decades as a result of progress in research in material design and techniques, and is expected to spread further in the future⁹⁹. The ideal material used to regenerate bone defects should possess 4 characteristics: osteoconduction, osteoinduction, osteogenesis and osseointegration.

Oseteoconduction is the ability of a material to stimulate bone growth by promoting optimal physical conditions like the porous spatial structure through which osteogenic cells infiltrate the bone. It serves as a scaffold. **Osteoinduction** implies the influence on stem cells by the matrix of bone grafting material that contains bone promotion substances, focusing cells to differentiate into osteoblasts, which are bone forming cells. One of the most known group of osteoinductive factors are bone morphogenetic proteins (BMPs). Finally, **osteogenesis** is the formation of new bone by osteogenic cells ¹⁰⁰. The selection of a material must also take into account the clinical feasibility, predictability, minimal operative hazards, minimal postoperative sequel and patient's acceptance.

4.2.2.1 Natural bone grafts

The ideal properties of bone grafts are shown in *Table 6*. **Natural bone grafts** are those which have a biological origin. They can be classified into autografts, allografts and xenografts, depending on the source of donor. These types of bone grafts are derived from human or animal tissues. The gold standard in maxillary bone regeneration is **autograft**. It consists to obtain a bone graft from the same individual and transferring it from one anatomic site to another (*Figure 18A*). For instance, the most common autograft is harvesting autologous bone from the iliac crest of a patient and then reimplanting it on his maxillary bone defect. Its use avoids any rejection problems as it is originated from the own patient's body. This bone graft meets the mechanical and biological requisites for a filling material ¹⁰¹.

IDEAL PROPERTIES OF BONE GRAFTS
✓ Mimic natural extracellular matrix
✓ Osteoblast adhesion and proliferation
✓ Incorporation of biomolecules
✓ Highly porous for nutrient transport and angiogenesis
✓ Biodegradable at a controllable rate
✓ Highly flexible design capacity
✓ Manipulation of their chemistry and structure

Table 6. Ideal properties of bone grafts ¹⁰².

Autograft presents all three mechanisms: osteoconduction, osteoinduction and osteogenesis ^{103,99}. However, this technique entails many drawbacks as well, being risk of infection and morbidity in the donor site the most important ones; **allografts** are the ones transferred between two different persons. It is obtained mostly from cadavers (*Figure 18B*). One of its main advantages is that avoids the surgical intervention of the donor site, reducing the pain and the period of rehabilitation of the patient. However, allografts failure rate is higher compared to autografts. They can have an inflammatory response on the host site, transmission of diseases and being an expensive and difficult task to find a

suitable bone tissue; **xenografts** are obtained from animals, like bovine or porcine species (*Figure 18C*). They are commonly applied as a calcified matrix.

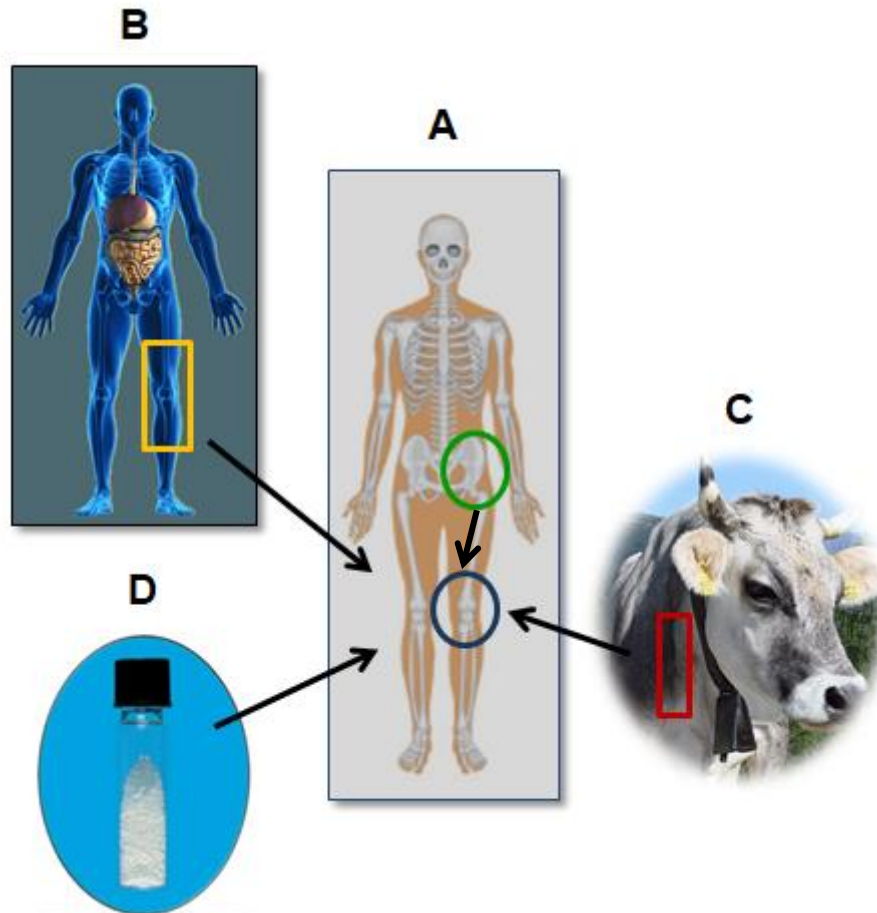


Figure 18. Types of bone grafts. **(A)**. Autograft: the surgeon harvests bone from another site of the patient's skeleton, often from the iliac crest, and implants it into the bone defect site. **(B,C)**. Allograft and xenograft: the bone graft is obtained from a human donor or animal model, respectively **(D)**. Synthetic bone graft: there are different types of new bone substitutes. These materials are safe and need no second surgery site. Modified from ¹⁰⁴.

A commercially well-known xenograft from bovine origin is Bio-Oss[®]. It is one of the most used bone substitutes in dentistry. One of its main advantages is the high availability. Nevertheless, the potential transmission of disease and immunological problems are the xenografts main disadvantages. Bone allograft

and xenograft exclude donor site complications, but some mechanical and biological properties, such as osteogenic and osteoconductive properties, can be reduced because of the bone graft processing variable ¹⁰⁵. The main advantages and drawbacks of natural bone grafts are shown in *Table 7* ^{106,107,108}.

TYPE OF BONE GRAFT	ADVANTAGES	DRAWBACKS
AUTOGRAFT	<ul style="list-style-type: none"> ✓ No immunogenic problems ✓ No transmission of disease ✓ Excellent biological outcomes 	<ul style="list-style-type: none"> - Limited graft volume availability - Donor pain - Morbidity in the donor site
ALLOGRAFT	<ul style="list-style-type: none"> ✓ Prepared into any shape or size ✓ Less surgical intervention ✓ Reduce period for rehabilitation 	<ul style="list-style-type: none"> - No osteoinductivity - Immunogenic problems - Transmission of disease - High cost
XENOGRAFT	<ul style="list-style-type: none"> ✓ Availability ✓ Inexpensive 	<ul style="list-style-type: none"> - Immunogenic problems - Transmission of disease - Osteoconductive only

Table 7. Advantages and drawbacks of natural bone grafts ^{101,103,108}.

4.2.2.2 Synthetic bone grafts

Because of the drawbacks of natural bone grafts and due to the enhancement of biomaterial technology, new approaches of bone substitutes are on the rise ¹⁰⁹. **Synthetic bone grafts** materials are those obtained from non-natural bone tissues (*Figure 18D*). In this sense, the materials are laboratory designed and manufactured in order to meet similar characteristics to those of natural bone grafts. Moreover, compared with natural bone grafts, they have no risk of disease transmission, their availability is highly superior and, most interestingly, they can be tuned and individually manufactured in order to better adapt to the bone site that has to be regenerated ¹¹⁰. As a result, this group of bone grafts is showing significant increase demand and that is why many synthetic bone grafts are under current investigations. A part of bone regeneration capacity, another interesting advantage of some of these grafts is that they can be used as local antibiotic carrier system. Depending on its material composition, they can be classified into metal-based, ceramic-based, polymer-based and composite-based bone grafts..

- **Metal-based** materials are more used in sites with a high mechanical resistance need, for instance in knee joint or hip orthopedic implants. Their main advantages are their superior mechanical properties, high biocompatibility, good corrosion resistance to body fluids, durability and low cost. Some examples are stainless steel, cobalt-chromium alloys, titanium, tantalum or magnesium materials ¹¹¹.
- **Ceramic-based** materials are solid inorganic compounds with different combinations of ionic and covalent bonds. They are extensively used as bone grafts with local antibiotic therapy. They can be divided in bioinerts (alumina, zirconia, calcium sulfate and calcium carbonate) and bioactive ceramics (calcium phosphate, bioactive glass). **Calcium sulfate** is a bioinert natural ceramic that is used as bone defect filler. It can restore the

morphological bone contours and form an osteoconductive matrix in the cavity. The disadvantages are the fast degradation and mild cytotoxic reactions that have been reported in some cases in human studies. **Calcium phosphate** (mostly tricalcium phosphates and hydroxyapatite) are bioactive ceramics that show the best similarity to the minerals found in bone. The main advantages are its excellent biocompatibility, biodegradability and osteoconductivity. They are capable to form molecular interaction with the surrounding tissue resulting in the deposition of an apatite layer on its surface. Calcium phosphate degradation is relatively slow compared to calcium sulfates. They can be used as local antibiotic delivery binding them on its surface. **Bioactive glasses** are solid bioceramics, nonporous and hard materials. Its main component is silicon dioxide (or silicate) apart from sodium dioxide, calcium oxide and phosphorous. They have been investigated for decades showing good results in bone regeneration. The degradation speed of this material depends on the composition of the glasses. They can also form a bonding interface with bone tissue ¹¹². Ceramic-based bone grafts are rigid and hard. However, its main disadvantage is brittleness ¹¹³. Majority of bone grafts available include ceramics, either alone or in combination with another material. We have chosen hydroxyapatite material as a component of our synthetic bone graft.

- **Polymer-based** materials have been extensively studied because of their great properties such as their biocompatibility, biodegradability and the characteristic that they can be tailored for specific applications ¹¹⁴. They can be divided into **synthetic** and **natural polymers**. Synthetic polymers can be non-degradable (like poly(methylmethacrylate) or PMMA) or fully biodegradable, allowing a total bone replacement in time (like polylactic acid (PLA)). Other examples are polyglycolic acid (PGA), poly(lactic-co-glycolic acid) (PLGA) and polycaprolactone (PCL). Natural polymers

examples are collagen, alginate and chitosan. They are protein based and derived from biologic tissues ^{99,101,115}. In the past years, polymer-based bone grafts have also been studied as a local antibiotic delivery system. Some drawbacks are the deformation with time and brittleness. We have chosen chitosan as a component of our synthetic bone graft.

- **Composite-based** materials are a combination of two or more types of materials that are essentially insoluble in each other. The objective of these materials is to increase its mechanical properties or to create materials with functional and structural properties that are not able to get with only one material. They can be tuned depending on its site of action. For instance, in the case of a composite designed with polymers and ceramics, the polymer part may act as the matrix and the ceramic part may act as the filler to reinforce it. The main properties of these materials may be ductility and hardness, without modifying its structure. The main drawback is its manufacturing difficulty ^{116,117}. One example is a polymer or a metal-based material with a hydroxyapatite covering, in order to gain bioactivity. *Table 8* shows synthetic bone grafts classification. In this thesis we have designed a composite bone graft, incorporating chitosan, hydroxyapatite and loaded with an antibiotic molecule.



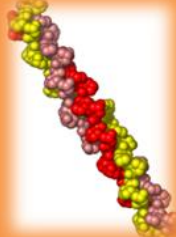

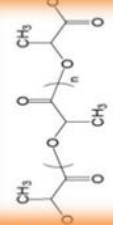
METAL-BASED	CERAMIC-BASED	POLYMER-BASED	COMPOSITE-BASED
		NATURAL 	
Stainless steel	Calcium phosphate (Hydroxyapatite)	SYNTHETIC 	Metal + Ceramic
Co-Cr alloys	Calcium sulfate	Collagen	Metal + Polymer
Titanium	Bioactive glass	Alginate	Polymer + Ceramic
Tantalum		Chitosan	
Magnesium		Hyaluronic acid	
		Cellulose	
		PLA	
		PGA	
		PLGA	
		PCL	

Table 8. Synthetic bone grafts classification depending on its material group. Co-Cr, cobalt-chromium; PLA, polylactic acid; PGA, polyglycolic acid; PLGA, poly(lactic-co-glicolicacid); PLC, polycaprolactone¹¹¹.

Polymer-based bone grafts are interesting biomaterials because they can be tailored and combined with other type of materials forming a composite-based bone graft, in order to enhance its properties. **Synthetic polymers** are mostly derived from petroleum oil and made by scientists and engineer. They can be manufactured with more reproducibility and can be fine-tuned so as to achieve controlled molecular weight compositions of polymer-desired degradation rates. Despite this, limitations of their bioactivity result in restricted cell interactions and tissue-forming capacity ¹¹⁸. On the other hand, **natural source polymers** occur in nature and can be extracted. They can replace petrochemical products by renewable, bio-sources components having a positive environmental impact ¹¹⁹. Natural polymers constitute the native extracellular matrix and, thereby, have an excellent biocompatibility ¹²⁰. This type of polymers seem to be beneficial to be used as bone substitutes due to their low cost, biocompatibility and aqueous solubility. Moreover, they present several interesting properties such as their capacity to interact with surrounding cells and tissues in order to mimic them, and to design them in a custom-made manner. *Table 9* shows the main natural and synthetic polymers and their principal characteristics ¹²¹.

	Polymer	Characteristics
N	Collagen	Major component of natural bone tissue. Excellent biocompatibility and cell-binding properties. Relatively weak mechanical stiffness and rapid biodegradation rate. Some crosslinking agents can be toxic
A	Gelatin	Denaturalized form of collagen. Similar properties as collagen
T	Silk fibroin (SF)	Structural protein of silk fibers. Flexible processibility, high mechanical strength and thermal stability. Easy chemical modification. May contain residue contaminant which can cause biocompatibility issue
U	Chitosan	Positively charged polysaccharide. Good biocompatibility. Antibacterial properties. Relatively weak mechanical strength and stability
R	Alginate	Negatively charged polysaccharide. Adjustable mechanical and biological properties by varying the content of two monomers. Crosslinkable and injectable. Relatively difficult to sterilize and to handle
A		
L	Hyaluronic acid (HA)	Negatively charged glycosaminoglycan. Soluble in water. Good biocompatibility. Easy manipulation. Can be crosslinked to form hydrogel
S	Poly(lactic acid) (PLA), poly(glycolic acid) (PGA), and copolymer PLGA	Aliphatic polyesters. Approved by FDA for various clinical uses. Tunable physical and mechanical properties by adjusting the copolymer ratio. Possible adverse tissue reactions due to acidic degradation products. Hydrophobic and lack of cellular adhesion
Y		
N	Polycaprolactone (PCL)	High crystallinity and good mechanical strength. Slow degradation rate (years). Poor water wettability and lack of cell adhesion
T		
H	Poly(vinyl alcohol) (PVA)	Polyalcohol synthesized by hydroxylation of polyvinyl acetate. Tunable water solubility and crystallinity by changing hydroxylation degree
E		
T	Poly(propylene fumarate) (PPF)	Possess multiple unsaturated double bonds. Crosslinkable <i>in situ</i> and injectable. Variable mechanical properties and degradation rate. Crosslinking agents can be toxic
I		
C	Polyurethane (PU)	Remarkable mechanical properties. Broad and variable range of mechanical, biological and physical properties

Table 9. Examples and characteristics of mostly used natural and synthetic polymers. Modified from ¹²².

Bone repair or regeneration is a part of a complex dynamic process that involves many molecules and cells. Using biomaterials in this area may take into account that its therapeutic effects should be harmonized with the biological processes and induce a better healing capacity. This kind of biomaterials not only provide a supporting matrix for cells, but also supply essential environments for cells spread, migrate, proliferate and differentiate. Because of this, bone biomaterials should be able to modify physico-chemically and to successfully repair and regenerate bone ¹²³. Biomaterials have higher risk to be infected, especially when the biomaterial is exposed to infected tissue or an area with high accessibility of

bacteria, such as the oral cavity. Thus, development of biomaterials with sufficient antibacterial properties may be a solution for these situations ¹²⁴. Infected bone defects are conventionally treated by a systemic administration of antibiotics and a posterior placement of bone grafts ¹²⁵. However, this option is time-consuming and entails bacterial resistance and lower effect of current antibiotics. To solve these problems, an interesting group of novel biomaterials with both antibacterial and osteoinductive properties have been developed in the last decade to be used as synthetic bone grafts.

Recently, due to the search for green chemistry and environmentally-friendly materials, there has been an increase in interest in the use of natural polymers as a source of bone regeneration biomaterials ^{119,126,127}. As we have explained before, collagen, hyaluronic acid, alginate and chitosan are some of the most studied natural polymers for bone regeneration. They have found different possibilities in the pharmaceutical and biomedical fields, especially to be used as drug-delivery systems, for wound dressing and as scaffolds for tissue engineering, between many other applications ^{126,127,128}. Thanks to their chemical composition they are pH-sensitive materials, being an advantage property because they can be modified in different ways to obtain tailor-made materials being optimal as drug carriers ¹²⁹. There are extensively documented studies about natural polymer-based bone grafts in the literature. We have chosen Chitosan-based biomaterial because its high availability, being the second most abundant polysaccharide in the world ¹²⁴; a part from all its advantages, it has a unique property: it is antibacterial and inhibits the growth of a wide variety of fungi, yeasts and bacteria, which can be beneficial for use in the dentistry field ^{130,131,132,133}. Recently, polymer-ceramic composite bone grafts have been intensively investigated, showing promise in mimicking the organic and inorganic parts of natural bone. Chitosan-hydroxyapatite composite have resulted in enhancement of *in vitro* mechanical properties and bioactivity ¹³⁴. For all these reasons, we have designed a synthetic composite-bone graft composed of

chitosan, hydroxyapatite and loaded with an antibiotic molecule in order to obtain an improved biomaterial to be used in the dentistry field. The antibiotic selected to accomplish this objective was Doxycycline (DX). It is a broad spectrum antibiotic of the tetracycline family which has been used to treat bacterial infections in the oral cavity ¹³⁵. Moreover, tetracyclines are the only type of antibiotic that stimulate bone mineralization ¹³⁶.

5. References

1. Ratner, B. *A History of Biomaterials. Biomaterials Science* (2013).
2. Medina-Fernandez, I. & Celiz, A. D. Acellular biomaterial strategies for endodontic regeneration. *Biomater. Sci.* **7**, 506–519 (2018).
3. Pacifici, L., De Angelis, F., Orefici, A. & Cielo, A. Metals used in maxillofacial surgery. *Oral Implantol. (Rome)*. **IX**, 107–111 (2016).
4. Buonocore, M. G. A simple method of increasing the adhesion of acrylic filling materials to enamel surfaces. *J. D. Res* **34**, 849–853 (1954).
5. Kumar, G. & Narayan, B. Osseointegrated Titanium Implants: Requirements for Ensuring a Long- Lasting, Direct Bone-to-Implant Anchorage in Man. *Acta Orthop Scand* **52**, 155–170 (1981).
6. Parirokh, M. & Torabinejad, M. Mineral Trioxide Aggregate: A Comprehensive Literature Review — Part III: Clinical Applications, Drawbacks, and Mechanism of Action. *J. Endod.* **36**, 400–413 (2010).
7. Low, I. M., Duraman, N. & Mahmood, U. Mapping the structure, composition and mechanical properties of human teeth. *Mater. Sci. Eng. C* **28**, 243–247 (2008).
8. Thompson, V. P. The tooth: An analogue for biomimetic materials design and processing. *Dent. Mater.* **In press**, 1–18 (2019).
9. Ahmed, H. M. A., Neelakantan, P. & Dummer, P. M. H. A new system for classifying accessory canal morphology. *Int. Endod. J.* **51**, 164–176 (2018).
10. Chu, T. G., Liu, S. S. & Babler, W. J. Craniofacial Biology, Orthodontics, and Implants. in *Basic and Applied Bone Biology* 225–242 (Elsevier Inc., 2014).
11. Hoyos Nogués, M. *Noves estratègies per la millora de les característiques biològiques dels implants dentals*. (Tesi doctoral. UPC, Departament d'Enginyeria de Sistemes, Automàtica i Informàtica Industrial, 2018).
12. Hanaoka H, Yabe H, B. H. The origin of the osteoclast. *Clin Orthop Relat Res* **239**, 286–298 (1989).
13. Matalová, E., Lungová, V. & Sharpe, P. Development of Tooth and Associated Structures. in *Stem Cell Biology and Tissue Engineering in Dental Sciences* 335–346 (2015).
14. Shao, C., Jin, B., Mu, Z. & Lu, H. Repair of tooth enamel by a biomimetic mineralization

- frontier ensuring epitaxial growth. *Sci. Adv.* **5**, 1–10 (2019).
15. Zhang, K., Wang, S., Zhou, C. & Cheng, L. Advanced smart biomaterials and constructs for hard tissue engineering and regeneration. *Bone Res.* **6**, (2018).
 16. Fernández, R. F., Bucchi, C. & Navarro, P. et al. Bone grafts utilized in dentistry: an analysis of patients' preferences. *BMC Med. Ethics* **16**, 1–6 (2015).
 17. Maekawa, T., Abe, T., Hajishengallis, E. & Hosur, K. B. Genetic and intervention studies implicating complement C3 as a major target for the treatment of Periodontitis. *J. Immunol.* **192**, 6020–6027 (2015).
 18. Teles, R., Teles, F., Frias-Lopez, J. & Paster, B. Lessons learned and unlearned in periodontal microbiology. *Periodontol 2000* **62**, 95–162 (2013).
 19. Yücel, O.O., Berker, E., Mesci, L. & Eratalay, K. Analysis of TNF- α (-308) polymorphism and gingival crevicular fluid TNF- α levels in aggressive and chronic periodontitis: A preliminary report. *Cytokine* **72**, 173–177 (2015).
 20. Vieira, A. R., & Albandar, J. M. Role of genetic factors in the pathogenesis of aggressive periodontitis. *Periodontol. 2000* **65**, 92–106 (2014).
 21. Abbott, P. V. Classification, diagnosis and clinical manifestations of apical periodontitis. *Endod. Top.* **8**, 36–54 (2004).
 22. Lima, S. et al. Antimicrobial peptide-based treatment for endodontic infections — Biotechnological innovation in endodontics. *Biotechnol. Adv.* **33**, 203–213 (2015).
 23. Van Der Weijden, F., Dell'Acqua, F. & Slot, D. E. Alveolar bone dimensional changes of post-extraction sockets in humans: a systematic review. *J. Clin. Periodontol.* **36**, 1048–1058 (2009).
 24. Ustaoglu, G., Göller-Bulut, D. & Gümüş, K. Ç. Evaluation of different platelet-rich concentrates effects on early soft tissue healing and socket preservation after tooth extraction. *Surg, J Stomatol Oral Maxillofac* **In press**, (2019).
 25. Belladonna, F. G., Calasans-Maia, M. D., Neves-Novellino-Alves, A. T. & Figueiredo-de Brito Resende, R. Biocompatibility of a Self-adhesive Gutta-percha – based Material in Subcutaneous Tissue of Mice. *J Endod* **40**, 1869–1873 (2014).
 26. Fukai, K., Yoshino, K., Ohyama, A. & Takaesu, Y. Dental Patient Preferences and Choice in Clinical Decision-Making. *Bull Tokyo Dent Coll* **53**, 59–66 (2012).
 27. Hoppe, A., Boccaccini, A. R. Biological impact of bioactive glasses and their dissolution products. *Biomater. Oral Craniomaxillofacial Appl.* **17**, 22–32 (2015).

28. Alves, M. J. *et al.* Antibacterial effect and biocompatibility of a novel nanostructured ZnO-coated gutta-percha cone for improved endodontic treatment. *Mater. Sci. Eng. C* **92**, 840–848 (2018).
29. Lee, D. K., Kee, T., Liang, Z. & Hsiou, D. Clinical validation of a nanodiamond-embedded thermoplastic biomaterial. *PNAS* **45**, 9445–9454 (2017).
30. Shrestha, A., Fong, S. & Khoo, B. Delivery of Antibacterial Nanoparticles into Dentinal Tubules Using High-intensity Focused Ultrasound. *J Endod* **35**, 1028–1033 (2009).
31. Ørstavik, D. Materials used for root canal obturation: technical, biological and clinical testing. *Endod. Top.* **12**, 25–38 (2005).
32. Ørstavik, D. Materials used for root canal obturation: technical, biological and clinical testing. *Endod. Top.* **12**, 25–38 (2005).
33. Wu, C., Chang, J. & Fan, W. Bioactive mesoporous calcium – silicate nanoparticles with excellent mineralization ability, osteostimulation, drug-delivery and antibacterial properties for filling apex roots of teeth. *J. Mater. Chem.* **22**, 16801–16809 (2012).
34. Friedman, C. M., Sandrik, J. L., Heuer, M. A. & Rapp, G. W. Composition and mechanical properties of Gutta-Percha endodontic points. *J. Dent. Res.* **54**, 921–925 (1975).
35. Möller, B. & Orstavik, D. Chemical and Energy-dispersive X-ray Analyses of Gutta-percha Points. *J Endod* **10**, 413–416 (1984).
36. Li, G. *et al.* Ability of New Obturation Materials to Improve the Seal of the Root Canal System – A Review. *Acta Biomater.* **10**, 1050–1063 (2014).
37. Gurgel-Filho, E. D., Andrade-Feitosa, J. P., Teixeira, F. B. & Monteiro De Paula, R. C. Chemical and X-ray analyses of five brands of dental gutta-percha cone. *Int. Endod. J.* **36**, 302–307 (2003).
38. Prakash, R., Gopikrishna, V. & Kandaswamy, D. Endodontology gutta-percha – an untold story. *Endodontology* 32–36
39. Lee, D.-K., Kim, S. V., Limansubroto, A. N. & Yen, A. Nanodiamond - Gutta Percha Composite Biomaterials for Root Canal Therapy. *ACS Nano* **9**, 11490–11501 (2015).
40. Friedman, C. E., Sandrik, J. L., Heuer, M. A. & Rapp, G. W. Composition and physical properties of gutta-percha endodontic filling materials. *J Endod* **3**, 304–308 (1977).
41. Shrestha, A. & Kishen, A. Antibacterial Nanoparticles in Endodontics: A Review. *J Endod* **42**, 1417–1426 (2016).
42. Maniglia-Ferreira, C., Valverde, G. B., Silva JR, J. B. A. & de Paula, R. C. M. Clinical

- Relevance of Trans 1,4-Polyisoprene Aging Degradation on the Longevity of Root Canal Treatment. *Eur. J. Dent.* **18**, 97–101 (2007).
43. Najar, A. L., Saquy, P. C., Vansan, L. P. & Sousa-Neto, M. D. Adhesion Of A Glass-Ionomer Root Canal Sealer To Human Dentine. *Aust Endod J* **29**, 20–22 (2010).
 44. Collado-González, M., Tomás-Catalá, C. J., Oñate-Sánchez, R. E. & Moraleda, J. M. Cytotoxicity of GuttaFlow Bioseal, GuttaFlow2, MTA Fillapex, and AH Plus on Human Periodontal Ligament Stem Cells. *J Endod* **43**, 816–822 (2017).
 45. Gandolfi, M. G., Siboni, F. & Prati, C. Properties of a novel polysiloxane-guttapercha calcium silicate-bioglass-containing root canal. *Dent. Mater.* **32**, 113–126 (2016).
 46. Tyagi, S., Mishra, P. & Tyagi, P. Evolution of root canal sealers: An insight story. *Eur. J. Gen. Dent.* **2**, 199–218 (2013).
 47. Parirokh, M., Torabinejad, M. & Dummer, P. M. H. Mineral trioxide aggregate and other bioactive endodontic cements: an updated overview – part I: vital pulp therapy. *Int. Endod. J.* **51**, 177–205 (2018).
 48. Aur, M., Rached-junior, F. J. A. & Kishen, A. Zinc Oxide Nanoparticles Enhance Physicochemical Characteristics of Grossman Sealer. *J Endod* **42**, 1804–1810 (2016).
 49. De-Deus, G. *et al.* Lack of correlation between sealer penetration into dentinal tubules and sealability in nonbonded root fillings. *Int. Endod. J.* **45**, 642–651 (2012).
 50. Bergmans, L., Moisiadis, P., De Munck, J., Van Meerbeek, B. & Lambrechts, P. Effect of polymerization shrinkage on the sealing capacity of resin fillers for endodontic use. *J Adhes Dent* **7**, 321–329 (2005).
 51. Schilder, H. Filling Root Canals in Three Dimensions. *J. Endod.* **32**, 281–290 (2006).
 52. Wolcott, J., Himel, V. T., Powell, W. & Penney, J. Effect of Two Obturation Techniques on the Filling of Lateral Canals and the Main Canal. *J. Endod.* **23**, 632–635 (1997).
 53. Venturi, M., Lenarda, R. Di & Breschi, L. An ex vivo comparison of three different gutta-percha cones when compacted at different temperatures: rheological considerations in relation to the filling of lateral canals. *Int. Endod. J.* **39**, 648–656 (2006).
 54. Reader, C. M., Himei, V. T., Germain, L. P. & Hoen, M. M. Effect of Three Obturation Techniques on the Filling of Lateral Canals and the Main Canal. *J. Endod.* **19**, 404–408 (1993).
 55. Melker, K. B., Vertucci, F. J. & Rojas, M. F. Antimicrobial Efficacy of Medicated Root Canal Filling Materials. *J Endod* **32**, 148–151 (2006).

56. Moorer, W. R. & Genet, J. M. Antibacterial activity of gutta-percha cones attributed to the zinc oxide component. *Oral Surgery, Oral Med. Oral Pathol.* **53**, 508–517 (1982).
57. Yamamoto, O. Influence of particle size on the antibacterial activity of zinc oxide. *Int. J. Inorg. Mater.* **3**, 643–646 (2001).
58. Podbielski, A. & Boeckh, C. Growth Inhibitory Activity of Gutta-percha Points Containing Root Canal Medications on Common Endodontic Bacterial Pathogens as Determined by an Optimized Quantitative In Vitro Assay. *J Endod* **26**, 398–403 (2000).
59. Jain, V. M., Karibasappa, G. N. & Dodamani, A. S. Comparative Assessment of Antimicrobial Efficacy of Different Antibiotic Coated Gutta-Percha Cones on *Enterococcus faecalis* An Invitro Study. *J. Clin. Diagnostic Res.* **10**, 65–68 (2016).
60. Fisher, M. A., Berzins, D. W. & Bahcall, J. K. An In Vitro Comparison of Bond Strength of Various Obturation Materials to Root Canal Dentin Using a Push-Out Test Design. *J Endod* **33**, 856–858 (2007).
61. Donadio, M., Jiang, J. & Safavi, K. E. Cytotoxicity evaluation of Active GP and Resilon cones in vitro. *Oral Surg. Oral Med. Oral Pathol. Oral Radiol. Endod.* **106**, 76–79 (2008).
62. Fransen, J. N., He, J. & Glickman, G. N. Comparative Assessment of ActiV GP/Glass Ionomer Sealer, Resilon/Epiphany, and Gutta-Percha/AH Plus Obturation: A Bacterial Leakage Study. *J Endod* **34**, 725–727 (2008).
63. Langalia, A. K., Dave, B., Patel, N. & Thakkar, V. Comparative Evaluation of Fracture Resistance of Endodontically Treated Teeth Obturated with Resin Based Adhesive Sealers with Conventional Obturation Technique: An In vitro Study. *J. Int. Oral Heal.* **7**, 6–12 (2015).
64. Sungur, D. D., Moinzadeh, A., Wesselink, P. R. & Tarhan, S. Ç. Sealing efficacy of a single-cone root filling after post space preparation. *Clin Oral Invest* **20**, 1071–1077 (2016).
65. Al-haddad, A. Y., Kutty, M. G., Adura, Z. & Ab, C. Push-Out Bond Strength of Experimental Apatite Calcium Phosphate Based Coated Gutta-Percha. *Int. J. Biomater.* **2018**, 1–5 (2018).
66. Mohn, D. *et al.* Composites made of flame-sprayed bioactive glass 45S5 and polymers: bioactivity and immediate sealing properties. *Int. Endod. J.* **2**, 1037–1046 (2010).
67. Eltair, M., Pitchika, V., Hickel, R., Kühnisch, J. & Diegritz, C. Evaluation of the interface between gutta-percha and two types of sealers using scanning electron microscopy (SEM). *Clin Oral Invest* **22**, 1631–1639 (2018).
68. Prado, M. *et al.* Surface modification of gutta-percha cones by non-thermal plasma. *Mater. Sci. Eng. C* **68**, 343–349 (2016).

69. Marending, M., Bubenhofer, S. B. & Sener, B. Primary assessment of a self-adhesive gutta-percha material. *Int. Endod. J.* **46**, 317–322 (2012).
70. Mohammadi, Z., Jafarzadeh, H., Shalavi, S. & Bhandi, S. Resilon: Review of a New Material for Obturation of the Canal. *J. Contemp. Dent. Pract.* **16**, 407–414 (2015).
71. Profeta, A. C. & Prucher, G. M. Bioactive-glass in Endodontic Therapy and Associated Microsurgery. *Open Dent. J.* **11**, 164–170 (2017).
72. Shanahan, D. J. & Duncan, H. F. Root canal filling using Resilon: a review. *Br. Dent. J.* **211**, 81–88 (2011).
73. Imai, Y. & Komabayashi, T. Properties of a New Injectable Type of Root Canal Filling Resin with Adhesiveness to Dentin. *J Endod* **29**, 20–23 (2003).
74. Oliet, S. & Sorin, S. M. Effect of aging on the mechanical properties of hand-rolled gutta-percha endodontic cones. *Oral Surgery, Oral Med. Oral Pathol.* **43**, 954–962 (1977).
75. Shipper, G., Ørstavik, D., Teixeira, F. B. & Trope, M. An Evaluation of Microbial Leakage in Roots Filled with a Thermoplastic Synthetic Polymer-Based Root Canal Filling Material (Resilon). *J Endod* **30**, 342–347 (2004).
76. Ying, W., Adura, Z., Ab, C. & Hayati, N. An in vitro Comparison of Bond Strength of Different Sealers / Obturation Systems to Root Dentin Using the Push-Out Test at 2 Weeks and 3 Months after Obturation. *Med Princ Pr.* **26**, 464–469 (2017).
77. Eldeniz, A. U. & Ørstavik, D. A laboratory assessment of coronal bacterial leakage in root canals filled with new and conventional sealers. *Int. Endod. J.* **42**, 303–312 (2009).
78. Carvalho, C. N., Martinelli, J. R., Bauer, J. & Haapasalo, M. Micropush-out dentine bond strength of a new gutta-percha and niobium phosphate glass composite. *Int Endod J* **48**, 451–459 (2015).
79. Carvalho, C. N., Wang, Z., Shen, Y. & Gavini, G. Comparative analyses of ion release, pH and multispecies biofilm formation between conventional and bioactive gutta-percha. *Int. Endod. J.* **49**, 1048–1056 (2015).
80. Raina, R., Loushine, R. J. & Weller, R. N. Evaluation of the Quality of the Apical Seal in Resilon/Epiphany and Gutta-Percha/AH Plus – filled Root Canals by Using a Fluid Filtration Approach. *J Endod* **33**, 944–947 (2007).
81. Al-Maswary, A. A., Alhadainy, H. A. & Al-Maweri, S. A. Coronal Microleakage of the Resilon and Gutta-Percha Obturation Materials with Epiphany SE Sealer: An in-vitro Study. *J. Clin. Diagnostic Res.* **10**, 39–42 (2016).

82. Sah, A. K., Dewangan, M. & Suresh, P. K. Potential of chitosan-based carrier for periodontal drug delivery. *Colloids Surfaces B Biointerfaces* **178**, 185–198 (2019).
83. Zaky, A. A., Mohamed, H. M., Harhsh, T. A. H. & Shalash, M. Can Low Level Laser Therapy Benefit Bone Regeneration in Localized Maxillary Cystic Defects? - A Prospective Randomized Control Trial. *Open Access Maced. J. Med. Sci.* **4**, 720–725 (2016).
84. Farivar, S., Malekshahabi, T. & Shiari, R. Biological Effects of Low Level Laser Therapy. *J. Lasers Med. Sci.* **5**, 58–62 (2014).
85. Park, J. J. & Kang, K. L. Effect of 980-nm GaAlAs diode laser irradiation on healing of extraction sockets in streptozotocin-induced diabetic rats: a pilot study. *Lasers Med. Sci.* **27**, 223–230 (2011).
86. Ebrahimi, T. *et al.* The Influence of Low-Intensity Laser Therapy on Bone Healing. *J. Dent.* **9**, 238–248 (2012).
87. Metin, R., Tatli, U. & Evlice, B. Effects of low-level laser therapy on soft and hard tissue healing after endodontic surgery. *Lasers Med. Sci.* **33**, 1699–1706 (2018).
88. Hamblin, M. R. & Demidova, T. N. Mechanisms of Low Level Light Therapy. *Proc. SPIE* **6140**, 1–12 (2006).
89. Sutherland, J. C. Biological Effects of Polychromatic Light. *Photochem. Photobiol.* **76**, 164–170 (2002).
90. Moreira, A. *et al.* Low-Level Laser Therapy Increases Transforming Growth Factor- β 2 Expression and Induces Apoptosis of Epithelial Cells During the Tissue Repair Process. *Photomed. Laser Surg.* **27**, 303–307 (2009).
91. Borutaite, V., Budriunaite, A. & Brown, G. C. Reversal of nitric oxide-, peroxynitrite- and S-nitrosothiol-induced inhibition of mitochondrial respiration or complex I activity by light and thiols. *Biochim. Biophys. Acta* **1459**, 405–412 (2000).
92. Alghamdi, K. M., Kumar, A. & Moussa, N. A. Low-level laser therapy: a useful technique for enhancing the proliferation of various cultured cells. *Lasers Med Sci* **27**, 237–249 (2012).
93. Pinheiro, C. & Bueno, D. F. Alternative strategies for stem cell osteogenic differentiation. in *Osteogenesis and Bone Regeneration* 1–17 (2018).
94. Takeda, Y. Irradiation effect of low-energy laser on alveolar bone after tooth extraction Experimental study in rats. *Int J Oral Maxillofac Surg* **17**, 388–391 (1988).
95. Luger, E. J., Rochkind, S., Wollman, Y., Kogan, G. & Dekel, S. Effect of Low-Power Laser Irradiation on the Mechanical Properties of Bone Fracture Healing in Rats. *Lasers Surg*

- Med* **22**, 97–102 (1998).
96. Khadra, M., Ronold, H. J., Lyngstadaas, S. P., Ellingsen, J. E. & Haanæs, H. R. Low-level laser therapy stimulates bone–implant interaction: an experimental study in rabbits. *Clin Oral Implant. Res* **15**, 325–332 (2004).
 97. Weber, J. B. B., Pinheiro, A. L. B., De Oliveira, M. G., Oliveira, F. A. M. & Ramalho, L. M. P. Laser Therapy Improves Healing of Bone Defects Submitted to Autologus Bone Graft. *Photomed. Laser Surg.* **24**, 38–44 (2006).
 98. Kassim, B., Ivanovski, S. & Mattheos, N. Current perspectives on the role of ridge (socket) preservation procedures in dental implant treatment in the aesthetic zone. *Aust. Dent. J.* **59**, 48–56 (2014).
 99. Kumar, P., Vinitha, B. & Fathima, G. Bone grafts in dentistry. *J. Pharm. Bioallied Sci.* **5**, 125–128 (2013).
 100. Stepniewski, M., Martynkiewicz, J. & Gosk, J. Chitosan and its composites: Properties for use in bone substitution. *Polim Med* **47**, 49–53 (2017).
 101. de Grado, G. F., Keller, L., Idoux-Gillet, Y. & Wagner, Q. Bone substitutes: a review of their characteristics, clinical use, and perspectives for large bone defects management. *J. Tissue Eng.* **9**, 1–18 (2018).
 102. Lan Levengood, S. & Zhang, M. Chitosan-based scaffolds for bone tissue engineering. *J Mater Chem B Mater Biol Med* **2**, 3161–3184 (2014).
 103. Misch, C. M. Maxillary Autogenous Bone Grafting. *Dent. Clin. NA* **55**, 697–713 (2011).
 104. Oryan, A., Alidadi, S., Moshiri, A. & Maffulli, N. Bone regenerative medicine: classic options, novel strategies, and future directions. *J. Orthop. Surg. Res.* **9**, 1–27 (2014).
 105. Shibuya, N. & Jupiter, D. C. Bone Graft Substitute Allograft and Xenograft. *Clin Pod. Med Surg* **32**, 21–34 (2015).
 106. Kashirina, A., Yao, Y., Liu, Y. & Leng, J. Biopolymers for bone substitutes: A review. *Biomater. Sci.* **7**, 3961–3983 (2019).
 107. Park, H., Lee, K. Y., Lee, S. J. & Park, K. E. Plasma-Treated Poly (lactic-co-glycolic acid) Nanofibers for Tissue Engineering. *Macromol. Res.* **15**, 238–243 (2007).
 108. Wang, W. & Yeung, K. W. K. Bone grafts and biomaterials substitutes for bone defect repair: A review. *Bioact. Mater.* **2**, 224–247 (2017).
 109. Elsalanty, M. E. & Genecov, D. G. Bone Grafts in Craniofacial Surgery. *Craniofacial. Trauma Reconstr.* **2**, 125–134 (2009).

110. Nkenke, E. *et al.* Morbidity of harvesting of bone grafts from the iliac crest for preprosthetic augmentation procedures: A prospective study. *Int J Oral Maxillofac Surg* **33**, 157–163 (2004).
111. Soman, S. & Ajitha, A. R. *Life cycle assessment of metallic biomaterials. Fundamental Biomaterials: Metals* (Elsevier Ltd, 2018).
112. Ning, C. Biomaterials for Bone Tissue Engineering. in *Biomechanics and Biomaterials in Orthopedics* 35–57 (2016).
113. Vugt, T. A. Van, Geurts, J. A. P., Arts, J. J. & Lindfors, N. C. *Biomaterials in treatment of orthopedic infections. Management of Periprosthetic Joint Infections (PJIs)* (Elsevier Ltd., 2017).
114. Dhandayuthapani, B., Yoshida, Y., Maekawa, T. & Kumar, D. S. Polymeric Scaffolds in Tissue Engineering Application: A Review. *Int. J. Polym. Sci.* **2011**, 1–19 (2011).
115. Naveed, N. & Dhanraj, M. CONTEMPORANEOUS TRENDS AND RECENT ADVANCES IN BONE AUGMENTATION FOR DENTAL IMPLANT PLACEMENT. *Int. J. Curr. Res.* **9**, 51853–51858 (2017).
116. Puska, M., Aho, A. J. & Vallittu, P. Polymer Composites for Bone Reconstruction. in *Advances in Composite Materials - Analysis of Natural and Man-Made Materials* 55–72 (2011).
117. Matassi, F., Nistri, L., Paez, D. C. & Innocenti, M. New biomaterials for bone regeneration. *Clin. Cases Miner. Bone Metab.* **8**, 21–24 (2011).
118. Vas, W. J., Shah, M., Hosni, R. Al, Owen, H. C. & Roberts, S. J. Biomimetic strategies for fracture repair: Engineering the cell microenvironment for directed tissue formation. *J. Tissue Eng.* **8**, 1–14 (2017).
119. Croisier, F. & Jérôme, C. Chitosan-based biomaterials for tissue engineering. *Eur. Polym. J.* **49**, 780–792 (2013).
120. Neto, A. S. & Ferreira, J. M. F. Synthetic and Marine-Derived Porous Scaffolds for Bone Tissue Engineering. *Materials (Basel).* **11**, 1–40 (2018).
121. Karandikar, S., Mirani, A., Waybhave, V. & Patravale, V. B. *Nanovaccines for oral delivery- formulation strategies and challenges. Nanostructures for Oral Medicine* (Elsevier Inc., 2017).
122. Kim, T., Bürklin, T., Schacher, B. & Ratka-krüger, P. Pharmacokinetic Profile of a Locally Administered Doxycycline Gel in Crevicular Fluid, Blood, and Saliva. *J Periodontol* **73**, 1285–1291 (2002).

123. Perez, R. A., Seo, S., Won, J. & Lee, E. Therapeutically relevant aspects in bone repair and regeneration. *Biochem. Pharmacol.* **18**, 573–589 (2015).
124. Jin, S., Li, J., Wang, J. & Jiang, J. Electrospun silver ion-loaded calcium phosphate/chitosan antibacterial composite fibrous membranes for guided bone regeneration. *Int. J. Nanomedicine* **13**, 4591–4605 (2018).
125. Lu, H., Liu, Y., Guo, J. & Wu, H. Biomaterials with Antibacterial and Osteoinductive Properties to Repair Infected Bone Defects. *Int. J. Mol. Sci.* **17**, 1–18 (2016).
126. Vroman, I. & Tighzert, L. Biodegradable Polymers. *Materials (Basel)*. **2**, 307–344 (2009).
127. Sibaja, B., Culbertson, E., Marshall, P. & Boy, R. Preparation of Alginate—Chitosan Fibers with Potential Biomedical Applications. *Carbohydr. Polym.* **134**, 598–608 (2015).
128. Anal, A. K. & Stevens, W. F. Chitosan–alginate multilayer beads for controlled release of ampicillin. *Int. J. Pharm.* **290**, 45–54 (2005).
129. Xu, Y., Zhan, C., Fan, L. & Wang, L. Preparation of dual crosslinked alginate–chitosan blend gel beads and in vitro controlled release in oral site-specific drug delivery system. *Int. J. Pharm.* **336**, 329–337 (2007).
130. Sun, K. & Li, Z. H. Preparations, properties and applications of chitosan based nanofibers fabricated by electrospinning. *Express Polym. Lett.* **5**, 342–361 (2011).
131. Camacho-Alonso, F., Julián-Belmonte, E., Chiva-García, F. & Martínez-Beneyto, Y. Bactericidal Efficacy of Photodynamic Therapy and Chitosan in Root Canals Experimentally Infected with *Enterococcus faecalis*: An In Vitro Study. *Photomed. Laser Surg.* **35**, 184–189 (2017).
132. Qi, L., Xu, Z., Jiang, X., Hu, C. & Zou, X. Preparation and antibacterial activity of chitosan nanoparticles. *Carbohydr. Res.* **339**, 2693–2700 (2004).
133. Liu, X., Ma, L., Mao, Z. & Gao, C. Chitosan-Based Biomaterials for Tissue Repair and Regeneration. *Adv Polym Sci* **244**, 81–128 (2011).
134. Zima, A. Hydroxyapatite-chitosan based bioactive hybrid biomaterials with improved mechanical strength. *Spectrochim. Acta Part A Mol. Biomol. Spectrosc.* **193**, 175–184 (2017).
135. Iqbal, H., Ali, M., Zeeshan, R. & Mutahir, Z. Chitosan/hydroxyapatite (HA)/hydroxypropylmethyl cellulose (HPMC) spongy scaffolds-synthesis and evaluation as potential alveolar bone substitutes. *Colloids Surfaces B Biointerfaces* **160**, 553–563 (2017).
136. Kallala, R. *et al.* In vitro and in vivo effects of antibiotics on bone cell metabolism and fracture healing. *Expert Opin Drug Saf* **11**, 15–32 (2012).

6. List of figures

FIGURE 1. This Mayan lower jaw found in Honduras is dated from 600 A.D. It shows three implanted incisors made of carved seashells. Calculus formation on these three implants indicates that they were not made solely for a burial display but served as fixed, functional and esthetic tooth replacements (*Image from the Peabody Museum of Archaeology and Ethnology, Harvard University, Cambridge, Mass.*). 4

FIGURE 2. Tooth anatomy. The crown contains the enamel, the dentin and the pulp cavity. The root contains the nerve, blood vessels and dentin inside the root canals, the periodontal ligament and the cement. The root is surrounded by the maxillary bone ⁷. 6

FIGURE 3. Root canal system that englobes the pulp chamber and the root canal parts. The root canal may have accessory canals (furcation canal, lateral canal) that communicate with the external surface of the root. The apical delta is the region near to the apex (which is the final part of the root), and the main root canal is divided in two or more accessory canals ⁹. 8

FIGURE 4. (A) Tooth alveolar process showing the different parts of maxillary bone cortical, trabecular and alveolar bone. **(B)** Chemical composition of the bone. Bone tissue has an inorganic phase (70%) mostly composed of hydroxyapatite (95%) and an organic phase (30%) mostly composed of collagen (95%) ¹⁰. 10

FIGURE 5. Illustration showing the coordination of different cells and molecules involved in osteoclastogenesis. After osteoclast precursors proliferation they merge in multicellular structures, and differentiate into matured osteoclasts. Both osteoclasts and osteoblasts proliferation is regulated by different cytokines, hormones and growth factors. Modified from ¹³. 12

FIGURE 6. Caries or tooth decay process. From enamel degradation to pulp involvement¹⁵. 14

FIGURE 7. Tooth with healthy periodontal tissue, gingivitis and with advanced periodontitis. Accumulation of plaque and calculus triggers the inflammation of supporting tissues. When there is advanced periodontitis, maxillary bone loss occurs and the tooth stability is in danger ²⁰. 15

FIGURE 8. Schematic figure of pulp and periapical pathology evolution. **1.** Progress of carious lesion with rupture of enamel and dentin barriers. **2.** Pulp inflammation, the first line of pulp defense with the migration of innate immune response cells. **3.** Pulp necrosis, to which pulp inflammation evolves. **4.** Periapical lesion, in which pulp necrosis makes the immune response migrate to the periapical area. The bone resorption starts. **5.** Immune-inflammatory response in periapical area with innate and adaptive cells and products. **6.** Bone resorption, started and maintained by osteoclasts and molecules involved, like cytokines among others. Modified from ²².

17

FIGURE 9. Tooth extraction steps. The maxillary bone will start the resorption process after this procedure.

18

FIGURE 10. Schematic representation of the tooth related and the bone related parts and their clinical problems. In the tooth related parts we have considered the enamel, dentin, pulp and root canals. Their most common clinical problems are caries and traumatism, which will cause an inflammation/infection of the pulp tissue; regarding the bone related parts we have focused on the gums, periodontal ligament and bone. Their most common clinical problems are periodontal disease and periapical lesions which are both caused by bacterial infections, and the bone resorption after a tooth loss, which may course with or without an infection process.

19

FIGURE 11. (A) Schematic representation of the tooth related clinical problems and the clinical treatment in which we will focus: the endodontic treatment. It has been represented with the core material used in this treatment. **(B)** Endodontic treatment of a tooth with an infected pulp tissue. This treatment is based 3 main steps: 1. The mechanical preparation and instrumentation by endodontic files in order to extract the pulp tissue and to widen the root canals. 2. The chemical disinfection with sodium hypochlorite solution in order to clean and eliminate the rests of dentin debris and pulp tissue inside the canals and 3. Root canals filling by a core material and a shell material in order to prevent a bacteria reinfection ³¹.

21

FIGURE 12. GP polymer is obtained from the sap of the trees of the *Palaquium* gender. Then it is mixed with zinc oxide, barium sulfate and wax and molded in a cone shape to better introduce it in the root canal space ⁴⁰.

23

FIGURE 13. Different strategies of RCF materials to use in endodontic treatments. **(A).** GP-coated with bioactive-glass ²⁵ **(B).** Nanoparticles incorporation into GP ³⁹ **(C).** GP surface treatment modification ⁶⁸ **(D).** Adhesion to dentin technique ⁴⁶

29

FIGURE 14. Illustration of the chemical bonding process between dentin tissue and RCF material. Calcium phosphate ions of dentin may interact with calcium or silicate phosphate components of the RCF material ³⁶. 30

FIGURE 15. (A) Periodontal surgery for bone augmentation with bone graft placement in a periodontal defect. (B) Endodontic surgery to eliminate a periapical lesion and to repair the bone defect. (C) Tooth extraction and bone graft placement for bone regeneration. In all cases, adjuvant treatments like low-level laser therapy could enhance wound healing and bone regeneration strategies. 32

FIGURE 16. Cell signaling pathways induced by LLLT. LLLT is proposed to act via mitochondria (cytochrome c oxidase) displacing nitric oxide (NO) from the respiratory chain and increasing levels of adenosine triphosphate (ATP) and low levels of reactive oxygen species (ROS). These changes act via intermediaries cyclic adenosine monophosphate (cAMP)-activated transcription factors AP-1. The interaction of the ROS and I κ B further transcription factor NF- κ B. The LLLT can be photoactive of calcium channels, resulting in higher intracellular calcium concentrations. All stimuli resulting in changes in gene expression and subsequent downstream production of chemical messengers implicated in the cellular changes increase cell proliferation, cell differentiation, cell motility and growth factors production. Image extracted from ⁹³. 35

FIGURE 17. Schematic representation of the bone related clinical problems and the clinical treatment in which we will focus, which is the bone regeneration treatment in three different situations (A) periodontal site, (B) endodontic site and (C) post-extraction site. 41

FIGURE 18. Types of bone grafts. (A). Autograft: the surgeon harvests bone from another site of the patient's skeleton, often from the iliac crest, and implants it into the bone defect site. (B,C). Allograft and xenograft: the bone graft is obtained from a human donor or animal model, respectively (D). Synthetic bone graft: there are different types of new bone substitutes. These materials are safe and need no second surgery site. Image inspired on ¹⁰⁴. 44

7. List of tables

TABLE 1. Ideal properties of a RCF material which are not fully accomplished by the materials that are used nowadays ^{32,33} .	22
TABLE 2. Advantages and drawbacks of GP material ^{38,40} .	25
TABLE 3. GP-based and non GP-based root canal fillings developed in the last 20 years.	26
TABLE 4. Effects of low-level laser therapy on different animal models. Adapted from ⁸⁶ .	36
TABLE 5. Effects of low-level laser therapy on different cell lines. Adapted from ⁹² .	37
TABLE 6. Ideal properties of bone grafts ¹⁰² .	43
TABLE 7. Advantages and drawbacks of natural bone grafts ^{101,103,108} .	45
TABLE 8. Synthetic bone grafts classification depending on its material group. Co-Cr, cobalt-chromium; PLA, polylactic acid; PGA, polyglycolic acid; PLGA, poly(lactic-co-glycolic acid); PLC, polycaprolactone ¹¹¹ .	49
TABLE 9. Examples and characteristics of mostly used natural and synthetic polymers. Extracted from ¹²² .	51

Chapter 1

A Bioactive Endodontic material for preventive treatments



1. Introduction

As explained in the previous chapter, Gutta-percha (GP) material remains as the gold standard to fill teeth root canals accompanied with a sealer material ¹. Nowadays, authors are mostly focused on obtaining a monoblock in which the core material, sealing agent and root canal dentin tissue form a single cohesive ensemble with the objective of increasing the GP mechanical and sealing properties. One of the modifications of GP is focused on its handling and flow abilities. We believe that decreasing the melting temperature of GP will enhance GP capacity to fill the root canal system. In this sense, taking into account from a chemical point of view that GP is based on the polymerization of *trans*-polyisoprene, we thought that the *trans*-polyisoprene could be combined with its isomer *cis*-polyisoprene. The interesting thing is that while the *trans* polymer has a melting temperature of 65°C, the *cis* polymer has a melting temperature of 45°C. We hypothesize that by reducing the melting temperature of the polymer by combining the two isomers at different ratios, we would improve GP flow ability; yet, to the best of our knowledge, GP has never been modified with the incorporation of *cis*-isomer in order to enhance this property. Generally, GP composite material is presented in the β -form in most commercial forms of GP. When thermal manipulation at 46°C is done it transforms to α -form; whereas when GP is heated at temperatures between 54 to 60°C an amorphous phase is reached ^{2,3,4}. There are some commercial types of GP polymer which are presented in the α -phase: thermo-mechanical compactible GP like Thermafill, in the form of heated α -phase GP on a rigid carrier of stainless steel, titanium or plastic ⁵. However, the main drawback of this material is the difficulty to retreat the root canal system. Recently, GuttaCore material is developed to solve these problems. It is presented in a core-carrier system that is composed of β -phase GP (in the core or inner part)

and cross-linked thermoset α -phase GP (in the shell or external part) ⁶. Nevertheless, GP still does not bond properly to dentine tissue. That is why it has to be introduced in the tooth root canal with a sealer. However, most sealers shrink and dissolve over time, leaving voids between dentin tissue and GP which can be colonized by bacteria ⁶. Among the strategies that are being explored to enhance GP sealing ability, bioactive elements are a promising strategy to improve root canal treatment ^{7,8}. The introduction of bioactivity, which refers to the ability to form hydroxyapatite on the surface of the materials and hence establish a direct chemical bonding with natural bone or dentin, is hypothesized as an interesting option to reduce leakage within the filling material and root canals. For instance, glass ionomer, calcium phosphate and bioceramics-GP composite have been proposed as bioactive GP options. In the cases of glass ionomer and calcium phosphate-GP composites, they use a sealer material as happens in the case of conventional GP cone, leading two bonding surfaces between the GP and the sealer and between the sealer and the root canal dentin^{9,10,11}. Instead, Bio-Gutta[®], which is a bioactive glass-based GP, and niobium phosphate glass-based GP, have been proposed to replace conventional GP material. As far as we know, only these two biomaterials have been designed in order to be used as a solely root canal filling material ^{12,13,14}. Silica-based microspheres (SiMS) are an example of bioactive elements that present a unique active surface and chemical composition. Thus, we hypothesize that they may provide a stronger adhesion to dentin tissue. These characteristic properties of ceramic based materials, and more specifically, silica based materials, may provide the missing features for the GP materials ^{15,16,17}. SiMS are a room temperature material that can be easily prepared and that may allow the encapsulation of biological molecules with the possibility to serve as a drug delivery system ^{15,16,17}. By providing a reinforcement into the polymeric matrix with a ceramic component, which in turn may allow a sustained drug release as well as with therapeutic ions ¹⁸, we hypothesize we

may provide the next generation of Gutta-Percha with better treatment outcomes. Hence, the aim of our first project is to develop a novel endodontic biomaterial, firstly by modifying the raw polymer of GP to obtain a more flowable root canal filling material; secondly by doping GP material with silica microspheres (SiMS-GP) in order to enhance the sealing ability and binding to dentin tissue of root canals, through the modification of GP from a bioinert to a bioactive material.

2. Objectives

The main objective of this chapter is to design and fabricate a bioactive endodontic material based on GP that has higher ability to flow combined with an increased ability to bind to dentin tissue. To tackle this challenge, we designed a strategy based on the following objectives:

- O1: To decrease the melting point of GP in order to increase its flow properties by combining two polyisoprene isomers to select the proper blend
- O2: To modify GP material from bioinert to bioactive by the fabrication and incorporation of silica microspheres within the GP composite
- O3: To determine the effect of silica microspheres in the physico-chemical properties of the SiMS-GP composite
- O4: To evaluate the *in vitro* response of mesenchymal stem cells on the SiMS-GP composites
- O5: To fabricate SiMS-GP material in a cone shape to assess its sealing properties
- O6: To analyze the sealing ability of SiMS-GP on simulated root canals and on extracted teeth

3. Materials and methods

➤ *Improvement of material's flowing ability*

3.1 Combining isomers to modify flowing properties

Chemically, GP polymer is a polyisoprene (PI), specifically *trans*-1,4-polyisoprene. The *trans*-isomer is highly crystalline at room temperature leading to a tough, hard and rigid material. This polymer has excellent mechanical strength and its adhesion and thermoplastic properties are desirable in the coating of porous materials. The *cis* structure of polyisoprene is the common natural latex elastomer. General properties are low raw polymer hardness and tensile strength, high resistance to tearing and abrasion, high resilience at 200°C and low heat build-up under mechanical vibrations. This material has a high viscosity, is flowable and crystallizes very slowly at room temperature, compared with *trans*- isomer that crystallizes rapidly at temperatures below 60° C^{19,20,21}. *Figure 1.1* shows geometric isometry of PI. We wanted to assess the properties of both isomers at different blends in order to enhance the rheological capacity of GP composite to flow better within teeth root canals, thus, enhancing its sealing properties.

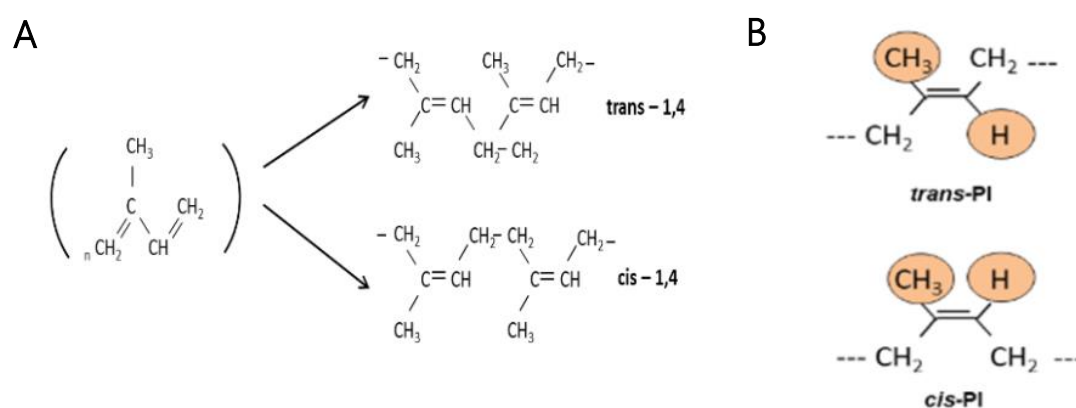


Figure 1.1. (A) Two of the stereospecific polyisoprenes that can be obtained with the polymerization of several units of isoprene. (B) Geometric isometry of *trans* and *cis* polyisoprenes (PI). Adapted from ²².

3.1.1 Synthesis and preparation

The main materials used in this study were *trans*-PI (TPI) and *cis*-PI (CPI) which were obtained from Sigma-Aldrich. These are conformation isomers which differ from each other by the position where the two residues are placed in the double bond. Materials were separately weighed and prepared by mixing the components thoroughly in the TPI/CPI weight ratio of 100/0, 70/30 and 60/40 % w/w composite. First, TPI which is in solid form was solvated in chloroform at a ratio of 6,75g/50 mL (w/v %) until a more viscous material was obtained; secondly, 0g (100 TPI/0 CPI) 2,9 g (70 TPI/30 CPI) or 4,5 g (60 TPI/40 CPI) of CPI, which is in a thick oil form, was added to TPI solution. The composites obtained were first left drying for one week before being moulded into teflon cylinders. After obtaining the desired form, the samples were left drying again for 3 weeks at room temperature in the fume hood in order to let the solvent evaporate.

3.1.2 Samples characterization

First, in order to analyze the morphology and microstructure of the samples, an optical microscope (Zeiss Stemi 305, Axiocam 512 mono) and Scanning Electron Microscopy (SEM; JEOL JSM-7001F) were used.

3.1.2.1 Chemical analysis: Fourier Transformed Infrared Spectroscopy (FTIR)

FTIR was used to characterise the chemical composition of the experimental materials and to verify if there were any chemical interactions between the components within the materials studied. The assay consisted on first obtaining

a disk from each sample; then the disk was placed in the spectrometer (Agilent Cary 630 FTIR) and the measurement was done. The infrared spectrum is detected at a wave number range of 650 to 4000 cm^{-1} with a resolution of 4 cm^{-1} . The spectrums were done 6 times and an average spectrum was obtained. A blank with no sample was measured in order to have the base line. The spectrums were obtained and analyzed using the MicroLab Lite software.

3.1.2.2 Mechanical properties

Samples were prepared by heating them at 50°C and the slurries were introduced into teflon cylinder moulds of 12 mm height and 6 mm diameter. Then, the samples were left dry for 3 weeks at room temperature in order to assure that the chloroform has evaporated after proceeding with the test. A standard number of ten cylinders were prepared for each composition and used for compression testing in Universal Testing Machine (Galdabini) at a crosshead speed of 1 mm/min. The force was axially applied. The samples analyzed were TPI/CPI 100/0, TPI/CPI 70/30 and TPI/CPI 60/40.

Yield strain, yield strength and elastic modulus of each sample were calculated. The maximum force applied was calculated versus the displacement. These units were given in Newtons and mm, respectively. The force was transformed into stress, by dividing the force by the area:

$$\sigma = F/A \quad [\text{MPa}]$$

Then strain was obtained by calculating the displacement divided by the original length of the material:

$$\varepsilon = (\text{displacement}/l_0) \times 100 \quad [\%]$$

where l_0 is original length (mm).

Elastic modulus values were obtained from the slope of the straight-line portion of a stress (σ) strain (ϵ) curve. Therefore, the modulus is the change in stress divided by the change in strain, calculated by the next equation:

$$\text{Elastic Modulus} = \sigma / \epsilon$$

➤ *Improvement of material's bioactivity*

3.2 Designing a bioactive composite

3.2.1 Synthesis and preparation

- Silica microspheres

Silica microspheres (SiMS) were prepared by a sol-gel process at room temperature as previously described ¹⁵. This chemical process is when a solution of molecules (sol) acts as the precursor for an integrated network (gel). In this case, Tetraethyl orthosilicate (TEOS, $C_8H_{20}O_4Si$, 98%, Sigma-Aldrich) (5 mL) was mixed with 0,1 M HCl (1,2 mL), with the addition of deionized water to form an acid catalyzed sol. It was stirred at 300 rpm and once the sol was obtained, 0,08 M ammonium hydroxide (NH_4OH , 28,0% NH_3 in water, 99,99% metal basis, Sigma-Aldrich) was added dropwise to the sol with agitation. The pH was adjusted to 5-5,5 and 6,25 mL of the sol was then added dropwise to 125 mL of olive oil. Then, it was stirred at 250 rpm to allow gelation. Gelled microspheres were gathered after precipitation at the bottom of the flask, vacuum filtered, rinsed with water, ethanol and acetone, and left overnight to dry (*Figure 1.2*). After drying, silica microspheres were sieved and the ones at size diameter of 20-100 μm were collected to use on further experiments. These sizes were chosen because dentine tubules are known to have a

diameter no superior to 5 μm ²³. Therefore, we hypothesize that smaller SiMS sizes would not been able to seal dentine tubules.

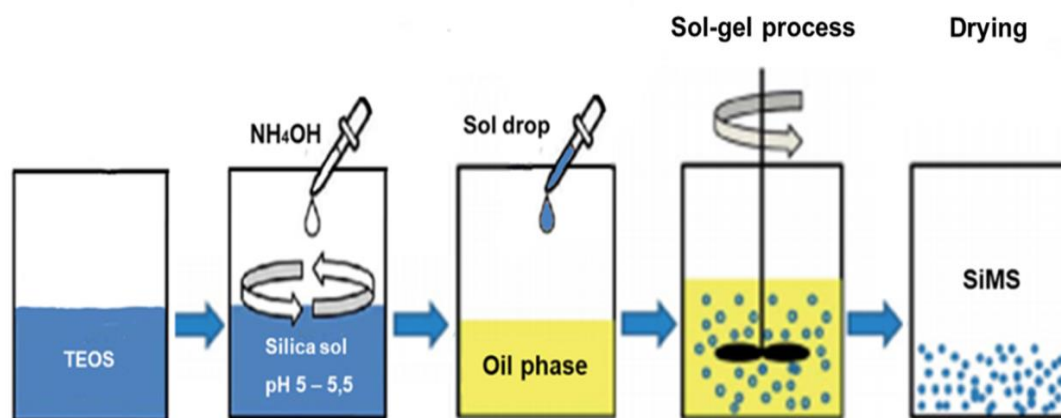


Figure 1.2. Schematic diagram for the preparation of silica microspheres by the sol-gel process. TEOS, tetraethyl orthosilicate; NH₄OH, ammonium hydroxide; SiMS, silica microspheres. Modified from ^{24,25}.

- **Composite**

Commercial GP cones are composed of 20% *trans*-polyisoprene (TPI), 66% zinc oxide (ZnO₂), 11% barium sulphate (BaSO₄) and 3% wax ^{26,27}. SiMS-GP was prepared with the same materials that commercial GP is composed, with the addition of 5% or 10% silica microspheres with diameters between 20-100 μm . The material ratios are based on a previous study by *Lee et al.* ²⁸. SiMS-GP was synthesized by mixing TPI, ZnO₂, BaSO₄ and wax (Sigma-Aldrich). First, TPI was prepared by dissolving 6,75 g of TPI in 50 mL of chloroform. Then, 22,4 g of ZnO₂, 3,74 g of BaSO₄ and 1,02 g of wax were added to the polyisoprene solution, with 15 minutes of sonication after the addition of each component. Finally, 1,79 g (5%) or 3,8 g (10%) of SiMS were then added to the composite and sonicated into the mix for 15 minutes to disperse any SiMS aggregates. Blanks composed with TPI alone (6,75 g) or mixed with 5% (0,35 g) or 10%

(0,75 g) SiMS were also prepared as control samples. The materials studied were: TPI and GP with and without SiMS, comGP and SiMS. *Table 1.1* shows the different codes of the samples studied. After preparing the samples, they were left to dry first for one week before being moulded into teflon cylinders. After obtaining the desired form, the samples were left drying again for 3 weeks at room temperature in the fume hood in order to let the solvent evaporate.

Code	Components and percentages
TPI	<i>trans</i> -polyisoprene (100%)
SiMS-TPI	<i>trans</i> - polyisoprene (95% or 90%) SiMS (5% or 10% from the total weight)
GP	TPI (20%), ZnO ₂ (66%), BaSO ₄ (11%) and wax (3%)
SiMS-GP	TPI (20%), ZnO ₂ (66%), BaSO ₄ (11%) and wax (3%) SiMS (5% or 10% from the total weight)
comGP (Dentsply Maillefer™)	Prefabricated commercial GP: TPI, ZnO ₂ , BaSO ₄ and wax
SiMS	Silica microspheres (100%)

Table 1.1. Samples studied and codes used for this chapter. The main variable studied was the SiMS percentage (5 and 10%) within TPI or GP composites.

3.2.2 Samples characterization

Chemical and mechanical properties were analyzed as explained before with the polymer samples. FTIR and universal testing machine were also used for the assays, respectively. Moreover, in order to analyze the morphology and microstructure of the materials and to observe the incorporation of the SiMS within the composite, SEM and optical microscope were used.

3.2.2.1 *In vitro* apatite forming ability

As previously explained, one of the main objectives of our material is to be bioactive in order to enhance its sealing ability, meaning that it will promote an optimal bonding to dentine tissue, which has a very similar composition to bone tissue. With that purpose in mind, we have immersed the materials in simulated body fluid (SBF) solution to study the apatite-forming ability on its surface. This assay is extensively used to evaluate the bone-bonding ability of a material because SBF solution has ion concentrations nearly equal to those of human blood plasma. We have prepared SBF solution as *Kokubo et al*²⁹. All components were obtained from Sigma-Aldrich. First of all, all containers and utensils were washed with diluted acid, neutral soap and deionized water. After that, the reagents presented in *Table 1.2* were mixed with 500 mL of deionized water in the order indicated and waiting for it to dissolve before adding the next reagent. Then, SBF solution was buffered at pH 7,4 with the addition of 50 mM Tris and 45 mM HCl (the last reagents of the *Table 1.2*), and the temperature was kept constant at 37°C. Finally, deionized water was added to complete 1 L of solution.

Order	Reagent	Amount
1	Sodium chloride (NaCl)	7,996 g
2	Sodium hydrogen carbonate (NaHCO ₃)	0.350 g
3	Potassium chloride (KCl)	0.224 g
4	Di-potassium hydrogen phosphate trihydrate (K ₂ HPO ₄ · 3H ₂ O)	0.228 g
5	Magnesium chloride hexahydrate (MgCl ₂ · 6 H ₂ O)	0.305 g
6	1 _M (mol/l) hydrochloric acid (1.0 _M -HCl)	37,5 mL
7	Calcium chloride (CaCl ₂)	0.278 g
8	Sodium sulfate (Na ₂ SO ₄)	0.074 g
9	Tris-hydroxymethyl aminomethane Tris	6.057 g
10	1 _M (mol/l) hydrochloric acid (1.0 _M -HCl)	0-5 mL

Table 1.2. Order and amounts of reagents for preparing 1000 mL of SBF ²⁹.

The material composites were prepared as previously explained at size of 3 mm height and 6 mm diameter. Moreover, one hundred milligrams of microspheres with diameters between 20 and 100 μm were collected to be used as control sample. All samples were incubated per triplicate in 50 mL of SBF solution for 14 and 21 days. The SBF solution volume needed was calculated by the next equation ²⁹:

$$V = A / 10$$

where V is the volume of the necessary medium for each sample and A is the apparently superficial area of the sample.

After the incubation period, the samples were collected and separated from the solution, gently rinsed with deionized water to remove any debris and finally they were left to dry for 24 hours. The samples were then mounted on

aluminium stubs, carbon-sputtered and examined with a Scanning Electron Microscopy (SEM) and Energy Dispersive X-ray Spectroscopy (EDS) (JEOL JSM-7001F). EDS is used to obtain information about which elements are present in the sample analyzed. This technique measures the X-ray energy emitted by the material, giving information about its composition. EDS was used in order to assess the presence of calcium phosphate and the different elements of the materials (Figure 1.3).

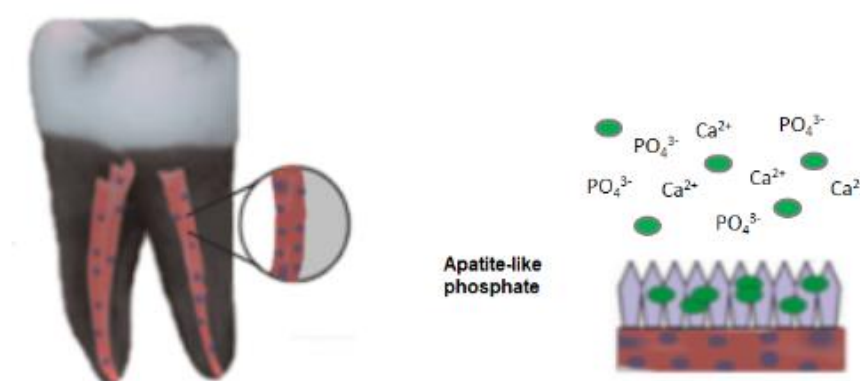


Figure 1.3. Schematic representation of the Gutta-percha containing silica based microspheres and the precipitation of hydroxyapatite on the surface of the material that will eventually enhance the bonding ability to dentin.

3.2.2.2 Cell proliferation assay

- **Materials**

Indirect cell proliferation assay was performed in order to assess the biocompatibility of SiMS-GP material. For that purpose, the material samples were prepared as follows: first of all, the ratio of material surface area to medium volume was set approximately $1,25 \text{ cm}^2/\text{mL}$ in accordance with the guidelines of the International Organization for Standardization 10993-12. Following this standard, the materials were shaped 7 mm height and 6 mm diameter. Moreover, 30 mg of SiMS were used for this assay. All samples were

sterilized by immersing them in ethanol solution for 3 times during 15 minutes and then in PBS solution during the same time. After that, ultraviolet irradiation was turned on during 30 minutes on each side of the samples and stored in the incubator at 37°C. All samples were used in triplicate. The eluates of the different materials were obtained in sterile conditions, using basal culture medium as extraction vehicle. The materials studied were TPI, SiMS-TPI, GP, SiMS-GP and SiMS. The extraction process was as follows: first, the materials were maintained in the basal medium for 24 hours at 37°C in a humid atmosphere containing 5% CO₂³⁰. The conditioned medium extracted was filtered with sterile filters of 0,22 µm diameter pores (Thermo Fisher), and several dilutions of basal medium with conditioned medium were prepared. Basal medium without materials served as a control.

- **Cell morphology in presence of conditioned medium**

Rat mesenchymal stem cells (rMSCs) were obtained in accordance with an ethics approved protocol from the Research Committee from the *Universitat Internacional de Catalunya*, under the project code IMR-2017-04 (supplementary data). Cells were isolated from 5 week old Sprague-Dawley male rat and were analyzed to confirm that they were optimal to be used in the next assay. Cells at passage 3 were used in order to assess the cell proliferation in an indirect experiment with the materials. The cells were cultured in DMEM with 4,5 g/L glucose supplemented with 20% fetal bovine serum (FBS), 1% L-glutamine (GlutaMax), 1% penicillin/streptomycin (Sigma-Aldrich), and incubated at 37°C in a humidified atmosphere of 5% CO₂ in air. The culture medium was exchanged every second day. Upon confluence, the cells were detached with a minimum amount of Accutase (Sigma-Aldrich). The cells were then seeded in 24-well plates at a density of 1 x 10⁴ cells per well with

500 μL of basal medium and allowed to attach for 24 hours. After that, the cells medium was changed for the conditioned medium of the materials at different dilutions (1, 1:5, 1:10 and 1:50). Cell-only with basal medium served as a control.

Cell morphology was assessed after 1 and 3 days of culture with the conditioned medium by optical microscopy images (Olympus CKX41, Nikon) in order to observe the overall cell morphology and to qualitatively evaluate their correct proliferation rate.

- **Cell proliferation assay**

Cell viability was evaluated at 1 and 3 days of the experiment using the commercial available Cell Counting Kit (CCK-8) (Sigma-Aldrich). This assay uses a water-soluble product known as WST-8 that is reduced by cells and generates a yellow-coloured product (formazan), as shown in *Figure 1.4*. This metabolized product is soluble in the culture medium. For that purpose, at each time point, the samples medium was changed for fresh one and added a 10% of CCK-8 solution to the cells. Then the plates were left in the incubator at 37°C for 3 hours for the reaction to take place. Aliquots of each sample were placed on 96 well-plate with a sample volume of 100 μL . A calibration curve with decreasing concentrations of cells was created to express results in cell number. The CCK-8 activity was then determined spectrophotometrically with a multi-detection microplate reader (Bio-Tek Synergy HT) by measuring absorbance at 450 nm.

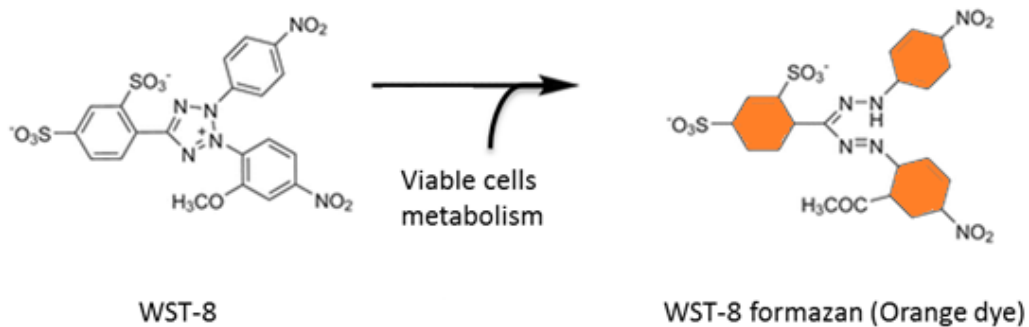


Figure 1.4. Structures of WST-8 and WST-8 formazan. Modified from manufacturer's protocol.

3.2.2.3 Sealing ability assay

This assay consists on performing an *in vitro* endodontic treatment following exactly the same steps as performed in the clinic. Its main objective is to assess and compare between different root canal filling materials or techniques.

- **On dental training blocks**

Commercial GP standardized cones and 10-SiMS-GP material were used for this assay. SiMS-GP samples were fabricated as explained before. The samples were heated with a blowtorch and manually shaped with a metal spatula until a cone-shape similar to comGP was obtained to be introduced in the dental training blocks. These blocks used were methacrylate *endotrain* beakers with a simulated root canal longitude size of 14 mm x 3 mm diameter (Dentsply Sirona). The mechanical preparation of the simulated root canal was done with the use of niqel titanium-made rotary Protaper files (Maillefer) with different tapers and diameters in order to wide and shape the canal. An automated torque control motor was used with a speed set to 300 rpm for all rotary files. The torque was set to 2.0 (N/cm). Between each rotary file instrumentation, an irrigation with 3 mL of 5% sodium hypochlorite solution was done in order to

eliminate the debris inside the canal and avoiding its blocking ³¹. The canals were then dried with paper points. Then, they were randomly divided into 2 groups of 3 specimens each and the cone-shaped materials were introduced in the canals to perform the canal filling:

- Group 1: commercial GP cones
- Group 2: 10-SiMS-GP manually-fabricated cones

Excess GP cone was seared off from the canal orifice using a heated endodontic metal instrument. After the filling procedure, the beakers were stored at room temperature for 24 hours and 10 µL of blue dye was applied on the top orifice of the beakers in order to assess the leakage. They were left for 7 days and photographs were taken to compare the filtration of the dye on the different samples.

- **On extracted teeth**

Patient-derived teeth samples were extracted for orthodontic or periodontal reasons at the UIC dental clinic. All the experiments were performed in accordance with an ethics approved protocol from the Research Committee from the *Universitat Internacional de Catalunya*, under the project code IMR-2017-04 (supplementary data). Teeth with caries, multiple canals, root resorption, open apex or root curvatures were excluded so that the level of expertise did not play a factor in the success of the root canal treatment. Six single-root incisors were chosen for the experiment. The teeth were immersed in a disinfection solution during one week and then in saline solution. They were decoronated using diamond disk at the cement-enamel junction uniformly. The root canal access was prepared using an endo access bur. After that, an endo Z bur was used to create and refine the proper walls of the chamber and the working length was determined using a 010 K-file. Finally, the mechanical preparation and root canal filling protocol was the same as

described above. In this case, we opted to compare self-fabricated GP with self-fabricated SiMS-GP in order to observe if there were differences with the same fabricated material at the same conditions, with the only difference of adding SiMS or not to the composite.

- Group 1: GP self-fabricated cones
- Group 2: 10-SiMS-GP self-fabricated cones

After the filling procedure, a final digital radiograph was taken to assess the quality of the filling. The X-ray tube and digital sensor were settled to allow radiographs to be exposed using the paralleling technique ³².

3.3 Statistical analysis

Statistical analysis was carried out with significance of 5%. One way analysis of variance (ANOVA) with Fisher post-hoc test was conducted. Data are expressed as mean \pm standard deviation, except in the case of mechanical properties, which are expressed as mean \pm standard error. The results were statistically analyzed using Minitab (Minitab[®] Software Inc. 17.1.0) and GraphPad Prism version 6 (Graphpad Software Inc.) was used to graph the data.

4. Results and Discussion

➤ *Improvement of material's flowing ability*

4.1 Isomers characterization

At the outset of our studies, we have evaluated a potential improvement in the flowing ability of polyisoprene by comparing pure *trans*-PI with mixtures of *trans* and *cis* PI. We hypothesized that by reducing the melting temperature of the polymer by combining the two isomers in different ratios, we would obtain a more flowable GP that will fill the root canal system much better. Yet, to the best of our knowledge, GP has never been modified by the incorporation of *cis*-isomer. We wanted to compare the mixtures with TPI alone and to assess if there was a significant improvement in the flowing ability. TPI was presented in a solid form. However, as CPI presentation was in a thick oil form, the material was too viscous and it did not set. For this reason, it was not possible to obtain a manipulable sample of CPI alone. That is why the ratios were maintained as they are presented in the assay. *Figure 1.5* shows the morphology and structure of the different samples: the morphology of TPI was more homogenous than TPI/CPI, showing a whitish colour compared to the blended samples, which had a brown darker tone because of the *cis* component. The 3D structure of all samples was maintained. TPI sample showed a harder consistency compared with TPI/CPI blends, which showed a softer consistency.

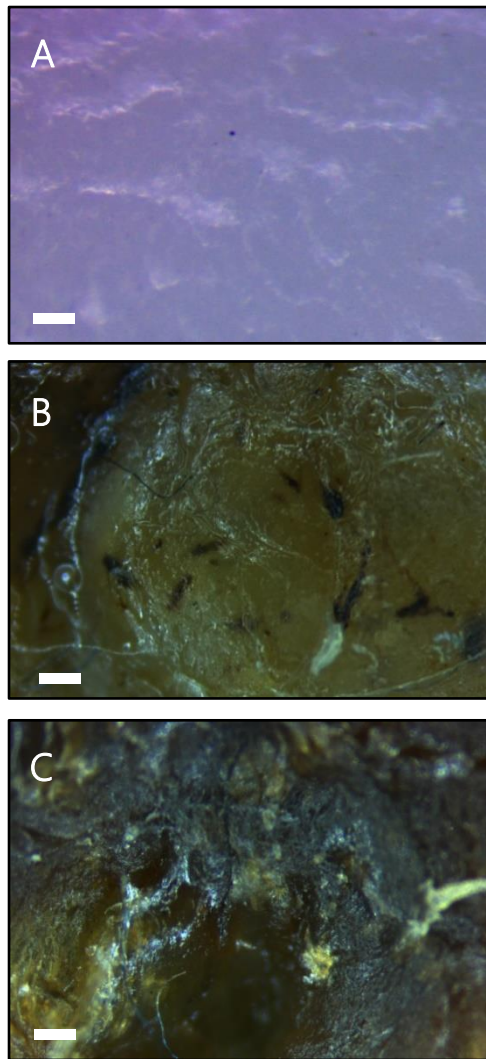


Figure 1.5. Optical microscopy images of (A) TPI (B) TPI/CPI 70/30 (C) TPI/CPI 60/40. Scale bars: 200 μm .

Taking all these considerations into account, we think it is important to find a strategy to convert GP in a more flowable material, which may chemically bind to dentin tissue avoiding gaps between GP and root canal walls, which would cause a bacteria reinfection and at the time the root canal treatment failure. In our study, TPI/CPI blends had good 3D maintained structure. With the characterization of the new materials in hand, we went on to study their chemical properties.

4.1.1 Chemical analysis: Fourier Transformed Infrared Spectroscopy (FTIR)

With the aim of characterising the chemical structure of the different polymers previously synthesized, and to verify the plausible chemical interactions between the compounds of the materials studied, we expected no new signals as we did not expect the formation of new covalent bonds. For this reason, we analyzed them by FTIR (*Figure 1.6*). We performed the sample analysis after allowing the material to dry for 3 weeks at room temperature in a fume hood. The assignment of the different bands observed in *Figure 1.6-1.7* is summarized in *Table 1.3*. Importantly, we observed a shift of the C-H stretching signal towards lower wavenumbers (from 2981 cm^{-1} of pure TPI to 2970 cm^{-1} , 2933 cm^{-1} and 2944 cm^{-1} for 70/30 TPI/CPI, 60/40 TPI/CPI and CPI respectively) demonstrating a weak interaction between the components within the composites. These results are in accordance with the knowledge of the vibration of hydrocarbons, in which C-H stretching vibrations are expected around 3000 cm^{-1} ³³. The same weak interaction happened regarding to C=C stretch, which was 1647 cm^{-1} for TPI and 1654 cm^{-1} for the rest of polymers. Another interesting change was C-H bending band at 1423 cm^{-1} for TPI and equal 1438 cm^{-1} for both concentrations of TPI/CPI and CPI alone.

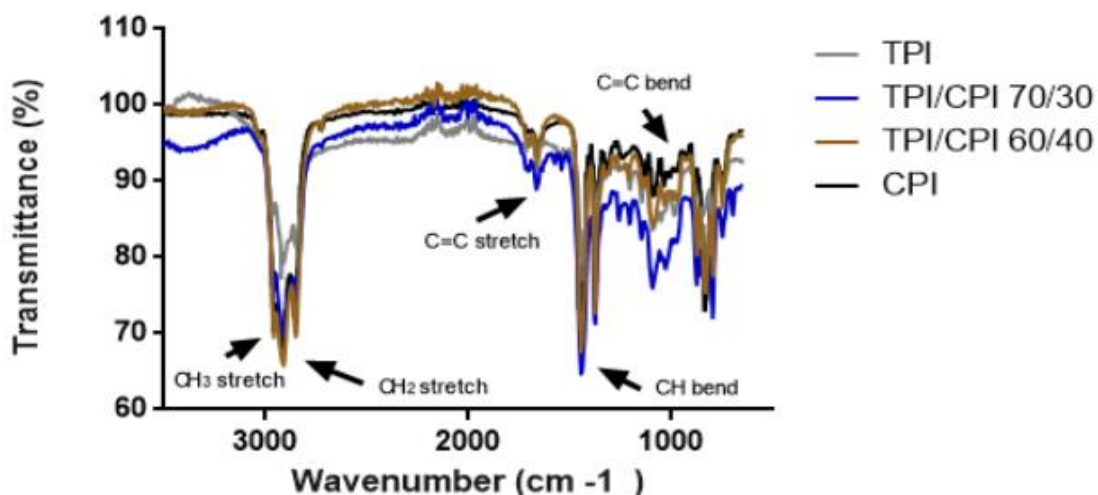


Figure 1.6. FTIR spectrum showing chemical bond structure of the different samples at different *trans*-isomer concentrations: TPI, TPI/CPI 70/30, TPI/CPI 60/40 and CPI.

In line with this observation, both the bands for C=C bending and C-H bending shifted to higher frequencies. Finally, C=C bend was 976 and 969 cm^{-1} for TPI and TPI/CPI 70/30, and equal 961 cm^{-1} for both TPI/CPI 60/40 and CPI respectively. *Chen et al.* also compared 1,4-TPI and 1,4-CPI by FTIR obtaining similar results. They explained that the difference of FTIR behavior of the polyisoprenes is due to the different microstructure of TPI and CPI polymers³⁴. Another explanation about the shifts observed in the IR bands may be because of the presence of amorphous polymer (CPI) that would affect the crystalline character of the TPI substantially³⁵.

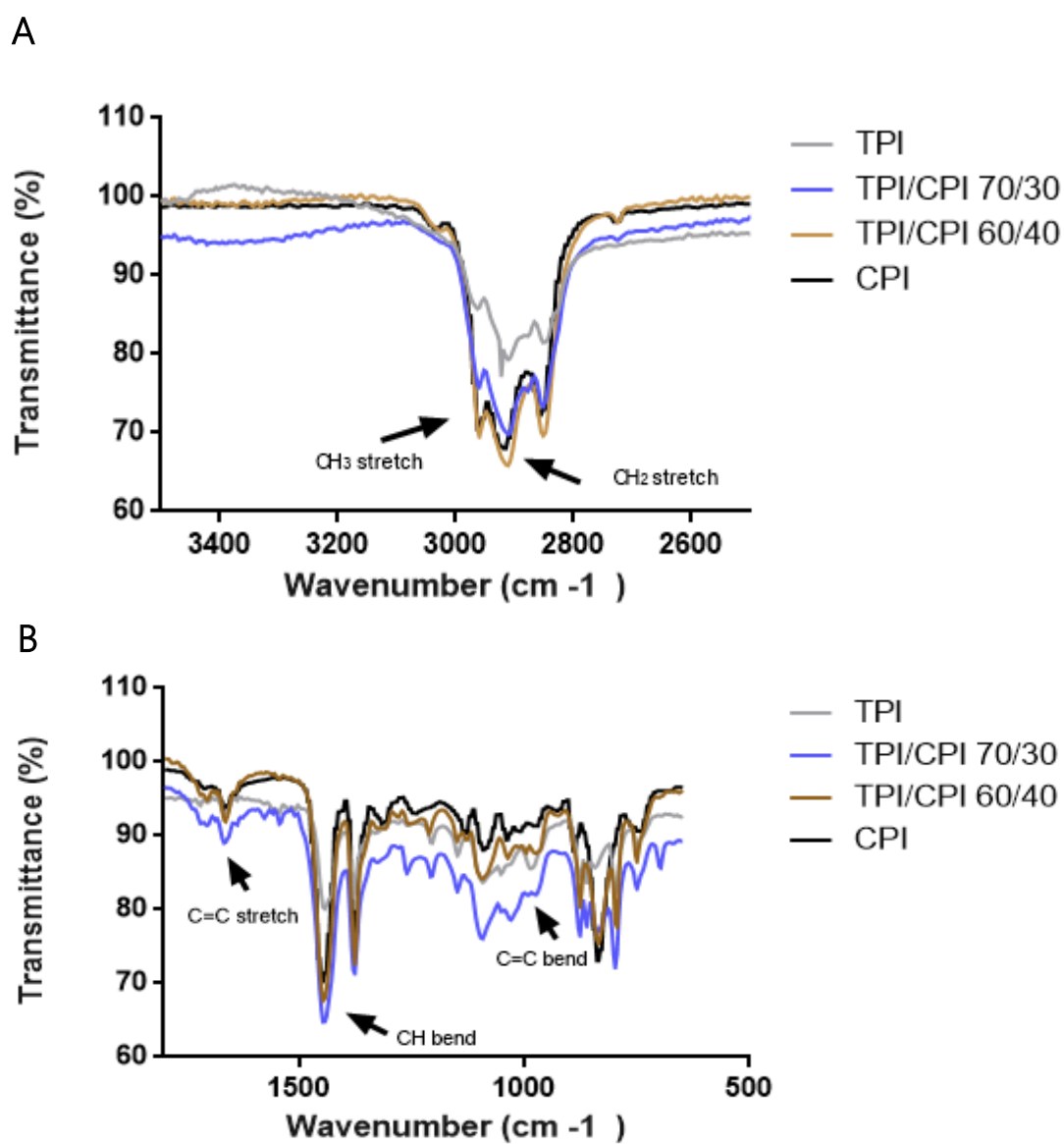


Figure 1.7. FTIR spectrum showing chemical bond structure of the different *trans*-isomer concentrations: TPI, TPI/CPI 70/30, TPI/CPI 60/40 and CPI. (A) Region from 4000-1800- cm⁻¹ (B) Region from 1800-600 cm⁻¹.

Interestingly, physically crosslinked elastomers like polyisoprenes, differ in the nature of the structure linking the chains together compared with chemically crosslinked elastomers. In physically crosslinked elastomers its polymer chains are held together by weak hydrogen bonds. The majority of thermoplastic elastomers have two separated microphases, the crystalline rigid segments and the amorphous segments. In contrast, in chemically crosslinked elastomers its polymer chains are linked together into a 3D network structure by covalent bonds³⁶. As expected, the absence of new bands in the FTIR spectra strongly suggests that no chemical reactions forming new covalent bonds took place. Besides, we observed shifts which may mean weak interactions took place. They were not forming new links and they did not act unexpectedly, as we only observed the shift of the aforementioned bands.

TPI (cm ⁻¹)	TPI/CPI 70/30 (cm ⁻¹)	TPI/CPI 60/40 (cm ⁻¹)	CPI (cm ⁻¹)	Vibration
2922	2899	2907	2914	C-H stretch
1423	1438	1438	1438	C-H bend
2981	2970	2933	2944	C-H stretch
1647	1654	1654	1654	C=C stretch
976	969	961	961	C=C bend

Table 1.3. Main FTIR bands observed for the three different samples. The same bands were observed for all the studied materials: TPI, TPI/CPI 70/30 and TPI/CPI 60/40.

With the characterization of the new materials in hand, we went on to study their physical properties.

4.1.2 Mechanical properties

The yield strain, yield strength and elastic modulus of TPI, TPI/CPI blends and commercial GP as control are shown in *Figure 1.8*. Compared to comGP (4,25%), the yield strain of all groups, with and without incorporation of *cis*-isomer, presented significant differences, being the highest value the one with the highest amount of *cis* component: TPI 6,87%, TPI/CPI 70/30 6,43% and TPI/CPI 60/40 7,81%. Yield strength presented higher values for TPI (6,63 MPa) and comGP (4,85 MPa) and the lowest values were obtained for the samples with the highest *cis* component: TPI/CPI 60/40 (0,87 MPa) and TPI/CPI 70/30 (2,33 MPa). All sample values had significant differences among them. Elastic modulus showed a similar pattern compared with yield strength, presenting significantly increased with the increment of concentration of TPI: 15,53 MPa; 42,04 MPa and 129,82 MPa for TPI/CPI 60/40, TPI/CPI 70/30 and TPI respectively. TPI (129,82 MPa) and comGP (149,43 MPa) have the highest values of elastic modulus compared with both concentrations of TPI/CPI samples, being statistically significant. The results showed that as much TPI concentration is incorporated in the sample, the elastic modulus significantly increased.

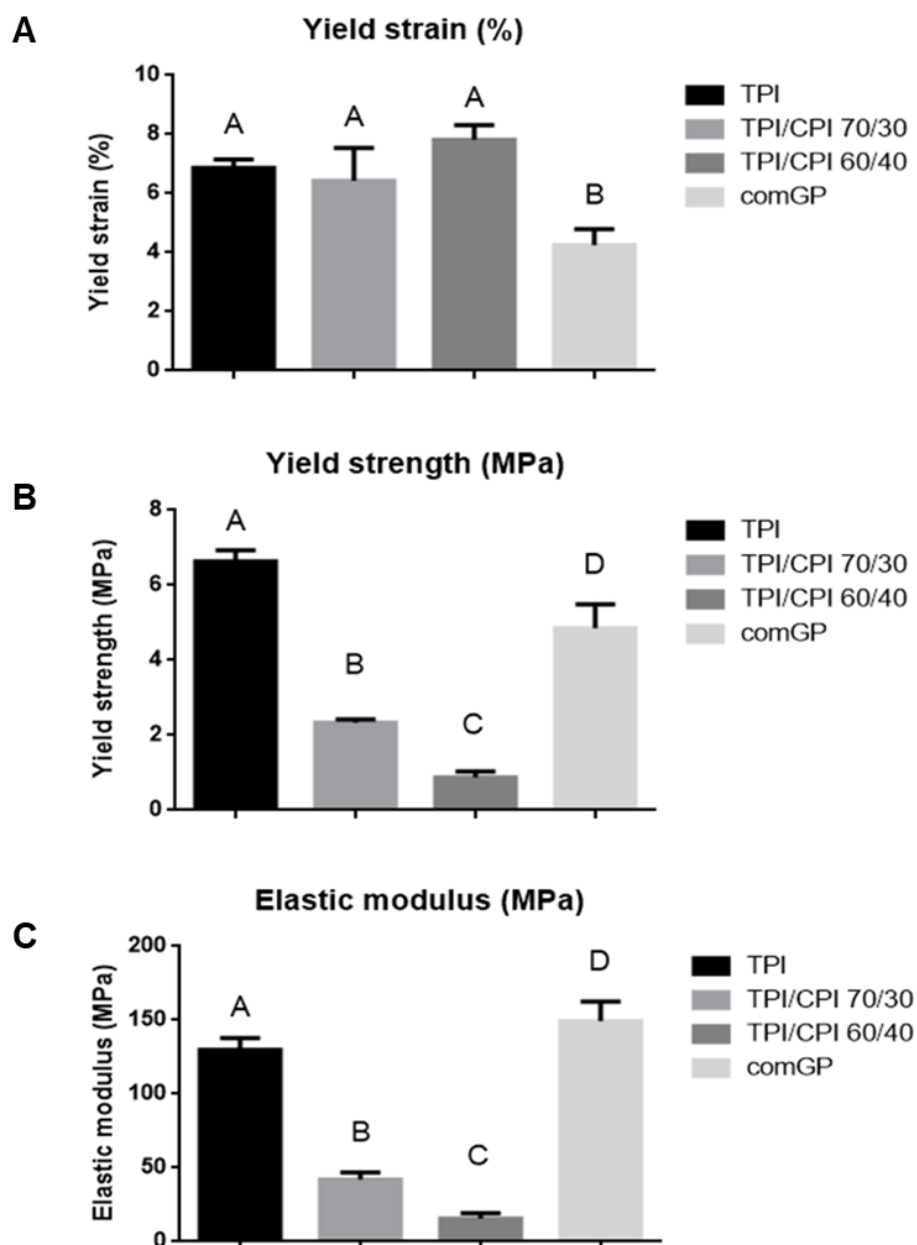


Figure 1.8. Mechanical properties of the different samples at different *trans* and *cis* isomer concentrations: TPI, TPI/CPI 70/30 and TPI/CPI 60/40 compared with comGP. Data are shown as mean \pm standard error ($n = 10$). Groups identified by the same superscript letter are not statistically different ($P \geq 0.05$).

As we have observed in *Figure 1.8*, with the increase of CPI the elastic region and yield strength highly decreases. Our results are consistent with those of *Baboo et al.*³⁵ which also blended TPI with CPI at similar concentrations (100/0,

75/25, 50/50 and 25/75), in order to enhance the properties of the individual constituents. They have used toluene in order to dissolve the materials separately and the solutions were cast on petri dish. Their results showed a reduction in elastic modulus, tensile strength and toughness while an enhancement of the elongation break. They observed that blending TPI with CPI induced a phase transition from a hard phase to a soft phase. It can be explained due to the fact that this mixture increases the glass transition temperature at the same time that decreases the crystallinity, which results in a softer material ³⁵. Regarding our results, the crystallinity and thus the mechanical properties of our material may also have changed because of the blend with CPI. Yield strain and yield strength of TPI were significantly higher compared with comGP. This result may be explained because with the addition of the rest of components of commercial GP, which are zinc oxide, barium sulphate and wax, these mechanical properties decrease. TPI is the 20% of the total weight in commercial GP. Knowing that a mechanical property is the description of the behavior of the material to physical forces ³⁷, the interesting fact is that the objective of this biomaterial will be to introduce it in tooth root canals. Teeth support many functional forces such as mastication, and in some cases they have to lead with parafunctional forces such as bruxism. If the root canal filling biomaterial does not reach a minimum of mechanical properties, the tooth may break and it will have to be extracted. An ideal root canal filling material would have an elastic modulus similar to dentin tissue, which is 14.000-18.600 MPa ¹. Unfortunately, the materials that serve as root canal fillers do not reach such high values. Mechanical properties are important in a root canal filling material because dentin tissue will receive the physiological masticatory forces (around 150-450 N). These forces are distributed by dentin which acts as a cushion for enamel, which is brittle but does not fracture because of the protection of dentin ³⁸. Taking this into account, we have measured yield strain, yield strength and elastic modulus of each material to

study if they reach a minimum desirable mechanical properties; stress is the internal resistance of the material to the force applied, whereas strain is the deformation of the material when this force reaches the material maximum support. Yield strength is the amount of stress that a material needs to experience for it to be permanently deformed whereas yield strain is essentially the maximum value of stress that a material can sustain without causing plastic deformation. Finally, elastic modulus or Young's modulus represents the relative stiffness or rigidity of the material within the elastic interval.

We have tried to optimize the GP flow ability by blending one of its matrix components, TPI, with CPI. As this material is found in a low proportion inside the total GP mix, and our results have not showed a significant difference in terms of flow capacity or mechanical properties, we have completed next assays with TPI component.

➤ *Improvement of material's bioactivity*

4.2 Composite characterization

The morphology and microstructure of TPI, SiMS-TPI, GP, SiMS-GP, comGP and SiMS are shown in *Figure 1.9*. The samples were observed by SEM and optical microscopy. TPI with and without SiMS was more homogenous (*Figure 1.9A*) than GP with and without SiMS (*Figure 1.9B*). This fact can be explained because GP was prepared by mixing the rest of the components a part from TPI, which are zinc oxide, barium sulphate and wax. Regarding the samples with SiMS incorporation it can be observed the microspheres well integrated within the materials in an homogeneous distribution (*Figure 1.9A2,A3 and B2,B3*). As expected, GP microstructure (*Figure 1.9B1*) was similar to comGP (*Figure 1.9C1*) as they are composed by the same materials. *Figure 1.9C2,C3* shows that uniform solid SiMS between 20-100 μm are spherical in shape.

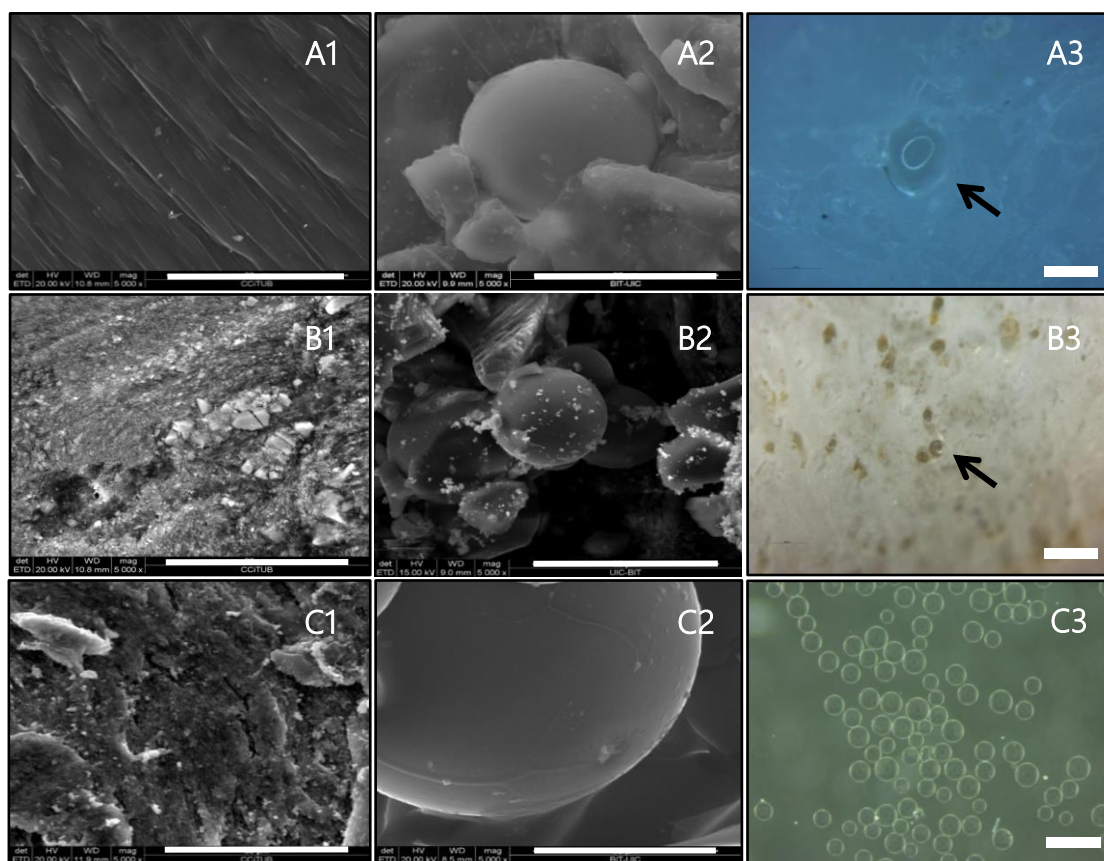


Figure 1.9. Images of (A1) TPI (A2,A3) 10-SiMS-TPI (B1) GP (B2,B3) 10-SiMS-GP (C1) comGP (C2,C3) SiMS; SEM images (A1, A2, B1, B2, C1, C2) scale bars: 30 μm ; optical microscopy images (A3,B3,C3) scale bars A3, B3: 100 μm ; C3 500 μm . Arrows show SiMS within the materials.

4.2.1 Chemical analysis: Fourier Transformed Infrared Spectroscopy (FTIR)

We analyzed GP, SiMS and 10-SiMS-GP in order to see the chemical interaction of silica microspheres within the GP material. SiMS-TPI was not analyzed in this section because we wanted to assess if there were differences between the whole GP composite with or without SiMS incorporation. *Figure 1.10-1.11* shows the IR spectra of these materials and the assignment of the different bands is summarized in *Table 1.4*. The C-H stretching bands are observed in GP with weak intensity at 2832-2922 cm^{-1} . The same fact happened with C-H bending

(1338-1423 cm^{-1}) and =C-H bonds (834 cm^{-1}). SiMS showed Si-O bond stretching vibration (1010 cm^{-1}). The 10-SiMS-GP composite showed a sharp signal in C-H stretching bands with strong intensity (2911-2847 cm^{-1}) compared with GP composite. The same trend is observed with C-H bending (1379-1438 cm^{-1}) compared with the GP. The C=C stretching seems to be only present in 10-SiMS-GP composite at 1636 cm^{-1} .

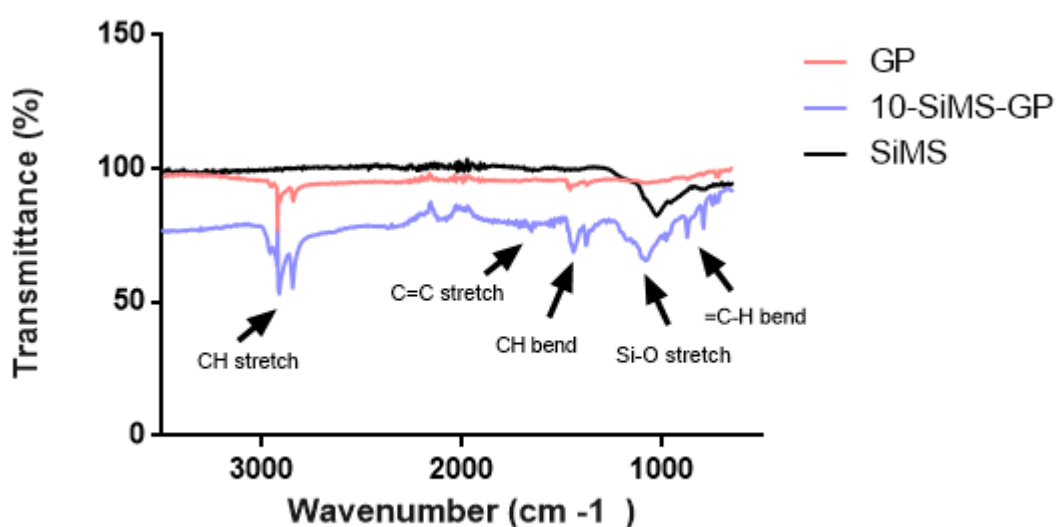


Figure 1.10. FTIR spectrum showing chemical bond structure of the different samples: GP, 10-SiMS-GP and SiMS alone.

Finally, Si-O stretching vibration bonds presented a shift to higher frequencies compared to SiMS alone, being 1062 cm^{-1} for 10-SiMS-GP compared to 1010 cm^{-1} for SiMS. Our results are consistent with the results of previous experimental work of *Poochai et al.*, who fabricated polyisoprene-coated silica composites obtaining such similar characteristic peaks³⁹. These observations confirm the incorporation of SiMS in 10-SiMS-GP composite with no changes in the GP chemical structure^{40,41}. Importantly, the shifts showed in the IR confirm

that there are interactions between the GP and the SiMS that preserve the integrity of the 3D structure of this composite. Previous studies hypothesize that this 3D network may be formed by covalent bonds between polymer chains and silica particles^{42,43,44,45}. However, the shift observed in Si-O stretching vibration bonds seems not to be so high to mean new covalent bonds were formed between the materials.

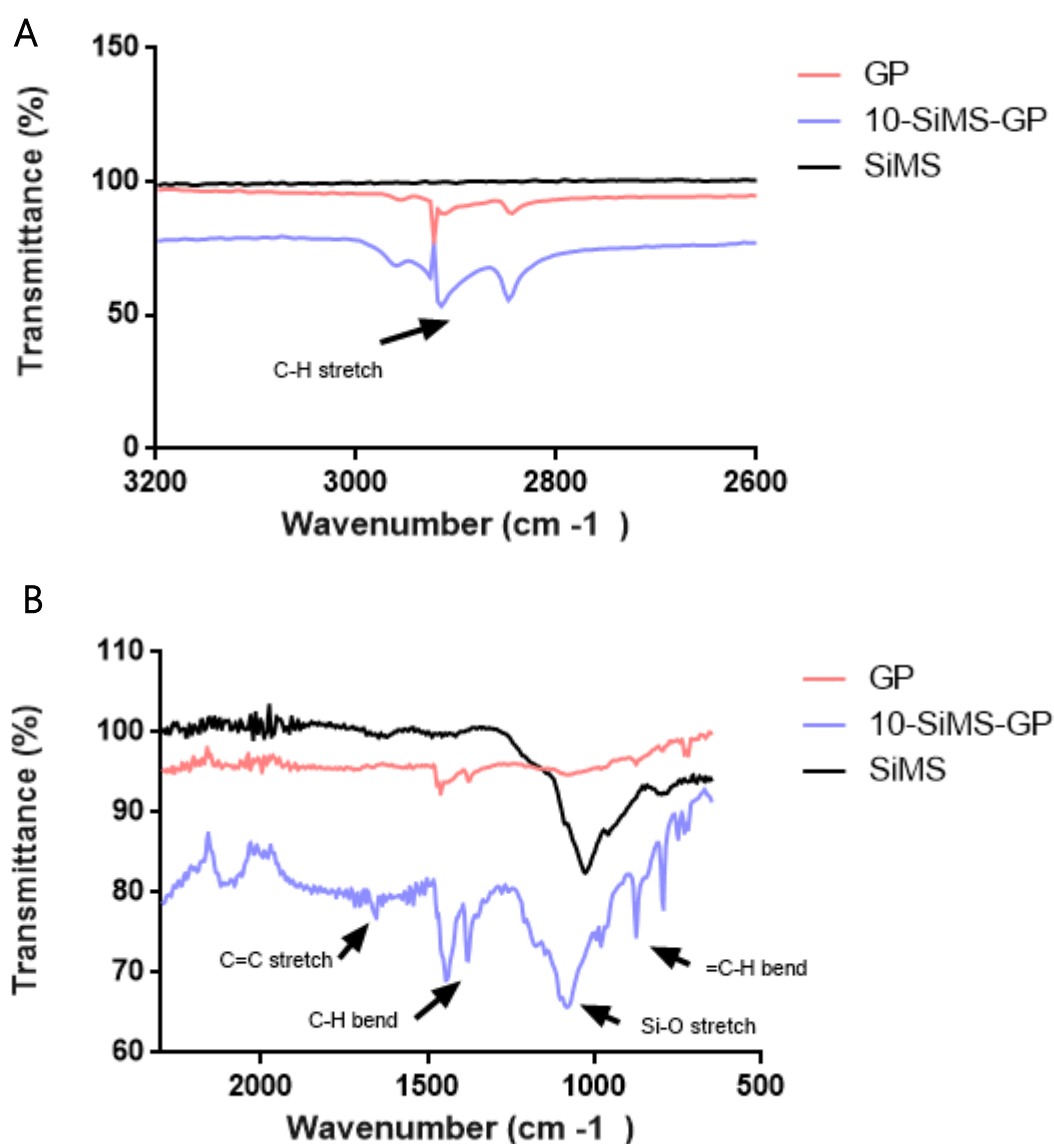


Figure 1.11. FTIR spectrum showing chemical bond structure of the different samples: GP, 10-SiMS-GP and SiMS alone. (A) Region from 3200-2600 cm⁻¹ (B) Region from 2600-500.

GP (cm ⁻¹)	10-SiMS-GP (cm ⁻¹)	SiMS (cm ⁻¹)	Vibration
834	872	----	=C-H bend
2832-2922	2911-2847	----	C-H stretch
1338-1423	1379-1438	----	C-H bend
----	1636	----	C=C stretch
----	1062	1010	Si-O stretch

Table 1.4. Main FTIR bands observed for the three different samples: GP, 10-SiMS-GP and SiMS.

These results may be interpreted as the carboxyl functional group of GP might interact with hydroxyl groups of silica. It has been reported that the high polar hydrophilic surface of silica may absorb components from the non-polar rubber matrix ⁴⁶, which GP is based on. It is fundamental to know that taking into account GP contains a 66% of ZnO, the stabilization of the negative charges of the deprotonated Si-O groups may bond via hydrogen bridges (Si-O ··· H-O-Zn, Si-O ··· HOH Zn ⁴⁷).

4.2.2 Mechanical properties

Dentin tissue is the main structure of the tooth. Although is a mineralized tissue, it has also an elastic consistency. Its elastic modulus is around 15.000 MPa, and its compressive strength is 100 MPa ⁴⁸. Many studies affirm that when a root canal treatment is performed, as higher amount of tooth structure is removed because of the instrumentation and the previous caries, fracture resistance of the tooth decreases ^{49,50}. That is why the biomaterial that will fill

root canals must have a minimum of optimal mechanical properties. For this reason, we have evaluated the yield strain, yield strength and elastic modulus of GP, 5-SiMS-GP, 10-SiMS-GP and commercial GP, which results are shown in *Figure 1.12*. The yield strain of GP without SiMS was 4,38%; with the addition of 5% SiMS into GP the result was 3,07%, after 10% SiMS incorporation increased to 4,05% and commercial GP (used as control) resulted in 4,25% (*Figure 1.12A*). No significant differences were observed referring to the yield strain of the different groups, with and without incorporation of SiMS. *Figure 1.12B* shows yield strength of the different samples. GP obtained the highest values (6,89 MPa) and with the addition of 5% SiMS the result was 2,56 MPa. Then, with the incorporation of 10% SiMS the value increased being 6,59 MPa with significant differences, compared with comGP that was 4,85 MPa. GP and 10-SiMS-GP did not show statistical differences among them. Elastic modulus of GP was 206,68 MPa and with the addition of 10% SiMS the value increased to 224,28 MPa, although it was not statistically significant. However, with only 5% SiMS incorporation within GP, the value decreased to 105,42 MPa, and resulted in 149,43 MPa for comGP. The decrease of the value obtained with 5% SiMS incorporation is an unexpected result. One explanation may be that with 10% of SiMS incorporation within the GP resulted in higher interactions between ZnO and silica components. In contrast, a lower amount of SiMS within the composite resulted to be instable, thus obtaining lower mechanical properties values (*Figure 1.12C*).

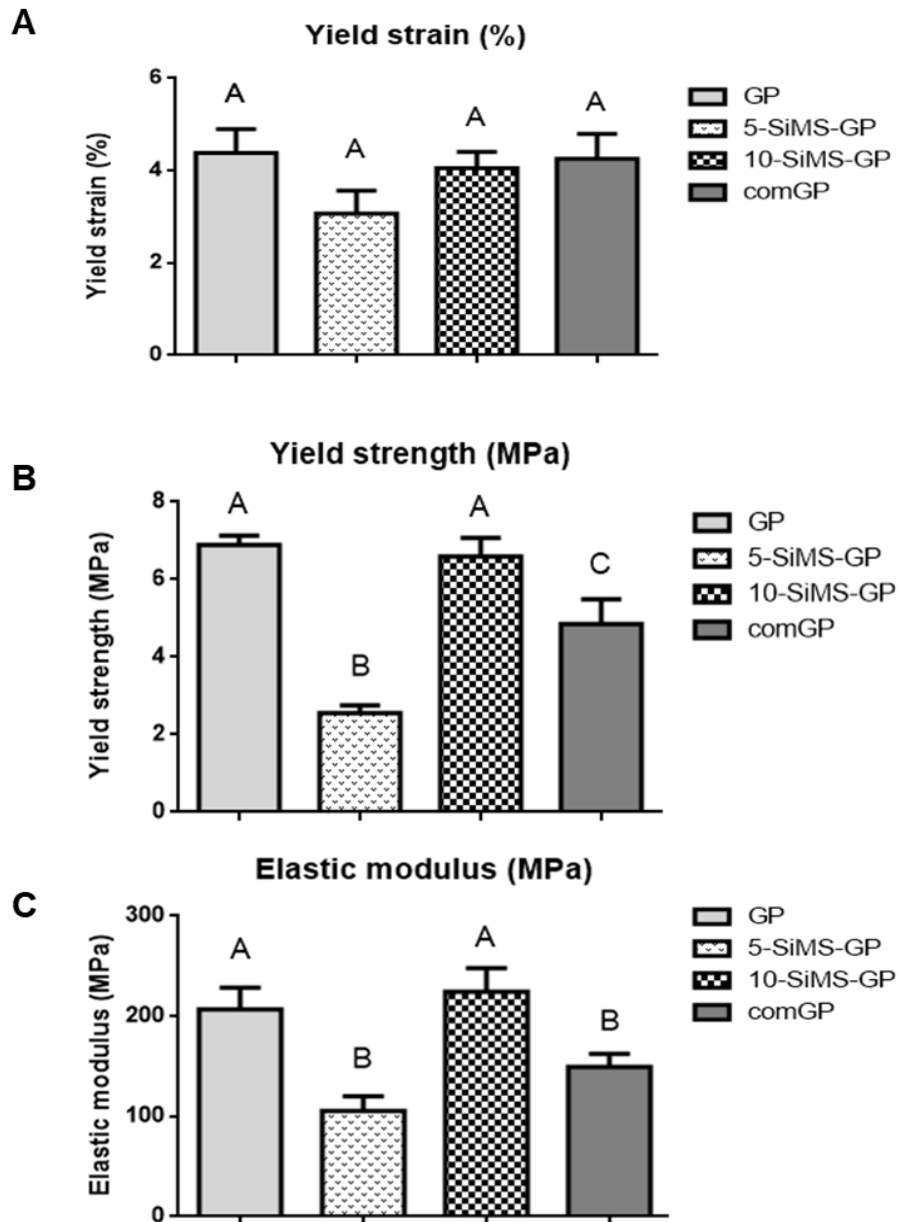


Figure 1.12. Mechanical properties of GP samples with and without 5 and 10% of SiMS incorporation: GP, 5-SiMS-GP and 10-SiMS-GP compared with comGP. Data are shown as mean \pm standard error ($n = 10$). Groups identified by one of the same superscript letter are not statistically different. ($P \geq 0.05$).

A study compared mechanical properties of commercial GP with Resilon, which is a newly developed polycaprolactone-based root canal filling material that uses an adhesive to bond to dentin. They observed that Resilon's elastic modulus was 86 MPa and for GP 78 MPa, and the yield strength was 7,83 MPa

for Resilon and 6,35 MPa for GP. In our study, SiMS-GP group had an elastic modulus of 224 MPa, being significantly higher than for comGP group, which resulted in 149 MPa. This fact may be explained because different brands of commercial GP are known to vary in terms of concentrations given the same component, which may vary the molecular weight distribution and the degree of crystallinity ^{5,51}. For instance, the incorporation of high zinc oxide amounts may result in a lower percentage of elastic modulus ⁵². Moreover, the thermal process applied on the GP material in order to cast the samples may differ between different studies and may also affect the mechanical properties of the material ⁵. However, the yield strength of SiMS-GP (6,59 MPa) was lower compared to Resilon (7,83 MPa) ⁵³. The study of Lee *et al.* compared the mechanical properties of commercial GP with their self-manufactured nano-diamonds loaded-GP (NDs-GP). They observed that 10% NDs-GP had an elastic modulus of 833 MPa which was significantly higher than comGP, which resulted on 240 MPa. Nano-diamonds are carbon nanoparticles that may form chemical bonds with the polymer chains in which they are integrated, affecting the inter-chain bonding characteristics and enhancing elastic modulus property ⁵⁴. Moreover, the interface strength between the additives and polymer may be improved because of the molecular-level uniform dispersion of nanoparticles that can lead to a large interfacial area in the polymer nanocomposites. This fact may improve the mechanical behavior of the polymer nanocomposite ^{28,55}; besides, yield strength of NDs-GP was 12 MPa and for GP was 7 MPa ²⁸. Elastic modulus was much higher in that study than in our results, meanwhile yield strength values were closer to ours. Providing reinforcement into GP polymeric matrix with the incorporation of SiMS as bioceramic component was one of the goals of this assay. This approach has also been reported by some authors that think that rubber matrix mechanical properties may be improved by the addition of a filler ^{56,57}. With this approach, we think it will be obtained an enhancement of the mechanical properties and thereby a reinforcement of the

tooth in order to higher supporting the physiological forces, thus providing a lower failure rate preventing the tooth's break.

4.2.3 *In vitro* apatite forming ability

One of the main characteristics that we wanted to study was the bioactivity of the GP-SiMS doped biomaterial. This property is highly interesting because is focused on the chemical interaction between the biomaterial and the surrounded tissues in which will be grafted. One of the possible assays to study this property is the *in vitro* apatite-forming ability which consists on the immersion of the solely material samples in simulated body fluid (SBF) solution. The objective of this study is to assess if the calcium phosphates deposition may occur on the biomaterial surface, simulating the clinical environment in which the biomaterial would be in contact to dentin fluids.

Thermoplastic polymer materials like GP are a good option as root canal filling material since they provide elasticity and are easy to introduce into the root canal space. In this case, a problem of critical significance is that this type of material does not spontaneously bond in terms of being integrated with the body's tissue. In this assay, GP, SiMS-GP, SiMS and comGP have been studied in terms of bioactivity. Our study was successful in proving that only SiMS-GP and SiMS samples showed apatite-forming ability on its surface after the immersion in SBF solution for 21 days. The graphic in *Figure 1.13* confirmed this observation with the representation of Energy Dispersive Spectrometry (EDS), which are spectrums that come from the scanning electron beam of the surface of the micrographs. These samples were the only ones that showed calcium phosphates (C and P) peaks in the graphic, confirming there was apatite deposition on its surfaces, a part from the presence of silicon and oxygen elements (Si and O) being SiMS components. Pure GP, SiMS-GP and

comGP graphics show C, Ba and S (for barium sulphate component) and Zn, O (for zinc oxide component). This non-biological examination with the SBF-immersion assay demonstrated an optimal improvement in the rate of apatite deposition on the biomaterials surface.

Silica incorporation in different materials like metals, PLA or PCL has been widely studied with the objective to add bone-bonding ability through the apatite layer on the material surface. The authors explain that the ionic breakdown products of silica-based materials have the attractive property of being osteoconductive ^{58,59,60,61}. Our results are in agreement with previous studies that reported a formation of hydroxyapatite on the surface of silica microcarriers after the immersion in SBF for 4 weeks ⁶². Bioactivity property is very interesting in the dentistry field because there is a need of biomaterials that may interact with dental tissues, improving the tissue response and thereby the treatment outcome. Recently, several studies have demonstrated that the presence of zinc and silicon increase the mineralization rate in SBF. These components may create favorable conditions for apatite formation ^{63,64}.

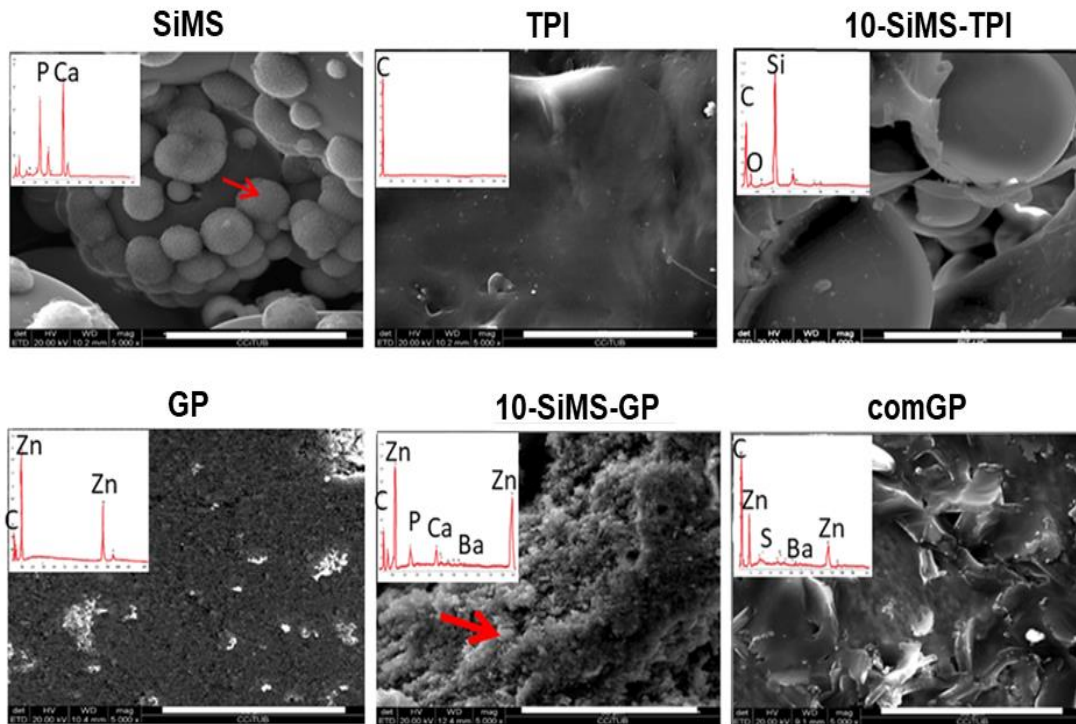


Figure 1.13 SEM micrographs for the different samples with or without 10% SiMS incorporation and with immersion in simulated body fluid (SBF) for 21 days at 37°C. SiMS and 10-SiMS-GP samples show the apatite forming ability on its surface (red arrows). On the left of each SEM image the representation of EDS spectrums that come from the scanning electron beam of the surface of the micrographs. SiMS and 10-SiMS-GP samples show calcium phosphates that are not showed in the rest of samples, meaning there is apatite forming ability on these samples. Scale bars 30 µm.

Although a range of materials, such as resin or ceramic sealers, have been developed to be used as root canal filling, they have failed to achieve permanent sealing because of the imperfect combination between these foreign materials and the native dentin tissue. Moreover, these materials may be prone to bacterial penetration along their entire length, due to dimensional changes that root canal sealers may suffer over time ⁶⁵. One of the main objectives of our study was to enhance this GP drawback, with the incorporation of bioactive microspheres. Moreover, we wanted to simplify and reduce the materials employed for root canal filling using only one core biomaterial, thus not needing the sealer material. We hypothesize that with

SiMS-GP we would replace the latter one. With the same objective of enhancing the adhesion of GP material to dentine tissue, making the use of an endodontic sealer unnecessary, a study of polyisoprene with nanometric bioactive glass 45S5 incorporation has been done. After immersing the samples in simulated body fluid, hydroxyapatite deposition was observed on material surface. This was not observed on the controls ¹². Following the same objective, another study assessed the bioactivity of a NaOH coated GP after immersing it in SBF solution for 10 days. They said that FTIR and XRD analysis confirm the presence of –OH in the coated GP, and with that finding they affirm that is an indicator to formation of hydroxyapatite ⁶⁶. In our study, we immersed SiMS-GP in SBF for 21 days and we obtained calcium phosphate ions on the surface of the biomaterial, as is showed in *Figure 1.13*. We hypothesize that our biomaterial may distinguish from the nanometric bioactive glass because SiMS platforms are fabricated at mild conditions, allowing the encapsulation of biological molecules with the possibility to serve as a drug delivery system ¹⁵. Moreover, we think that the hydroxyapatite layer induced by the mineralization in the SiMS-GP surface stimulated by silica microspheres can be integrated into native dentin such that the root canal sealing would be permanent and more predictable, as it would be a chemical union. An ion-exchange reaction between the bioactive material and surrounding body fluids (dentin fluids) will result in the formation of a calcium phosphate apatite (HA) on its surface that will be chemically and crystallographically equivalent to the mineral phase in bone. This process may be developed as an effective routine treatment in root canal sealing in the clinical practice.

4.2.4 Cell proliferation

- Cell morphology in presence of conditioned medium

Indirect cell viability assay was conducted in order to assess cell response on the different materials studied. SiMS-GP biomaterial is expected to be used in endodontic treatments, in which case the biomaterial will be enclosed inside a root canal in an indirect contact with periradicular cells, which are encompassed in cementum, periodontal ligament and bone tissue (for more detail see *Figure 11* in the chapter of *General Introduction*). *Figure 1.14* shows optical microscopy images of rMSCs after 1 and 3 days of culture with conditioned medium of the different materials, and the control group cultured with basal medium. The cells presented good morphology and shape at different time intervals studied in all groups, which mean there is a preservation of cell anatomy. At day 1, SiMS group seemed to have higher cell number compared with the rest of groups. However, at day 3, GP and control (CT) groups showed the highest amount of cell number. Importantly, when comparing the samples at days 1 and 3 of the experiment, SiMS-GP and CT groups apparently exhibited a higher cell number.

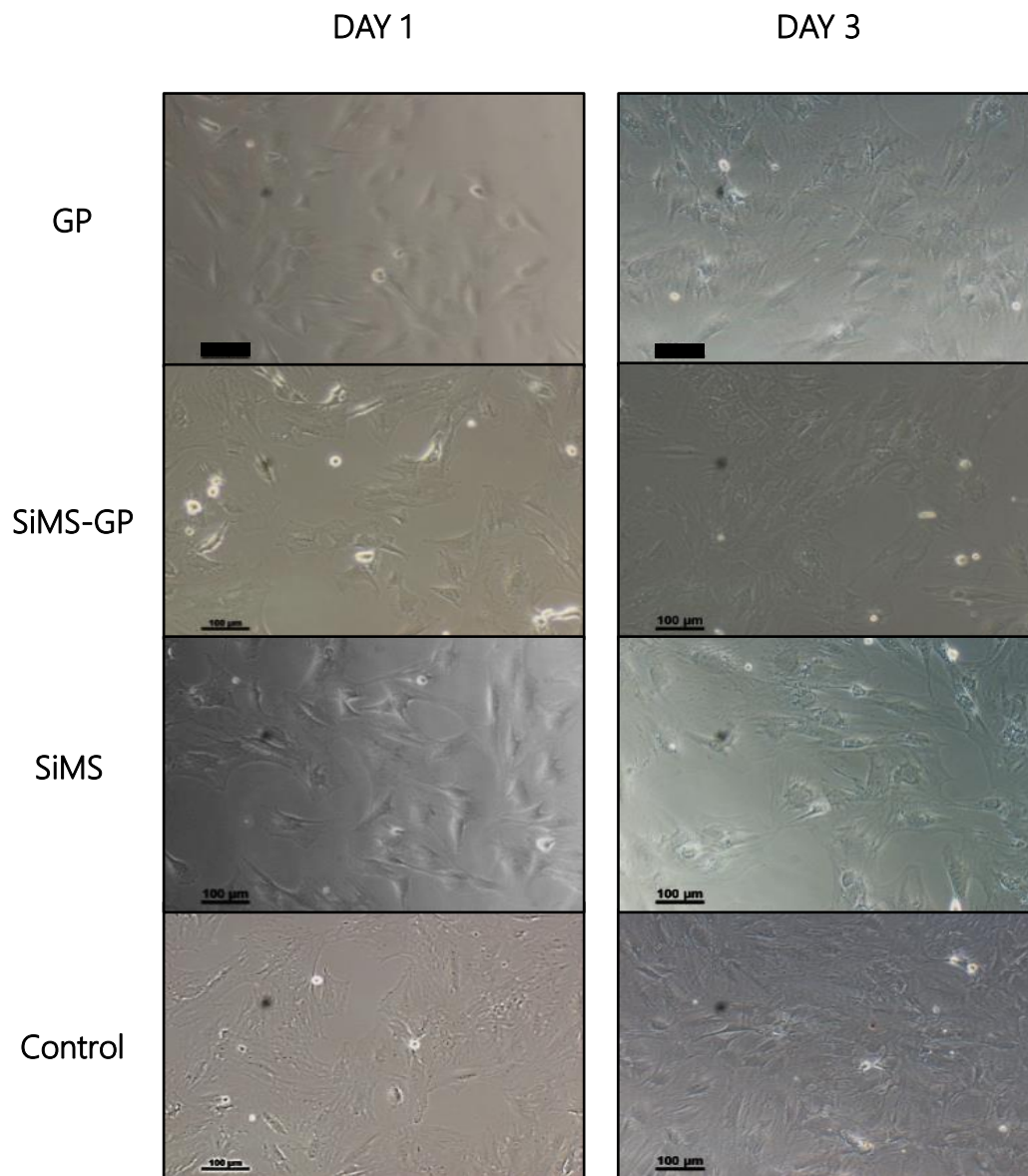


Figure 1.14. Optical microscopy images of rMSCs. Good cell morphology is observed with the eluates of the different biomaterials and the control group with basal medium at days 1 and 3 of the experiment. Scale bars 100 μm .

- Cell proliferation

Periapical tissues englobe osteoblasts and MSCs ^{67,68,69} which are involved in the healing and regeneration of periapical bone defects ⁷⁰. That is the reason why new biomaterials have to be studied in terms of cell viability, and that is why we have used mesenchymal stem cells for this assay. The viability of rMSCs was studied with the Cell Counting Kit-8 (CCK-8). This experiment was interesting in order to assess that the materials were not cytotoxic, and to compare the cell proliferation capacity of the different materials. Different concentrations of biomaterials have been used (1, 1:5, 1:10 and 1:50) to evaluate a potential threshold concentration at days 1 and 3. As the results of the different eluate concentrations did not showed significant differences between them, only 1:50 concentration is presented. *Figure 1.15* shows the percentage of viability obtained for each sample at different time points. The graphic shows that at day 1 of cells culture there were no statistical differences between the different materials, although there is a trend to higher viability in SiMS-GP and SiMS samples, with a 99% and 101% respectively, compared with 96% in GP sample. Regarding at day 3, the graphic shows differences between SiMS-GP (105%), SiMS (106%), GP (100%) and the control without any material (100%) This fact may indicate that silicon ions elution has promoted cell proliferation ^{71,72,73,74}. However, these results were not statistically significant.

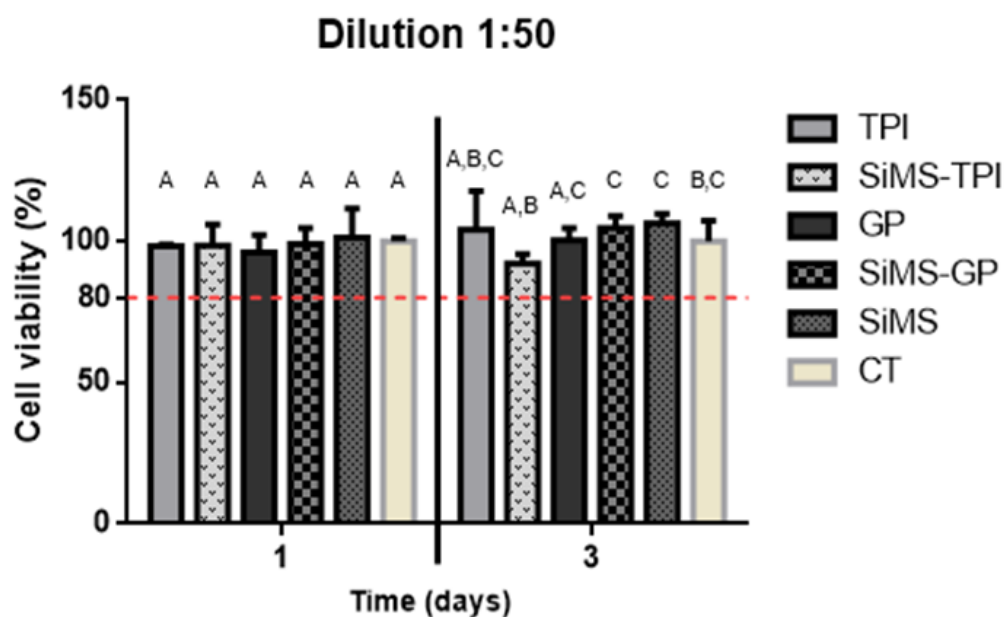


Figure 1.15. CCK-8 for the proliferation rate of rMSCs after 1 and 3 days of exposure to conditioned medium of different materials (1:50 concentration). Red horizontal dot line indicates 80% of viability. Data are shown as mean \pm standard deviation ($n = 3$). Groups identified by the same superscript letter are not statistically different. ($P \geq 0.05$).

As expected, excellent results of cell proliferation were obtained, which means no cytotoxic effects were found for any of the different materials studied. These results are in agreement with other authors. For instance, a study compared cell proliferation of tricalcium phosphate (TCP) material doped with ZnO and SiO₂. They used human osteoblast cells to determine the influence of dopants on the cell-materials interaction, obtaining better results in cell proliferation in the doped samples compared with pure TCP. We have fabricated SiMS-GP samples composed of TPI, ZnO, BaSO₄, wax and SiMS. As showed in *Figure 1.15*, SiMS-GP group together with SiMS samples, have obtained the highest results in cell proliferation rate after 3 days of the experiment (105 and 106% respectively) ⁶⁴. Another study used a root canal filling material based on GP, polyethylene and hydroxyapatite particles of 3-5 μm to study the indirect cytotoxicity of the material. The eluates showed no statistically significant

differences from the control group ⁷⁵. Glass-ionomer coated GP (ActiV GP) has its own sealer made of barium aluminosilicate glass powder and polyacrylic acid. This material is claimed to bond to dentin tissue, fluoride release, antimicrobial activity and biocompatibility. ActiV GP has a 2- μ m coating of glass ionomer particles on its surface and also into the body of the GP cone ⁷⁶. Compared with SiMS-GP, ActiV GP has the drawback that it must be used with a sealer material, undergoing two bonding phases instead of only one, with a higher possibility of failure rate if the bonding is not accomplished. Moreover, it consumes more time which hinders the filling procedure. Recently, a bioactive glass GP-based root canal filling material has been proposed. It consists of glass nanoparticles (45S5) incorporated into GP. The material has been studied in terms of cytotoxicity using human osteoblasts in an indirect assay. They did not find differences among the experimental material compared to conventional GP after 24 hours of cell culture ⁷⁷. In our study, we assessed the cytotoxic effects during 1 and 3 days in order to follow cell activity at higher time intervals, because at lower time the material may not be releasing its products. Our results showed an enhancement of rMSCs proliferation in SiMS-GP group, after 3 days exposure of 1:50 material dilution, compared with the rest of groups.

Moreover, current research in the field of endodontics is focused on studying new materials with bioactive molecules-incorporated in order to progressively release them. For example, growth factors that could favour MSCs multiplication and differentiation ⁶⁹. That research agree with our in terms that we proposed microspheres incorporation to GP material in order to introduce, in the near future, bioactive molecules or drugs, to induce a response in periapical tissues with the aim to enhance the endodontic treatment outcome.

4.2.5 Sealing ability

Sealing ability assay was performed in order to confirm the *in vitro* capacity of SiMS-GP biomaterial to fill the canals, both on dental training blocks and on extracted teeth.

- **On dental training blocks**

Dental training blocks (or simulated root canals) were instrumented and filled with comGP and 10-SiMS-GP in triplicate and then stained with a blue dye to assess the possible filtration within the simulated root canals. This assay was performed to reproduce the possible bacteria or fluid filtration within the biomaterial and dentin tissue. *Figure 1.16A* shows the different samples with the cone shape (like is used in the clinic), before cut and condensed using a heated instrument in order to fill the simulated root canal. *Figure 1.16B* shows the blue stain within the standardized samples. A greater amount of blue dye filtration can be observed in the comGP samples compared with the SiMS-GP samples after 2 weeks of the experiment. The figure also shows the optimal adaptation of SiMS-GP which was hand-rolled, compared with the comGP which has been prefabricated at the same taper and diameter as the files used for instrumenting the canals.

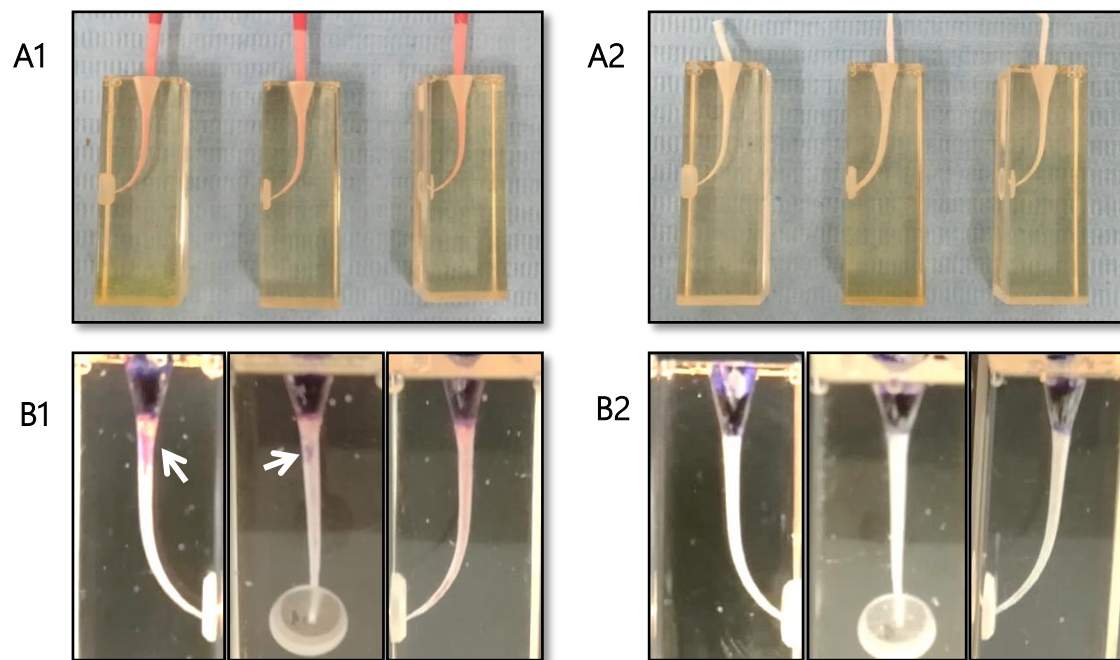


Figure 1.16. Macroscopic images of standardized dental training blocks used as simulated root canals filled with comGP cones (**A1, B1**) and SiMS-GP cones (**A2, B2**) and stained, after 14 days of the experiment. Arrows show the blue stain filtration.

Our results agrees with previous research in which they compared dye leakage on simulated root canals filled with comGP, Resilon, polyisoprene polymer coated with 30 wt% bioactive glass nanoparticles and polycaprolactone polymer coated with bioactive glass nanoparticles. They concluded that there was no leakage in both experimental polymers with bioactive glass, compared with comGP and Resilon, which showed coronal leakage¹². Several studies are in agreement that one of the main undesirable property of GP is leakage because of the lack of adhesiveness between the polymer and the dentin tissue^{78,79,80,81}. Commercial GP and self-fabricated GP may plasticize at different temperatures and behave differently when compacted. Consequently, it may be questionable whether optimal three-dimensional filling could be realized with different GP products without knowledge of the physical events involved

⁸². Usually, commercial GP may have plasticizers that our GP does not, making a difference in the sealing outcome on simulated root canals.

- **On extracted teeth**

The final step in order to better evaluate the sealing ability of SiMS-GP material was to introduce it on extracted teeth. Teeth were instrumented and filled with single-cone technique (and without any sealer as it was not the purpose of this study) with self-fabricated GP and 10-SiMS-GP. Single-root maxillary teeth were used to simplify the filling procedure and to allow greater overall amount of filling material to place within the canal, accordingly allowing any differences to be noted more easily ⁸³. *Figure 1.17* shows the extracted teeth used for this assay and the teeth digital radiography images showing the root canal fillings (RCF).

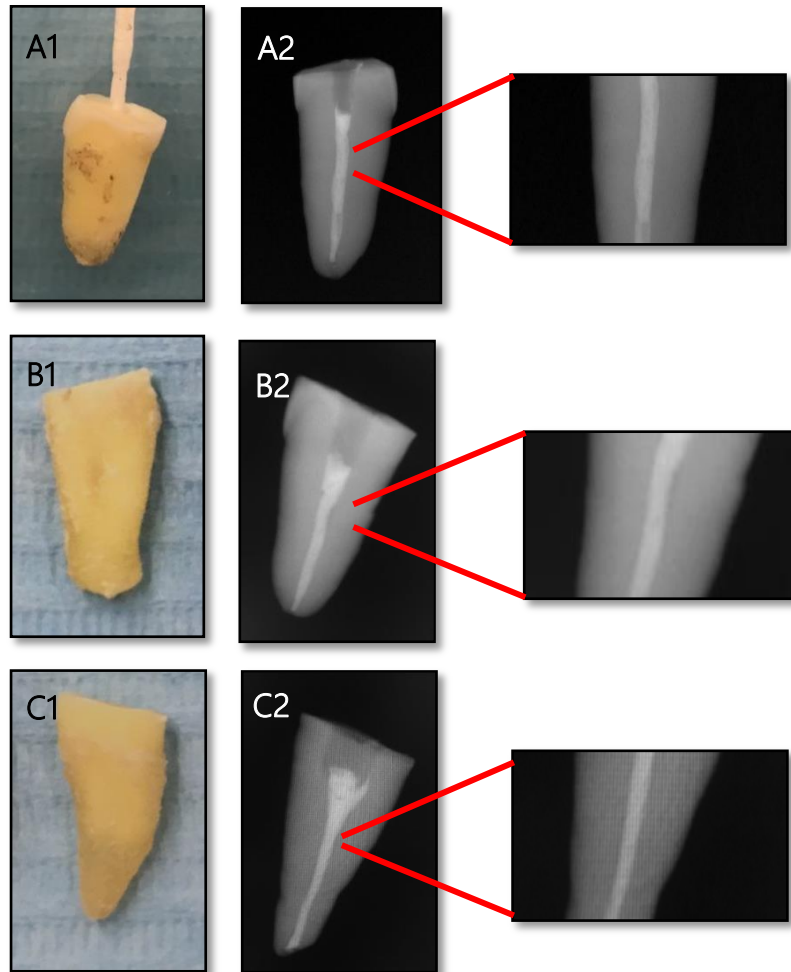


Figure 1.17. Macroscopic and X-ray digital images of extracted teeth filled with **(A,B)** SiMS-GP cones and **(C)** self-fabricated GP cone.

The radiopacity of SiMS-GP is not uniform because SiMS did not have any radiopaque element within them, such as barium sulphate, which is incorporated in the composite. However, both GP and SiMS-GP seem to fill in an acceptable manner all the root canal longitude. The tooth apical part is not well filled because of the complexity of hand-rolling the cones samples and not having a standard machine to uniformly manufacture them. Knowing that, the root coronal and middle thirds are able to be compared between both GP samples; but the apical third would not be able to be compared with.

Recently, *Lee et al.* have manufactured a nanodiamond-loaded GP functionalized with an antibiotic. They have also assessed the biomaterial sealing ability with X-ray digital radiography. They have used one tooth sample for commercial GP and another for ND-GP ²⁸. There were not differences noted between the different materials. In their case, they have used nanodiamond nanoparticles, which may not affect visually in radiopacity properties. In our case, we have used silica microparticles, and even the components were homogeneously mixed by sonication, the fact that SiMS do not have a radiopacifier component itself, may have affected visually on the radiopacity property. This fact could be enhanced by founding a more standardized protocol to mix the SiMS with the GP matrix. For instance, by using a spin mixer that would be able to mix more homogeneously these type of materials. Moreover, SiMS may be placed both inside and on the GP surface, in order to ensure the contact between dentin and SiMS.

GP shrinkage during cooling is an important drawback that might jeopardize the seal of the root canal ^{84,85}. Silica, among other solid materials such as calcium carbonate, have been used as a filler for reducing shrinkage of a variety of polymers in the building industry ⁸⁶. Recently, silica nanoparticles have been studied as filler in order to improve polymer composites properties. The advantages of these particles may include reinforcement with excellent mechanical strength, heat stability and reduced shrinkage ⁸⁷. For that reason, we hypothesize that SiMS-GP may enhance the longevity of root canal therapy, minimizing the polymer shrinkage thus reducing gaps within GP material, due to silica microparticles incorporation. Nevertheless, we think that a higher concentration of SiMS within the composite may enhance this ability, as the bioceramic proportion will be greater. When comparing a potential use of SiMS-GP towards bioactive glass (BAG) material as RCF, we state that SiMS-GP has more advantages referring specifically in this treatment. For instance, the

manufacturing conditions of BAG are at high temperatures (around 600°C)^{88,89}, comparing with mild conditions of SiMS-GP fabrication, allowing the incorporation of biomolecules. Furthermore, knowing that an important characteristic of a RCF is to be able to perform a retreatment, in the case of BAG material this option would not be able to be performed; instead, using GP material as a matrix, the retreatment could be done. Finally, the material must have a good handle property in order to place it inside the root canal system complexity. Thus, we think SiMS-GP may accomplish better with these requirements.

Moreover, with the known capacity of these platforms to incorporate and have a sustained release of biomolecules, during some hours or few days, SiMS-GP would deal with bacteria resistance problems, which is one of the main causes of oxidative process of GP degradation and endodontic failure⁴¹.

5. Conclusions and future perspectives

The evidence from this study suggests that *trans*-polyisoprene can be combined with *cis*-polyisoprene, although the mechanical properties of the blend are lower than with pure *trans*-polyisoprene. The main principle of this fact is because the flowable state of *cis*-PI.

An important finding was that incorporating 10% SiMS into GP had increase its mechanical properties and had demonstrated bioactive capacity, compared with comGP. Moreover, incorporation of 10% SiMS carriers into GP material had demonstrated no cytotoxic effects on rMSCs, and showed cell proliferation was maintained in the CCK-8 assay. Finally, 10-SiMS-GP had showed sealing ability both on simulated root canals and on extracted teeth, preventing filtration on simulated root canals.

Gutta-percha is an economic material and it has been given extensive use for more than 150 years. However, GP no longer lives up to the current advanced endodontic treatments. We have designed a biomaterial to be used as root canal filling, studying its mechanical properties, bioactivity, biocompatibility and sealing ability. Moreover, we hypothesize the filling technique may be simplified because clinicians will only use one biomaterial instead of two, reducing the working time. Recently, there has been a huge advancement in the area of root canal filling instruments technology in comparative with the root canal filling materials. Instrumentation is an important part of root canal treatments; however, the filling part is such a crucial step too. We must offer to our patients the best treatments combined with the best biomaterials, taking into account that we treat patients with different economic capacities. We think

that future assays must be done to complement our results, such as bioactivity assay and mechanical properties on extracted teeth, drug-incorporation in silica microspheres and *in vitro* release assays. We are positive about the future use of GP with SiMS-loaded-bioactive molecules, such as different drugs or growth factors, in order to obtain a sustained release from the biomaterial. In the case of GP-loaded-growth factors, the release would be in order to promote cell homing in open apex in cases with avulsioned teeth, or immature teeth with necrotic pulp. With this in mind, we think that in the near future, endodontic field will be able to individualize the treatments enhancing the outcomes, with the same final objective which is collaborate into patient's health. Moreover, knowing that approximately 15 million of root canal treatments are effectuated per year only in the USA, we consider that the introduction of SiMS-GP biomaterial in the Endodontic field would be a competitive and viable possibility. Taking together, this study represents a clinically translatable approach of a bioactive endodontic material for preventive treatments.

6. References

1. Tay, F. R. & Pashley, D. H. Monoblocks in root canals - a hypothetical or a tangible goal. *J Endod* **33**, 391–398 (2007).
2. Fisher, D. Crystal Structures of Gutta Percha. *Proc. Phys. Soc. Sect. B* **66**, 1–16 (1952).
3. Schilder, H., Goodman, A. & Winthrop, A. The thermomechanical properties of gutta-percha I. The compressibility of gutta-percha. *Oral Surgery, Oral Med. Oral Pathol.* **37**, 946–953 (1974).
4. Goodman, A., Schilder, H. & Aldrich, W. The thermomechanical properties of gutta-percha. Part IV. A thermal profile of the warm gutta-percha packing procedure. *Oral Surgery, Oral Med. Oral Pathol.* **51**, 544–551 (1981).
5. Maniglia-Ferreira, C., Gurgel-Filho, E. D., Silva-Jr, J. B. A. & Monteiro De Paula, R. C. Chemical composition and thermal behavior of five brands of thermoplasticized gutta-percha. *Eur. J. Dent.* **7**, 201–206 (2013).
6. Schäfer, E., Schrenker, C., Zupanc, J. & Bürklein, S. Percentage of Gutta-percha Filled Areas in Canals Obturated with Cross-linked Gutta-percha Core-carrier Systems, Single-Cone and Lateral Compaction Technique. *J. Endod.* **42**, 294–298 (2016).
7. Patel, E., Pradeep, P., Kumar, P., Choonara, Y. E. & Pillay, V. Oroactive dental biomaterials and their use in endodontic therapy. *J Biomed Mater Res B Appl Biomater* **108**, 201–212 (2019).
8. Jitaru, S., Hodisan, I., Timis, L., Lucian, A. & Bud, M. The use of Bioceramics in Endodontics - Literature Review. *Clujul Med.* **89**, 470–473 (2016).
9. Fisher, M. A., Berzins, D. W. & Bahcall, J. K. An In Vitro Comparison of Bond Strength of Various Obturation Materials to Root Canal Dentin Using a Push-Out Test Design. *J Endod* **33**, 856–858 (2007).
10. Al-haddad, A. Y., Kutty, M. G., Adura, Z. & Ab, C. Push-Out Bond Strength of Experimental Apatite Calcium Phosphate Based Coated Gutta-Percha. *Int. J. Biomater.* **2018**, 1–5 (2018).
11. Eltair, M., Pitchika, V., Hickel, R., Kühnisch, J. & Diegritz, C. Evaluation of the interface between gutta-percha and two types of sealers using scanning electron microscopy (SEM). *Clin Oral Invest* **22**, 1631–1639 (2018).

12. Mohn, D. *et al.* Composites made of flame-sprayed bioactive glass 45S5 and polymers: bioactivity and immediate sealing properties. *Int. Endod. J.* **2**, 1037–1046 (2010).
13. Carvalho, C. N., Martinelli, J. R., Bauer, J. & Haapasalo, M. Micropush-out dentine bond strength of a new gutta-percha and niobium phosphate glass composite. *Int Endod J* **48**, 451–459 (2015).
14. Santos, O., Coelho, M., Moreno, E., Vitor, P. & Luís, S. Effect of Root Repair Materials and Bioactive Glasses on Microhardness of Dentin. *Iran. Endod. J.* **13**, 337–341 (2018).
15. Perez, R. A. *et al.* Therapeutic bioactive microcarriers : Co-delivery of growth factors and stem cells for bone tissue engineering. *Acta Biomater.* **10**, 520–530 (2014).
16. Dashnyam, K., Jin, G.-Z., Kim, J.-H. & Perez, R. Promoting angiogenesis with mesoporous microcarriers through a synergistic action of delivered silicon ion and VEGF. *Biomaterials* **116**, 145–157 (2017).
17. Dashnyam, K. *et al.* Hybrid scaffolds of gelatin – siloxane releasing stromal derived factor-1 effective for cell recruitment. *J. Biomed. Mater. Res. - Part A* **102**, 1859–1867 (2014).
18. Perez, R. A., Seo, S., Won, J. & Lee, E. Therapeutically relevant aspects in bone repair and regeneration. *Biochem. Pharmacol.* **18**, 573–589 (2015).
19. Cheremisinoff, N. . Natural rubber. in *Condensed Encyclopedia of Polymer Engineering Terms* (ed. Butterworth-Heinemann) 183–192 (2001).
20. Rudin, A. & Choi, P. Ionic and Coordinated Polymerizations. in *The Elements of Polymer Science & Engineering* (eds. Rudin, A. & Choi, P.) 449–493 (2013).
21. Kent, E. . & Swinney, F. . Properties and applications of trans-1,4-polyisoprene. *Ind. Eng. Chem. Prod. Res. Dev.* **5**, 134–138 (1966).
22. Rodríguez, O. Estudio Espectroscópico de la Formación de Análogos de Resinas Fósiles. *Thesis* (2013).
23. Lo Giudice, G. *et al.* Dentine Morphology of Root Canal Surface: A Quantitative Evaluation Based on a Scanning Electronic Microscopy Study. *Biomed Res. Int.* **2015**, 1–7 (2015).
24. Yun, S. & Gao, Y. Superhydrophobic silica aerogel microspheres from methyltrimethoxysilane: rapid synthesis via ambient pressure drying and excellent absorption properties. *RSC Adv.* **4**, 4535–4542 (2014).
25. Alif, Z. *et al.* Dispersion of polymeric coated – silica aerogel particles in unsaturated

- polyester composites: Effects on thermal – mechanical properties. *J. Dispers. Sci. Technol.* **39**, 1093–1101 (2017).
26. Friedman, C. M., Sandrik, J. L., Heuer, M. A. & Rapp, G. W. Composition and mechanical properties of Gutta-Percha endodontic points. *J. Dent. Res.* **54**, 921–925 (1975).
 27. Möller, B. & Orstavik, D. Chemical and Energy-dispersive X-ray Analyses of Gutta-percha Points. *J Endod* **10**, 413–416 (1984).
 28. Lee, D.-K., Kim, S. V., Limansubroto, A. N. & Yen, A. Nanodiamond - Gutta Percha Composite Biomaterials for Root Canal Therapy. *ACS Nano* **9**, 11490–11501 (2015).
 29. Kokubo, T. & Takadama, H. How useful is SBF in predicting in vivo bone bioactivity? *Biomaterials* **27**, 2907–2915 (2006).
 30. Rodríguez-Lozano, F. J., Collado-González, M., Tomás-Catalá, C. J. & García-Bernal, D. GuttaFlow Bioseal promotes spontaneous differentiation of human periodontal ligament stem cells into cementoblast-like cells. *Dent. Mater.* **35**, 114–124 (2018).
 31. Ahuja, L., Jasuja, P., Verma, K. G. & Juneja, S. A Comparative Evaluation of Sealing Ability of New MTA Based Sealers with Conventional Resin Based Sealer: An In-vitro Study. *J. Clin. Diagnostic Res.* **10**, 76–79 (2016).
 32. Alhashimi, R. A. & Mannocci, F. Synthesis and Preliminary Evaluation of a Polyolefin-based Core for Carrier-based Root Canal Obturation. *J. Endod.* **38**, 983–986 (2012).
 33. Mohan, S. Vibrational Spectra of Cis-1,4-Polyisoprene. *Arab. J. Sci. Eng.* **29**, 17–26 (2004).
 34. Chen, D., Shao, H., Yao, W. & Huang, B. Fourier Transform Infrared Spectral Analysis of Polyisoprene of a Different Microstructure. *Int. J. Polym. Sci.* **2013**, 1–5 (2013).
 35. Baboo, M., Dixit, M. & Sharma, K. The Structure and Thermomechanical Properties of Blends of Trans-polyisoprene with Cis-polyisoprene. *Int. J. Polym. Mater. Polym. Biomater.* **58**, 636–646 (2009).
 36. Chen, Q., Liang, S. & Thouas, G. A. Elastomeric biomaterials for tissue engineering. *Prog. Polym. Sci.* **38**, 584–671 (2013).
 37. Manappallil, J. J. *Basic Dental Materials Book*. (2016).
 38. Bharath, R. K. *Fundamentals of Oral Anatomy, Physiology and Histology*. (2018).
 39. Poochai, C., Pae-on, P. & Pongpayoon, T. Polyisoprene-coated Silica/Natural rubber Composite. *World Acad. Sci. Eng. Technol.* **41**, 969–973 (2010).

40. Jr, A. S. *et al.* In Vivo Aging of Gutta-Percha Dental Cone. *J. Appl. Polym. Sci.* **100**, 4082–4088 (2006).
41. Maniglia-Ferreira, C., Valverde, G. B., Silva JR, J. B. A. & de Paula, R. C. M. Clinical Relevance of Trans 1,4-Polyisoprene Aging Degradation on the Longevity of Root Canal Treatment. *Eur. J. Dent.* **18**, 97–101 (2007).
42. Novak, B. M. Hybrid Nanocomposite Materials—Between Inorganic Glasses and Organic Polymers. *Adv. Mater.* **5**, 422–433 (1993).
43. Donnet, J. B. Nano and microcomposites of polymers elastomers and their reinforcement. *Compos. Sci. Technol.* **63**, 1085–1088 (2003).
44. Guseva, D. V *et al.* Molecular-dynamics simulations of thin polyisoprene films confined between amorphous silica substrates Molecular-dynamics simulations of thin polyisoprene films confined between amorphous silica substrates. *J. Chem. Phys.* **140**, 1–14 (2014).
45. Papon, P., Leblond, J. & Meijer, P. H. E. Gelation and Transitions in Biopolymers. in *The Physics of Phase Transitions: Concepts and Applications* 190–191 (2007).
46. Kandyrin, K. L. & Karpova, A. N. Basic approaches to creating bonds between silica filler and rubber. *Int. Polym. Sci. Technol.* **33**, 71–76 (2006).
47. Ochs, H., Bublak, D., Wild, U., Muhler, M. & Kolbesen, B. O. Depth distribution of zinc adsorbed on silicon surfaces out of alkaline aqueous solutions. *Appl. Surf. Sci.* **133**, 73–83 (1998).
48. Chieruzzi, M. *et al.* Nanomaterials for Tissue Engineering In Dentistry. *Nanomaterials* **6**, 9–13 (2016).
49. Teixeira, F. B., C., T. E., Thompson, J. Y. & Trope, M. Fracture resistance of roots endodontically treated with a new resin filling material. *J. Am. Dent. Assoc.* **135**, 646–652 (2004).
50. Kazandag, M. K., Sunay, H., Tanalp, J. & Bayirli, G. Fracture resistance of roots using different canal filling systems. 705–710 (2009). doi:10.1111/j.1365-2591.2009.01571.x
51. Tsukada, G., Tanaka, T., Torii, M. & Inoue, K. Shear modulus and thermal properties of gutta percha for root canal filling. *J. Oral Rehabil.* **31**, 1139–1144 (2004).
52. Friedman, C. E., Sandrik, J. L., Heuer, M. A. & Rapp, G. W. Composition and physical properties of gutta-percha endodontic filling materials. *J Endod* **3**, 304–308 (1977).
53. Williams, C., Loushine, R. J., Weller, R. N., Pashley, D. H. & Tay, F. R. A Comparison of

- Cohesive Strength and Stiffness of Resilon and Gutta-Percha. *J Endod* **32**, 553–555 (2006).
54. Maitra, U., Prasad, K. E., Ramamurty, U. & Rao, C. N. R. Mechanical properties of nanodiamond-reinforced polymer-matrix composites. *Solid State Commun.* **149**, 1693–1697 (2009).
55. Ovid'ko, I. A. Enhanced mechanical properties of polymer-matrix nanocomposites reinforced by graphene inclusions: A Review. *Rev. Adv. Mater. Sci* **34**, 19–25 (2013).
56. Baboo, M., Dixit, M., Sharma, K. & Saxena, N. S. of cis -polyisoprene and trans -polyisoprene blends. 661–672 (2011). doi:10.1007/s00289-010-0378-7
57. Sharma, S., Srivastava, D., Grover, S. & Sharma, V. Biomaterials in Tooth Tissue Engineering: A Review. *J. Clin. Diagnostic Res.* **8**, 309–316 (2014).
58. Oyane, A. *et al.* Sol-gel modification of silicone to induce apatite-forming ability. *Biomaterials* **20**, 79–84 (1999).
59. Vallet-Regí, M. & Salinas, A. J. *Sol-Gel Silica-Based Biomaterials and Bone Tissue Regeneration*. (In: Klein L., Aparicio M., Jitianu A. (eds) Handbook of Sol-Gel Science and Technology. Springer, Cham, 2016).
60. Ballarre, J. & Ceré, S. M. *Bioactive Silica-Based Coating on Stainless Steel Implants*. (In: Klein L., Aparicio M., Jitianu A. (eds) Handbook of Sol-Gel Science and Technology. Springer, Cham, 2016).
61. Turnbull, G. *et al.* 3D bioactive composite scaffolds for bone tissue engineering. *Bioact. Mater.* **3**, 278–314 (2017).
62. Angelopoulou, A., Efthimiadou, E. K., Boukos, N. & Kordas, G. A new approach for the one-step synthesis of bioactive PS vs. PMMA silica hybrid microspheres as potential drug delivery systems. *Colloids Surfaces B Biointerfaces* **117**, 322–329 (2014).
63. Fielding, G. A., Bandyopadhyay, A. & Bose, S. Effects of silica and zinc oxide doping on mechanical and biological properties of 3D printed tricalcium phosphate tissue engineering scaffolds. *Dent. Mater.* **28**, 113–122 (2011).
64. Bandyopadhyay, A., Bernard, S., Xue, W. & Bose, S. Calcium Phosphate-Based Resorbable Ceramics: Influence of MgO, ZnO, and SiO₂ Dopants. *J. Am. Ceram. Soc.* **89**, 2675–2688 (2006).
65. Ørstavik, D., Nordahl, I. & Tibballs, J. E. Dimensional change following setting of root canal sealer materials. *Dent. Mater.* **17**, 512–519 (2001).

66. Al-haddad, A. *et al.* Physicochemical Properties of Calcium Phosphate Based Coating on Gutta-Percha Root Canal Filling. *Int. J. Polym. Sci.* **2015**, 1–5 (2015).
67. Prati, C. & Giovanna, M. Calcium silicate bioactive cements: Biological perspectives and clinical applications. *Dent. Mater.* **31**, 351–370 (2015).
68. Gandolfi, M. G., Siboni, F. & Prati, C. Properties of a novel polysiloxane-guttapercha calcium silicate-bioglass-containing root canal. *Dent. Mater.* **32**, 113–126 (2016).
69. Leprince, J. G., Zeitlin, B. D., Tolar, M. & Peters, O. A. Interactions between immune system and mesenchymal stem cells in dental pulp and periapical tissues. *Int Endod J* **45**, 689–701 (2012).
70. Collado-González, M., Tomás-Catalá, C. J., Oñate-Sánchez, R. E. & Moraleda, J. M. Cytotoxicity of GuttaFlow Bioseal, GuttaFlow2, MTA Fillapex, and AH Plus on Human Periodontal Ligament Stem Cells. *J Endod* **43**, 816–822 (2017).
71. Shie, M., Ding, S. & Chang, H. The role of silicon in osteoblast-like cell proliferation and apoptosis. *Acta Biomater.* **7**, 2604–2614 (2011).
72. Hongxu, L. *et al.* In vitro Proliferation and Osteogenic Differentiation of Cultured with Hardystonite (Ca₂ZnSi₂O₇) and β-TCP Ceramics. *J. Biomater. Appl.* **25**, (2010).
73. Sun, J. *et al.* Proliferation and gene expression of osteoblasts cultured in DMEM containing the ionic products of dicalcium silicate coating. *Biomed. Pharmacother.* **63**, 650–657 (2009).
74. Zou, S., Ireland, D., Brooks, R. A., Rushton, N. & Best, S. The Effects of Silicate Ions on Human Osteoblast Adhesion, Proliferation, and Differentiation. *J Biomed Mater Res B Appl Biomater* **90B**, 123–130 (2009).
75. Alhashimi, R. A., Mannocci, F., Foxton, R. & Deb, S. Fabrication and characterisation of polymer composites for endodontic use. *Int Endod J* **47**, 574–582 (2013).
76. Fransen, J. N., He, J. & Glickman, G. N. Comparative Assessment of ActiV GP/Glass Ionomer Sealer, Resilon/Epiphany, and Gutta-Percha/AH Plus Obturation: A Bacterial Leakage Study. *J Endod* **34**, 725–727 (2008).
77. Nascimento, J. *et al.* Cytocompatibility of a self-adhesive gutta-percha root-filling material. *J Conserv Dent* **20**, (2017).
78. Suzuki, Y., Hayashi, M., Yasukawa, T., Kobayashi, H. & Makino, K. Development of a novel fluorapatite-forming calcium phosphate cement with calcium silicate: In vitro and in vivo characteristics. **34**, 263–269 (2015).

79. Shipper, G., Ørstavik, D., Teixeira, F. B. & Trope, M. An Evaluation of Microbial Leakage in Roots Filled with a Thermoplastic Synthetic Polymer-Based Root Canal Filling Material (Resilon). *J Endod* **30**, 342–347 (2004).
80. Shanahan, D. J. & Duncan, H. F. Root canal filling using Resilon: a review. *Br. Dent. J.* **211**, 81–88 (2011).
81. Selem, L. C. *et al.* Quality of Obturation Achieved by a Non–gutta-percha–based Root Filling System in Single-rooted Canals. *J. Endod.* **40**, 2003–2008 (2014).
82. Venturi, M., Lenarda, R. Di & Breschi, L. An ex vivo comparison of three different gutta-percha cones when compacted at different temperatures: rheological considerations in relation to the filling of lateral canals. *Int. Endod. J.* **39**, 648–656 (2006).
83. James, B. L., Brown, C. E., Legan, J. J., Moore, B. K. & Vail, M. M. An In Vitro Evaluation of the Contents of Root Canals Obturated With Gutta Percha and AH-26 Sealer or Resilon and Epiphany Sealer. *J. Endod.* **33**, 1359–1363 (2007).
84. Al-Maswary, A. A., Alhadainy, H. A. & Al-Maweri, S. A. Coronal Microleakage of the Resilon and Gutta-Percha Obturation Materials with Epiphany SE Sealer : An in-vitro Study. *J. Clin. Diagnostic Res.* **10**, 39–42 (2016).
85. Hammad, M., Qualtrough, A. & Silikas, N. Extended Setting Shrinkage Behavior of Endodontic Sealers. **34**, 90–93 (2008).
86. Bakis, C. E. Fiber-Reinforced-Plastic (FRP) Reinforcement for Concrete Structures: Properties and Applications. in *Developments in Civil Engineering* (ed. Nanni, A.) 36–37 (Elsevier, 1993).
87. Rahman, I. A. & Padavettan, V. Synthesis of Silica Nanoparticles by Sol-Gel: Size-Dependent Properties, Surface Modification, and Applications in Silica-Polymer Nanocomposites—A Review. *J. Nanomater.* **2012**, 1–15 (2012).
88. Hench, L. L. The story of Bioglass. *J Mater Sci Mater Med* **17**, 967–978 (2006).
89. Li, R., Clark, A. E. & Hench, L. L. An Investigation of Bioactive Glass Powders by Sol-Gel Processing. *J. Appl. Biomater.* **2**, 231–239 (1991).

7. List of figures

FIGURE 1.1. (A). Two of the stereospecific polyisoprenes that can be obtained with the polymerization of several units of isoprene. (B) Geometric isomery of *trans* and *cis* polyisoprenes (PI). Adapted from ²² 74

FIGURE 1.2. Schematic diagram for the preparation of silica microspheres by the sol-gel process. TEOS, tetraethyl orthosilicate; NH₄OH, ammonium hydroxide; SiMS, silica microspheres. Modified from ^{24,25}. 78

FIGURE 1.3. Schematic representation of the Gutta-percha containing silica based microspheres and the precipitation of hydroxyapatite on the surface of the material that will eventually enhance the bonding ability to dentin. 82

FIGURE 1.4. Structures of WST-8 and WST-8 formazan. Modified from manufacturer's protocol. 85

FIGURE 1.5. Optical microscopy images of (A) TPI (B) TPI/CPI 70/30 (C) TPI/CPI 60/40. Scale bars: 200 μm . 89

FIGURE 1.6. FTIR spectrum showing chemical bond structure of the different samples at different *trans*- isomer concentrations: TPI, TPI/CPI 70/30, TPI/CPI 60/40 and CPI. 91

FIGURE 1.7. FTIR spectrum showing chemical bond structure of the different samples at different *trans*- isomer concentrations: TPI, TPI/CPI 70/30, TPI/CPI 60/40 and CPI. (A) Region from 4000-1800- cm^{-1} (B) Region from 1800-600 cm^{-1} . 92

FIGURE 1.8. Mechanical properties of the different samples at different *trans* and *cis* isomer concentrations: TPI, TPI/CPI 70/30 and TPI/CPI 60/40 compared with comGP. Data are shown as mean \pm standard error (n = 10). Groups identified by the same superscript letter are not statistically different (P \geq 0.05). 95

FIGURE 1.9. Images of (A1) TPI (A2,A3) 10-SiMS-TPI (B1) GP (B2,B3) 10-SiMS-GP (C1) comGP (C2,C3) SiMS; SEM images (A1, A2, B1, B2, C1, C2) scale bars: 30 μm ; optical microscopy images (A3,B3,C3) scale bars A3, B3: 100 μm ; C3 500 μm . Arrows show SiMS within the materials. 98

FIGURE 1.10. FTIR spectrum showing chemical bond structure of the different samples: GP, 10-SiMS-GP and SiMS alone. 99

FIGURE 1.11. FTIR spectrum divided by regions showing chemical bond structure of the different samples: GP, 10-SiMS-GP and SiMS alone. **(A)** Region from 3200-2600 cm^{-1} **(B)** Region from 2600-500. 100

FIGURE 1.12. Mechanical properties of GP samples with and without 5 and 10% of SiMS incorporation: GP, 5-SiMS-GP and 10-SiMS-GP compared with comGP. Data are shown as mean \pm standard error ($n = 10$). Groups identified by one of the same superscript letter are not statistically different. ($P \geq 0.05$). 103

FIGURE 1.13. SEM micrographs for the different samples with or without 10% SiMS incorporation and with or without immersion in simulated body fluid (SBF) for 21 days at 37°C. SiMS and 10-SiMS-GP samples show the apatite forming ability on its surface (red arrows). On the left of each SEM image the representation of EDS spectrums that come from the scanning electron beam of the surface of the micrographs. SiMS and 10-SiMS-GP samples show calcium phosphates that are not showed in the rest of samples, meaning there is apatite forming ability on these samples. Scale bars 30 μm . 107

FIGURE 1.14. Optical microscopy images of rMSCs. Good cell morphology is observed with the eluates of the different biomaterials and the control group with basal medium at days 1 and 3 of the experiment. Scale bars 100 μm . 110

FIGURE 1.15. CCK-8 for the proliferation rate of rMSCs after 1 and 3 days of exposure to conditioned medium of different materials (1:50 concentration). Red horizontal dot line indicates 80% of viability. Data are shown as mean \pm standard deviation ($n = 3$). Groups identified by the same superscript letter are not statistically different. ($P \geq 0.05$). 112

FIGURE 1.16. Macroscopic images of standardized dental training blocks used as simulated root canals filled with comGP cones **(A1, B1)** and SiMS-GP cones **(A2, B2)** and stained, after 14 days of the experiment. Arrows show the blue stain filtration. 115

FIGURE 1.17. Macroscopic and X-ray digital images of extracted teeth filled with **(A,B)** SiMS-GP cones and **(C)** self-fabricated GP cone. 117

8. List of tables

TABLE 1.1. Samples studied and codes used for this chapter. The main variable studied was the SiMS percentage (5 and 10%) within TPI or GP composites. **79**

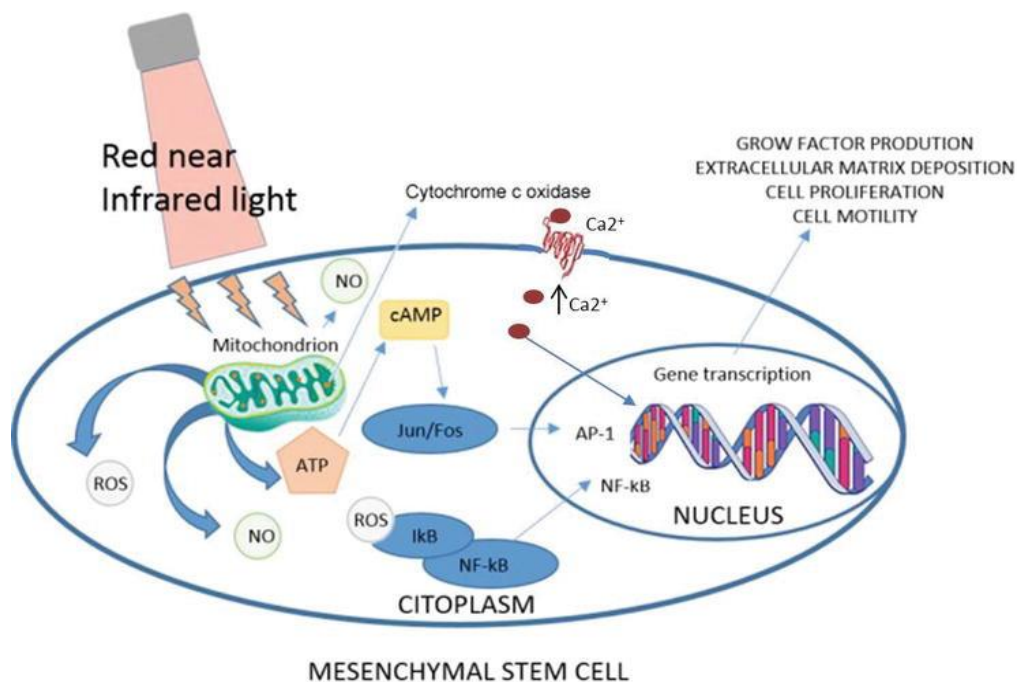
TABLE 1.2. Order and amounts of reagents for preparing 1000 mL of SBF ²⁹. **81**

TABLE 1.3. Main FTIR bands observed for the three different samples. The same bands were observed for all the studied materials: TPI, TPI/CPI 70/30 and TPI/CPI 60/40. **93**

TABLE 1.4. Main FTIR bands observed for the three different samples: GP, 10-SiMS-GP and SiMS. **101**

Chapter 2

Low-level Laser Therapy for Bone Regeneration



1. Introduction

This chapter is focused on low level laser therapy (LLLT) which may be used as an adjuvant treatment for bone regeneration defects. One of the main situations in which this objective has to be achieved is when conservative dental treatments cannot be applied and at that time the tooth must be extracted. This procedure entails maxillary bone resorption that has to be repaired in order to replace the tooth with a dental implant in a prosthetically suitable position ^{1,2}. As explained at *section 4.2.2* in the general **Introduction (Bone substitutes)**, bone grafting is one of the most commonly used surgical methods to replace missing bone. This procedure may be accomplished by using material from patient's own body, synthetic or natural material substitute ³. Although bone grafting is a good option for this purpose, the healing process of bone defect is time-consuming ^{4,5}. To address this challenge, LLLT has been suggested for clinical use as an adjuvant treatment to accelerate bone regeneration. This therapy has increased in popularity and is being used by clinicians not only for the enhancement of wound healing, but also to modulate and stimulate the potential for bone remodeling and repair ^{6,7}. In this context, several authors affirm that this process may act by the modulation of various biological and metabolic processes both *in vitro* and *in vivo* ^{8,9,10}. They observed that there is a photochemical conversion of the energy absorbed by photoacceptor molecules. These molecules can transfer the energy to another molecule, causing chemical reactions in the surrounding tissue ⁹. For instance, by increasing mitochondrial respiration and ATP synthesis, increasing DNA activity and the RNA and proteins synthesis ¹¹; consequently, there is an enhancement of osteoblastic activity, organization of collagen fibers and higher vascularization ^{10,12,13,14}. It has been reported that LLLT modulates this process by activating mitogen-activated protein kinase/extracellular signal-

regulated protein kinase (MAPK/ERK) phosphorylation in cells, inducing cell proliferation^{15,16,17}. However, the effects of laser therapy on bone remain controversial, as previous reports show different or conflicting results¹⁸. Such differences may be attributable to discrepancies in the radiation protocols and the experimental models used¹. Recently, a review has evaluated the outcome of LLLT for the treatment of maxillary bone defects showing positive results. They have reported that LLLT promotes an improvement of bone healing in the maxillofacial area¹. Nevertheless, mostly of them were qualitative analysis and no quantitative ones. It is important to consider that specific combinations of LLLT parameters can variate the results obtained^{1,19,20}. Besides, that differences between the parameters used in the studies difficult the issue of making meaningful comparisons²¹. It is possible that the laser effect on bone regeneration depends not only on the total dose, but also on the irradiation time and mode¹⁸. Importantly, it has been evaluated that low energy densities applied stimulates cell proliferation. However, higher energy densities have a suppressive action^{22,23}. That is why there is a need of clear and consistent methodology referring to the laser parameters to be used both *in vitro* and in clinical studies^{24,25,26}. We thus addressed this question, investigating the importance of laser irradiation during the stimulation of cells relation to energy density and time intervals. We think it will be highly useful to have an *in vitro* standardized protocol to extrapolate to the clinic. Regarding this, we wanted to study which was the minimum power range and time application of the laser which resulted to have optimal proliferation and osteogenic capacities, in order to analyze the results obtained to better understand the clinical outcomes.

2. Objectives

The main objective of this chapter is to analyze the LLLT *in vitro* effects both in cell proliferation and osteogenesis. For this purpose, we have established different output powers and different irradiation times to compare the results obtained.

- O1: To study different irradiation parameters to obtain the optimal mesenchymal stem cells proliferation rate
- O2: To determine the *in vitro* osteogenic response of mesenchymal stem cells after the irradiation by low-level laser therapy

3. Materials and methods

3.1 Cell culture

For the isolation of DPMSCs, healthy human third molars were extracted for orthodontic and prophylactic reason from patients with ages between 14 and 18 years old. All the experiments were performed in accordance with an ethics approved protocol from the Research Committee from the *Universitat Internacional de Catalunya*, under the project code IMR-2017-04 (supplementary data). The teeth were then washed with a gauze soaked in 70% ethanol, followed by a second wash with distilled water. The teeth apices were opened cutting the teeth and the dental pulp was extracted using a sterile nerve-puller file 15 and forceps. The dental pulp was then placed in falcon tubes that contained 1X phosphate-buffered saline (PBS) (Sigma-Aldrich) with 5% of 0.25% trypsin-EDTA and 1% Penicillin-Streptomycin (Thermo Fisher Scientific). Samples were transferred to the laboratory and they were digested

with 3 mg/mL collagenase type 1 (Sigma-Aldrich) at 37°C for 60 minutes. Disaggregated dental pulps were washed twice with PBS and the tissue extracts were then cultured in DPSC expansion medium in culture flasks, at 37°C in a 5% CO₂ incubator. The medium was composed of 60% DMEM low glucose (Sigma) and 40% MCDB (Sigma) supplemented with Insulin-Transferrin-Selenium (ITS) (Sigma), linoleic acid bovine serum albumin (LA-BSA) (Sigma), 10⁻⁹ M dexamethasone (Sigma), 10⁻⁴ M ascorbic acid 2-phosphate (Sigma), 1% penicillin/streptomycin (Sigma), 2% fetal bovine serum (Sigma), 10 ng/mL hPDGF-BB (R&D Systems), 10 ng/mL EGF (R&D Systems), Chemically Defined Lipid Concentrate (Gibco) and 0.8 mg/mL BSA (Sigma). The medium was changed every 2-3 days. When the cells reached 70% confluence, they were detached using TrypLE™ Express Enzyme (Thermo Fisher Scientific).

3.2 Laser irradiation

Laser irradiation was applied with a diode laser (SciCan Aseptim™ Denfotex Light Systems Ltd, Inverkeithing, Scotland) (*Figure 2.1*). The light source was emitted in a continuous beam at a wavelength of 635 nm. Three different output powers of 50, 70 and 100 mW were applied in a daily dose during a total of 10 days. For the calculation of the energy density, we used the irradiated beam area of the well-plates and the time dose applied. Then, the following equations were applied ^{27,28}:

$$1 \text{ mW} = 0,001 \text{ W}$$

$$\text{Energy density (J/cm}^2\text{)} = (\text{energy (J)} / \text{beam area (cm}^2\text{)}) \times \text{time irradiation (s)}$$

$$\text{Beam area (cm}^2\text{)} = \pi \text{ radio}^2$$

W=watt, J=joule, s=seconds

We have converted the output powers (50, 70 and 100 mW) into the energy density by multiplying by the time irradiation (seconds). The values used are showed in *Table 2.1*.

The output powers were chosen regarding the type of laser that we had, which had an output power from 50 to 100 mW, adjustable at intervals of 10 mW; besides, the selection of this parameters was made after evaluating that in different *in vitro* studies the range of output power used was from 30 to 110 mW²⁹. Then, 10 or 50 seconds of irradiation times were used in each group for the same laser output power in order to study different parameters and to evaluate which was the best one in this study. These irradiation times were chosen because they may be a no time-consuming in the clinic. Moreover, some clinical trials have used an irradiation time from 30 to 60 seconds obtaining good effect on tissue regeneration³⁰. The distance between the light source and the cells was set at a constant distance of 15 cm using a support for the laser instrument and the irradiation was perpendicularly applied above the culture plate containing the DPMSCs monolayer. Some of the wells within the plate were left empty in order to physically separate the groups to avoid a collateral irradiation. A group without laser irradiation served as the control. All the experiments were done in triplicates.



Figure 2.1. Low-level laser used for the experiments.

Output Power (mW)	Time of irradiation (s)	Energy density (J/cm ²)
50	10	0,5
	50	2,5
70	10	0,7
	50	3,5
100	10	1
	50	5

Table 2.1. Parameters used for cells irradiation in order to determine the effect of different power settings. mW=milliwatts, s=seconds, J=joules.

3.3 Cell morphology after laser irradiation

DPMSCs were re-plated in 24-well plates at a cell density of 10^3 cells/well during 24 hours before the performance of laser irradiation treatment. After 3 days of daily laser irradiation, cells morphology was assessed by optical microscopy images (Olympus CKX41, Nikon) in order to observe the overall cell morphology and to qualitatively evaluate their correct proliferation rate.

3.4 Cell proliferation assay

Meanwhile, cell viability was evaluated after 3 and 10 days of low-level laser irradiation using the commercial available CyQUANT Cell Proliferation Assay kit (Invitrogen) based on cells-DNA content. This assay uses a sensitive fluorescence-based method for quantifying cells and assessing cell proliferation and cytotoxicity, as shown in *Figure 2.2*. For that purpose, cells medium was removed and then cells were washed once with PBS gently, at each time point of the assay. Then, 200 μ L 0,1% Triton X-100 buffer per well was added to lyse the cells. Plates were frozen at -70°C for one week (until the experiment was finalized). After the freeze-thawing cycle, the DNA content was measured by CyQUANT cell proliferation assay kit following the manufacturer's instructions. Briefly, CyQUANT reagent dye was added in a volume of 100 μ L and incubated for 5 minutes protected from light at room temperature. Aliquots of each sample were placed on 96-well-plate with a sample volume of 100 μ L. A standard curve was performed with λ DNA provided with the kit and treated equally to the sample plates. Fluorescence signals (excitation 485 nm, emission 530 nm) were then determined spectrophotometrically with a multi-detection fluorescence microplate reader (Bio-Tek Synergy HT).

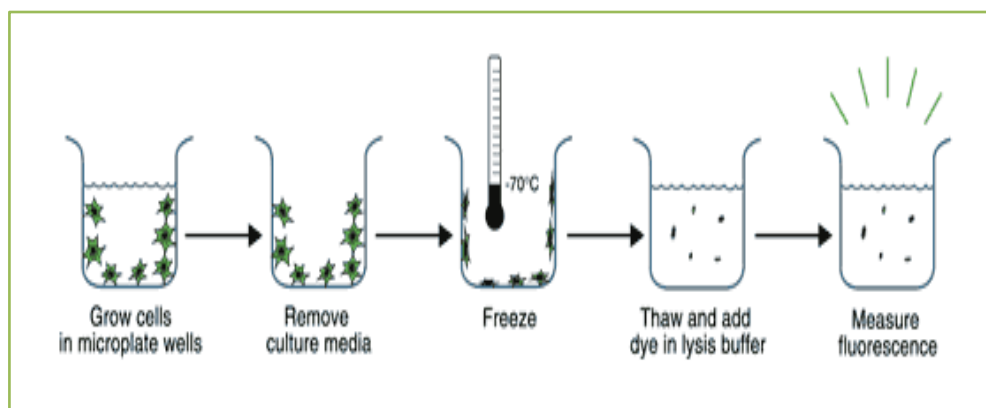


Figure 2.2. Workflow for CyQUANT Cell Proliferation Assays multiday tests. Quantitation of cells using the CyQUANT kit. Fluorescence measurements were made using a microplate reader with excitation at 485 nm and emission detection at 530 nm. Modified from manufacturer's protocol.

3.5 Cell osteogenic assay

First, cells were seeded in 24-well plates at a density of 10^3 cells/well enriched with osteogenic medium which was changed every 2 days. The osteogenic medium was composed of α -MEM containing 10% heat inactivated FBS, 10 mM β -glycerol phosphate, 50 μ M of L-ascorbic acid/Vit-C, 0.01 μ M dexamethasone and 1% penicillin/streptomycin. All products were obtained from Sigma-Aldrich. Then, cell osteogenic capacity was evaluated after the irradiation was applied at the same parameters showed in *section 3.2 Laser irradiation (Table 2.1)*. After 10 days of daily irradiation the assay was performed using the commercial available Alkaline Phosphatase (ALP) kit (BioSystems). ALP catalyses the hydrolysis of phosphate esters in alkaline buffer and produces an organic radical and inorganic phosphate. This is a cellular enzyme assay, which is based on the conversion of para-nitrophenylphosphate (p-NPP) to para-nitrophenol and on the determination of the resulting yellow coloured product by spectrophotometry. In short, Alkaline buffer solution and substrate solution (4 mg/mL) were mixed to obtain the working solution, by multiplying by the number of samples studied. The lysates obtained (as explained in the previous

section) were mixed with 20 μL of the working solution and incubated for 15 minutes at 37°C. The reaction was stopped with 1 M NaOH and the production of para-nitrophenol was determined by measuring its absorbance at 405 nm according to the manufacturer's instructions.

3.6 Statistical analysis

Statistical analysis was carried out with significance of 5%. One way analysis of variance (ANOVA) with Fisher post-hoc test was conducted. Data are expressed as mean \pm standard deviation. The results were statistically analyzed using Minitab (Minitab® Software Inc. 17.1.0) and GraphPad Prism version 6 (Graphpad Software Inc.) was used to graph the data.

4. Results and Discussion

4.1 Cell morphology after laser irradiation

Low-level laser therapy has been studied since early 1960s. The objective of using LLLT is to biomodulate cells by supplying light energy source. Its effects are non-thermal, but are considered to be mediated by a photochemical reaction that modifies cell membrane permeability, promoting increased mRNA synthesis and cell growth³¹. This reaction may be due to the light adsorption inside the mitochondria, or by cellular photoreceptors. Cellular photoreceptors are thought to be respiratory chain molecules, such as cytochrome C oxidase, which can adsorb the low level laser light and pass the energy to the mitochondria, increasing ATP production. At the same time, this fact produce cell intern changes in genetic intermediators, increasing protein synthesis and cellular proliferation. This phenomenon is the responsible of the

enhancement of tissue repair^{8,32,33}. Cells with stress condition, damaged or inflamed have a major adsorption due to a higher fluid content in the inflamed area^{27,34}. Recently, LLLT has been used to stimulate the proliferation of several cell types, including stem cells, which is essential for studying the different effects that may cause²².

In this study, we have first analyzed post-irradiation morphology of DPMSCs by optical microscopy images after 3 consecutive days of laser irradiation at different output powers comparing with non-irradiated cells (CT). The wavelength of the laser was 635 nm (*Figure 2.3*).

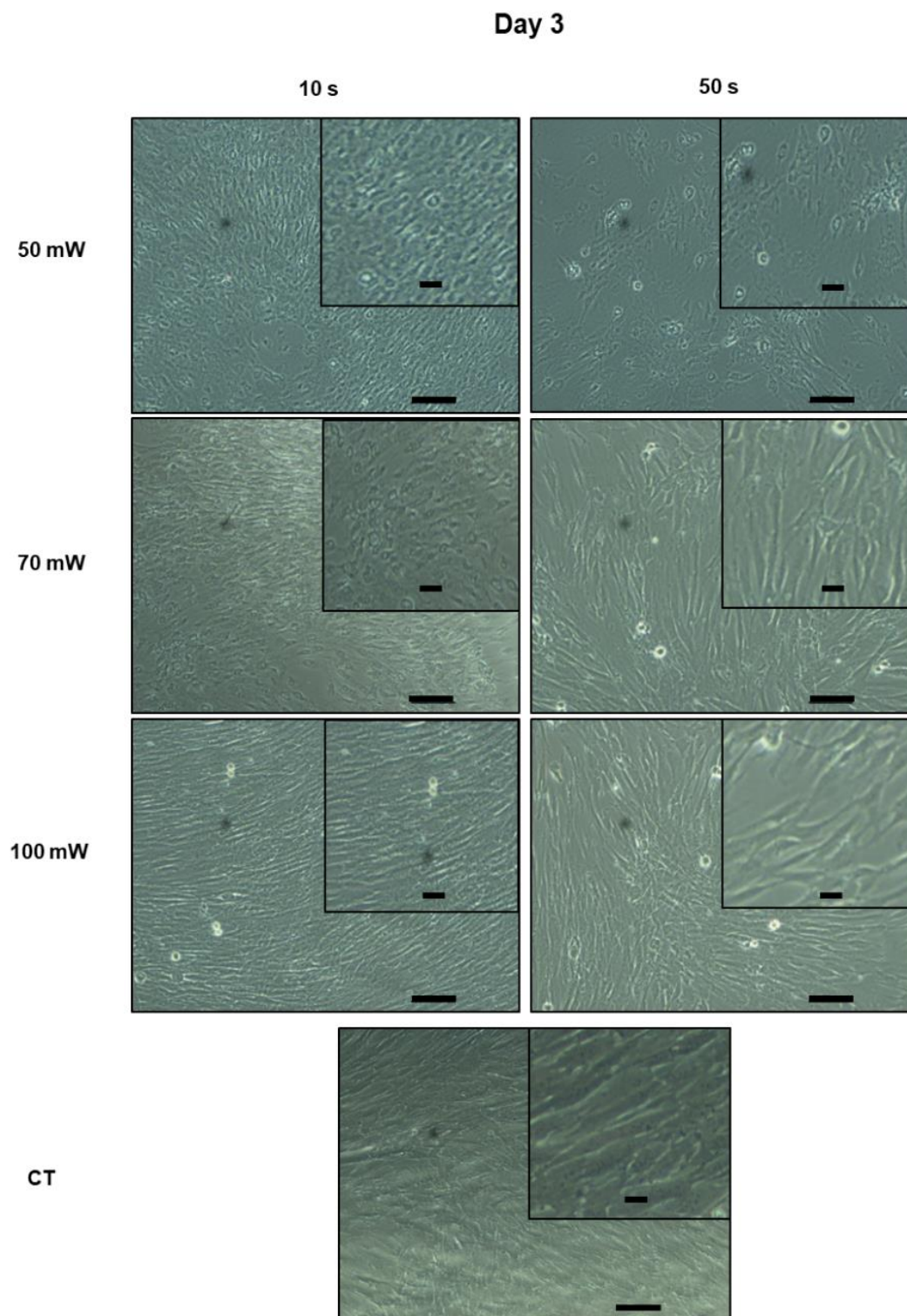


Figure 2.3. Optical microscopy images of DPMSCs after 3 days of low-level laser irradiation at different output powers (50, 70 and 100 mW) and at different irradiation times (10 and 50 seconds). Scale bar 100 μm .

The images show that DPMSCs have proliferated and were elongated in a normal way compared with the control group (CT). Apparently, no morphologic changes are visible between different laser treatments neither compared with the control. This fact may confirm that laser treatment applied at different doses do not affect cell viability and cell morphology. Other studies that have analyzed stem cells morphology after the irradiation with LLLT did not described differences between the irradiated and non-irradiated cells after 3 days of the experiment ^{35,36}.

4.2 Cell proliferation

In the present study, we aimed to make an approach of the clinical positive results by studying the effects of LLLT on DPMSCs isolated from human third molars. For this purpose, we have used a low-level laser with a wavelength of 635 nm which have been applied at different output powers of 50, 70 and 100 mW, and translated into different energy densities: 0.5, 0.7, 2.5, 3.5, 1 and 5 J/cm². The aim of this assay was to better understand the results of existing clinical treatments such as the acceleration of wound healing and maxillary bone repair, using this technique as an adjuvant therapy. Moreover, cell viability was quantitatively evaluated after 3 and 10 days of laser irradiation using the commercial available CyQUANT Cell Proliferation Assay kit. *Figure 2.4* shows the results of the assay with cell samples irradiated and non-irradiated.

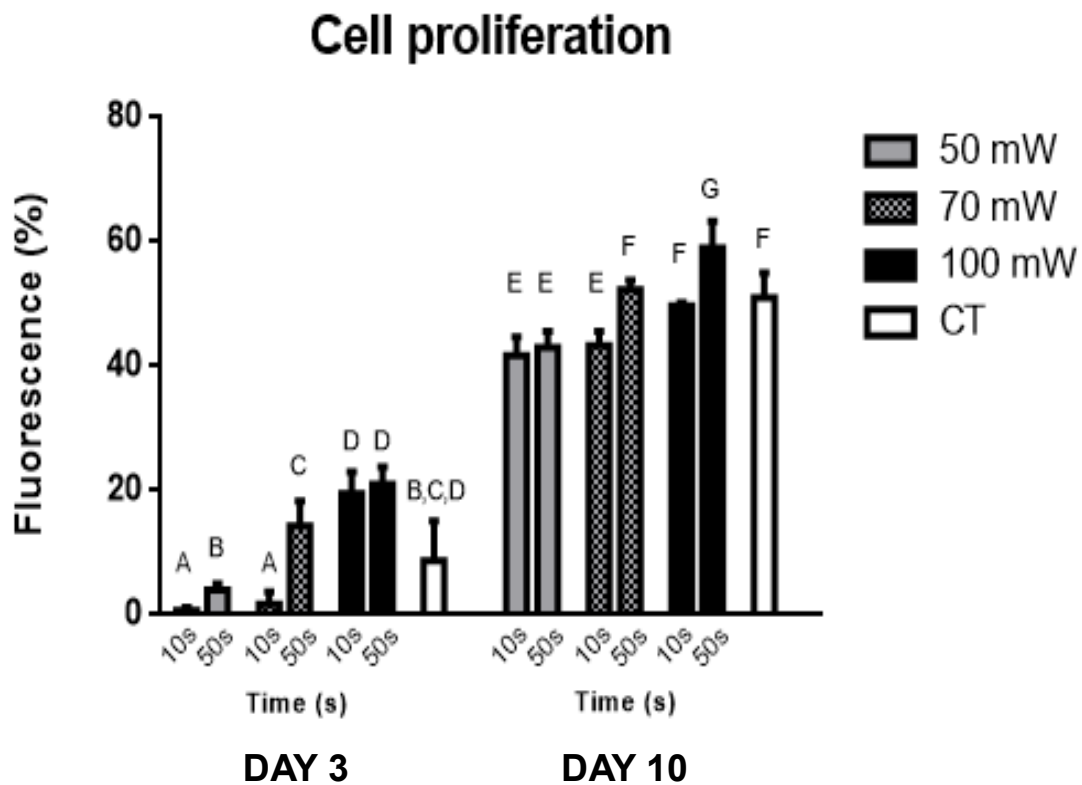


Figure 2.4. CyQUANT cell Proliferation Assay Kit was performed to analyze the proliferation of DPMSCs after 3 and 10 days of low-level laser irradiation at different output powers (50, 70 and 100 mW) at different time intervals (10 s = 10 seconds; 50 s = 50 seconds). Data are shown as mean \pm standard deviation ($n = 3$). Groups identified by one of the same superscript letter are not statistically different. ($P \geq 0.05$).

The graphic shows good cell proliferation capacity after LLLT application at different potencies and at different time dose, both after 3 and 10 days of the experiment. Moreover, after 3 days of treatment, the highest output powers at the largest irradiation time showed a significant increase in proliferation rate compared with lower potency and the control. These results are in accordance with *Oliveira et al.* who studied osteoblast viability and proliferation after irradiating the cells during 3 days with LLLT with an energy density of 10 J/cm^2 (Figure 2.5)³⁷. In our study, after 10 days of the experiment, the highest energy

density used (5 J/cm^2) presented significant higher values of cell proliferation compared with the rest of groups. Interestingly, only the group with the longest time and higher output power showed a significant increase regarding cell proliferation compared with the control. Another study demonstrated that after the irradiation at a wavelength of 636 nm and dose of 5 J/cm^2 promoted cell proliferation and viability on human adipose-derived stem cells, as well as the expression of proteins, like epidermal growth factor ³⁸.

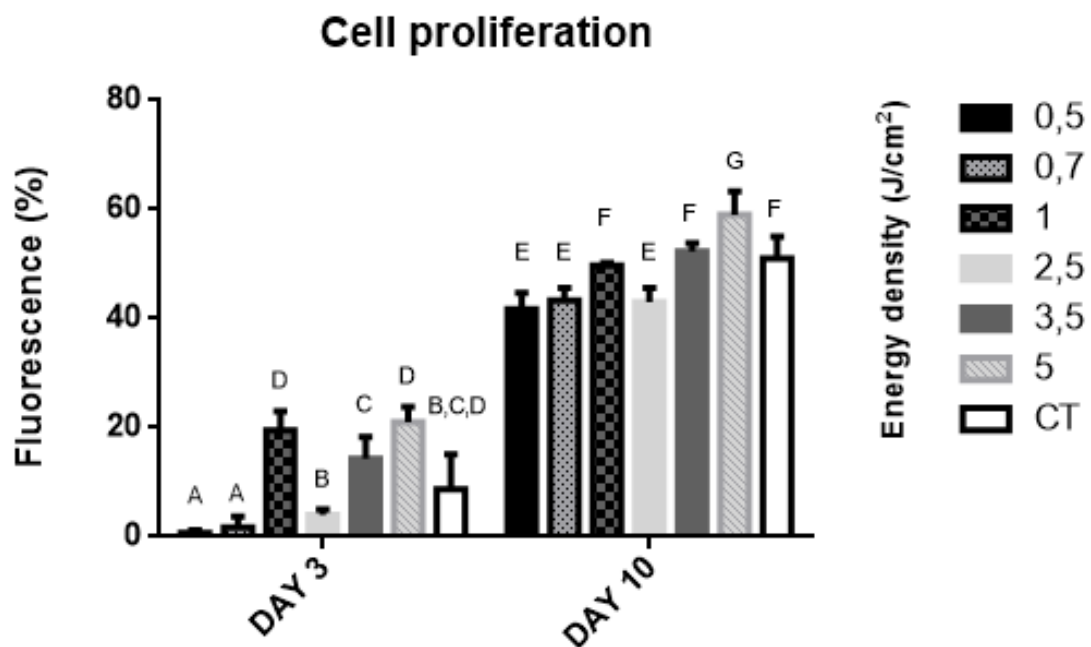


Figure 2.5. CyQUANT cell Proliferation Assay Kit expressed with energy density parameters. Data are shown as mean \pm standard deviation ($n = 3$). Groups identified by one of the same superscript letter are not statistically different. ($P \geq 0.05$).

Researchers in this field have extensively tried to determine the optimal laser protocol to promote the optimal biostimulatory effects which are attributed to low-level laser irradiation. Unfortunately, nowadays there is not a clear guideline in this treatment. However, several clinical studies in this field have

obtained good results, demonstrating beneficial LLLT effects on different diseases and injuries ^{10,15}. The main parameters stipulated are that LLLT delivered at low energy density resulted in better results than the same wavelength delivered at higher energy density. Mostly, fluences of red or infrared (600-1070 nm) as low energy densities as 3 or 5 J/cm² are beneficial *in vivo*, but at higher energy densities like 50 or 100 J/cm² may lose the beneficial effect ³⁹. Besides, most studies suggest that laser applied at a wavelength of 600-700 nm and at energy densities from 0,5 to 5 J/cm² stimulates cell proliferation ^{22,29}. In a similar way, *Li et al.* obtained good hMSCs proliferation when stimulating by daily irradiation after 5 days at an energy density of 2 and 4 J/cm² ⁴⁰. Instead, irradiation at an energy density of 16 J/cm² had suppressive effects for cells ^{22,23,41}. The same negative result was reported using an energy density from 20 to 50 J/cm² ⁴². These cellular effects may support clinical applications.

Recently, some authors suggest that the union of stem cells with LLLT is not beneficial, decreasing its proliferation ability. Other studies propose that LLLT does not have any effect on cell proliferation capacity or may cause cytotoxicity ^{41,42}. The difference may be because of the energy densities that they employed, which were from 4 to 10 fold higher than in our study. Nitric oxide (NO) is thought to be involved in LLLT, and may be photo-released from its binding sites in the respiratory chain. Several papers discuss the so-called two-faced molecule nitric oxide (NO). This molecule can be either beneficial in a low dose, or harmful in a higher dose, depending on the energy fluence applied and on the cell type where it is generated ³⁹. In this chapter, we have used human dental pulp mesenchymal stem cells and the energy density used for irradiation was between a range of 0,5 to 5 J/cm², founding differences between irradiated and non-irradiated cells in terms of cell proliferation ability (*Figure 2.5.*).

Although in the study of *Pereira et al.* have used the same type of cells, they did not find statistically significant differences between cell proliferation rates of irradiated and non-irradiated cells, either from hDPMSCs from normal or inflamed dental pulps. The difference was that they have used an energy density of 0.05, 0.30, 7 and 42 J/cm², which may explain the discrepancy of our results⁴³. The laser wavelength also may influence in the negative results, resulting an inhibitory response for those cells irradiated in the infra-red range (830 nm)³⁶. Wavelength is an important factor because it relates to penetration of laser light across biological tissue¹². Longer wavelengths are more resistant to scattering than shorter ones⁴⁴. This study agrees with the latest in terms on that the biological response of laser therapy is dependent on the dose and the wavelength. In fact, it is widely known that each type of cell respond in a different way to laser irradiation depending on the parameters used, such as wavelength, power output, energy density and irradiation time⁴⁵. In our study, we found that the extent of enhancement of the DPMSCs proliferation is in close correlation with the radiant exposure (5 J/cm²). Thus, these results may endorse the clinical use for LLLT. Nevertheless, we state the importance of having an accurate protocol to follow.

4.3 Cell osteogenic ability

Some researchers have analyzed that exposure to low-level laser irradiation can improve the bone density when applied postoperatively in maxillofacial bony defects^{1,26,37}. Regarding this fact, we wanted to analyze if there was an osteogenic effect *in vitro* in order to better understand, at a cellular level, the clinical findings. For this reason, we have quantified the alkaline phosphatase (ALP) activity on hDPMSCs, which is known to be an early marker of osteoblast differentiation^{13,25}. *Figures 2.6* and *2.7* show the results of Alkaline phosphatase (ALP) activity. The samples irradiated with the highest output power (100 mW)

showed significant differences regarding ALP values compared with the ones irradiated with the lowest output power (50 mW). Nevertheless, there was not statistical significant difference between the highest output power group and the control group. These results are in agreement with *Bloise et al.* who studied ALP activity in Saos-2 cells after 14 days of laser treatment at an energy density of 3 J/cm². They did not find significant differences between laser irradiated/non-irradiated samples ⁷. This data suggest that the effect of LLLT on osteogenic stimulation of DPMSCs is dose-dependent. However, further experiments with higher potencies are needed to be performed in order to study if osteogenic differentiation may be enhanced.

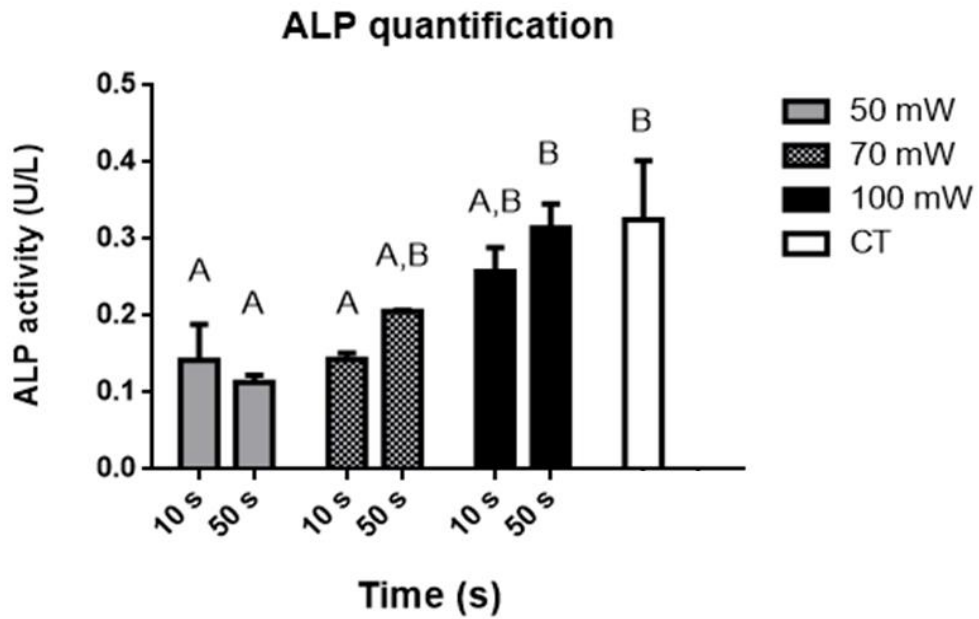


Figure 2.6. Cell osteogenic capacity was evaluated after 10 days of low-level laser irradiation at different energy potencies (50, 70 and 100 mW) and at different irradiation times (10 and 50 seconds) using the Alkaline Phosphatase (ALP). Data are shown as mean \pm standard deviation ($n = 3$). Groups identified by one of the same superscript letter are not statistically different. ($P \geq 0.05$).

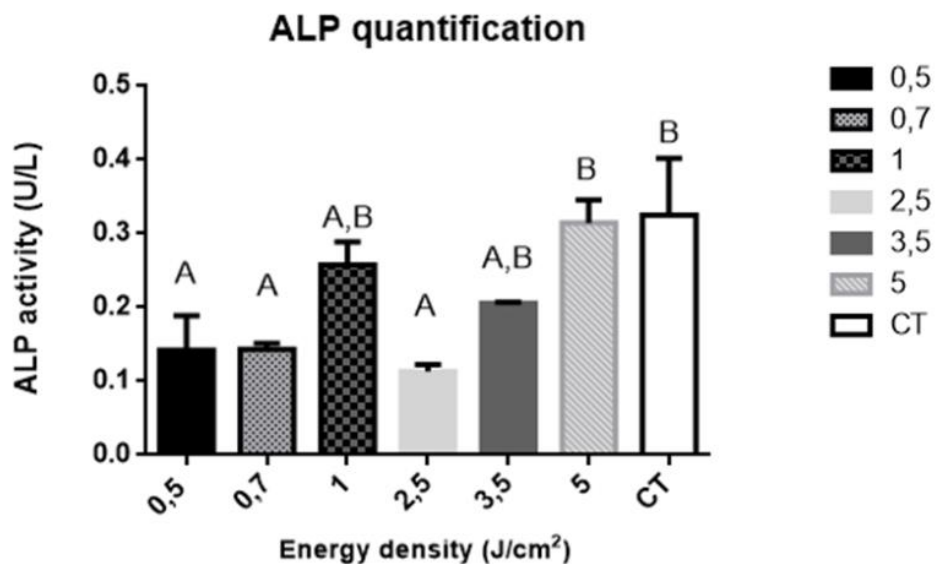


Figure 2.7. Cell osteogenic capacity was analysed using the Alkaline Phosphatase (ALP) after 10 days of irradiation expressed with energy density parameters. Data are shown as mean \pm standard deviation ($n = 3$). Groups identified by one of the same superscript letter are not statistically different. ($P \geq 0.05$).

Normalization between ALP activity to cellular proliferation of DPMSCs using CyQUANT assay was carried out (*Figure 2.8*). The objective was to make a relation among the proliferation and the osteogenic differentiation rates. Interestingly, the graphic shows that the group 100 mW;50 seconds presented significant higher values compared with the group 70 mW;10 seconds, This result may be explained because of the fact that with a higher output power, the ALP/cell proliferation relation is enhanced. It can be noticed a trend of rate increase when the cells were irradiated with the highest potency (100 mW) and during the longest time (50 s), despite not being significantly different.

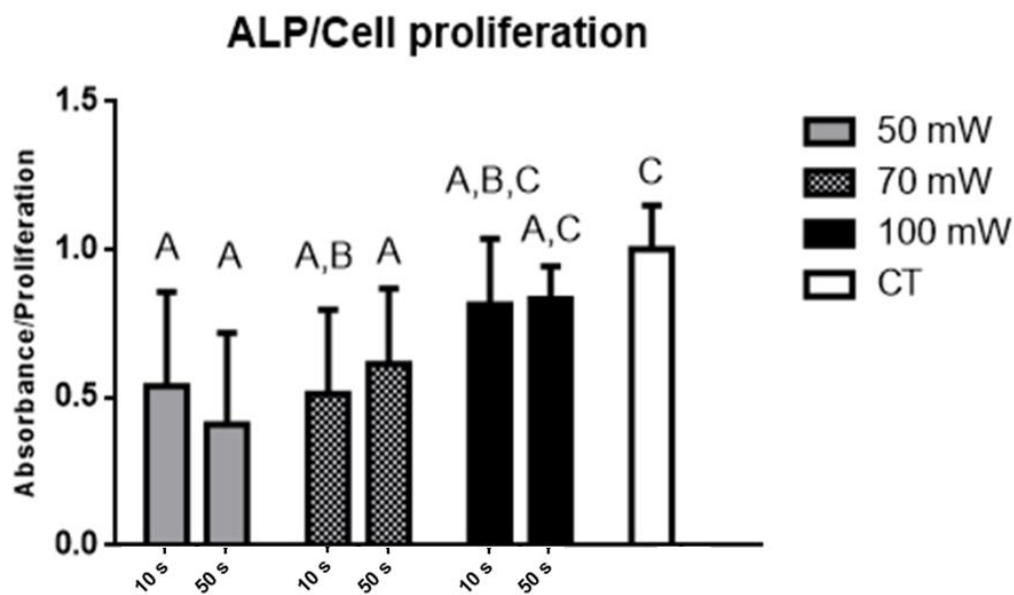


Figure 2.8. Alkaline phosphatase (ALP) activity normalized to cellular proliferation of DPMSCs in relation with the control group after 10 days of low-level laser irradiation at different output powers (50, 70 and 100 mW) and at different irradiation times (10 and 50 seconds).

Some studies support that LLLT induces an increase of ALP synthesis. One study which used bone marrow-derived mesenchymal stem cells to differentiate into osteoblasts by LLLT (wavelength of 810 nm; energy density of

2 or 4 J/cm²) have showed an increment of ALP activity after 10 days of the experiment and increased in a dose dependent manner ⁴⁶. Explanations may include the different wavelengths used or sensitivity due to the redox state of mitochondria in the target cells ³⁹. Moreover, they differ in the laser irradiation time (4 minutes instead of seconds), and the time interval used which was every 4 hours instead of every 24 hours. Besides, laser beam measurement problems may also be considered. It is known that laser beams have higher irradiance in the middle and they are weaker towards the edge. That is why cells in the center of a culture well may be exposed to higher irradiances than those on the periphery ³⁹.

In our experiment, we observed that LLLT (wavelength of 635 nm; maximum output power 100 mW) at daily exposure during 10 days at an energy density of 5 J/cm² had the highest values of ALP quantification compared with lower values of energy density applied (*Figure 2.7*). Laser irradiation was applied in another study after 24 and 48 hours of osteoblasts cells seed. The irradiation times were 1, 3 and 10 seconds at an output power of 180 mW; the corresponding energy densities were 0.14, 0.43 and 1.43 J/cm², respectively. The results showed a significant increment of ALP activity after 1 and 3 seconds of irradiation, compared with the control. However, the maximum energy density applied (1,43 J/cm²) did not show a significant increase of ALP activity. Comparing with our results, which the maximum output power was 100 mW, these differences may be explained because when applying different output powers values (mW) but the same energy densities (J/cm²), the results recorded may be different ^{39,47}. Another explanation may include that when DPMSCs are in the proliferation rate, they are not differentiating ⁴⁸. This fact may corroborate our results because after laser irradiation cells proliferation rate was increased, meanwhile ALP activity was not.

Kim et al. studied the effect of LLLT on osteogenic differentiation of mouse MSCs (D1 cells) that were also cultured in the presence of osteogenic medium. ALP activity was found to be significantly increased 5 days after LLLT (wavelength of 647 nm; energy density of 279 mW) ²⁵. These results demonstrate that different laser parameters are involved in the final outcome. Our results may hypothesize that ALP transcription was immediately activated after laser irradiation, allowing protein translation, and eventually the effect was lost. Although cell viability was not affected after the laser irradiation, the energy densities used were not enough to observe osteogenic changes. Nevertheless, several clinical studies in this field have obtained good results. One study with 70 patients used a laser with a wavelength of 810 nm and an energy density of 3,87 J/cm². The laser was applied after the maxillary surgery and daily for postoperative during 7 days. The results were compared with the control in terms of pain, clinical and radiological findings. In short, the laser group showed significantly better results in bone density, defect volume area, edema and wound healing ⁴⁹. Another clinical study used a combination of LLLT at a wavelength of 631 nm and an energy density of 12 J/cm² in combination with a grafted biomaterial. Two tooth extractions were performed in the same patient in order to compare both surgical sites, and synthetic hydroxyapatite biomaterial was placed in both extraction sockets. Then, only one site was treated daily with LLLT during 21 days. Histologic results showed that the socket grafted with HA and treated with LLLT produced significantly more bone than the control socket ⁵⁰.

Laser therapy is a non-invasive, effective, stimulator of cell proliferation and osteogenesis ⁵¹. These findings may be clinically relevant, pointing that repeated treatments are needed to achieve a positive laser effect in cells.

5. Conclusions and future perspectives

Our work has led us to conclude that irradiation with a diode low-level laser at a wavelength of 635 nm and with an energy density of 5 J/cm² have promoted DPMSCs proliferation after 10 days of daily treatment. Different energy densities were studied in order to assess which parameters were effective regarding cell proliferation and ALP activity. Laser irradiation did not affect cell morphology and cell viability. Moreover, it might have a dose-response effect regarding cell proliferation and ALP activity. Interestingly, there was significantly increase of cell proliferation directly proportional to the increase of power energy and the time of irradiation. However, the doses used in this study are not high enough to observe osteogenic differences among the control.

An important point that should be considered is the need of standardization of all the parameters used with LLLT in order to allow a more accurate comparison of results. Nevertheless, our study may affirm that exposure to laser light has beneficial effects at cellular level, supporting its current clinical application. Further investigations are needed in the near future to explain the mechanism underlying the effect of laser on the osteogenic differentiation of DPMSCs. These advances will lead to better acceptance of LLLT in mainstream dentistry and to use it in combination with other strategies, like bone grafts, in the cases of bone maxillary defects. Importantly, LLLT protocols need to be standardized before strongest conclusions can be affirmed about this subject.

6. References

1. Santinoni, S. *et al.* Influence of low-level laser therapy on the healing of human bone maxillofacial defects : A systematic review. *J. Photochem. Photobiol. B Biol.* **169**, 83–89 (2017).
2. Ustaoglu, G., Göller-Bulut, D. & Gümüş, K. Ç. Evaluation of different platelet-rich concentrates effects on early soft tissue healing and socket preservation after tooth extraction. *Surg. J Stomatol Oral Maxillofac* **In press**, (2019).
3. Kumar, P., Vinitha, B. & Fathima, G. Bone grafts in dentistry. *J. Pharm. Bioallied Sci.* **5**, 125–128 (2013).
4. Zaky, A. A., Mohamed, H. M., Harhsh, T. A. H. & Shalash, M. Can Low Level Laser Therapy Benefit Bone Regeneration in Localized Maxillary Cystic Defects? - A Prospective Randomized Control Trial. *Open Access Maced. J. Med. Sci.* **4**, 720–725 (2016).
5. de Almeida, A. L. P. F. *et al.* The effect of low-level laser on bone healing in critical size defects treated with or without autogenous bone graft : an experimental study in rat calvaria. *Clin. Oral Implants Res.* **25**, 1131–1136 (2014).
6. Moreira, A. *et al.* Low-Level Laser Therapy Increases Transforming Growth Factor- β 2 Expression and Induces Apoptosis of Epithelial Cells During the Tissue Repair Process. *Photomed. Laser Surg.* **27**, 303–307 (2009).
7. Bloise, N., Ceccarelli, G., Minzioni, P., Vercellino, M. & Benedetti, L. Investigation of low-level laser therapy potentiality on proliferation and differentiation of human osteoblast-like cells in the absence/presence of osteogenic factors. *J. Biomed. Opt.* **18**, 1–14 (2013).
8. Hu, W.-P. *et al.* Helium–Neon Laser Irradiation Stimulates Cell Proliferation through Photostimulatory Effects in Mitochondria. *J. Invest. Dermatol.* **127**, 2048–2057 (2007).
9. Karu, T. Primary and secondary mechanisms of action of visible to near-IR radiation on cells. *J. Photochem. Photobiol. B Biol. Photobiol* **49**, 1–17 (1999).
10. Oron, U. *et al.* Low-Energy Laser Irradiation Reduces Formation of Scar Tissue After Myocardial Infarction in Rats and Dogs. *Circulation* **103**, 296–301 (2001).
11. Barboza, C. A., Ginani, F., Soares, D. M., Henriques, A. C. & Freitas, R. A. Low-level laser irradiation induces in vitro proliferation of mesenchymal stem cells. *Einstein (Sao Paulo)* **12**, 75–81 (2014).

12. Shakouri, S. K., Soleimanpour, J., Salekzamani, Y. & Oskuie, M. R. Effect of low-level laser therapy on the fracture healing process. *Lasers Med Sci* **25**, 73–77 (2010).
13. Abramovitch-Gottlib, L., Gross, T., Naveh, D., Geresh, S. & Rosenwaks, S. Low level laser irradiation stimulates osteogenic phenotype of mesenchymal stem cells seeded on a three-dimensional biomatrix. *Lasers Med. Sci.* **20**, 138–146 (2005).
14. Hamad, A. S., Naif, J. S. & Abdullah, M. A. Effect of Diode Laser on Healing of Tooth Extraction Socket: An Experimental Study in Rabbits. *J. Maxillofac. Oral Surg.* **15**, 308–314 (2016).
15. Shefer, G., Oron, U. R. I., Irintchev, A., Wernig, A. & Halevy, O. Skeletal Muscle Cell Activation by Low-Energy Laser Irradiation: A Role for the MAPK/ERK Pathway. *J. Cell. Physiol.* **187**, 73–80 (2001).
16. Stein, A., Benayahu, D., Maltz, L. & Oron, U. Low-Level Laser Irradiation Promotes Proliferation and Differentiation of Human Osteoblasts in Vitro. *Photomed. Laser Surg.* **23**, 161–166 (2005).
17. Ahrabi, B. *et al.* The Effect of Photobiomodulation Therapy on the Differentiation, Proliferation, and Migration of the Mesenchymal Stem Cell: A Review. *Laser Appl. Med. Sci. Res. Cent.* **10**, 96–103 (2019).
18. Pinheiro, A. L. B. & Gerbi, M. E. M. Photoengineering of Bone Repair Processes. *Photomed. Laser Surg.* **24**, 169–178 (2006).
19. Haxsen, V., Schikora, D., Sommer, U. & Remppis, A. Relevance of laser irradiance threshold in the induction of alkaline phosphatase in human osteoblast cultures. *Lasers Med. Sci.* **23**, 381–384 (2008).
20. Schwartz-filho, H. O., Reimer, A. C., Marcantonio, C., Jr, E. M. & Marcantonio, R. A. C. Effects of low-level laser therapy (685 nm) at different doses in osteogenic cell cultures. 539–543 (2011). doi:10.1007/s10103-011-0902-5
21. Posten, W. *et al.* Low-Level Laser Therapy for Wound Healing: Mechanism and Efficacy. *Dermatol Surg* **31**, 334–339 (2005).
22. Alghamdi, K. M., Kumar, A. & Moussa, N. A. Low-level laser therapy: a useful technique for enhancing the proliferation of various cultured cells. *Lasers Med Sci* **27**, 237–249 (2012).
23. Wang, L. *et al.* Low-level laser irradiation modulates the proliferation and the osteogenic differentiation of bone marrow mesenchymal stem cells under healthy and inflammatory condition. *Lasers Med. Sci.* **34**, 169–178 (2018).

24. Tuby, H., Maltz, L. & Oron, U. Low-Level Laser Irradiation (LLLI) Promotes Proliferation of Mesenchymal and Cardiac Stem Cells in Culture. *Lasers Surg. Med.* **39**, 373–378 (2007).
25. Kim, H. K. *et al.* Red light of 647 nm enhances osteogenic differentiation in mesenchymal stem cells. *Lasers Surg. Med.* **24**, 465–466 (2009).
26. Eduardo, F. D. P., Bueno, D. F., Freitas, P. M. De & Marques, M. Stem Cell Proliferation Under Low Intensity Laser Irradiation: A Preliminary Study. *Lasers Surg. Med.* **40**, 433–438 (2008).
27. Carroll, J. D., Milward, M. R., Cooper, P. R., Hadis, M. & Palin, W. M. Developments in low level light therapy (LLLT) for dentistry. *Dent. Mater.* **30**, 465–475 (2014).
28. Jenkins, P. A. & Carroll, J. D. How to Report Low-Level Laser Therapy (LLLT)/Photomedicine Dose and Beam Parameters in Clinical and Laboratory Studies. *Photomed. Laser Surg.* **29**, 785–787 (2011).
29. Fekrazad, R., Asefi, S., Allahdadi, M. & Kalhori, K. A. Effect of Photobiomodulation on Mesenchymal Stem Cells. *Photomed. Laser Surg.* **4**, 813–822 (2016).
30. Cotler, H. B., Chow, R. T., Hamblin, M. R., Carroll, J. & Hospital, M. G. The Use of Low Level Laser Therapy (LLLT) For Musculoskeletal Pain. *Orthop heumatol* **2**, 1–16 (2015).
31. Nesioonpour, S. *et al.* The Effect of Low-Level Laser on Postoperative Pain After Tibial Fracture Surgery: A Double-Blind Controlled Randomized Clinical Trial. *Anesth Pain Med* **4**, 1–4 (2014).
32. Abrahamse, H. Regenerative Medicine, Stem Cells, and Low-Level Laser Therapy: Future Directives. *Photomed. Laser Surg.* **30**, 1–2 (2012).
33. Farivar, S., Malekshahabi, T. & Shiari, R. Biological Effects of Low Level Laser Therapy. *J. Lasers Med. Sci.* **5**, 58–62 (2014).
34. Oltra-Arison, D., España-Tost, A. J., Berini-Aytés, L. & Gay-Escoda, C. Aplicaciones del láser de baja potencia en Odontología. *RCOE* **9**, 517–524 (2004).
35. de Villiers, J. A., Houreld, N. N. & Abrahamse, H. Influence of Low Intensity Laser Irradiation on Isolated Human Adipose Derived Stem Cells Over 72 Hours and Their Differentiation Potential into Smooth Muscle Cells Using Retinoic Acid. *Stem Cell Rev Rep* **7**, 869–882 (2011).
36. Abrahamse, H., Tech, N. N. H. D., Tech, S. M. B. & Dip, L. N. N. Fluence and wavelength of low intensity laser irradiation affect activity and proliferation of human adipose derived stem cells. *Med. Technol. SA* **24**, 15–20 (2010).

37. Oliveira, A. *et al.* Low intensity lasers differently induce primary human osteoblast proliferation and differentiation. *Photochem. Photobiol.* **163**, 14–21 (2016).
38. Mvula, B., Moore, T. J. & Abrahamse, H. Effect of low-level laser irradiation and epidermal growth factor on adult human adipose-derived stem cells. *Lasers Med. Sci.* **25**, 33–39 (2010).
39. Huang, Y.-Y., Chen, A. C.-H., Carroll, J. & Hamblin, M. R. Biphasic dose response in low level light therapy. *Int. Dose-Response Soc.* **7**, 358–383 (2009).
40. Li, W., Chen, H. & Wang, C. Effect of Light Emitting Diode Irradiation on Proliferation of Human Bone Marrow Mesenchymal Stem Cells. *J. Med. Biol. Eng.* **26**, 35–42 (2006).
41. Hawkins, D. & Abrahamse, H. Effect of Multiple Exposures of Low-Level Laser Therapy on the Cellular Responses of Wounded Human Skin Fibroblasts. *Photomed. Laser Surg.* **24**, 705–714 (2006).
42. Bayat, M. & Jalalifirouzkouhi, A. Presenting a Method to Improve Bone Quality Through Stimulation of Osteoporotic Mesenchymal. *Photomed. Laser Surg.* **35**, 622–628 (2017).
43. Pereira, L. O., Longo, J. P. F. & Azevedo, R. B. Laser irradiation did not increase the proliferation or the differentiation of stem cells from normal and inflamed dental pulp. *Arch. Oral Biol.* **57**, 1079–1085 (2012).
44. Basford, J. R. Low Intensity Laser Therapy: Still Not an Established Clinical Tool. *Lasers Surg. Med.* **16**, 331–342 (1995).
45. Pinheiro, C. C. G., de Pinho, M. C., Fregnani, E. & Bueno, D. F. Low laser Therapy: a strategy to promote the osteogenic differentiation of deciduous dental pulp stem cells from Cleft Lip and Palate patients. *Tissue Eng. Part A* **24**, 569–575 (2018).
46. Soleimani, M. *et al.* The effects of low-level laser irradiation on differentiation and proliferation of human bone marrow mesenchymal stem cells into neurons and osteoblasts—an in vitro study. *Lasers Med. Sci.* **27**, 423–430 (2012).
47. Bolton, P., Young, S. & Dyson, M. Macrophage responsiveness to light therapy with varying power and energy densities. *Laser Ther.* **3**, 6–9 (1991).
48. Cooper, G. M. *The Cell: A Molecular Approach.* (Sinauer Associates, 2000).
49. Metin, R., Tatli, U. & Evlice, B. Effects of low-level laser therapy on soft and hard tissue healing after endodontic surgery. *Lasers Med. Sci.* **33**, 1699–1706 (2018).
50. Brawn, P. R. & Kwong-Hing, A. Histologic Comparison of Light Emitting Hydroxyapatite-Grafted Extraction Sockets: A Same-Mouth Case Study. *Implant Dent.* **16**, 204–211

(2007).

51. Hilal, A., Nigar, V., Cem, O., Ahmet, H. & Umit, Y. Comparison of the Effects of Low-Level Laser Therapy and Ozone Therapy on Bone Healing. *J. Craniofac. Surg.* **26**, 396–400 (2015).

7. List of figures and tables

FIGURE 2.1. Low-level laser used for the experiments. **140**

FIGURE 2.2. Workflow for CyQUANT Cell Proliferation Assays multiday tests. Quantitation of cells using the CyQUANT kit. Fluorescence measurements were made using a microplate reader with excitation at 485 nm and emission detection at 530 nm. Modified from manufacturer's protocol. **142**

FIGURE 2.3. Optical microscopy images of DPMSCs after 3 days of low-level laser irradiation at different energy potencies (50, 70 and 100 mW) and at different irradiation times (10 and 50 seconds). Scale bar 100 μm . **145**

FIGURE 2.4. CyQUANT cell Proliferation Assay Kit was performed to analyze the proliferation of DPMSCs after 3 and 10 days of low-level laser irradiation at different output powers (50, 70 and 100 mW) at different time intervals (10 s = 10 seconds; 50 s = 50 seconds). Data are shown as mean \pm standard deviation ($n = 3$). Groups identified by one of the same superscript letter are not statistically different. ($P \geq 0.05$). **147**

FIGURE 2.5. CyQUANT cell Proliferation Assay Kit expressed with energy density parameters. Data are shown as mean \pm standard deviation ($n = 3$). Groups identified by one of the same superscript letter are not statistically different. ($P \geq 0.05$). **148**

FIGURE 2.6. Cell osteogenic capacity was evaluated after 10 days of low-level laser irradiation at different energy potencies (50, 70 and 100 mW) and at different irradiation times (10 and 50 seconds) using the Alkaline Phosphatase (ALP). Data are shown as mean \pm standard deviation ($n = 3$). Groups identified by one of the same superscript letter are not statistically different. ($P \geq 0.05$). **152**

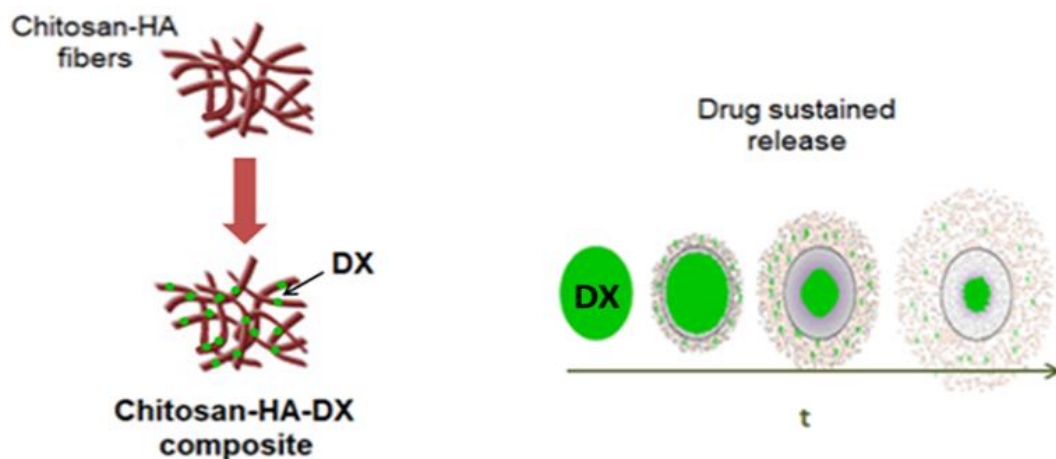
FIGURE 2.7. Cell osteogenic capacity was analysed using the Alkaline Phosphatase (ALP) after 10 days of irradiation expressed with energy density parameters. Data are shown as mean \pm standard deviation ($n = 3$). Groups identified by one of the same superscript letter are not statistically different. ($P \geq 0.05$). **152**

FIGURE 2.8. Alkaline phosphatase (ALP) activity normalized to cellular proliferation of DPMSCs in relation with the control group after 10 days of low-level laser irradiation at different output powers (50, 70 and 100 mW) and at different irradiation times (10 and 50 seconds). **153**

TABLE 2.1. Parameters used for cells irradiation in order to determine the effect of different power settings. mW=milliwatts, s=seconds, J=joules. **140**

Chapter 3

Novel Chitosan-based Biomaterial for Bone Regeneration



1. Introduction

This last chapter will focus on the design, manufacture and characterization of a new biomaterial to use as synthetic bone graft in maxillary defects, with the characteristic of sustained-drug release, emphasizing a solution to solve the aggregated problem of bacterial infections, which are really common in the oral area. As we have explained at *section 4.2.2.2* in the general **Introduction** (*New generation of bone grafts*) natural polymer-based bone substitutes are recently receiving tremendous popularity. We have chosen Chitosan (CS)-based biomaterial due to its renewable source and its high availability, being derived of chitin, which is the second most abundant polysaccharide in the world ^{1,2,3,4}. Marine crustacean shells are mainly used as primary sources for the obtaining of chitin, which is composed of randomly distributed β -(1 \rightarrow 4)-linked D-glucosamine and N-acetyl-D-glucosamine ^{5,6}. *Figure 3.1* shows the chemical structure of CS, which is the N-deacetylated product of chitin ⁷. Furthermore, it has a polymeric cationic character, biodegradability, biocompatibility and non-toxicity ⁸; as CS is positively charged, it makes this material able to bind to the bacterial cell wall which is negatively charged. Then, it will attach to the DNA thus preventing the replication of bacteria ^{9,10}. The antibacterial property renders CS a unique material, inhibiting the growth of a wide variety of fungi, yeasts and bacteria, which can be beneficial for use in the dentistry field ^{11,12,13,14}. Interestingly, CS can be molded into different forms in order to adapt to the different maxillary bone defects. Thus, CS fibers would be good candidates to resolve different bone regeneration situations. However, a pure CS biomaterial is mechanically weak and lacks the bioactivity to promote hard tissue formation, which limits its application as a bone graft biomaterial ^{15,16}. Synthetic bone grafts can be classified depending on its material group: metal, ceramic, polymer or composite-based. Composite-based group is an excellent option

because of the different advantages and synergies of materials that can compose the biomaterial. For that, we have designed a bone graft composed of CS with the incorporation of a ceramic material. We have chosen hydroxyapatite (HA) because it is biocompatible, non expensive and abundant¹⁷. Moreover, this ceramic has a chemical composition similar to the mineral phase of natural bone, being calcium phosphate, thus exhibiting bone-bonding ability^{18,19,20,21} (*Figure 3.1*). For that reason, the CS-HA composites have been claimed as bioactive materials for bone regeneration²⁰. Nevertheless, bone grafting procedures might develop bacterial infections which may compromise the tissue regeneration outcome. To avoid these infections, local drug-release is an excellent approach to prevent general adverse effects by protecting surrounded tissues from fast drug exposure while also improving drug efficacy by achieving sustained release directly at the infection site. This procedure may also benefit patients by avoiding unnecessary systemic undesired effects, because the drug will not pass the gastrointestinal barrier; moreover, it will be more efficiency and easy for the patient, avoiding possible forgetfulness of the drug intake from the patient. Antibiotic loading on bone regenerative biomaterials is a promising way to prevent augmentation procedures from infection during the resorption stage of bone substitutes²². That is why Doxycycline (DX) has been combined with the CS-HA composite biomaterial. It is a broad spectrum antibiotic of the tetracycline family which has been used to treat bacterial infections in the oral cavity²³ (*Figure 3.1*).

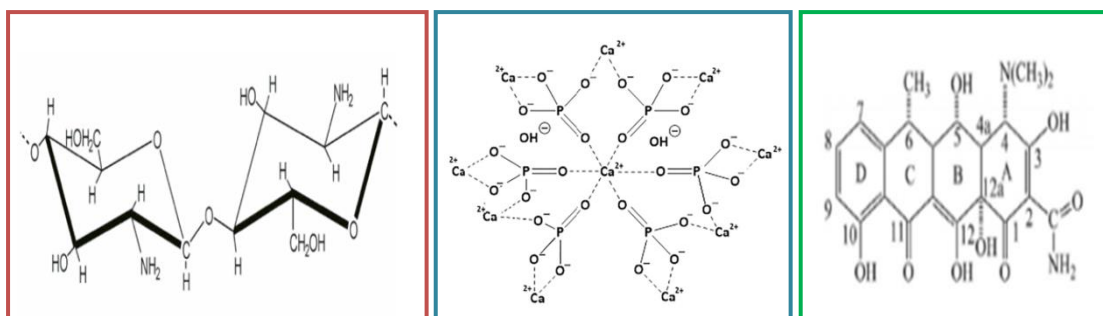


Figure 3.1. From left to right: chemical structure of chitosan³ hydroxyapatite²⁴ and doxycycline.

Interestingly, some researchers have reported the enhancement of bone mineralization and stimulation of apoptosis of osteoclasts *in vitro*, preventing bone resorption^{25,26}. Hence, the goal of our third project is to develop a biomimetic and bioactive CS-HA DX-loaded biomaterial which resembles the extracellular matrix so as to create conducive living environment to stimulate cells to repair maxillary bone naturally. At the same time, it will prevent reinfections in the implanted area because of the sustained-antibiotic release ability.

2. Objectives

The main objective of this chapter is to design and manufacture a bone grafting composite based on CS-biomaterial combined with sustained-drug release ability. To address this challenge, we designed a strategy based on the following objectives:

- O1: To optimize the hydrogel/ceramic ratio to obtain an injectable bone graft composite with good handling and setting properties
- O2: To control the chemical parameters of the bone graft composite
- O3: To study the sustained drug release of doxycycline within the bone graft composite at different time points

3. Materials and methods

3.1 Chitosan fibers synthesis and characterization

CS fibers were designed as follows. First, CS was prepared by dissolving 1 mL of glacial acetic acid (CH_3COOH) (Panreac) into 99 mL of distilled deionized water (DI water, from Milli-Q water system) and stirring at 800 rpm. Then, an amount of 1-3g of chitosan were added to the solution and stirred at 450 rpm during one hour at room temperature, in order to obtain from 1 to 3% chitosan solutions. After that, a volume of 3 mL of CS solution was introduced on a 5 mL plastic syringe. The syringe was then placed into an injection pump (kd Scientific pump KDS-200-CE) which was used to manufacture the fibers at a constant rate from 60 to 150 mL/h using a needle diameter of 0,5 or 0,9 mm. NaOH solutions from 0,05 to 0,5 molar ratios were prepared to use as the fibers crosslinking agent, at a pH of 12 (*Figure 3.2*). We have selected the fibers

form because they can be tailored through different parameters such as polymer concentration, molar ratio of the gelation solution and the alteration of the fiber size. Chitosan is an amino glucose containing small proportion of amide groups through an amide linkage with acetic acid ²⁷. Crosslinking is a physiochemical technique in which a charged polymer, in this case CS, is forming intermolecular chemical bonds between chains of the polymer, gaining stability and resistance ⁴. CS crosslinking to form the fiber shape was obtained with a solution of sodium hydroxide (NaOH). The capacity of CS fibers to be tunable is very important, taking into account that clinically, every maxillary bone defect may have different shape and size. The samples were fabricated per triplicate. In the present work, the effect of the different variables on the fibers fabrication and its properties were analyzed. The studied variables included:

- a) Chitosan concentration: 1, 2 and 3%
- b) Injection pump flow rate: 60, 75, 100 and 150 mL/h
- c) Needle diameter: 0,5 and 0,9mm
- d) Molar ratio of the NaOH crosslinking solution: 0.05, 0.1 and 0.5 M

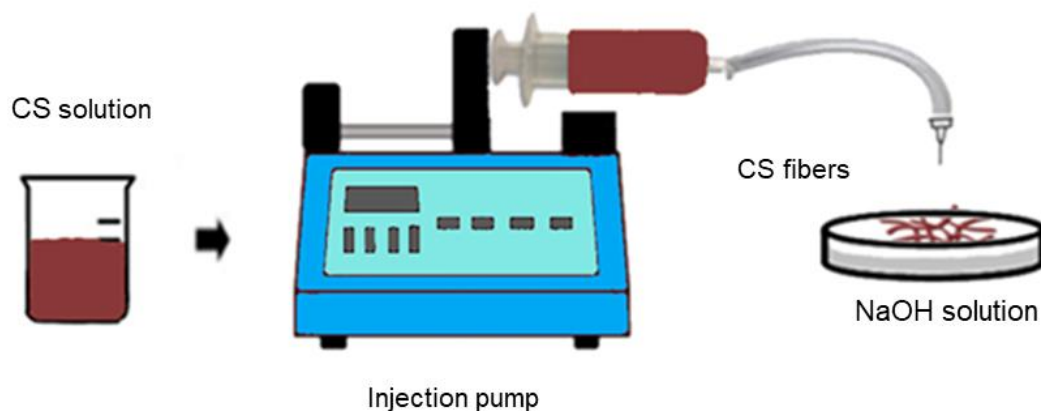


Figure 3.2. Schematic illustration of the CS fibers manufactured with the injection pump and the NaOH crosslinking solution agent.

3.1.1 Fibers structure analysis

Once the CS fibers were prepared, their stability and manipulation were evaluated under qualitative parameters in order to compare between the different variables studied. The maintenance of 3D structure of the fibers was evaluated and scored as low/bad, resulting in a non manipulable fiber which may easily loose its structure when handling with tweezers; correct, meaning the fiber was manipulable but not stable in aqueous media; or optimal, obtaining an excellent manipulable and stable fiber in aqueous media and maintenance of its structure when handling with tweezers. An optical microscope (Olympus CKX41, Nikon) was used to characterize the structure and to measure the size diameter of the fabricated biomaterials.

3.1.2 pH evolution

After 5 minutes of crosslinking time in NaOH solution, each biomaterial sample was immersed in 20 mL DI water bath during 10 minutes for 4 times in order to neutralize the basic pH of the solution (n=3). After each bath, the supernatant pH was analyzed and also after different periods until the pH reached 7,4 using a pH-meter (SensION™+ PH31).

3.2 Chitosan composite synthesis and characterization

After characterizing CS fibers, the values of the main variables studied were selected. The ones with the best stability and manipulation parameters were chosen in order to continue with the CSHA composite fabrication:

- a) Chitosan concentration: 1%
- b) Injection pump flow rate: 75 mL/h
- c) Needle diameter: 0,9mm
- d) Molar ratio of the NaOH crosslinking solution: 0,5 M

Chitosan was prepared as explained in *section 3.1*. At this point, 1% CS composite was used and different amounts of HA were incorporated. First, hydroxyapatite (HA) powder (Sigma-Aldrich) was mixed with the CS solution at ratios of 10, 50 or 75 wt (weight) % of HA respect to the composite to obtain CSHA biomaterials. Since the viscosity of CS varied with the HA concentration, the L/P ratio used for the mix of the HA powder was adjusted to the minimum value of water at which HA75% was well dispersed. According to this criterion, HA 10, 50 and 75% was dispersed in 400 μ L DI water and placed on the vortex to homogenize. A volume of 3 mL of CSHA composite was introduced on a 5 mL plastic syringe to fabricate the fibers with the injection pump as explained before. A constant rate of 75 mL/h was established and the needle diameter used was 0,9 mm. NaOH solution of 0,5 M was used as the fibers crosslinking agent. All samples were fabricated per triplicate.

3.2.1 Chitosan composite structure analysis

Once the CSHA fibers were manufactured, the characterization of their structure and the measurement of the size diameter were evaluated. As explained before, an optical microscope was used for this assay.

3.2.2 pH evolution

The pH evolution experiment was assessed with the same steps followed for the CS fibers.

3.2.3 Chemical analysis: Fourier Transformed Infrared Spectroscopy (FTIR)

FTIR was used to characterize the chemical composition of the experimental materials and to verify the changes in the chemical structure. The material studied consisted of CS with different HA concentrations in each sample. The assay consisted on taking one small piece of each sample and to place it in the spectrometer (Agilent Cary 630 FTIR) and recording the measurement. The infrared spectrum is detected between a range of 650 to 4000 cm^{-1} with a resolution of 4 cm^{-1} . The spectrums were done 6 times and an average spectrum was obtained. A blank with no sample was measured in order to have the base line. The spectrums were obtained and analyzed using the MicroLab Lite software.

3.2.4 Doxycycline-loaded composite fabrication

DX was selected to be incorporated into the CSHA composite because it is a broad spectrum antibiotic and is known to have an osteogenic regeneration capacity. The amount of DX powder used was 833 $\mu\text{g}/\text{mL}$. This concentration was selected taking into account a study that was similar to ours, in which they used 1mg DX/mL of the material ²³. Moreover, DX minimum inhibitory concentration (MIC) is known to be 16 $\mu\text{g}/\text{mL}$ ²⁸. We assumed a high lost of DX because of the water baths. That is why we choose a higher DX concentration as a first study. Thus, the antibiotic was added to the solution (either 1% CS or 1% CSHA composites) following the steps explained in *section 3.2* and using the same HA concentrations (0-75 wt %). In order to obtain CSHADX composites, a constant doxycycline (DX) powder (Sigma Aldrich) weight of 0,0025 g was added to the CSHA composite. As DX is sensitive to light, the DX-loaded biomaterials were kept in the dark until used ²⁹. A volume of 3 mL of CSHADX composite was introduced on a 5 mL plastic syringe to fabricate the

fibers with the injection pump as explained before. A constant rate of 75 mL/h was established and the needle diameter used was 0,9 mm. NaOH solution of 0,5 M was used as the fibers crosslinking agent. All samples were fabricated per triplicate. *Table 3.1* shows the samples studied. The CSHADX composites structure analysis, pH evolution and FTIR were assessed as explained before for the CS fibers.

HA concentration (%)	Without DX	With DX
0	CS	CSDX
10	CSHA10	CSHA10DX
50	CSHA50	CSHA50DX
75	CSHA75	CSHA75DX

Table 3.1. Samples studied and codes used for this section. The main variable studied was the HA percentage (0, 10, 50 and 75%) with or without DX incorporation.

3.3 *In vitro* doxycycline release study

After crosslinking the samples for 5 minutes into 0,5 M NaOH solution, the amount of DX was analyzed from the supernatant to detect the loading quantity. The amount of DX released was measured using a spectrophotometer by measuring the absorbance at 351 nm (Bio-Tek Synergy HT). Moreover, the effect of HA amount in the mixture solution with CS was also investigated. To study the release of DX from the biomaterials after the crosslinking time, each sample was immersed in 1 mL DI water for different

periods and maintained at the incubator at 37°C. The release quantity was interpreted after normalized to the loaded quantity. Then, 1 mL of medium was refreshed at each time point of the assay.

3.4 Statistical analysis

Statistical analysis was carried out with significance of 5%. Mann-Whitney test was conducted. Data are expressed as mean \pm standard deviation. The results were statistically analyzed using Minitab (Minitab® Software Inc. 17.1.0) and GraphPad Prism version 6 (Graphpad Software Inc.) was used to graph the data.

4. Results and discussion

4.1 Chitosan fibers synthesis and characterization

4.1.1 Fibers structure analysis

Natural polymers are nowadays widely used as biomaterials for periodontal and bone regeneration treatments because of their excellent biocompatibility. Among biopolymers, chitosan has gained more attention due to its extent biomedical applications like tissue engineering and drug carrier. This biomaterial has FDA approval for wound dressing ³⁰. Moreover, CS is widely useful for these situations because it is biodegradable, non-toxic and it has a mucoadhesive nature ⁶. Furthermore, it has a sustainable and low-cost process for the manufacturing of bone tissue reducing the consumption of toxic materials ³¹. In this study, we have first evaluated different variables within the fabrication process such as the CS concentration, the flow rate, the needle diameter and the molarity of the NaOH solution used to manufacture the fibers. The aim of this section was to evaluate and select the best parameters

used in order to proceed to the composite fabrication. *Table 3.2* shows the stability and manipulation capacity of different NaOH solution molarities that were evaluated to select the best crosslinking solution concentration. This fact was important to ensure the maintenance of the 3D fiber structure. The solution concentration that resulted in an optimal stability and manipulation of the fibers was 0,5 M. The CS transition from the solution to the fiber form is determined by the immersion in basic media, such as NaOH.

NaOH solution (M)	Low/bad	Correct	Optimal
0,05	X		
0,1	X		
0.5			X

Table 3.2. Visible stability and manipulation of CS fibers at different NaOH solution molarities (0,05-0,5). The parameters were scored as low/bad, correct or optimal marked with an X.

The fact that the higher molarity of the NaOH solution resulted to be the best in terms of stability and manipulation of CS fibers, could be explained because of the higher concentration of OH⁻ ions, which are conducted by diffusion gradient interacting with CS cationic groups to penetrate into the composite in less time leading to a faster CS neutralization; this fact may lead to a rapid formation of a stable fiber network³⁰. Our results are in agreement with *Bergonzi et al.* who evaluated different crosslinking media at different molarities, obtaining good fiber constructs from 0,5-1 M. Besides, they did not obtain a maintenance of the 3D structure at lower crosslinking media

molarities, such as 0,1 M ³⁰. Furthermore, the use of a basic solution like NaOH for the crosslinking process of CS under mild conditions requires short time of gelation, compared with other studies that used NaCl or phosphate buffer saline ³².

Once NaOH 0,5 M was selected as the best crosslinking solution, CS fibers with different needle diameters, polymer concentrations and flow rates were fabricated. *Table 3.3* shows the stability and manipulation of different CS fibers with different needle diameters. Interestingly, the highest needle diameter resulted in fibers better formation compared with the lower needle diameter.

Needle diameter (mm)	Score
0,5	0
0,9	++

Table 3.3. Visible stability and manipulation of CS fibers manufactured with different needle diameters: 0,5 mm and 0,9 mm. The parameters were scored as low/bad = 0, correct = + or optimal = ++.

Table 3.4 shows the effect of different CS concentrations used (1, 2 and 3%) to fabricate the fibers regarding different rates assessed (60, 75, 100 and 150 mL/h). All CS concentrations demonstrated good fiber forming ability, which means they did not disintegrate and were able to maintain its 3D structure when were manipulated with tweezers. However, flow rates at 60 mL/h had lower stability than the higher rates studied.

		Rate (mL/h)			
CS (%)	60	75	100	150	
1	0	++	++	++	
2	+	++	++	++	
3	0	++	++	++	

Table 3.4. Visible stability and manipulation of fibers at different CS percentages (1, 2 and 3%) and at different rates (60, 75, 100 and 150 mL/h). The parameters were scored as low/bad = 0, correct = + or optimal = ++.

The wet spinning process steps are: preparation of the polymer solution, extrusion of polymer solution into the crosslinking bath and coagulation in this bath. Polymer concentration in the spinning solution depends mainly on polymer solubility and spinning pressure limitations. The formation of the fibers in the crosslinking bath is a complex process that involves parameters of bath composition, temperature, flow rate, among others³³. Thus, in this process, the polymer dropping from the needle tip onto the collector may occur, and if the flow rate is not optimal, it will then spoil the fibers already collected. The pressure required to deliver the solution at a constant rate will depend on different factors, including the diameter of the needle and the solution viscosity³⁴, which will depend on the CS concentration. If the flow rate is too low, there will be insufficient polymer at the NaOH solution surface. The diffusion of the NaOH solution into the CS macrofilaments may be in relation with the CS concentration and the flow rate, having higher bonds between CS chains as

higher CS concentration, resulting in better fiber stability. Indeed, the CS chains reorganization occurs as the crosslinking agent diffuses into the CS solution³⁵. The needle diameter issue may be better at a higher diameter because the polymer was able to flow better through the needle at the moment of the fiber fabrication. This ability of the polymer to flow may be related to how fast and how far individual CS chains can move in relation to each other, and can influence the fiber diameter, thus influencing its stability and manipulation³⁴. Although very fine fibers can be produced using 1% CS at a flow rate of 60 mL/h in NaOH bath, the fibers disintegration may be because of lack of crosslinking at that lower rate³⁶. *Figure 3.3* shows optical microscope images at the different variables studied before, fabricated in a constant 0,5 M NaOH solution. CS fibers at 1% concentration manufactured with the lowest needle diameter had a smoother profile compared with higher CS concentrations and the highest needle diameter used. Comparing fibers obtained with the same needle diameter, the ones with 1% CS resulted to be the thickest compared with higher CS concentrations. When comparing different flow rates used, there were not apparently differences between them. However, when combining the highest CS concentration with the lowest rate, it was not possible to manufacture the fibers because of the high CS solution viscosity. Moreover, because of the higher viscosity of 3% CS, it showed a non-uniform shape presenting beads, compared with the rest of the fibers.

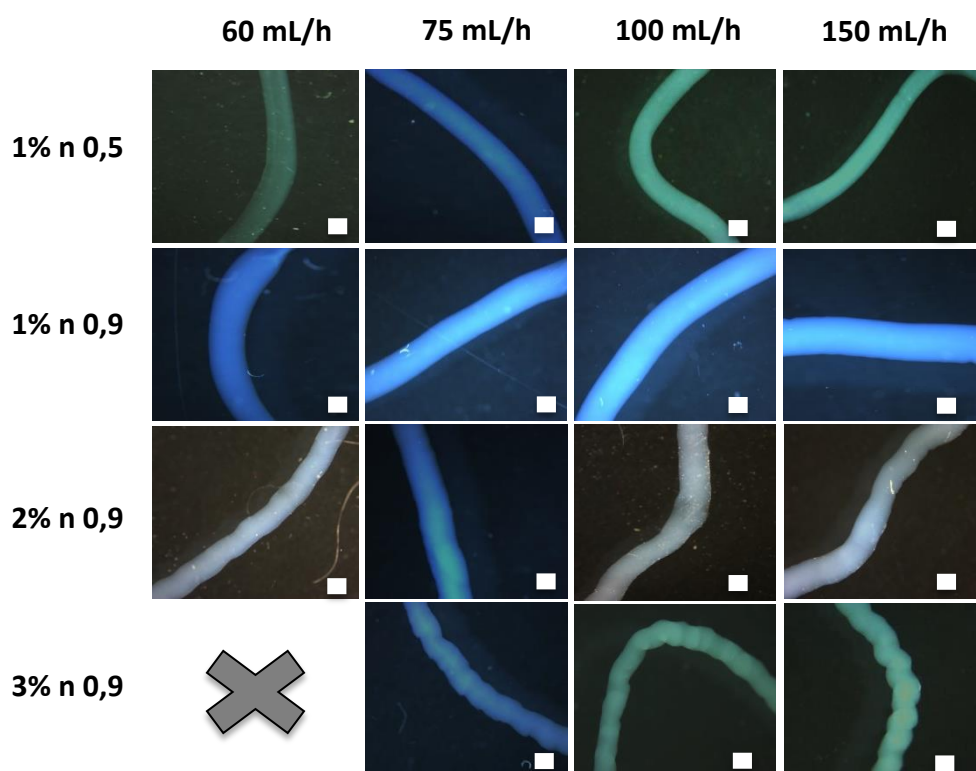


Figure 3.3. Optical microscope images of CS fibers at different percentages (1, 2 and 3%) and at different rates (60, 75, 100 and 150 mL/h). CS fibers at 1% were manufactured with 0,5 and 0,9 mm needle diameter, and the rest of fibers with 0,9 mm needle diameter. The NaOH solution was 0,5 M. Scale bar 500 μm .

These results were confirmed with the size fiber quantification measured by optical microscopy. First, regarding the combination of different needle diameters at different flow rates, *Figure 3.4* shows that when using the highest needle diameter the fibers significantly increased in size, compared with the results of lower needle diameter. Referring to the different flowing rates studied with the needle diameter 0,5 mm, fibers manufactured at 100 and 150 mL/h had increased sizes compared with the ones fabricated at 60 and 75 mL/h. This finding may suggest that the flow rate has an effect on the diameter of the fibers. A study explained this fact stabilising that when we have a larger volume of solution in motion over a set distance, the obtained fibers will be

thicker³⁴. However, there were not statistically significant differences when a diameter of 0,9 mm was used at different rates.

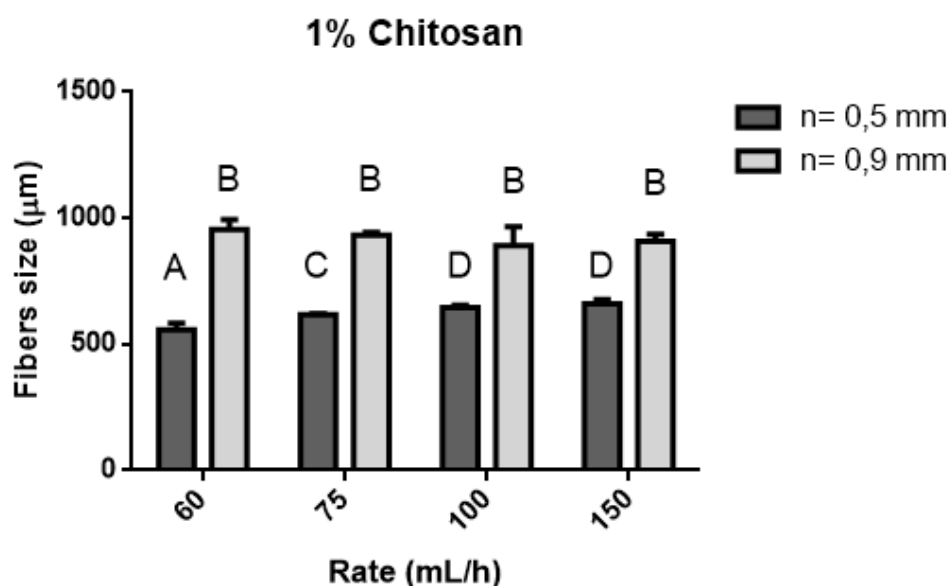


Figure 3.4. CS fibers size with the two needle diameters (0,5 and 0,9 mm) and at different rates (60-150 mL/h). Data are shown as mean \pm standard deviation ($n = 6$). Groups identified by the same superscript letter are not statistically different. ($P \geq 0.05$).

After that, we have studied the combination of different CS concentrations at different flow rates, maintaining a constant needle diameter of 0,9 mm. The graphic in *Figure 3.5* corroborates the images showed before obtained by optical microscopy. The 1% CS concentration resulted on the highest values of fiber size compared with the rest of the concentrations analyzed, being statistically significant. Regarding the different flow rates, there were no differences between them at 1% CS concentration. Our results showed that 1% CS had the highest fibers size. Thus, we hypothesize that fabricating the fibers at lower CS concentration has allowed more expansion of the polymer within the crosslinking solution, obtaining thicker fibers. A study showed that there

was a non-linear relation between the polymer concentration and fiber diameter³⁷. However, the authors studied nanofibers instead of microfibers.

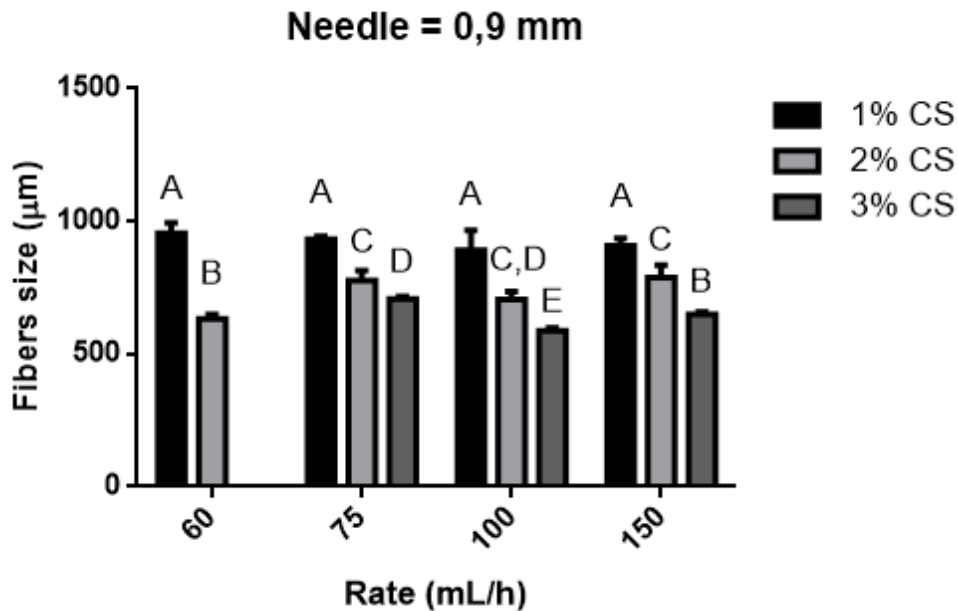


Figure 3.5. CS fibers size at 1, 2 and 3% concentration fabricated with a needle diameter 0,9 mm and at different rates (60-150 mL/h). Data are shown as mean \pm standard deviation ($n = 6$). Groups identified by the same superscript letter are not statistically different. ($P \geq 0.05$).

The stability and manipulation capacity are extremely important because this biomaterial will be clinically used to fill bone defects. Besides, the clinician must have an optimal biomaterial manipulation in order to short the time of the treatment. That is why we think fiber shape is a good option both to better adapt to the host tissue and to repair the irregular bone defect more efficiently. Furthermore, the fibers at 1% CS were the highest in terms of size, which may be an excellent property in terms of needing less biomaterial to fill a wider defect. Moreover, these fibers had good cutability, making them optimal for clinical requirements to be gathered by cutting the composite biomaterials into individualized shapes and sizes.

4.1.2 pH evolution

At this point, the assesment of the pH evolution was performed. pH is one environmental stimuli at which CS polymer may change in response to this parameter. This pH sensitive behaviour is because of the large quantities of amino groups presented on its chains. After manufacturing CS fibers, they were immersed in baths of DI water 4 times and the pH was measured at different time points. First, we studied the pH of 1% CS fabricated with a needle diameter of 0,5 or 0,9 mm at a flow rate of 75 mL/h. The lower needle diameter reached a lower mean pH (8,4) compared with the higher needle diameter (8,7), although there were not significant differences (*Figure 3.6*).

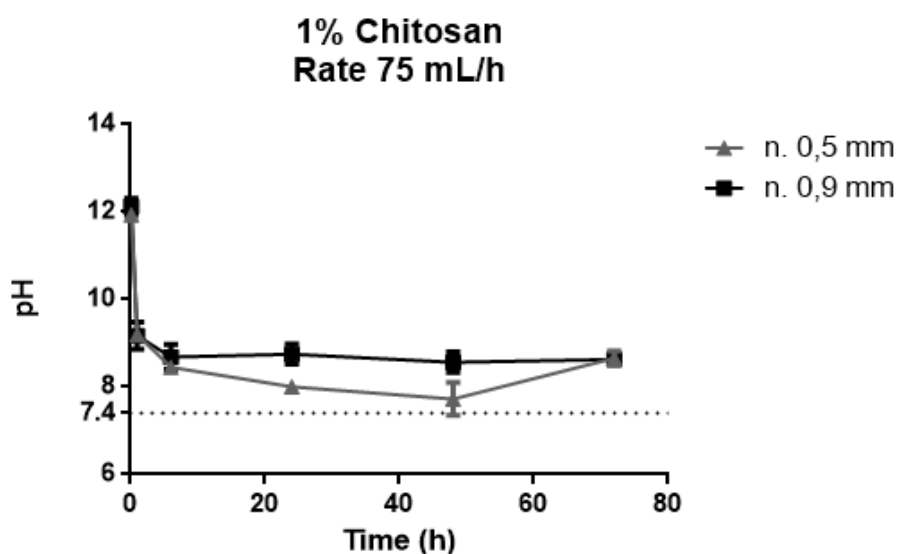


Figure 3.6. pH analysis of 1% CS at a rate of 75mL/h and with different needle diameters (0,5 or 0,9 mm).

Then, we evaluated the pH of 1-3% CS at a flow rate of 75 mL/h. The 1% CS sample showed slightly higher pH values (8,7) compared with 2 and 3% CS samples (8,6 and 8,5), although significant differences were not found (*Figure 3.7*). All samples reached a pH near 7,4 after 48h of the study.

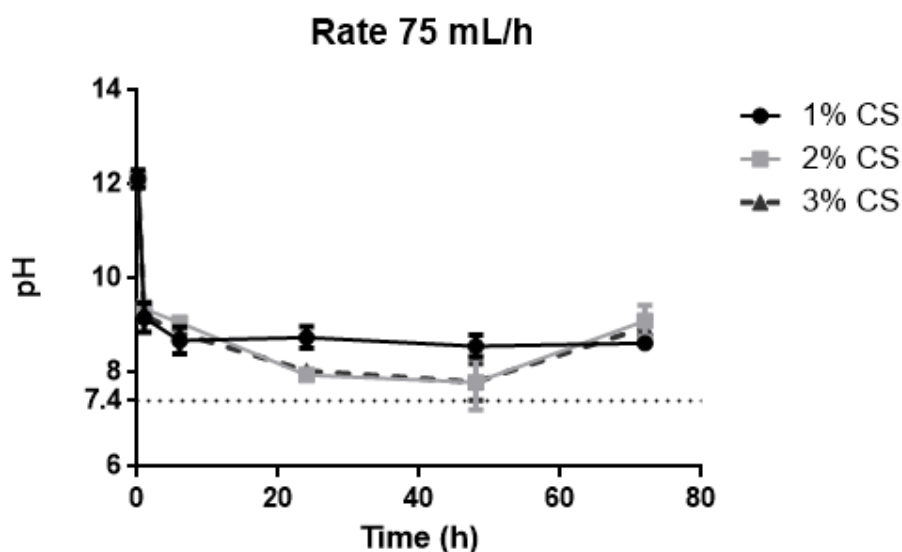


Figure 3.7. pH analysis of different CS concentrations (1-3%) at a constant rate of 75 mL/h (n=3).

Finally, 1% CS at different flow rates was evaluated in order to study the differences between them (Figure 3.8). The highest pH value was 8,9 for the lowest rate (60 mL/h), and the lowest value was 8,2 for the highest rate (75 mL/h). However, they were not statistically significant.

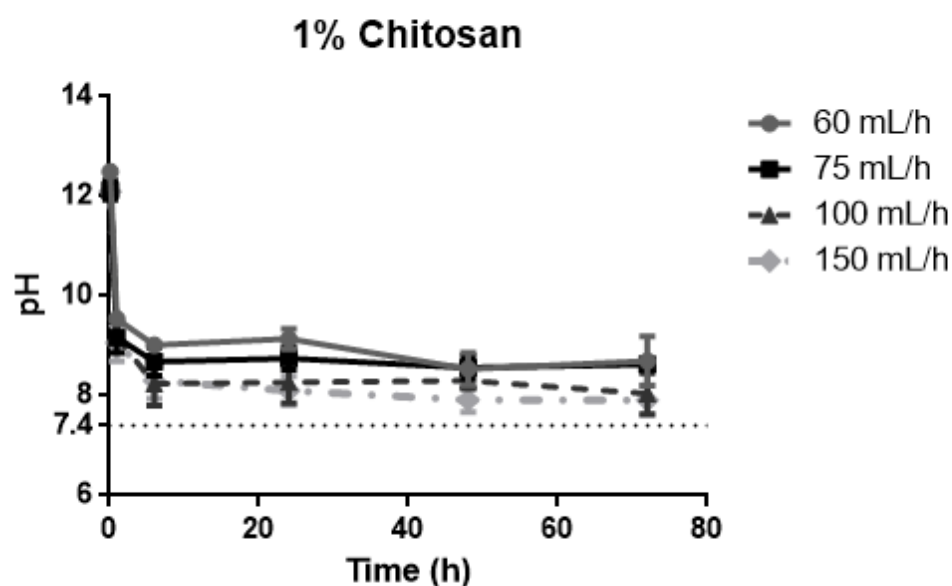


Figure 3.8. pH analysis of 1% CS at different rates (60-150 mL/h) (n=3).

CS has a cationic nature and it is a pH-sensitive polymer. When it reaches weak acids ($\text{pH} < 6$) the protonated free amino groups of glucosamine allows solubility of the molecule. The formation of CS fibers is accomplished after immersing CS solution into a basic NaOH solution with a $\text{pH}=12$. This is a common approach to perform sol-to-gel transition for water soluble, pH-sensitive polymers. CS usually undergo phase transition because of the functional groups on the polymer that either accept or donate protons as a result of pH changes in the environment ³⁸. As CS fibers initially had a $\text{pH}=12$ because of the NaOH crosslinking solution, we have immersed the polymer in several DI water baths in order to decrease its pH and change it to a physiological pH. For this reason, we wanted to evaluate the pH stability of CS at different fiber fabrication parameters in order to select the best results. Taking into account there were no significant differences between the samples studied, 1% CS at a flow rate of 75 mL/h and with a needle diameter of 0,9 mm was chosen for the next experiments.

4.2 Chitosan composite synthesis and characterization

4.2.1 Composite fibers structure analysis

Human bones are mainly formed of organic and inorganic components, particularly HA and collagen. Composite biomaterials that mimic the bone matrix may have important clinical applications in bone grafting ¹⁸. CS is claimed as an excellent biomaterial to be used as a bone graft. In the literature we can find a wide range of methods for CS processing to be used in tissue engineering ³⁹ (*Figure 3.9*). Furthermore, the combination of polymers with inorganic phases leads to materials with improved mechanical characteristics due to the higher stiffness and strength of the inorganic material, because CS itself do not possess optimal mechanical properties to satisfy bone tissue repair requirements ^{21,40,41,42}.

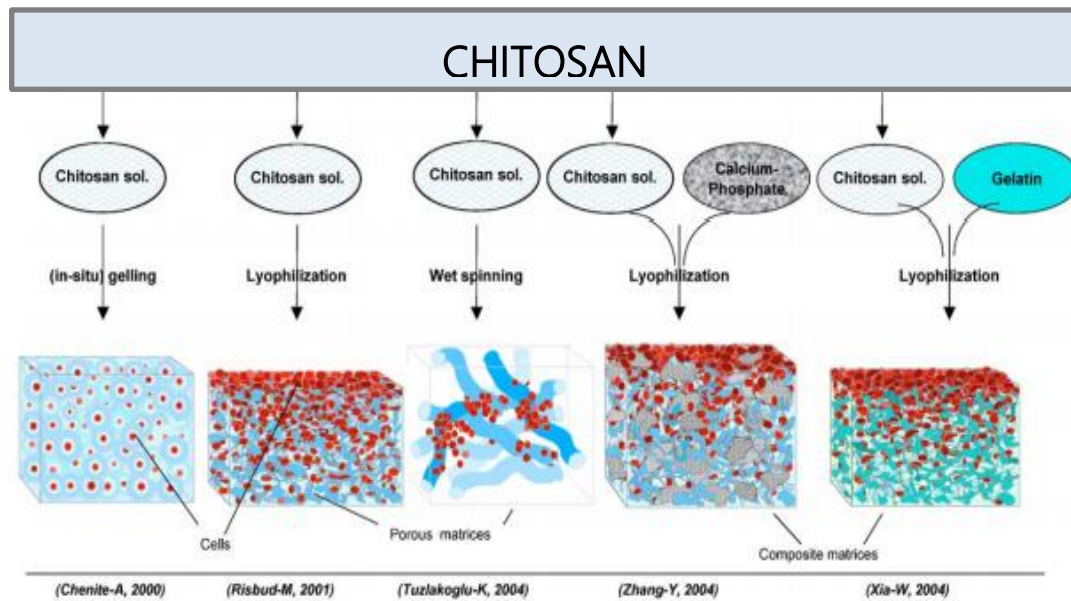


Figure 3.9. Illustration of selected examples of CS processing for use in tissue engineering: Cells may be encapsulated in gels or seeded in porous matrices including sponge-like or fibrous structures. Combinations of CS with other biocompatible materials such as calcium phosphate or gelatin are applied to modify biomechanical and cell-matrix-interaction properties. Different adaptations of CS may help to optimize cell and tissue differentiation and tailor the transplant to different clinical cell delivery situations ^{43,44,10,45,46}. Modified from ³⁹.

Moreover, we think that the addition of HA, which exhibits bone bonding ability, will enhance the biomaterial osteogenic properties as this combination has been extensively studied ^{18,23,47,48,49,50}. Besides, we have incorporated into the composite DX powder, which is an antibiotic and is also known to promote bone growth ⁵¹. For these reasons, we have fabricated a composite biomaterial with different amounts of HA and a constant DX concentration in order to characterize the fibers size and morphology. The morphology of the CS and CSHA fibers obtained by means of coagulating in NaOH solution is shown in *Figure 3.10*. As HA concentration increased, the composite macrostructure seemed denser and more well-packed. The explanation may be that the greater the quantity of HA, the amount of water is reduced. This fact leads to a

less hydrogel and more ceramic material. Moreover, higher HA concentration rendered the fibers a whitish color. Optical microscope images of the composite fibers revealed the individual structure of the different samples analyzed. The sizes of the CS and CSHA75 fibers apparently seem the thickest.

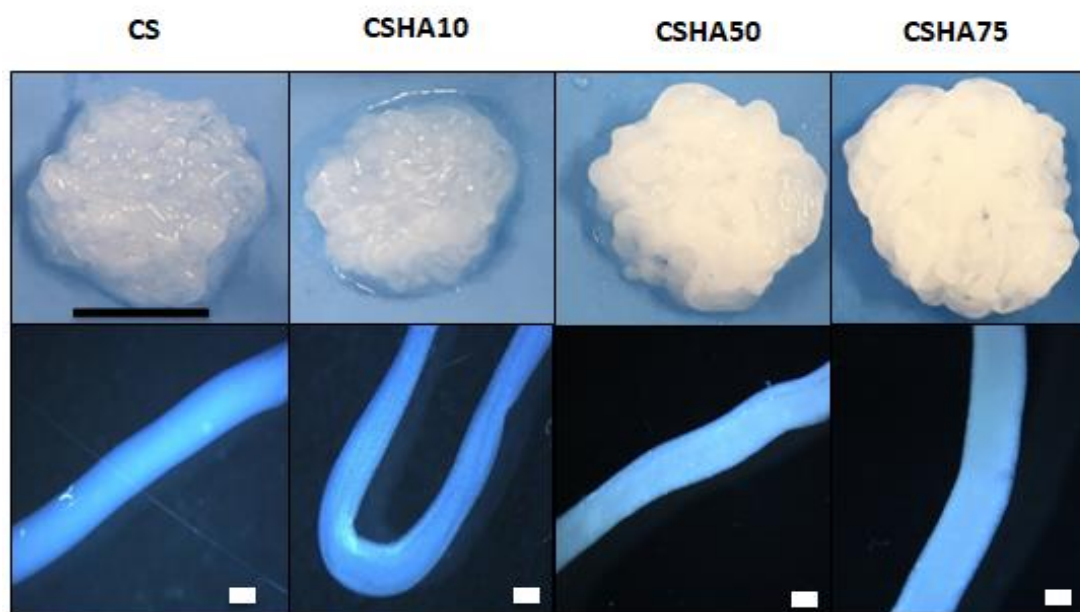


Figure 3.10. Digital photographs and optical microscope images of 1% CS fibers manufactured with a needle diameter of 0,9 mm and at a constant rate of 75 mL/h mixed with different concentrations of HA (0-75%). Scale bars 0,5 cm and 500 μ m.

Figure 3.11 shows CS and CSHA fibers with DX incorporation. Similar pattern was followed in these samples, in which it can be observed a denser and more well-packed macrostructure at higher amounts of HA, but less whitish color because of the yellowish color of DX powder. Optical microscope images showed well defined fiber shape being CSHA75DX the thickest composites.

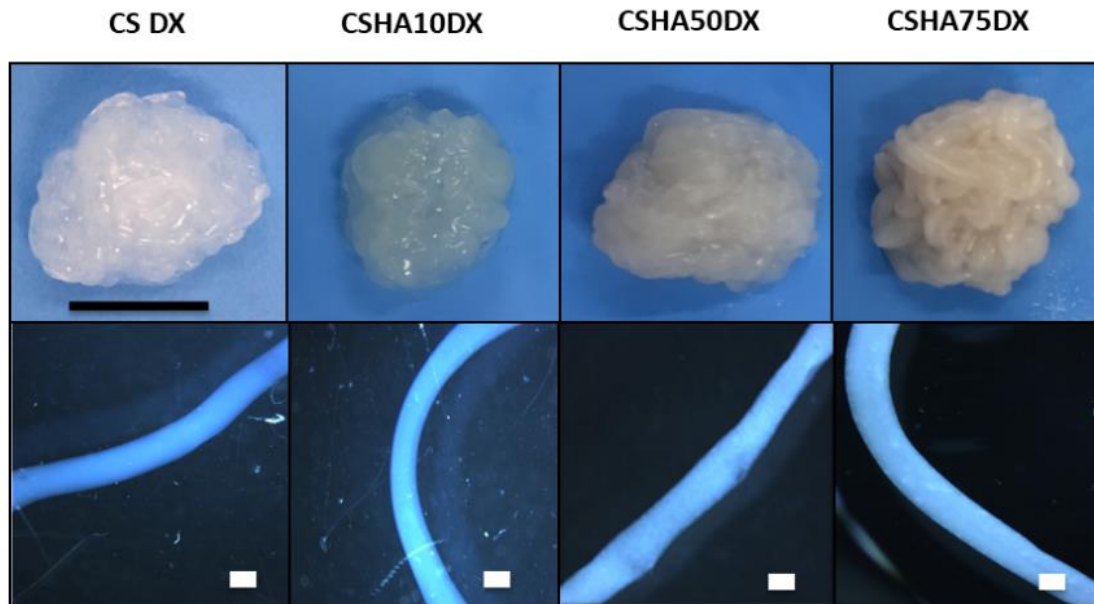


Figure 3.11. Digital photographs and optical microscope images of 1% CS fibers manufactured with a needle diameter of 0,9 mm and at a constant rate of 75 mL/h mixed with different concentrations of HA (0-75%) with DX incorporation. Scale bars 0,5 cm and 500 μ m.

The graphic in *Figure 3.12* corroborates the optical microscopy images showed before. Regarding the group without DX, CS sample showed significantly increased values of fiber size compared with the rest of the groups with HA. CSHA75 obtained the highest fiber size comparing between CSHA samples, being statistically significant. Referring to the samples with DX incorporation, CSHA75 had higher fiber size comparing to the rest of the samples less with CSHA50, which resulted in similar sizes. DX did not seem to affect the fiber size of the composites containing HA. However, the CS fibers without HA decreased its size when incorporating DX.

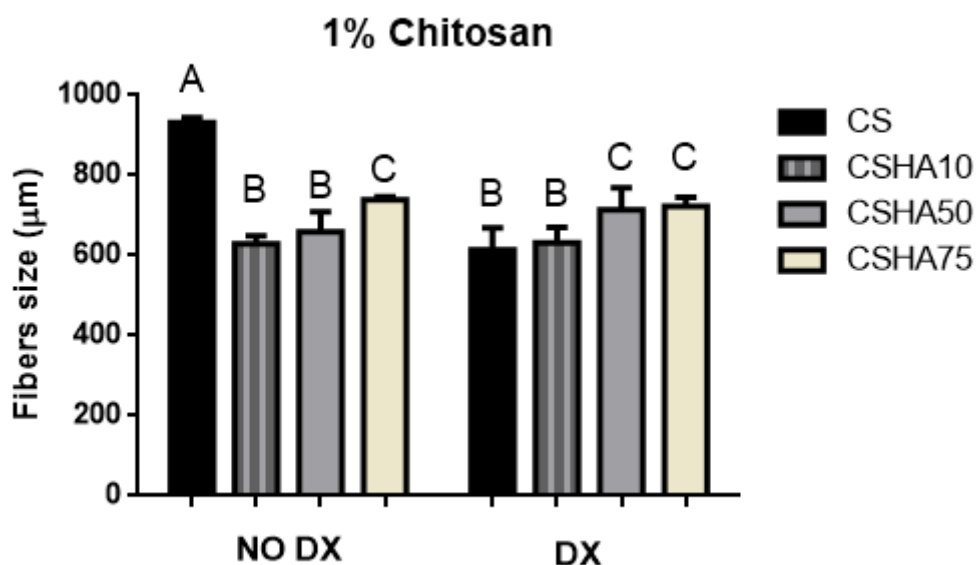


Figure 3.12. CSHA fibers size with and without DX incorporation. Data are shown as mean \pm standard deviation ($n = 6$). Groups identified by the same superscript letter are not statistically different. ($P \geq 0.05$).

It should be borne in mind that CS fibers were fabricated immersing the polymer in NaOH solution; however, CS composites were mixed before with 400 μ L of DI water in order to disperse DX particles. This fact may explain the fibers size differences between CS and CSHA composites with or without DX incorporation.

4.2.2 pH evolution

The effect of pH did not have statistically differences between the groups studied. Nevertheless, it could be noticed a direct proportional correlation with the increasing HA concentration into CS composites which resulted in decreasing pH values (*Figure 3.13A*). CSHA composites with DX addition revealed the same pattern (*Figure 3.13B*). CSHA composites analyzed, both with or without DX, reached nearby a pH of 7,4 before 48h of the experiment;

however, CS samples decreased its pH near 7,4 after a minimum of 48h of the study.

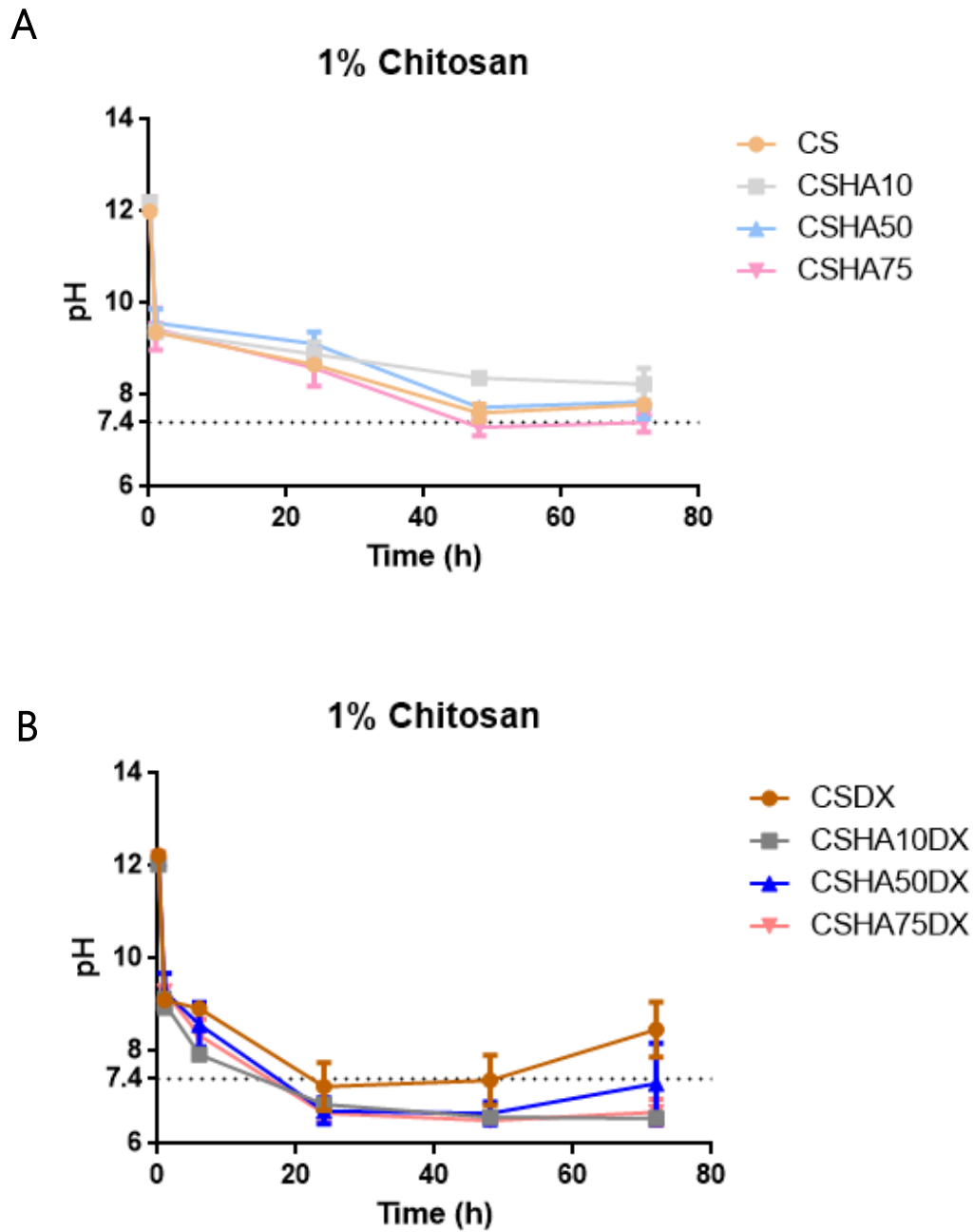


Figure 3.13. (A) pH analysis of 1% CS at a constant rate of 75 mL/h with different HA concentrations (0-75%) without DX addition and (B) with DX addition (n=3).

There are several factors that may affect to the pH value. One of the most important is the relation of absorption between anions and cations. Generally, a higher absorption of cations causes a lower pH, and a higher absorption of anions causes a higher pH. The ion pairs formed by negatively charged phosphate groups of HA with protonated amine functionality of CS in the crosslinking process ⁵² may allowed a higher absorption of cations in the media, resulting in a decrease of the pH when CS was combined with HA. It is known of the possibility to form bonds between the $-NH_2$ of CS and Ca^{2+} of HA ^{5,53}. However, HA did not make a substantial change in the pH. This may be because the addition of ceramic particles in the polymer makes it more resistant and less susceptible to pH variation ²³. When incorporating DX within the CSHA composite, the pH decreased substantially compared with CSDX composite. This fact may be explained because DX chemical structure is composed by NH_2 (which remains neutral) and OH (which has negative charge). DX may interact with CS and HA, resulting in a lower pH value. Moreover, acetic acid was first mixed with CS in order to obtain a solution. The HADX addition to CS solution may have retained some acetic acid, making the pH decrease compared with CSDX composite. CS is a polyelectrolyte, which is a class of polymer with ionizable groups along its matrix. Interestingly, it can be protonated or deprotonated depending on the pH of the surrounding medium ^{30,54}. When CS and CSHA were mixed with DX, it caused a change in the environmental pH, faster decreasing its value within the first 20 hours compared with the control without DX. This fact can be explained because DX has an acidic pH of 2-3 ⁵⁵. CS has several advantages such as the possibility to link with different elements and to modify its pH in order to obtain a nearby physiological one, with the aim to place it as a bone graft biomaterial.

4.2.3 Chemical analysis: Fourier Transformed Infrared Spectroscopy (FTIR)

With the aim of characterizing the chemical structure of the different composites previously synthesized, we analyzed them by FTIR. Specifically, FTIR allowed us to study the chemical interactions between the different components of the biomaterial. We hypothesized that weak interactions between CS, HA and DX impart stability to the composite preventing the disaggregation of the components. CS composites with different HA concentrations (10, 50, 75%) were analyzed and the same trend was observed in all the measurements. Thus, for clarity, only the spectra of HA75% concentration is represented. The infrared spectra of 1% CS is shown in *Figure 3.14*. The assignment of the different bands observed in *Figure 3.14* is summarized in *Table 3.5*. Chitosan is an amino glucose containing small proportion of amide groups through an amide linkage with acetic acid ²⁷. Therefore, signals at 1584 cm^{-1} and 1531 cm^{-1} are ascribed to amide I and amide II bands. The peak at 2843 cm^{-1} and 2825 cm^{-1} corresponds to C-H symmetric and asymmetric stretching bands characteristics of polysaccharide, which chitosan nature is (*Figure 3.14; Table 3.3*). A band between 3100 and 3300 cm^{-1} is seen due to the stretching vibration of N-H and O-H bonds ⁵⁶. HA, on the other hand, showed very intense bands at 961 cm^{-1} and 1017 cm^{-1} corresponding to the PO_4 group in hydroxyapatite ^{48,57}.

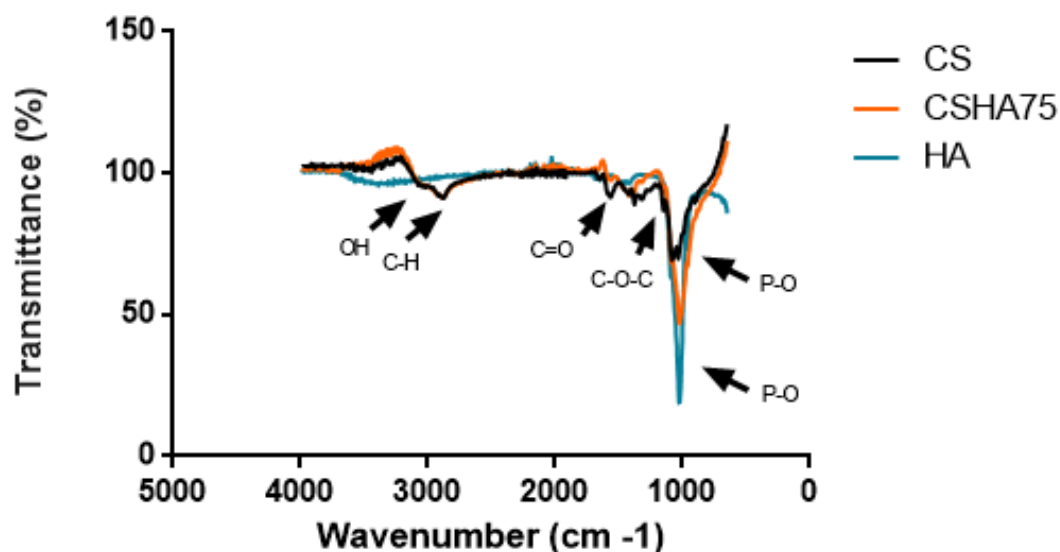


Figure 3.14. FTIR spectrum showing chemical bond structure of 1% CS samples with or without HA75 and HA alone.

The spectra of the pure compounds are consistent with those reported in the literature ^{58,59,60}. Regarding FTIR of CSHADX series, we can observe that the most intense absorbance bands of spectra correspond to HA (*Figure 3.15*; *Table 3.5*). These results are in agreement with *Danilchenko et al.* who also investigated CSHA composites at different CS:HA ratios and obtained similar vibration bands ⁴⁸. Attention should be focused on the shifts resulted in CSHA and CSHADX compared with the polymer alone. C-H symmetric stretching bands changed from CS (2843 cm^{-1}) to CSHADX (2810 cm^{-1}); C-H asymmetric stretching was 2825 cm^{-1} for CS and 2836 cm^{-1} when adding HA. Interestingly, amide I and II band had also showed a shift when adding HA and DX to form the composite.

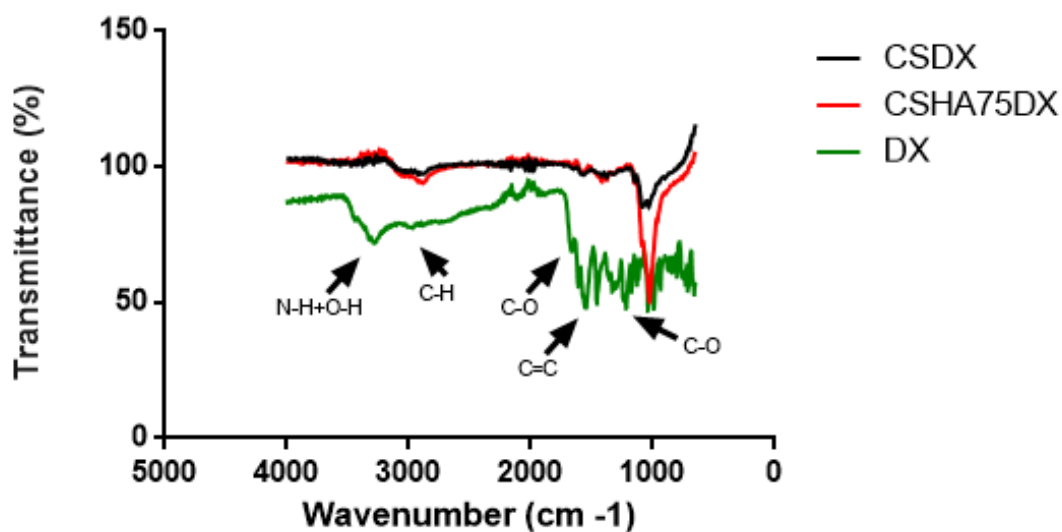


Figure 3.15. FTIR spectrum showing chemical bond structure of 1% CSDX samples with or without HA75 and DX alone.

Similar results were also found in the literature for CS nanoHA blends. They suggest that the hydroxyl and phosphate ions on the surface of HA may interact with the amino and hydroxyl ions of CS by the formation of hydrogen bonds^{49,53,61,62}. These shifts were subtle, thus we hypothesize that the interactions between the different components were weak (hydrogen bond, van der Waals bond and/or electrostatic interaction)⁶⁰. Besides, fiber formation in alkaline bath may occur when protonated amino residues are neutralized and thus there is a decrease of charge density of CS. Then, posterior regular arrangement of CS network through weak intra- and inter- molecular interactions and hydrogen bonds are favored, inducing the formation of physical junctions^{35,63}. The FTIR spectra of pure doxycycline is characterized by the presence of a wide band in the region 3100-3300 cm^{-1} due to both O-H and N-H stretching bands. Peak of C-O in the glucopyranose ring is present at 1174 cm^{-1} . All the doxycycline-doped biomaterials prepared did not show the typical absorption bands corresponding to the drug. This fact may be due to

the low amount of DX loaded into the composite (Figure 3.15; Table 3.3). This data is in accordance to *Yadav et al.* who also studied CSDX FTIR spectra. They used CS nanoparticles blended with 40 mg of DX and did not find any chemical interaction between CS and DX ⁶⁴.

CS (cm ⁻¹)	HA (cm ⁻¹)	DX (cm ⁻¹)	CSHA (cm ⁻¹)	CSHADX (cm ⁻¹)	Vibration
2843	---	---	2843	2810	C-H symmetric stretching
2825	---	---	2836	2821	C-H asymmetric stretching
1584	---	---	1587	1602	Amide I band
1531	---	---	1517	1517	Amide II band
1162	---	---	1162	1125	C-O-C stretching
---	1017	---	1010	984	P-O asymmetric stretching
---	961	---	954	950	P-O symmetric stretching
3100-3300	---	3100-3300	---	---	N-H and O-H stretching
---	---	1174	---	---	C-O

Table 3.5. Main FTIR bands observed for the three different components of the biomaterial: chitosan (CS), hydroxyapatite (HA), doxycycline (DX) and the hybrid biomaterials.

Similar results were obtained by *Soriano et al.* who designed HA microspheres containing DX. The FTIR results only showed phosphate and hydroxyl peaks from HA, and did not show DX vibration bands. Instead, they analyzed DX adsorption within HA microspheres by UV-Vis spectrophotometry ⁶⁵. Another study used Ibuprofen instead of DX to load in CS hydrogel, which was fabricated similar to our fabrication of CS polymer. They reported that CS

physical mixture with ibuprofen exhibited the features of both materials with no visible changes in the FTIR. This fact was regarding the lowest CS concentration of the composite. Instead, a shift was observed in Ibuprofen when CS concentration increased ⁶⁶. We have studied 1% CS that may be a low concentration to observe any interaction when blended with DX. As the lack of information in the literature regarding FTIR and CSHADX biomaterial, our results have also been compared with a study that fabricated silver (Ag) ion-loaded calcium phosphate/CS composite. They found that the characteristic bands of HA-Ag were almost the same of those of HA, indicating that Ag had little effect on HA chemical structure ¹.

4.3 *In vitro* doxycycline release study

DX is an inexpensive broad spectrum drug used to treat bacterial infections such as aerobic and anaerobic Gram-positive and Gram-negative bacteria, among other microorganisms. Its antimicrobial activity is due to the suppression of the bacterial protein biosynthesis. DX also inhibits the activity of collagenase, thus inhibiting bone resorption via osteoclasts ^{67,68,69}. DX release efficiency was studied in two different groups: in the first one, the fibers were manufactured and then the measure of the DX release was assessed; in the second group, the fibers were manufactured and then 4 deionized water baths of 10 minutes each were performed; meanwhile the DX release was measured in order to study if there were differences between both groups in terms of drug release. The DX release values of the first group studied can be observed in *Figure 3.16*.

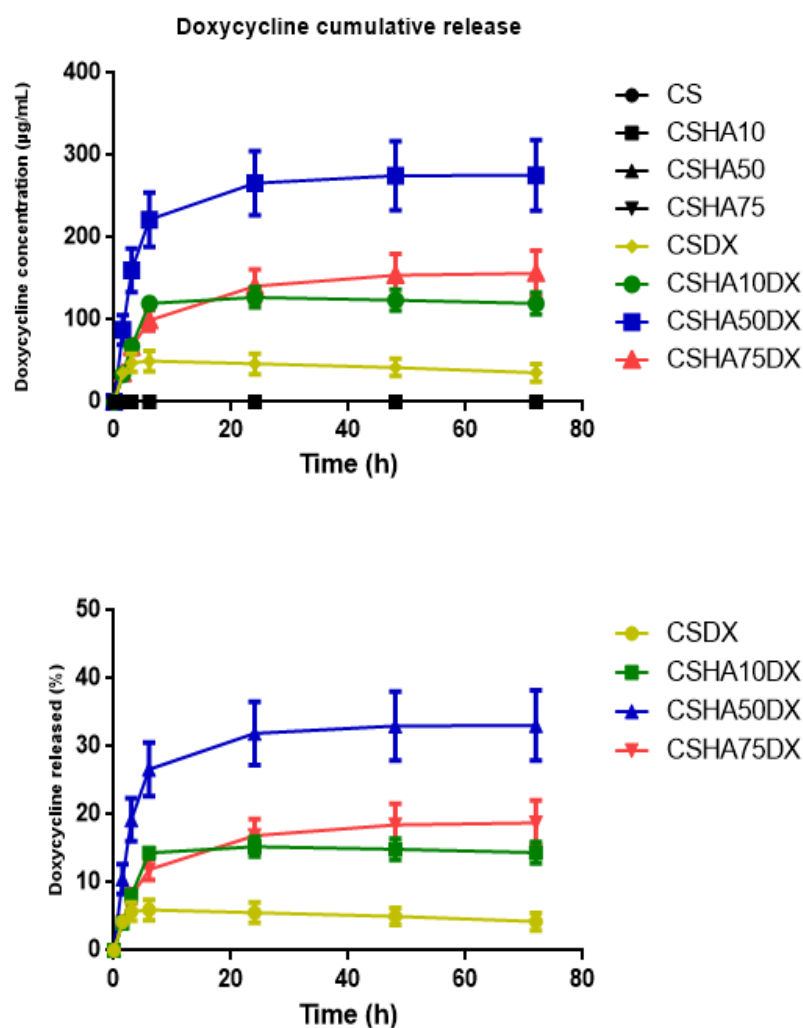


Figure 3.16. Cumulative amount of doxycycline (DX) released and percentage of DX released as a function of time for samples 1% chitosan (CS) with different amounts of hydroxyapatite (HA) from 0 to 75%.

First, the graphic shows that control samples (CS and CSHA without DX) had no release. Then, it can be observed that DX was released from the CSDX fibers in a burst-effect manner within the first 6 hours followed by a slow sustained release. Interestingly, the addition of HA to the CS composite had significant differences from CSDX, obtaining higher release amounts. In the case of CSHA samples, the burst release was observed within the first 24 hours. DX release of CSHA50DX was significantly higher compared with CSDX, having

approximately 5-fold higher values. After the first 2 hours of the initial release, the amount of drug released has decreased. Then, a sustained release was followed for the remaining time of the experiment. Regarding the samples with higher amounts of HA, they had a 2% of increment of the release compared with the rest of the CSHADX samples. CSHA50DX had significant differences compared with the rest of the samples at all time points studied. CSHA50DX sample had released a total of 32% after 24 hours of the study. In the second group (with DI water baths), the drug release pattern also consisted of two distinguishing stages observed in *Figure 3.17*.

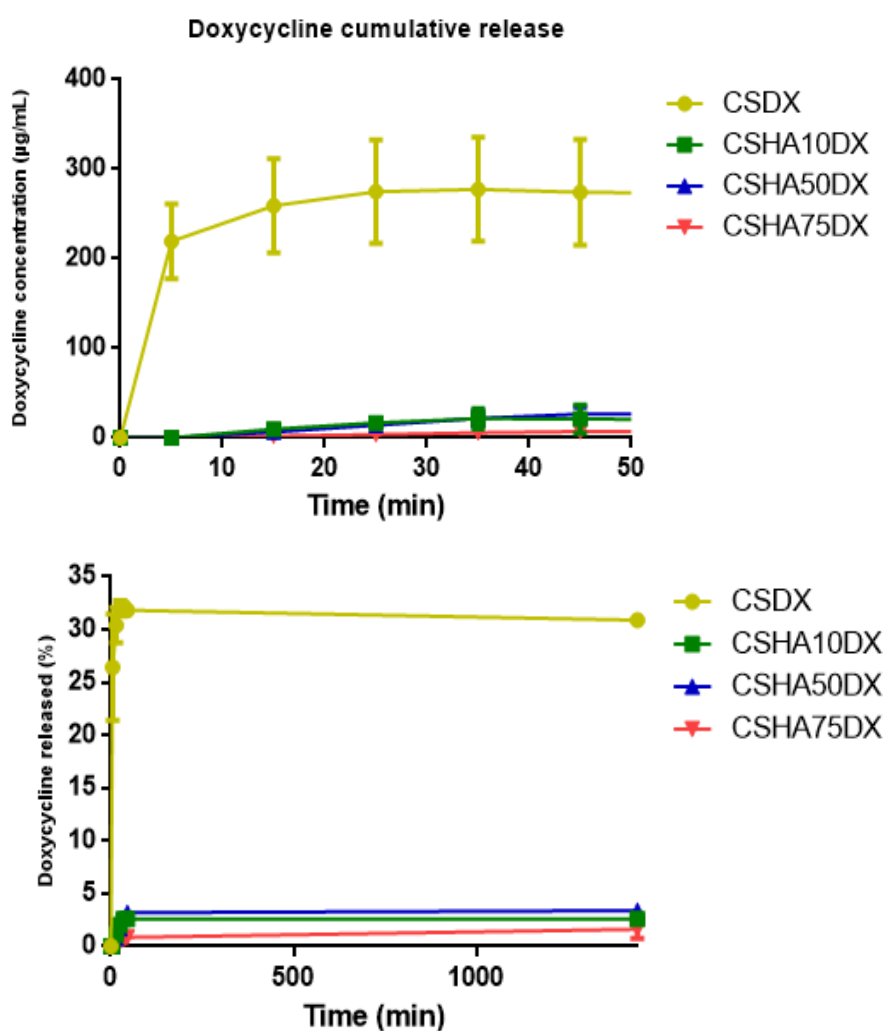


Figure 3.17. Cumulative amount of doxycycline (DX) released and percentage of DX released as a function of time for samples 1% chitosan (CS) with different amounts of hydroxyapatite (HA) from 0 to 75% with previous deionized water baths.

The first is characterized by a burst release of DX within the first 5 minutes of crosslinking and 3 DI water baths of 10 minutes each (a total of 35 minutes) followed by a slow sustained release. These results had significant differences; for CSHADX samples, within the first 45 minutes. The hybrid biomaterials were apparently more effective in releasing DX in a controlled way than their CS equivalent. Within the next 24 hours after the initial release, the amount of drug released decreased and then was followed by a sustained release for the remaining time, except for CSHA75DX, which after 24 hours increased its release from 0,86% to 1,62%, before having a sustained release for the remaining time. By the end of 24 hour monitoring period, CSHA50DX had released more total drug than the rest of the samples analyzed with HA, being statistically significant. That could be explained because of the more acidic pH resulted with the addition of higher amounts of HA that may interfere with the DX release. The interaction between the positive CS charged and the negative HA and DX particles may suggest a remarkable affinity between CS, HA and DX, having an intermolecular attraction ⁷. Our results are in agreement with *Semyari et al.*, who had studied the DX release from a collagen/nanohydroxyapatite scaffold obtaining 29% of release during the same time interval. However, they also have obtained 66% DX release over 14 days of the assay. Their results may be different because they have manufactured collagen scaffolds containing nanohydroxyapatite with DX. Moreover, the DX amount they have used was 6,7 mg/mL compared with our DX concentration used that was 0,83 mg/mL. Besides, they have used the freeze-drying method in order to fabricate the scaffold, which generates a highly porous architecture that may explain the differences between the studies ⁶⁸. *Iqbal et al.* have manufactured a spongy scaffold containing CS, HA, DX and hydroxypropylmethyl cellulose as a crosslinking agent. They have used the freeze-drying method to prepare the scaffolds. Their material resulted that a 60-70% of the drug had a burst release within the first 6-8 hours. After that, a

sustain release profile was maintained for the next 64 hours. The samples with the crosslinking agent had interconnected pores facilitating high concentration of drug entrapment²³. Our results showed that by the end of 72 hour of the monitoring period, CSHA50DX had released more total drug than the rest of the samples analyzed. The differences between the first and the second group studied may be explained because of the DI water baths of the second group. In that group, there may have been a release within the 4 water baths, resulting in a lower release at the time of the measurement. Similar results were obtained by *Ramirez et al.*, who designed nanofibers made of polycaprolactone/gelatin/HA nanoparticles-loaded DX to study antibacterial activity. They have also measured the DX release obtaining a first phase of burst release of about 60% at the first hour⁷⁰. The difference between the amounts of DX released by the 4 samples in both groups studied can be attributed to the differences in HA concentration. The explanation may be because of the chemical retention of DX by HA particles, making a more durable and sustained drug release when HA is present in the composite. Moreover, they have used nanofibers which have a lower surface for DX diffusion compared with the fibers we have designed. CSHA porosity may provide proper loading and sustain release of antibacterial drugs. CS and HA tend to interact with each other through hydrogen bonds between $-NH_2$ and Ca^{2+} from HA⁵⁰. In our study, pure CS with DX exhibited burst release while the composites with apatite component showed both fast and sustained release profiles. The adsorption of tetracyclines on HA is mainly produced by Van der Waals forces and the major mechanism of the release from the composite may be via diffusion of the entrapped DX through the porous network, even the formation of a chelate could also be involved^{29,67}. That explanation is in agreement with *Ding et al.*, who had studied the effect of HA-coated implants treated with DX, clearly demonstrating new bone formation around the HA-coated surface in mice. The DX concentration used was 5

mg/mL⁶⁷. DX minimum inhibitory concentration (MIC) is known to be ≤ 16 $\mu\text{g/mL}$, although it depends on the bacteria strain²⁸. In our experiment, we have obtained a DX release with a MIC in accordance to this data, in all groups studied.

Regarding the CSHADX fibers size (*Figure 3.12*), a relation could be established between the thickness of the fibers and the sustained release obtained. In this sense, the thickest fibers had a higher sustained release. This fact could be explained because when the diameter of the fibers is higher the bonds within its components will be increased, resulting in a higher retention of DX and thus a higher sustained release. Moreover, *Anomolu et al.* stand that the formation of a well-defined crosslinked network helps to a slower drug release from the hydrogel. By changing the concentration of the polymers and the crosslinking density, drug release from the hydrogel can be tailored⁷¹.

We have investigated CSHA biomaterial as a potential carrier of DX. We are positive that introducing CSHADX fibers to maxillary bone defects will be able to produce sustained drug levels locally by the adhesion of the biomaterial to the target tissue as well as the absorption of the fibers into the tissue, increasing the bone volume tissue and the complete pathogen elimination. CS is claimed as an attractive biomaterial to be used as a bone scaffold because it promotes the attachment and proliferation of osteoblasts cells, as well as formation of mineralized bone matrix *in vitro*²¹. Thus, we hypothesize that the major advantages of HA as an additive to our biomaterial is the enhancement of the mechanical properties. Besides, it may establish chemical bonds with the host tissue which, at the same time, may lead to faster and greater bone tissue regeneration and integration. With this preliminary study, we present a simple but efficient method to prepare CSHADX-loaded biomaterial to be used as bone graft in different maxillary defects.

5. Conclusions and Future perspectives

The evidence from this study points towards the idea that 1% chitosan concentration was stable, easy to manipulate and exhibited adequate cutability and pH parameters. An interesting finding was that incorporating HA and DX powder into CS fibers had decreased their pH values. Moreover, we have observed that the integration of HA and DX within the CS composite resulted in a chemical stability. The results of the present study suggest that chitosan/hydroxyapatite/doxycycline complex exhibited combined fast and sustained release profile dictated by hydroxyapatite concentration. In this chapter, we have designed a drug-polymer-bioceramic conjugate to be used as multifunctional regulated drug delivery for maxillary bone regeneration treatments. In fact, the combination of biocompatibility of the three biomaterial components, added to the CS intrinsic antibacterial activity and its ability to bind to anionic molecules such as growth factors, and the antibacterial plus osteogenic capacity of DX, renders our proposed biomaterial a promising candidate graft material for bone tissue engineering in dental clinical practice. In future, the progress will focus in the fabrication of biomaterials for minimally invasive surgery enhancing injectable forms, optimal degradation rate and mechanical strength parameters. Patients with bone regeneration needs will have better outcomes with this type of biomaterials, being safer and more predictable treatments. 3D printing will be an important technique in this field, giving precise and accurate control for individualized bone defects to regenerate.

6. References

1. Jin, S., Li, J., Wang, J. & Jiang, J. Electrospun silver ion-loaded calcium phosphate/chitosan antibacterial composite fibrous membranes for guided bone regeneration. *Int. J. Nanomedicine* **13**, 4591–4605 (2018).
2. Croisier, F. & Jérôme, C. Chitosan-based biomaterials for tissue engineering. *Eur. Polym. J.* **49**, 780–792 (2013).
3. López-García, J., Lehocký, M., Humpolíček, P. & Sáha, P. HaCaT Keratinocytes Response on Antimicrobial Atelocollagen Substrates: Extent of Cytotoxicity, Cell Viability and Proliferation. *J. Funct. Biomater.* **5**, 43–57 (2014).
4. Nie, J., Wang, Z. & Hu, Q. Difference between Chitosan Hydrogels via Alkaline and Acidic Solvent Systems. *Sci. Rep.* **6**, 1–8 (2016).
5. Venkatesan, J. & Kim, S. Chitosan Composites for Bone Tissue Engineering — An Overview. *Mar. Drugs* **8**, 2252–2266 (2010).
6. Kumar, A., Vimal, A. & Kumar, A. Why Chitosan? From properties to perspective of mucosal drug delivery. *Int. J. Biol. Macromol.* **91**, 615–622 (2016).
7. Aguilar, A. *et al.* Application of Chitosan in Bone and Dental Engineering. *Molecules* **24**, 1–17 (2019).
8. Anal, A. K. & Stevens, W. F. Chitosan–alginate multilayer beads for controlled release of ampicillin. *Int. J. Pharm.* **290**, 45–54 (2005).
9. Yu, W. *et al.* Synergistic antibacterial activity of multi components in lysozyme/chitosan/silver/hydroxyapatite hybrid coating. *Mater. Des.* **139**, 351–362 (2017).
10. Tuzlakoglu, K., Alves, C. M., Mano, J. F. & Reis, R. L. Production and Characterization of Chitosan Fibers and 3-D Fiber Mesh Scaffolds for Tissue Engineering Applications. *Macromol. Biosci.* **4**, 811–819 (2004).
11. Sun, K. & Li, Z. H. Preparations, properties and applications of chitosan based nanofibers fabricated by electrospinning. *Express Polym. Lett.* **5**, 342–361 (2011).
12. Qi, L., Xu, Z., Jiang, X., Hu, C. & Zou, X. Preparation and antibacterial activity of chitosan nanoparticles. *Carbohydr. Res.* **339**, 2693–2700 (2004).

13. Camacho-Alonso, F., Julián-Belmonte, E., Chiva-García, F. & Martínez-Beneyto, Y. Bactericidal Efficacy of Photodynamic Therapy and Chitosan in Root Canals Experimentally Infected with *Enterococcus faecalis*: An In Vitro Study. *Photomed. Laser Surg.* **35**, 184–189 (2017).
14. Liu, X., Ma, L., Mao, Z. & Gao, C. Chitosan-Based Biomaterials for Tissue Repair and Regeneration. *Adv Polym Sci* **244**, 81–128 (2011).
15. He, X., Liu, Y., Yuan, X. & Lu, L. Enhanced Healing of Rat Calvarial Defects with MSCs Loaded on BMP-2 Releasing Chitosan/Alginate/Hydroxyapatite Scaffolds. *PLoS One* **9**, (2014).
16. Zhang, Y. & Zhang, M. Calcium phosphate/chitosan composite scaffolds for controlled in vitro antibiotic drug release. *J. Biomed. Mater. Res.* **62**, 378–386 (2002).
17. Pighinelli, L. & Kucharska, M. Chitosan – hydroxyapatite composites. *Carbohydr. Polym.* **93**, 256–262 (2013).
18. Gao, Y., Wang, Y., Wang, Y. & Cui, W. Fabrication of Gelatin-Based Electrospun Composite Fibers for Anti-Bacterial Properties and Protein Adsorption. *Mar. Drugs* **14**, 1–14 (2016).
19. Wang, H. *et al.* Biointerfaces Osteogenic effect of controlled released rhBMP-2 in 3D printed porous hydroxyapatite scaffold. *Colloids Surfaces B Biointerfaces* **141**, 491–498 (2016).
20. Okada, T. *et al.* Preparation of chitosan-hydroxyapatite composite mono-fiber using coagulation method and their mechanical properties. *Carbohydr. Polym.* **175**, 355–360 (2017).
21. Lan Levengood, S. & Zhang, M. Chitosan-based scaffolds for bone tissue engineering. *J Mater Chem B Mater Biol Med* **2**, 3161–3184 (2014).
22. Chai, F. *et al.* Antibacterial activation of hydroxyapatite (HA) with controlled porosity by different antibiotics. *Biomol. Eng.* **24**, 510–514 (2007).
23. Iqbal, H., Ali, M., Zeeshan, R. & Mutahir, Z. Chitosan/hydroxyapatite (HA)/hydroxypropylmethyl cellulose (HPMC) spongy scaffolds-synthesis and evaluation as potential alveolar bone substitutes. *Colloids Surfaces B Biointerfaces* **160**, 553–563 (2017).
24. Pai, S., Kini, M. S. & Selvaraj, R. A review on adsorptive removal of dyes from wastewater by hydroxyapatite nanocomposites. *Env. Sci Pollut Res* (2019).
25. Ong, S. M. & Taylor, G. J. S. Doxycycline inhibits bone resorption by human interface

- membrane cells from aseptically loose hip replacements. *J. bone Jt. Surg.* **85**, 456–461 (2002).
26. Kallala, R. *et al.* In vitro and in vivo effects of antibiotics on bone cell metabolism and fracture healing. *Expert Opin Drug Saf* **11**, 15–32 (2012).
 27. Sahoo, S., Sasmal, A., Sahoo, D. & Nayak, P. Synthesis and Characterization of Chitosan-Polycaprolactone Blended with Organoclay for Control Release of Doxycycline. *J. Appl. Polym. Sci.* **118**, 3167–3175 (2010).
 28. Bell, S., Pham, J., Saab, J. & Nguyen, T. Calibration of doxycycline for use in urinary tract infections with enterococci. *Pathology* **44**, 654–675 (2012).
 29. Teng, S. *et al.* Functionally Gradient Chitosan/ Hydroxyapatite Composite Scaffolds for Controlled Drug Release. *J. Biomed. Mater. Res. Part B Appl. Biomater.* **90**, 275–282 (2008).
 30. Bergonzi, C. *et al.* Study of 3D-printed chitosan scaffold features after different post-printing gelation processes. *Sci. Rep.* **9**, 1–11 (2019).
 31. Jahangirian, H., Lemraski, E. G., Moghaddam, R. R. & Webster, T. J. A review of using green chemistry methods for biomaterials in tissue engineering. *Int. J. Nan* **13**, 5953–5969 (2018).
 32. Xu, Y., Han, J. & Lin, H. Fabrication and characterization of a self-crosslinking chitosan hydrogel under mild conditions without the use of strong bases. *Carbohydr. Polym.* **156**, 372–379 (2017).
 33. Ozipek, B. & Karakas, H. *Wet spinning of synthetic polymer fibers. Advances in filament yarn spinning of textiles and polymers* (Woodhead Publishing Limited, 2014).
 34. Robb, B. & Lennox, B. The electrospinning process, conditions and control. in *Electrospinning for Tissue Regeneration* (eds. Bosworth, L. A. & Downes, S.) 51–66 (2011).
 35. Rivas Araiza, R. N., Rochas, C., Laurent, D. & Domard, A. Interrupted Wet-Spinning Process for Chitosan Hollow Fiber Elaboration. *Macromol Symp* **266**, 1–5 (2008).
 36. Pati, F., Adhikari, B. & Dhara, S. Development of Ultrafine Chitosan Fibers Through Modified Wetspinning Technique. *J. Appl. Polym. Sci.* **121**, 1550–1557 (2011).
 37. Deitzel, J. M., Kleinmeyer, J., Harris, D. & Tan, N. C. B. The effect of processing variables on the morphology of electrospun nanofibers and textiles. *Polymer (Guildf)*. **42**, 261–272 (2001).

38. Enache, A., Laurent, D., Puaux, J. P., Banu, I. & Bozga, G. An experimental study of chitosan wet spinning process. *UPB Sci. Bull. Ser. B Chem. Mater. Sci.* **80**, 13–26 (2018).
39. Di Martino, A., Sitterling, M. & Risbud, M. V. Chitosan: A versatile biopolymer for orthopaedic tissue-engineering. *Biomaterials* **26**, 5983–5990 (2005).
40. Ding, S. Biodegradation behavior of chitosan/calcium phosphate composites. *J. Non. Cryst. Solids* **353**, 2367–2373 (2007).
41. Maurmann, N. *et al.* Highly defined 3D printed chitosan scaffolds featuring improved cell growth. *Biomed Mater* **12**, 1–11 (2017).
42. Dhandayuthapani, B., Yoshida, Y., Maekawa, T. & Kumar, D. S. Polymeric Scaffolds in Tissue Engineering Application: A Review. *Int. J. Polym. Sci.* **2011**, 1–19 (2011).
43. Chenite, A. *et al.* Novel injectable neutral solutions of chitosan form biodegradable gels in situ. *Biomaterials* **21**, 2155–2161 (2000).
44. Risbud, M. V & Bhone, R. R. Polyacrylamide-Chitosan Hydrogels: In Vitro Biocompatibility and Sustained Antibiotic Release Studies. *Drug Deliv.* **7**, 69–75 (2000).
45. Zhang, Y. & Zhang, M. Cell growth and function on calcium phosphate reinforced chitosan scaffolds. *J. Mater. Sci. Mater. Med.* **15**, 255–260 (2004).
46. Xia, W. *et al.* Tissue Engineering of Cartilage with the Use of Chitosan-Gelatin Complex Scaffolds. *J. Biomed. Mater. Res. Part B Appl. Biomater.* **71**, 373–380 (2004).
47. Pastorino, D., Canal, C. & Ginebra, M. Acta Biomaterialia Drug delivery from injectable calcium phosphate foams by tailoring the macroporosity – drug interaction. *Acta Biomater.* **12**, 250–259 (2014).
48. Danilchenko, S. N. *et al.* Characterization and in vivo evaluation of chitosan-hydroxyapatite bone scaffolds made by one step coprecipitation method. *J. Biomed Mater Res A* **96**, 639–647 (2011).
49. Wawro, D. & Pighinelli, L. Chitosan Fibers Modified with HAp/ β -TCP Nanoparticles. *Int. J. Mol. Sci.* **12**, 7286–7300 (2011).
50. Stepniewski, M., Martynkiewicz, J. & Gosk, J. Chitosan and its composites: Properties for use in bone substitution. *Polim Med* **47**, 49–53 (2017).
51. Mederle, N. *et al.* Innovative Biomaterials Based on Collagen-Hydroxyapatite and Doxycycline for Bone Regeneration. *Adv. Mater. Sci. Eng.* **2016**, 1–5 (2016).
52. Rogina, A. *et al.* Cellular hydrogels based on pH-responsive chitosan-hydroxyapatite system. *Carbohydr. Polym.* **166**, 173–182 (2017).

53. Xianmiao, C. *et al.* Properties and in vitro biological evaluation of nano-hydroxyapatite/chitosan membranes for bone guided regeneration. *Mater. Sci. Eng. C* **29**, 29–35 (2009).
54. Zhang, R., Zaslavski, E., Vasilyev, G., Boas, M. & Zussman, E. Tunable pH-responsive Chitosan-Poly (acrylic acid) electrospun fibers. *Biomacromolecules* **19**, 588–595 (2018).
55. Doxycycline Hyclate. in *Drugs for the Geriatric Patient* (eds. Shorr, R. I., Hoth, A. B. & Rawls, N.) 320–413 (Elsevier Inc, 2007).
56. Sakkara, S., Santosh, M. S. & Reddy, N. Chitosan Fibers. in *Handbook of Fibrous Materials* 125–156 (2020).
57. Bollino, F., Armenia, E. & Tranquillo, E. Zirconia/Hydroxyapatite Composites Synthesized Via Sol-Gel: Influence of Hydroxyapatite Content and Heating on Their Biological Properties. *Materials (Basel)*. **10**, 1–19 (2017).
58. Pawlak, A. & Mucha, M. Thermogravimetric and FTIR studies of chitosan blends. *Thermochim. Acta* **396**, 153–166 (2003).
59. Moosa, A. A., Ridha, A. M. & Kadhim, N. A. Use of Biocomposite Adsorbents for the Removal of Methylene Blue Dye from Aqueous Solution. *Am. J. Mater. Sci.* **6**, 135–146 (2016).
60. Sibaja, B., Culbertson, E., Marshall, P. & Boy, R. Preparation of Alginate—Chitosan Fibers with Potential Biomedical Applications. *Carbohydr. Polym.* **134**, 598–608 (2015).
61. Zima, A. Hydroxyapatite-chitosan based bioactive hybrid biomaterials with improved mechanical strength. *Spectrochim. Acta Part A Mol. Biomol. Spectrosc.* **193**, 175–184 (2017).
62. Kumar, B. Y. S., Isloor, A. M., Kumar, G. C. M., Inamuddin & Asiri, A. M. Nanohydroxyapatite Reinforced Chitosan Composite Hydrogel with Tunable Mechanical and Biological Properties for Cartilage Regeneration. *Sci. Rep.* **9**, 1–15 (2019).
63. Pati, F., Adhikari, B. & Dhara, S. Development of chitosan – tripolyphosphate fibers through pH dependent ionotropic gelation. *Carbohydr. Res.* **346**, 2582–2588 (2011).
64. Yadav, M., Parle, M., Sharma, N., Dhingra, S. & Raina, N. Brain targeted oral delivery of doxycycline hydrochloride encapsulated Tween 80 coated chitosan nanoparticles against ketamine induced psychosis: behavioral , biochemical , neurochemical and histological alterations in mice. *Drug Deliv.* **24**, 1429–1440 (2017).
65. Soriano-Souza, C. *et al.* Doxycycline containing hydroxyapatite ceramic microspheres as a bone-targeting drug delivery system. *J Biomed Mater Res B Appl Biomater* **108**, 1351–

- 1362 (2020).
66. Abioye, A. O., Armitage, R. & Kola-mustapha, A. T. Thermodynamic Changes Induced by Intermolecular Interaction Between Ibuprofen and Chitosan : Effect on Crystal Habit , Solubility and In Vitro Release Kinetics of Ibuprofen. (2015). doi:10.1007/s11095-015-1793-0
 67. Ding, L. *et al.* Effect of doxycycline-treated hydroxyapatite surface on bone apposition: A histomophometric study in murine maxillae. *Dent. Mater.* **37**, 130–138 (2018).
 68. Semyari, H. *et al.* Fabrication and characterization of collagen–hydroxyapatite-based composite scaffolds containing doxycycline via freeze-casting method for bone tissue engineering. *J. Biomater. Appl.* **33**, 501–513 (2018).
 69. Castro, M. L. *et al.* Down-Regulation of Protease Activated Receptor 2 , Interleukin-17 and Other Pro-Inflammatory Genes by Subantimicrobial Doxycycline Dose in a Rat Periodontitis Model. *J. Periodontol.* **87**, 203–210 (2015).
 70. Ramírez-agudelo, R. *et al.* Hybrid nanofibers based on poly-caprolactone/gelatin/hydroxyapatite nanoparticles-loaded Doxycycline: Effective anti-tumoral and antibacterial activity. *Mater. Sci. Eng. C* **83**, 25–34 (2018).
 71. Anumolu, S. S. *et al.* Doxycycline loaded poly(ethylene glycol) hydrogels for healing vesicant-induced ocular wounds. *Biomaterials* **31**, 964–974 (2010).

7. List of figures

- FIGURE 3.1.** From left to right: chemical structure of chitosan³ hydroxyapatite and doxycycline. 167
- FIGURE 3.2.** Schematic illustration of the CS fibers manufactured with the injection pump and the NaOH crosslinking solution agent. 169
- FIGURE 3.3.** Optical microscope images of CS fibers at different percentages (1, 2 and 3%) and at different rates (60, 75, 100 and 150 mL/h). CS fibers at 1% were manufactured with 0,5 and 0,9 mm needle diameter, and the rest of fibers with 0,9 mm needle diameter. The NaOH solution was 0,5 M. Scale bar 500 μ m. 179
- FIGURE 3.4.** CS fibers size with the two needle diameters (0,5 and 0,9 mm) and at different rates (60-150 mL/h). Data are shown as mean \pm standard deviation (n = 6). Groups identified by the same superscript letter are not statistically different. ($P \geq 0.05$). 180
- FIGURE 3.5.** CS fibers size at 1, 2 and 3% concentration fabricated with a needle diameter 0,9 mm and at different rates (60-150 mL/h). Data are shown as mean \pm standard deviation (n = 6). Groups identified by the same superscript letter are not statistically different. ($P \geq 0.05$). 181
- FIGURE 3.6.** pH analysis of 1% CS at a rate of 75mL/h and with different needle diameters (0,5 or 0,9 mm). 182
- FIGURE 3.7.** pH analysis of different CS concentrations (1-3%) at a constant rate of 75 mL/h (n=3). 183
- FIGURE 3.8.** pH analysis of 1% CS at different rates (60-150 mL/h) (n=3). 183
- FIGURE 3.9.** Illustration of selected examples of CS processing for use in tissue engineering: Cells may be encapsulated in gels or seeded in porous matrices including sponge-like or fibrous structures. Combinations of CS with other biocompatible materials such as calcium phosphate or gelatin are applied to modify biomechanical and cell-matrix-interaction properties. Different adaptations of CS may help to optimize cell and tissue differentiation and tailor the transplant to different clinical cell delivery situations^{43,44,10,45,46}. Modified from³⁹. 185
- FIGURE 3.10.** Digital photographs and optical microscope images of 1% CS fibers manufactured with a needle diameter of 0,9 mm and at a constant rate of 75 mL/h mixed with different concentrations of HA (0-75%). Scale bars 0,5 cm and 500 μ m. 186

FIGURE 3.11. Digital photographs and optical microscope images of 1% CS fibers manufactured with a needle diameter of 0,9 mm and at a constant rate of 75 mL/h mixed with different concentrations of HA (0-75%) with DX incorporation. Scale bars 0,5 cm and 500 μ m. **187**

FIGURE 3.12. CSHA fibers size with and without DX incorporation. Data are shown as mean \pm standard deviation (n = 6). Groups identified by the same superscript letter are not statistically different. ($P \geq 0.05$). **188**

FIGURE 3.13. (A) pH analysis of 1% CS at a constant rate of 75 mL/h with different HA concentrations (0-75%) without DX addition and **(B)** with DX addition (n=3). **189**

FIGURE 3.14. FTIR spectrum showing chemical bond structure of 1% CS samples with or without HA75 and HA alone. **192**

FIGURE 3.15. FTIR spectrum showing chemical bond structure of 1% CSDX samples with or without HA75 and DX alone. **193**

FIGURE 3.16. Cumulative amount of doxycycline (DX) released and percentage of DX released as a function of time for samples 1% chitosan (CS) with different amounts of hydroxyapatite (HA) from 0 to 75%. **196**

FIGURE 3.17. Cumulative amount of doxycycline (DX) released and percentage of DX released as a function of time for samples 1% chitosan (CS) with different amounts of hydroxyapatite (HA) from 0 to 75% with previous deionized water baths. **197**

8. List of tables

TABLE 3.1. Samples studied and codes used for this chapter. The main variable studied was the HA percentage (0, 10, 50 and 75%) with or without DX incorporation. **173**

TABLE 3.2. Visible stability and manipulation of CS fibers at different NaOH solution molarities (0, 05-0,5). The parameters were scored as low/bad, correct or optimal marked with an X. **175**

TABLE 3.3. Visible stability and manipulation of CS fibers manufactured with different needle diameters: 0,5 and 0,9 mm. The parameters were scored as low/bad = 0, correct = + or optimal = ++. **176**

TABLE 3.4. Visible stability and manipulation of fibers at different CS percentages (1, 2 and 3%) and at different rates (60, 75, 100 and 150 mL/h). The parameters were scored as low/bad = 0, correct = + or optimal = ++. **177**

TABLE 3.5. Main FTIR bands observed for the three different components of the biomaterial: chitosan (CS), hydroxyapatite (HA), doxycycline (DX) and the hybrid biomaterial. **194**

o

Chapter 4

Conclusions and Future perspectives

1. Conclusions

A Bioactive Endodontic material for conservative treatments

1. *Trans*-polyisoprene had better mechanical and handling properties than *trans/cis*-polyisoprene blend.
2. Adding 10% silica microspheres into gutta-percha material enhanced the mechanical properties of the raw material.
3. The infrared analysis showed there are electrostatic interactions between the gutta-percha and the silica microspheres.
4. The analysis by scanning electron microscopy and energy dispersive X-ray spectroscopy revealed that silica microspheres-GP composite had bioactivity capacity, showing calcium phosphate deposition on its surface.
5. Cell proliferation assay demonstrated that silica microspheres-GP was no cytotoxic for rat MSCs.
6. Silica microspheres-GP revealed an adequate sealing ability, both in simulated root canals and on extracted teeth, preventing filtration on simulated root canals.

Low-level laser therapy for bone regeneration

1. Irradiation with a diode low-level laser with a wavelength of 635 nm and at an energy density of 5 J/cm² has promoted higher proliferation rates on DPMSCs after 10 days of daily treatment, compared with the control group.
2. LLLT did not have a significant effect on ALP activity compared with the control, although irradiation at an energy density of 5 J/cm² obtained higher ALP quantity compared with the other irradiation groups at different energy densities.

Novel Chitosan-based Biomaterial for Bone Regeneration

1. An optimization of the biomaterial has been carried out. We have chosen 1% CS concentration which was stable and easy to manipulate.
2. Once the fibers were stabilized, a physiological pH was maintained. This parameter is crucial in order to may integrate the biomaterial into the patient's body.
3. The analysis by FTIR revealed that electrostatic interactions were formed between the components of the biomaterial. This fact showed that there was an integration of HA within the CS composite. We have optimized the sustained release of doxycycline. The incorporation of 50% HA into the CS fibers resulted in a more sustained DX release compared with the rest of the samples studied.

2. Future perspectives

The results obtained in the present thesis are promising regarding the field of dentistry. We have focused in endodontics in a first stage. Its main objective is to preserve the tooth of the patient by performing the root canal treatment. The final step is the root canal filling and the gold standard material used is GP. In order to improve this treatment, it would be of great interest to may incorporate some type of signaling molecules to the proposed SiMS-GP biomaterial, such as antibiotics or anti-inflammatory molecules. This could prevent future re-infections in the endodontic treated tooth or enhance its healing process once implanted. Moreover, this fact could avoid the patient from taking systemic-drugs because they would receive a drug local controlled action. However, the first step would be corroborating the bioactive activity of the biomaterial once implanted on extracted teeth, in order to verify the chemical adhesion of SiMS-GP with the dentine tissue.

We have to bear in mind there are several cases in which the patient presents a more advanced dental pathology, which has led to the tooth loss and/or bone loss surrounding the tooth. Thus, the second area of this thesis research is bone tissue engineering. We have studied low level laser therapy as an adjuvant treatment for bone regeneration. Nowadays, this technique is used in the clinic to enhance the tissue regeneration. Nevertheless, cell mechanistic studies at different laser potency and time interval parameters will be needed in order to better understand the underlying mechanisms of the effects of laser in the clinical practice. Once this concept is understood, low-level laser therapy will have the potential not only in the bone tissue engineering field but also in other clinical specialties.

Regarding the work of the chitosan-based biomaterial to be used as a bone graft, future studies may be accomplished. For instance, the fibers loaded with doxycycline could be studied *in vitro* both in cell culture and bacterial culture in order to analyze if osteogenesis and antibacterial capacity would take place. One of the approaches would be to further encapsulate the drug inside the composite, by designing a biomaterial with core-shell characteristics so that the drug will be released in a more sustain manner. For this purpose, the biomaterial manufacturing can be modified, such as combining the drug with the core CS material and adding outside layers into the fiber. Another interesting approach will be to design and manufacture a 3D printing model of CS-HA scaffold that would be suitable to optimize the fibers structure. This fact would be an important contribution in the cases with complex anatomy that require an individualized design and fabrication. Furthermore, growth factors or ions could be incorporated in order to enhance the scaffold bone regeneration capacity.

Supplementary data

Ethics committee approval

**APROVACIÓ PROJECTE PEL CER/ APROBACIÓN PROYECTO POR EL CER**

Codi de l'estudi / Código del estudio: IMR-2017-04
Versió del protocol / Versión del protocolo: 1.0
Data de la versió / Fecha de la versión: 18/01/18
Títol / Título: Development of novel biomaterials for endodontic treatments

Sant Cugat del Vallès, 6 de febrer de 2018

Investigadora: Ana Barbara Giordano
Director de Tesi: Dr. Roman Pérez Antónanzas

Títol de l'estudi / Título del estudio: Development of novel biomaterials for endodontic treatments

Benvolgut/da,

Valorat el projecte presentat, el CER de la Universitat Internacional de Catalunya, considera que, el contingut de la investigació, no implica cap inconvenient relacionat amb la dignitat humana, tracte ètic per als animals ni atempta contra el medi ambient, ni té implicacions econòmiques ni conflicte d'interessos, però no s'han valorat els aspectes metodològics del projecte de recerca degut a que tal anàlisi correspon a d'altres instàncies.

Per aquests motius, el Comitè d'Ètica de Recerca, **RESOLT FAVORABLEMENT**, emetre aquest **CERTIFICAT D'APROVACIÓ**, per que pugui ser presentat a les instàncies que així ho requerixin.

Em permeto recordar-li que, si en el procés d'execució es produís algun canvi significatiu en els seus plantejaments, hauria de ser sotmès novament a la revisió i aprovació del CER.

Atentament,

Apreciada,

Valorado el proyecto presentado, el CER de la Universidad Internacional de Catalunya, considera que, el contenido de la investigación, no implica ningún inconveniente relacionado con la dignidad humana, trato ético para los animales, ni atenta contra el medio ambiente, ni tiene implicaciones económicas ni conflicto de intereses, pero no se han valorado aspectos metodológicos del proyecto de investigación debido a que tal análisis corresponde a otras instancias.

Por estos motivos, el Comité d'Ètica de Recerca, RESUELVE FAVORABLEMENTE, emitir este CERTIFICADO DE APROBACIÓN, para que pueda ser presentado a las instancias que así lo requieran.

Me permito recordarle que si el proceso de ejecución se produjera algún cambio significativo en sus planteamientos, debería ser sometido nuevamente a la revisión y aprobación del CER.

Atentamente,

Dr. Josep Argemí
President CER-UIC